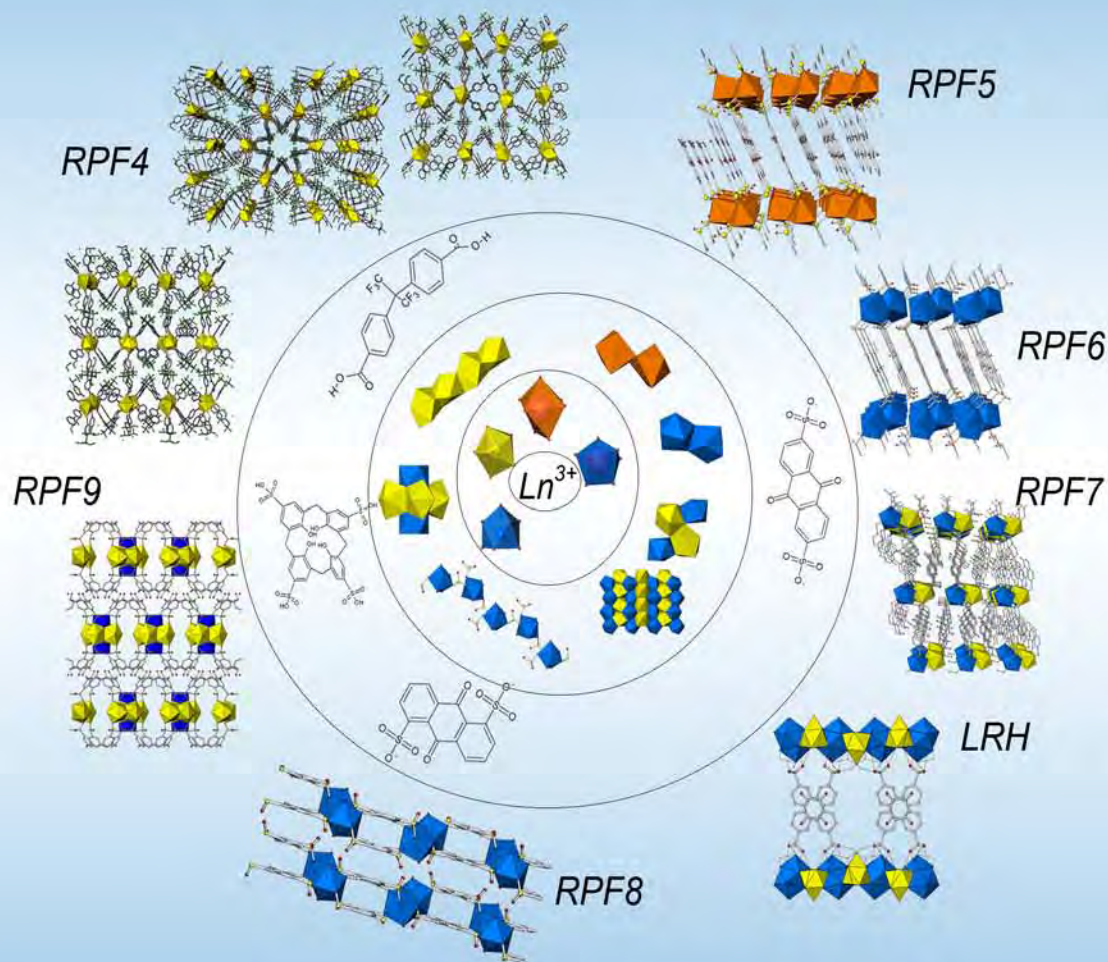


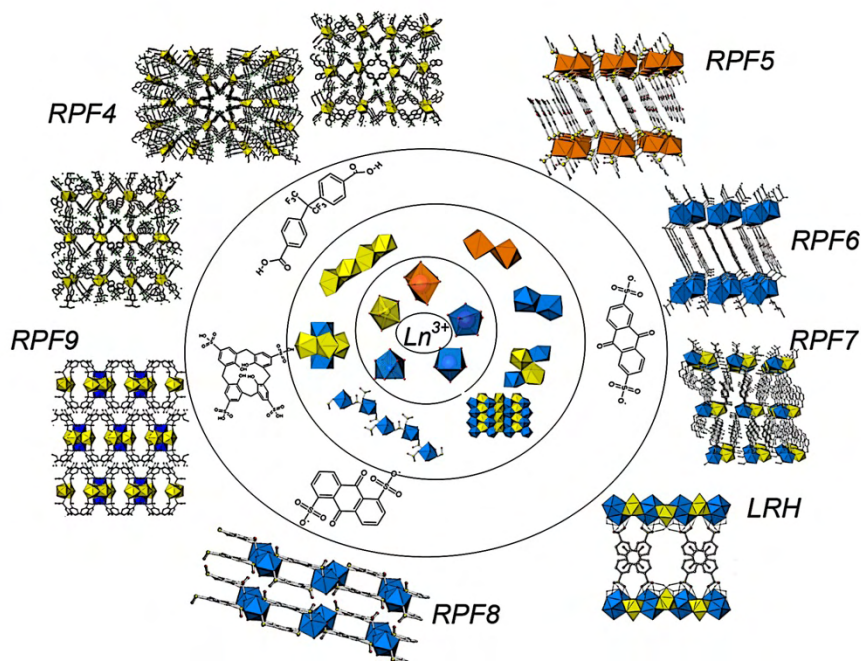
New Rare-earth Coordination Polymers as Multifunctional Materials



*Memoria presentada por Felipe Gándara Barragán
para optar al grado de Doctor en Química*

Madrid, Junio 2009

New Rare-earth Coordination Polymers as Multifunctional Materials



Tesis Doctoral dirigida por la Doctora M. Ángeles Monge Bravo y por la Doctora Natalia Snejko.

Trabajo realizado en el Departamento de Síntesis y Estructura de Óxidos, del Instituto de Ciencia de Materiales de Madrid – CSIC

Memoria presentada en el Departamento de Química-Física Aplicada, Facultad de Ciencias, Universidad Autónoma de Madrid, por Felipe Gándara Barragán para optar al grado de Doctor en Química.

Madrid, Junio de 2009

Para mis padres y mis hermanas.

Para Mari Jose, mi compañera de viaje

Resumen

Los polímeros de coordinación son un tipo de compuestos en los que centros metálicos coordinan con ligandos orgánicos para dar lugar a estructuras que forman redes extensas en al menos una dirección del espacio. Durante los últimos quince años, la investigación centrada en este tipo de compuestos ha experimentado un gran desarrollo, debido a las potenciales aplicaciones que presentan. Así, se han sintetizado materiales que presentan estructuras abiertas con porosidad permanente, y su utilización como materiales para adsorción, separación y almacenamiento de gases está actualmente siendo objeto de estudio por numerosos grupos de investigación en todo el mundo. Otras aplicaciones para las que estos materiales están siendo investigados se encuentran dentro del área de la catálisis heterogénea, o en su uso como sensores, gracias a que pueden presentar, entre otras, propiedades ópticas, magnéticas, o de conducción. Dentro de la gran evolución que estos materiales han sufrido, la cristalografía y la cristalografía han jugado y juegan un papel determinante, tanto por permitir conocer las características estructurales de los nuevos materiales, como por ocuparse del entendimiento y racionalización de las nuevas redes formadas. En la actualidad, y a pesar de que en los últimos años ha habido una gran explosión en la aparición de nuevos polímeros de coordinación en la literatura, la investigación continúa centrada en la obtención racional de nuevos tipos estructurales diseñados para su aplicación en las áreas ya mencionadas.

El presente trabajo ha sido realizado con el objetivo de preparar nuevos polímeros de coordinación utilizando elementos de las tierras raras y diversos ligandos orgánicos.

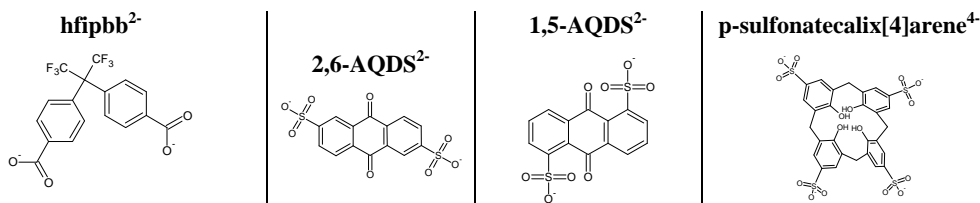
En general, el uso de elementos de tierras raras está menos extendido en comparación con el de los metales de transición, principalmente debido a la variabilidad en la coordinación que presentan los primeros. Sin embargo, con la incorporación de estos metales dentro de los polímeros de coordinación se

puede dotar a estos materiales con las interesantes propiedades de estos elementos.

Entre los ligandos seleccionados encontramos un ligando dicarboxílico. Los ligandos con grupos carboxilato han demostrado ser capaces de formar estructuras robustas órgano-inorgánicas. El ligando utilizado en este trabajo ha sido seleccionado por sus características geométricas, ya que tiende a adoptar una conformación en forma de V. Ligandos con esta conformación no son muy comunes. Su uso ha sido anteriormente evaluado en nuestro grupo de investigación. En combinación con metales de transición ha dado lugar a estructuras con topologías poco habituales, debido sin duda a las características de la molécula. Su utilización para la construcción de polímeros de coordinación de tierras raras en el presente trabajo ha dado lugar a la formación de tres nuevos tipos estructurales, que resultan ser tres polimorfos de una misma fase. Nuevamente, las características del ligando se ven reflejadas en las topologías de estas nuevas redes.

Por otro lado, el resto de ligandos utilizados presentan como grupo funcional al grupo sulfonato. El grupo sulfonato ha sido tradicionalmente considerado como poco apropiado para la construcción de polímeros de coordinación. Sin embargo, en nuestro grupo empezamos a evaluar sus posibilidades para la construcción de polímeros de coordinación con tierras raras. De esta forma se prepararon tres tipos estructurales, con buena estabilidad térmica e interesantes propiedades. Siguiendo con estos resultados obtenidos, nuevos tres ligandos con grupos sulfonatos han sido utilizados para la elaboración de este trabajo, dado lugar a la obtención de seis nuevos tipos estructurales. La comparación de estos nuevos resultados con los ya obtenidos permitirá extraer interesantes conclusiones sobre la preparación de polímeros de coordinación con tierras raras y ligandos sulfónicos. Además, todos estos nuevos materiales preparados presentan diferentes e interesantes propiedades, las cuales han sido evaluadas.

Los materiales preparados durante la elaboración del presente trabajo están resumidos en la siguiente tabla:



<i>Y³⁺</i>	RPF4α					
<i>La³⁺</i>	RPF4α	RPF4β	RPF4γ	RPF7	RPF8	RPF9
<i>Ce³⁺</i>	RPF4α					
<i>Pr³⁺</i>	RPF4α			RPF7	RPF8	RPF9
<i>Nd³⁺</i>	RPF4α			RPF6	RPF8	RPF9
<i>Sm³⁺</i>	RPF4α			RPF6	RPF8	
<i>Eu³⁺</i>	RPF4α				RPF8	
<i>Gd³⁺</i>	RPF4α			RPF6	RPF8	
<i>Tb³⁺</i>	RPF4α				RPF8	
<i>Dy³⁺</i>	RPF4α		RPF6	LRH	RPF8	
<i>Ho³⁺</i>	RPF4α		RPF6	LRH	RPF8	
<i>Er³⁺</i>	RPF4α		RPF6	LRH	RPF8	
<i>Yb³⁺</i>	RPF4α			RPF5	LRH	RPF9

A continuación, el trabajo elaborado y los resultados obtenidos durante la elaboración de la presente tesis doctoral son expuestos en detalle.

Abbreviations:

RPF: Rare earth Polymeric Framework

LRH: Layered Rare earth hydroxide

MOF: Metal-Organic Framework

H₂hfipbb: 4,4'-(hexafluoroisopropylidene)bis(benzoic acid)

NDS: Naphthalenedisulfonate

AQDS: Anthraquinonedisulfonate

Bipy: 4,4'-bipyridil

SBU: Secondary Building Unit

Et₃N: Triethylamine

Ln: Lanthanide element

R³⁺: trivalent rare earth cation

ORTEP: Oak Ridge Thermal Ellipsoid Plot

Outline

I.	INTRODUCTION AND OBJECTIVES.....	1 – 39
	1. Introduction.....	3
	• Coordination polymers	
	• Rare-earth elements	
	• Topological and reticular concepts	
	• Ligands	
	• Preparation of coordination polymers	
	2. Objective and content.....	21
	• Objectives	
	• Content	
	3. References.....	27
II.	EXPERIMENTAL.....	41 – 58
	1. Experimental	
	details.....	43
	• Hydrothermal synthesis	
	• X-ray diffraction	
	– Single crystal X-ray diffraction	
	– Powder X-ray diffraction	
	• Thermal analysis	
	• Catalytic experiments and gas chromatography	
	2. References.....	57
III.	Results.....	59 – 167
	1. Rare-earth + hfipbb: RPF4.....	61
	• Introduction	
	• Synthesis	
	• Crystal structure description	
	• Characterization	
	– Powder X-ray diffraction	
	– Thermal and elemental analysis	
	• Properties	
	– Photoluminescence	

-
- Catalytic activity experiments
2. Rare-earth + 2,6AQDS: RPF5, RPF6, RPF7, LRH.....83
- Introduction
 - Synthesis
 - RPF5 structural type
 - Crystal structure description
 - Topological analysis
 - X-ray powder diffraction
 - Elemental analysis
 - Thermal analysis
 - RPF6 structural type
 - Crystal structure description
 - Elemental analysis
 - X-ray powder diffraction
 - Thermal analysis
 - RPF7 structural type
 - Crystal structure description
 - Topological analysis
 - X-ray powder diffraction and elemental analysis
 - Thermal analysis
 - LRH structural type
 - Crystal structure description
 - Topological analysis
 - X-ray powder diffraction and elemental analysis
 - Thermal analysis
 - Structural comparison
 - Catalytic activity experiments
3. Rare-earth + 1,5AQDS: RPF8.....123
- Introduction
 - Synthesis
 - Crystal structure description
 - Characterization
 - Conductivity measurements

	• Magnetic measurements	
4.	Rare-earth + calix[4]arene-p-sulfonic acid: RPF9.....	141
	• Introduction	
	• Synthesis	
	• Crystal structure description	
	• X-ray powder diffraction	
	• Thermal behavior	
	• Catalytic activity experiments	
5.	References.....	159
IV.	Discussion and Conclusions.....	169-188
1.	Comparative analysis.....	171
	• Structural considerations	
	• Topological comparison of sulfonate containing frameworks	
	• Comparison of catalytic activity	
2.	General conclusions.....	181
3.	Conclusiones.....	185
V.	Supplementary material.....	189-203
1.	Additional crystal structures.....	191
	• Gd, Ho and Er RPF6 crystals	
	• Fe and Co 1,5-AQDS compounds	
	• Additional Pr-RPF9 crystals	
	• P1 refinement of RPF9 crystals	
2.	Atomic coordinates tables.....	197
VI.	Published articles.	205-239

I. Introduction and objectives

1. Introduction

Coordination polymers

The term “coordination polymer” appeared in the literature in the early 60s, mainly regarding to polymeric compounds in which there are present inorganic entities, coordinatively bonded to organic moieties^{1, 2}. The crystal structures of coordination compounds composed by metal centers and organic ligands, which are infinite in, at least, one dimension of the space, appear also in these years^{3, 4}. This could actually be a definition of what it is now understood with the term “coordination polymer”. Thus, it can be defined as a compound in which metallic centers are joined together through organic ligands with coordination bonds, giving rise to a network that is extended in the space. On the basis of the extended net dimensionality, we can find one, two or three dimensional polymeric frameworks. Other less general terminologies are found in the literature, especially in the last years, referring to compounds of this type, such as hybrid organo-inorganic compounds, organic zeolite analogues, or metal-organic frameworks. This latter term has become very popular in the last decade. A definition of metal-organic framework (MOF) (or what a material should be to be named as MOF) is found in reference 5. According to this definition, a MOF must be a crystalline, robust compound with organic linking units. Metal-organic frameworks are now considered as a new class of solid materials, being subject of study by several researching groups. The interest in this new class of compounds is easily understood taking into account the high versatility that this type of materials offers, with many potential applications coming from their inherent properties. This versatility is due to the wide range of possibilities that we have in the combination of the two main components of the MOFs (and of coordination polymers in general): the metallic centers (connectors), and the organic ligands (linkers). In principle, through the wide

choice of metal, and the infinite choice and design of ligands, a broad range of magnetic, electrical, optical, catalytic and other properties might be rationally incorporated into such materials. Besides, properties inherent to the structural features of the frameworks are of special interest. For example, many studies have been performed on the sorption properties of porous metal-organic framework. Porous coordination polymers appear now as an alternative to other classic porous materials, such as zeolites or other related inorganic compounds (AlPOs, MeAPOs, etc...). Materials with very high specific surface area, selective sorption properties, or high sorption capability can be found in the family of the coordination polymers.

The field of coordination polymers has undergone a high development during the past fifteen years. The discovery of coordination polymers exhibiting permanent porosity in the middle 90s⁶⁻⁸ made these compounds to be subject of investigation of numerous groups. Initially, the greatest efforts were directed toward the preparation of compounds with the highest values of specific surface area, as well as pore diameters. Thus, compounds with specific surface area above 5000 m²/g have been obtained⁹, as well as others¹⁰ with cavities of ~20600 Å³. Parallely, during those years the interest in hydrogen as alternative energetic source substantially increased and together with this, the use of MOFs as materials for hydrogen storage appeared as the most important (and popular) of their potential applications. Their H₂ sorption properties have also been subject of different studies to better understand the interactions and the sorption mechanism processes of the H₂ into the framework¹¹⁻¹³. The target value of 6% w/w of hydrogen sorption of the US department of energy has been achieved by some MOFs¹⁴⁻¹⁷. However, to reach these excellent values, high pressures and low temperatures are needed, exhibiting more modest values at room temperature and moderate pressure, which make them non suitable for current industrial applications in H₂ storage yet. Together with the H₂ storage, studies on the sorption of other molecules with industrial and environmental interest have been made in porous

coordination polymers. Studies on the selective sorption and sequestration of CO₂ molecules have been carried out¹⁸⁻²², as well as on the sorption of methane²³⁻²⁵ or acetylene²⁶. Alternatively, it has also been demonstrated that MOFs can exhibit selective adsorption for some molecules²⁷⁻³².

Research focused on the porosity and adsorption properties of coordination polymers continues being very active, since the behavior of these materials during the sorption processes has revealed to be very rich and interesting. Some coordination polymers have a high degree of flexibility, being able to modify their structures to accommodate the guest molecules. For example, rotation around a single bond provides structure flexibility and the structures response to the sorption / desorption of molecules varying their cell volume, in a sponge like manner³³⁻³⁶, without loss of crystallinity. Compounds suffering this so-called breathing process³⁷⁻³⁹ are able to expand their structure depending on the adsorbed molecules, with reported changes in the cell volume up to 270% compared with the “dry” material⁴⁰. Other applications related to the porosity of the coordination polymers are in the gas separation area. They can be employed to separate different molecules on basis on the specific interaction with the framework^{38, 41}. More recently, the application of MOFs for drug delivery is also being subject of study⁴²⁻⁴⁵, offering the materials a controlled release of the target molecules.

In the search of materials with extra-large cavities and areas, the synthesis procedures have been rationalized, with the aim of obtaining frameworks with the desired structural features, in what is known as *crystal engineering* process. Within this area, there is a great fascination of the researchers to obtain coordination polymers with zeolitic (probably influenced by the industrial interest of this materials), or zeolite related topologies. There are compounds described as built up from zeolitic cages⁴⁶⁻⁴⁸. In others, specific ligands with bond angles similar to that of the O–Si–O in the inorganic zeolites have been selected, in combination with metals with preference to tetrahedral coordination^{21, 49-58}. With them, MOFs with topologies already

known in zeolites have been prepared, as well as other predicted but still unprecedented in inorganic materials, with the advantage of exhibiting larger cavities, and the possibility of chemically functionalize the framework yet in the synthesis procedure, with the variations of the organic ligands.

Properties related to the porosity in coordination polymer are probably the most extensively investigated. However, the intrinsic nature of these materials confer them a multifunctionality⁵⁹ that not many kinds of materials have. Looking further than at the empty space in the coordination polymers, one can find a lot of possible applications defined by the components of the frameworks and their combinations. One of them, and also with a remarkably industrial interest, is the use of coordination polymer in catalysis^{29, 60-71}. Usually, the combination of catalytically active elements and porous structures results in a material with a high potential as heterogeneous catalyst. This idea has been extensively explored in zeolites and in open-structure AlPOs and related, with the substitution of part of the components of the framework by catalytically active metal atoms. In the case of coordination polymers, despite of being one of the early studied applications⁷², it still remains less explored than those related to gas storage. On the other hand, the fact that the active metal is a fundamental part of the framework opens the possibilities to use compounds without porosity in catalytic reactions. Within the area of catalysis, the formation of compounds with chirality is receiving great attention⁷³ since they could be able to offer enantioselectivity.

Coordination polymers have been evaluated to be used in several other applications. Compounds with no-centrosymmetric frameworks appear as candidates to be used as nonlinear optical materials⁷⁴⁻⁷⁸. There is also considerable interest in the optical properties of hybrid frameworks. The incorporation of optically active elements in the framework results in materials of interest for applications as phosphors or fluorescent probes⁷⁹⁻⁸³. An adequate organic ligand can act as antenna, transferring the energy to the optically active centers. The optical properties in porous coordination

polymers may be affected by the presence of guest molecules, with potential applications of these materials as sensors. The magnetic properties of coordination polymers have also been studied in compounds incorporating elements that can present ferromagnetic interactions⁸⁴⁻⁸⁸.

Rare-earth elements

Coming back to the definition of coordination polymer, we can describe with more detail the two main components of this type of solids. The first of them is the metallic center. As mentioned above, there is a wide range of possibilities in the choice of the metal (or metals) employed. By far, transition metals are the most employed in the synthesis of coordination polymers. The fact that their coordination spheres are more controllable makes them, in principle, more suitable for their use in the preparation of compounds with specific structural features. There are many examples of MOFs with, for example, Zn, Ni, or Co. The metallic center could be not only a single atom, but also, and very commonly, an aggregate (cluster) of metal atoms. By analogy with zeolites, these aggregates are called secondary building units (SBUs). The geometry of the SBUs can in principle be controlled by an adequate control of the synthesis conditions, and it is highly influenced by the kind of ligand employed, and more precisely, by the kind of functional group through which the ligand is joined to the metals. More details about the SBUs are given below.

Less studied are, however, compounds built with rare earth elements. Precisely, a main difference in the coordination chemistry of the rare earth elements is their variable coordination number, which generally goes from 6 to 12. This fact has made the rare earth elements to be regarded as less suitable for the construction of MOFs. However, these elements exhibit very interesting properties, including, for example, optical or catalytic properties. All the presented materials in this report are constructed using exclusively

rare earth elements as metal centers, and because of this, it is worth describing with more details these elements.

The International Union for Pure and Applied Chemistry recommended in 1968 that the elements 58 through 71 be referred to as “lanthanides” and that the name rare earth be reserved for the elements scandium, yttrium, lanthanum and the lanthanides. In 1794 Johann Gadolin successfully obtained an oxide, in those times called “earth”, from the gadolinite mineral, which was discovered in 1787 by C. A. Arrhenius near Ytterbi, Sweden. He called it the earth yttria, and with it, it began the chemistry of the rare earth elements. Soon later, another “earth”, ceria, was isolated from the mineral cerite. More than 40 years later, these two earths were found to be a mixture of different oxides, yttrium, erbium and terbium in the case of yttria, and oxides of lanthanum, cerium, and didymia, a mixed oxide of the metals from Pr through Gd, in the case of ceria. In 1869 Mendeleev published his first periodic chart, leaving a blank where scandium is now placed. In 1879, scandium was discovered. In this initial chart, there was also a place for lanthanum, but no place seems to be for the other rare earths. Actually they even were believed to be modifications of lanthanum. There were also mistakes in the assignment of the elements (for example terbium and erbium), and wrong reports of “new” elements. Only after the work of Moseley relating X-ray spectra to atomic number in 1912, it could be known how many rare earth elements should exist. Now it is known that at element 57 there is a change in the way that the electrons are added to the atoms as the atomic number increases. At this point, the electrons start entering into an inner 4f shell, leaving the number of valency electrons undisturbed. This f shell can accommodate up to 14 electrons, giving rise to the 14 lanthanides with atomic number 58 to 71. The 4f orbitals penetrate the xenon core appreciably. Because of this, they cannot overlap with ligand orbitals and therefore do not participate significantly in bonding. The 5s and 5p orbitals penetrate the 4f subshell and are not shielded from increasing nuclear charge, and hence because of the

increasing effective nuclear charge the atomic radii contract as the atomic number increases. This effect is called the lanthanide contraction.

The presence of the f electrons makes the lanthanides to be different in their chemistry, which differentiate them from the d-block elements. Some of their differences are: a wide range of coordination numbers; coordination geometries determined by ligand steric factors rather than crystal field effects; spectroscopic and magnetic properties largely uninfluenced by the ligand, since the 4f orbitals do not participate in bonding; preference for anionic ligands with donor atoms of high electronegativity; not formation of multiple bonds as it is known for transition metals. Besides, the physical properties of the lanthanide elements make them as suitable elements to be used in different applications. Many lanthanide ions exhibit luminescence, emitting radiation from an excited electronic state, the emitted light having sharp lines characteristic of f-f transitions of an Ln^{3+} ion. Thanks to this, complex of lanthanides are used in applications such as sensory probes, in television tubes, lighting applications, lasers, and also as security markers in banknotes. Complex of gadolinium are also used to assist diagnosis with magnetic resonance imaging^{89, 90}. With the incorporation of rare earth elements within the framework of coordination polymers, these are expected to be provided with the interesting properties inherent to the rare earth elements. In particular, those related to luminescence are receiving great attention. However, the number of compounds with rare earth elements is still much lower than that with transition elements. Some details on the structural chemistry of MOFs will help us to understand in some way the preference for transition metals.

Topological and reticular concepts

As for any periodic structure, we can describe the networks of the coordination polymers on the basis of their connectivity, performing what is known as a topological analysis⁹¹. In any periodic structure the basic components are nodes and links. The way in which the nodes are connected among them will produce a net with specific structural features. The work by A. F. Wells⁹²⁻⁹⁴ was a fundamental contribution in the classification of crystal structures on basis of their connectivity. He analyzed a great number of nets in terms of their basic topology, and also introduced a method for the generation of 3D nets from 2D nets, predicting networks that were later discovered. The topological analysis of networks has also been important in the field of zeolites and related materials. J. V. Smith^{95, 96} focused on the classification of zeolites, describing them as networks consisting of tetrahedral nodes of the TO₄ type; several databases have appeared later predicting the possible networks resulting from the combinations of 4 connected nodes^{97, 98}. A first problem that has appeared in the topological classification of nets is the fact that a same net has been described with several names and symbols. This problem has increased in the last years, since more and more frameworks appear every day in the literature. An appropriate way of unequivocal classification consists on the assignment of two symbols, vertex symbol and coordination sequence, for each node in a net. The vertex symbol was introduced by O’Keeffe⁹⁹ as an alternative to the point symbol (also known as Schläfli symbol). With the point symbol, a n-connected node is identified as A^a.B^b.C^c..., where A < B < C... and a + b + c ... = n(n-1)/2, and represent the sizes (A, B, C...) and numbers (a, b, c...) of the “shortest circuits” contained at each angle. The point symbol is extensively used, but it is not sufficient to identify a net. Because of this, it was introduced the vertex symbol. In it, the size of the shortest rings at each angle is given with a subscript to denote the number of such rings. The coordination sequence CS(k) of a node is defined

as a sequence of numbers in which the k^{th} term is the number of nodes in “shell” k that are connected to nodes in “shell” $k-1$. It should be noticed that while that the point symbol is defined with circuits, the vertex symbol employs rings for its representation (figure I.1.01). A ring is a circuit that has the property that there is no shorter path between any two vertices on the circuit than the shortest one that is part of the circuit. Besides, O’Keeffe and co-workers have suggested using a lower-case three letter code nomenclature¹⁰⁰, in a similar way to the upper-case three letter classification employed for the zeolitic networks¹⁰¹.

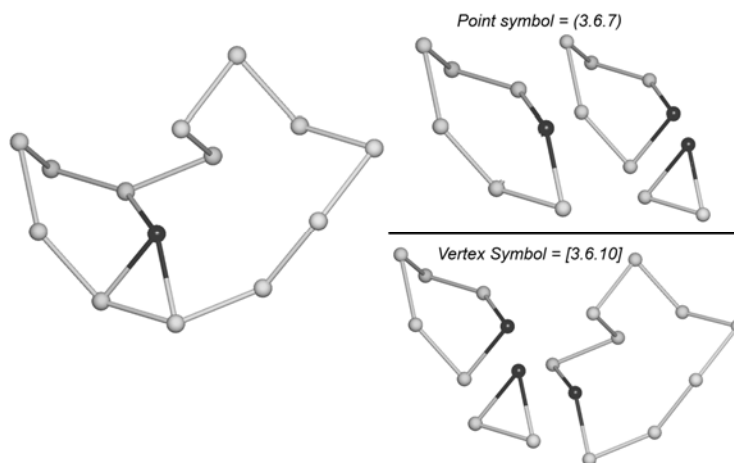


Figure I.1.01: The three connected vertex represented in black has a point symbol = (3.6.7), and a VS = [3.6.10]. The seven member circuit considered in the point symbol is the sum of the 3-member and the 6-member circuits, and therefore is not a ring.

Regarding to polymeric framework, it must be pointed out the work by Robson, who probably was the first who obtained a compound with a predefined topology¹⁰². He could obtain diamond related networks by combining elements with preference to tetrahedral environment (Zn and Cu), linked by linear ligands. Yet in this early work, Robson suggested that using tetrahedral centers, the frameworks are expected to adopt structure based on either the diamond or the lonsdaleite (dia and lon according to O’Keeffe’s classification) networks, and those constructed from octahedral centers should yield a framework related to the α -polonium (pcu) net. This first example

clearly shows the importance of the geometry of the metal center on the final topology of the network. Besides, the use of linear rigid linkers seems to be a simple and efficient way for connecting the nodes. In a higher degree of complexity in the construction of coordination polymers, aggregates of metal atoms are used instead of unique metallic atoms as nodes of the nets. These aggregates are known as secondary building units (SBUs), in a parallel way to the zeolites construction. The aggregates can also be geometrically simplified to related polyhedra. An example of this is the compound known as MOF-5¹⁰³. Constructed with Zn and benzenedicarboxylate, it exhibits a cubic network in which the nodes are formed by 4 ZnO₄ tetrahedra, sharing a central vertex, in such a way that a SBU with octahedral geometry can be described. The SBUs are joined by the linear organic linkers, and as it was predicted by Robson, the joining of the octahedral centers gives rise to a pcu network. The existence of this type of octahedral aggregate was already known, as it was found in metal carboxylates (acetate, benzoate and pivalate), and it was used later for the synthesis of isorecticular MOFs¹⁰⁴, compounds with the same net, in which the difference was in the length of the organic linker, in such a way that frameworks with different pore volumes were prepared. The number of possible secondary building units and their geometries are varied and the control of the synthesis conditions will allow obtaining them. In the most of the cases, these SBUs are formed by aggregates of metal atoms with geometrically well defined coordination environment (i.e. aggregate of tetrahedra) (figure I.1.02). The coordination environment of the rare earth elements is more varied, and therefore, its control is harder than in the case of the transition elements. Despite of this, there are examples of coordination polymers constructed with lanthanides¹⁰⁵⁻¹⁰⁹. Besides, the ability of these elements to form clusters with different geometries is already known.

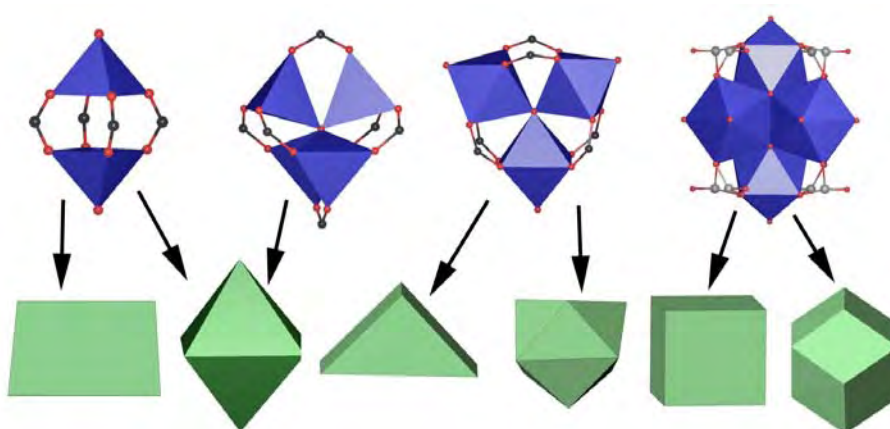


Figure I.1 02: Representation of different metallic aggregates, and the SBUs that they can form.

In the next step of this reticular depiction of coordination polymers, we can describe with more details the other components of the framework, the organic ligands. In the simplest way, as the examples presented above, linear molecules with two functional groups are the linkers of the networks. In these cases, the structural role of the organic part of the compounds is just to link the metals or the inorganic SBUs. The only variation that can be made in this case, is the length of the ligand, in such a way that a same net can be constructed employing ligands that only differs in the distance between their functional groups. Nevertheless, this variation can be important, producing phenomena such as interpenetration. If organic molecules with geometries different to a simple rod are employed, a new degree of complexity is introduced into the system. If the molecule used is connected to more than 2 nodes (having more than two functional groups) it is not a linker anymore, and then this organic secondary building unit is also a node in the topological simplification of the framework. As a result of this, the possibilities of obtaining new networks, with less common topologies, are multiplied. There exist numerous examples of this, with organic molecules with, for example, triangular or tetragonal geometries, resulting in the simplest cases in binodal networks.

Ligands

Another important point regarding to the ligands, is the type of functional group through which they are connected to the metals. Being chemically coordination compounds, the coordination polymers follow the rules of the coordination chemistry. Thus, in the organic ligand there have to be found atoms with high electronegativity so that they could coordinate to the metallic centers. Cyano- and amino- derivatives have been extensively employed, with the N atom coordinated to the metals. Even more extensively are found the carboxylate derivatives, with oxygen atoms coordinated to the metals. The differences among them are manifest, since the carboxylates own two oxygen atoms to bond the metals, with more possible coordination modes. The variation of the coordination modes offers a wide range of possibilities in which the metallic nodes of the network can be connected. The dicarboxylate anions may appear, for example, coordinated in chelating manners, or as bridges between two metal atoms. Besides, the torsion angle of the C-CO₂ bond allows different geometries in their coordination. The phosphonate group has also been employed in the construction of extended networks, especially those based on the connection of tetrahedral entities, as in AlPOs or MePOs (metal phosphonates), but it is not so common in the case of coordination polymers. Its use in the formation of layered structures with pendant organic parts is more extensive, due to the regularity of the PO₃²⁻ group coordination mode within this kind of structures. There are also examples of coordination polymers with ligands having different mixed functional groups, and it is also usual to find examples in which more than one type of ligand is employed, for example using pyridine derivatives in combination with dicarboxylate ligands.

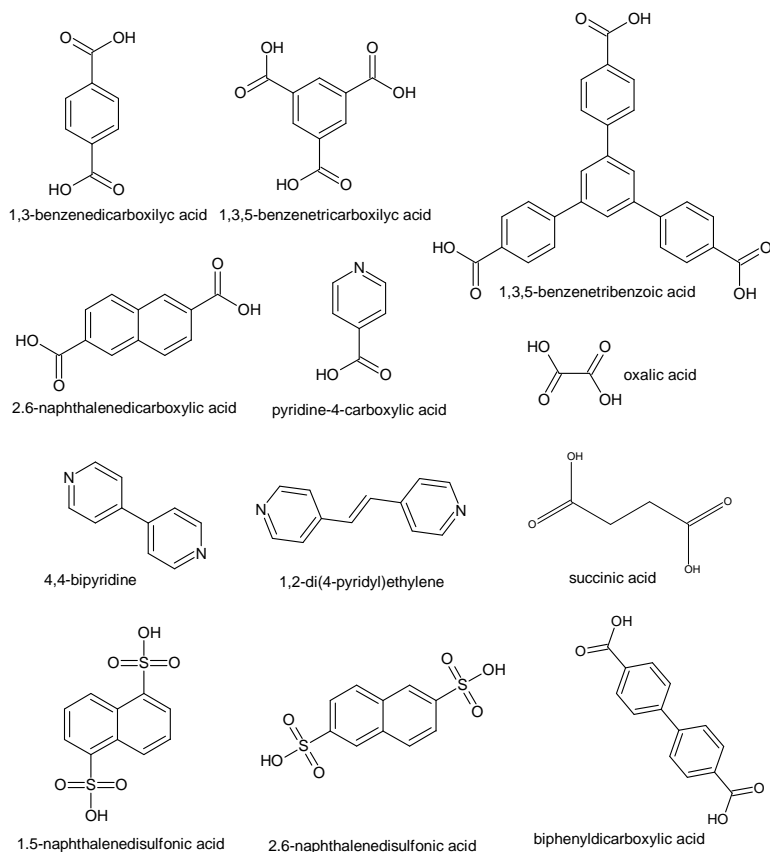


Figure I.1.03: Some of the most commonly used organic ligands

Another potential candidate, which has been evaluated in a part of this work, is the sulfonate group. In comparison with the dicarboxylate anions, there are relatively few examples of MOFs with sulfonate derivatives as ligands. The coordination chemistry of the sulfonate group has been less investigated, due to the perception that the sulfonate is a poor ligand, and therefore, its use in the chemistry of coordination polymer remains less explored than those of other ligands. Organosulfonate molecules have been employed to form supramolecular structures, built up with hydrogen bonds. For instance, hydrogen bonded guanidinium sulfonates have been systematically studied by M. D. Ward¹¹⁰⁻¹¹⁴.

The coordination chemistry of metal-arenesulfonates have been studied, among others, by Côte and Shimizu¹¹⁵ and Cai¹¹⁶, and there is also a recent review on metal- disulfonate compounds with alkali, alkali-earth and transition metals¹¹⁵.

In many of the examples of compounds with direct coordination of the sulfonate group to the metal, there is an additional functional group in the ligand, or even an auxiliary ligand is employed to form a polymeric structure. The presence of nitrogen ligands is favorable to ease the coordination of the SO₃ group in its competition with the solvent molecules to be part of the coordination sphere of the metals. Thus, in the case of arenedisulfonate ligands, there are studies with naphthalenedisulfonate (NDS) employed in combination with amine derivatives ligands, to form extended networks with copper^{117, 118} or cadmium¹¹⁹⁻¹²¹ as well as an example with mercury¹²², and another with zinc¹²³.

Among the transition metals, silver derivatives are the most studied and abundant sulfonate compounds. Thus, there are compounds with NDS¹²⁴, as well as with other different ligands, both exclusively sulfonate¹²⁵⁻¹²⁷, and mixed¹²⁸⁻¹³⁰. Apart from silver, the most abundant sulfonate derivatives coordination polymers are formed with alkali and alkali-earth cations. There are examples of compounds with exclusively these metals, including 1,5-NDS^{131, 132}, 2,7-NDS¹³³, hydroxybenzenedisulfonate^{134, 135} biphenyldisulfonate¹³⁶, and others¹³⁷⁻¹³⁹. In other structures, group 1A and 2A elements are present together with lanthanides cations¹⁴⁰⁻¹⁴². With exclusively rare earth elements coordinated to sulfonate groups there are few examples of polymeric compounds. With naphthalenedisulfonate ligand, we prepared three families of compounds in our group^{143, 144}. Besides, there is a report with 1,5-NDS and 2,7-NDS in combination with o-phenantroline¹⁴⁵, and another with exclusively 1,5-NDS¹⁴⁶. Benzenedisulfonate (BDS) has also been employed, both the 1,2-BDS isomer¹⁴⁷, and the 1,4-BDS, this latter together with sulfobenzoic acid¹⁴⁸. There are also a couple of structures with

sulphoisophthalic acid, one of them with only this ligand¹⁴⁹, and the other in combination with *o*-phenantroline¹⁵⁰. Finally, calixarene sulfonate derivatives have also been used to form polymeric rare-earth structures¹⁵¹⁻¹⁵⁴.

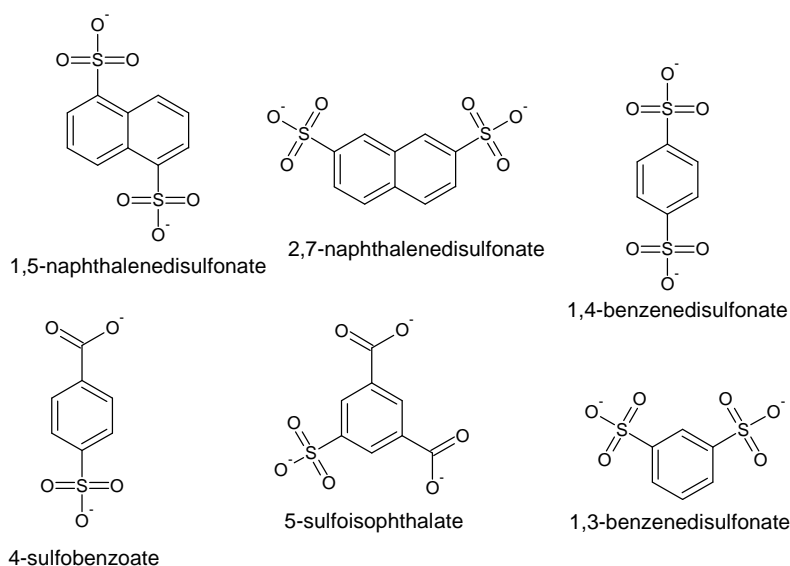


Figure I.1.04: Some sulfonate ligands found in the literature.

Another reason with traditionally negative influence in the selection of the sulfonate ligands is the variability in their coordination modes, being the SO_3^- coordination modes very flexible and sensitive to the chemical environment. However, precisely this feature of the sulfonate group can make it a very interesting type of ligand for the building of compounds with unexpected structures and topologies. This versatility of the sulfonate ligands makes also possible to obtain different compounds with different properties, employing the same components. As mentioned above, the control of the synthetic conditions will be a key step in the control of the coordination modes, and to reach a good control of this, synthetic studies, including those with combinatorial approaches, are essential for a better understanding of the formation of these compounds.

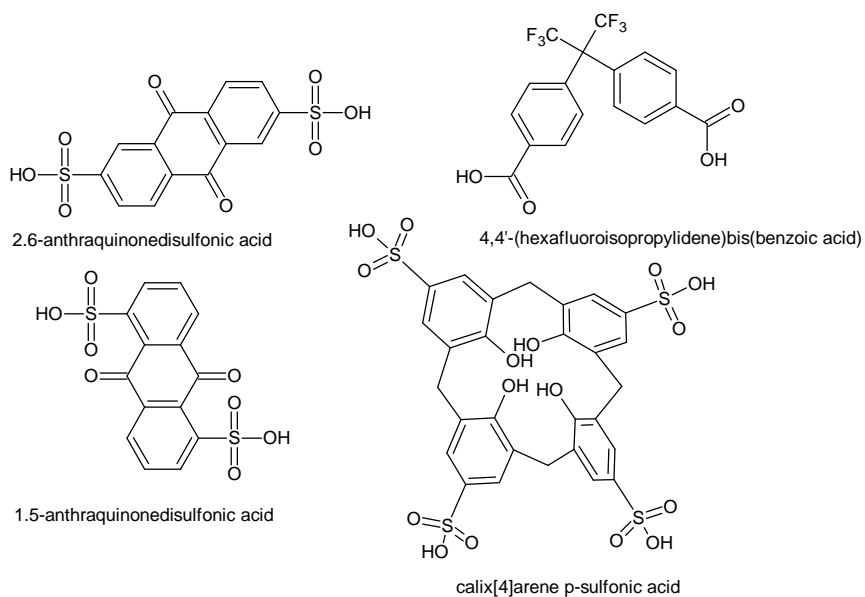


Figure I.1.05 The ligands employed in this work.

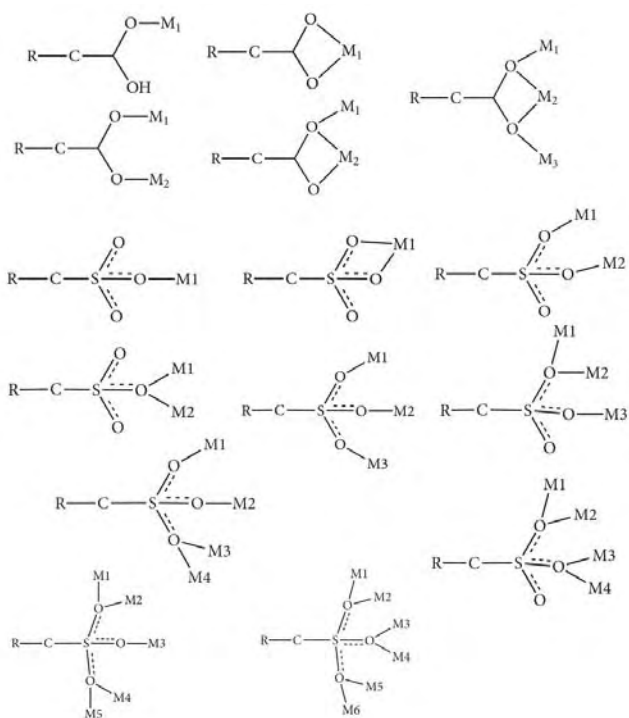


Figure I.1.06: Representation of the possible coordination modes of the carboxylate and sulfonate groups.

Preparation of coordination polymers

The first examples of coordination polymers were obtained under traditional coordination chemistry synthetic methods¹⁰², with crystallization at room or mild temperatures, and open systems. These methods were used with the aim of obtaining good quality single crystals of the products. They include slow evaporation of a solution of the precursors¹⁵⁵⁻¹⁵⁷, layering of solution¹⁵⁸⁻¹⁶⁰, or slow diffusion of one component solution into another through a membrane or an immobilizing gel^{161, 162}.

Nowadays, the hydrothermal synthesis has become the most extended technique for the preparation of MOFs. In a hydrothermal, or more generally solvothermal, synthesis, the reaction takes place at more elevated temperature and pressure. Basically, a mixture containing the adequate amounts of reagents and solvent is heated into a sealed autoclave in which an autogenous pressure is produced. The use of solvothermal techniques allows the obtaining of kinetically controlled phases over the most stable dense phases, and so the hydrothermal synthesis has been widely employed for the preparation of porous inorganic materials, such as zeolites or AlPOs. In the most of the cases, the presence of a structure directing agent (SDA) which commonly is an organic molecule is required to obtain the desired zeolitic structure, in combination with the correct choice of the synthesis conditions: temperature, time of heating, time of aging, reagents ratio, solvents, stirring, etc. Similarly to the preparation of inorganic porous materials, the hydrothermal methods have successfully been employed in the preparation of coordination polymers. Some differences have to be considered; for instance, the presence of organic molecules as structure directing agents is by far less common in the preparation of coordination polymers. The SDAs are usually amine derivatives, and they could react with the metal atoms if they are used in the synthesis of, especially transition metal, coordination polymers. Besides, the number of solvents employed is larger, and in many cases, precisely the

molecules of solvent may act in some way as directing agents. This can be made with a controlled decomposition of the employed solvent, for example dimethylformamide. Other related methods are used for the synthesis of coordination polymers. Thus, microwaves are now used to heat the synthesis mixtures¹⁶³⁻¹⁶⁸ and they are believed to accelerate the synthesis procedure¹⁶⁹. In the ionothermal synthesis¹⁷⁰⁻¹⁷³ ionic liquids (ionic salts with low melting points) are used instead of conventional solvents. Thanks to all this techniques, many different materials have been successfully prepared.

2. Objectives and content

Objectives

The objective of the present work is the preparation of new coordination polymers with multifunctional properties. Within this general objective, the following steps are included:

- Search for new structural types with rare earth elements as metal centers.

With the construction of rare earth coordination polymers, the properties of these elements are expected to be displayed by the new frameworks. Among them, optical and catalytic properties are included.

- Selection of suitable organic ligand to provide the new frameworks with additional features and properties:

A dicarboxylate ligand with a bent geometry has been selected, with the aim of obtaining frameworks with open structures and new topologies.

A disulfonate ligand with the aim of obtaining diverse coordination environments of the rare earth elements, which will be appropriated for selected applications.

An anthraquinone derivative suitable to be reduced, to include an extra functionality from its redox properties.

A calixarene derivative to obtain capsule-containing frameworks.

- Structural characterization of the new compounds.

X-ray diffraction methods are used to solve the crystal structures of each new prepared compound. Usually, conventional X-ray sources are used

for single crystal and powder diffraction. Synchrotron data will also be employed when required. Once the crystal structures are solved, and the atomic positions are known, the structural features of the new compounds can be analyzed. The local chemical environment of the metal centers, including the diverse coordination modes of the ligands is studied.

- A topological analysis of the frameworks.

This gives information about the connectivity of the nodes in a network, and it is an appropriate way to rationalize the study for the preparation of new MOFs.

- Optimization of the synthesis conditions.

A synthetic study is carried out to obtain the new compounds as pure phases. This study includes the variation of several synthesis conditions and the analysis of the obtained compounds in each case. The compounds have to be obtained purely, and in a good yield. To evaluate the purity of the products, powder X-ray diffraction is used. When each crystalline phase is purely obtained, elemental chemical analysis, and thermal analysis are performed.

- Evaluation of the new compounds potential applications.

The possibilities that the new compounds offers are evaluated. The application of each compound is selected based upon the structural features that they exhibit. With the results obtained in this evaluation, some conclusions on the structure-properties relationship are extracted. Through the statement of the properties related with the network of each material, a new one is designed in order to improve their properties.

To achieve the goals above described, the work for this thesis has been carried out according to a general sketch as the shown in figure I.2.01.

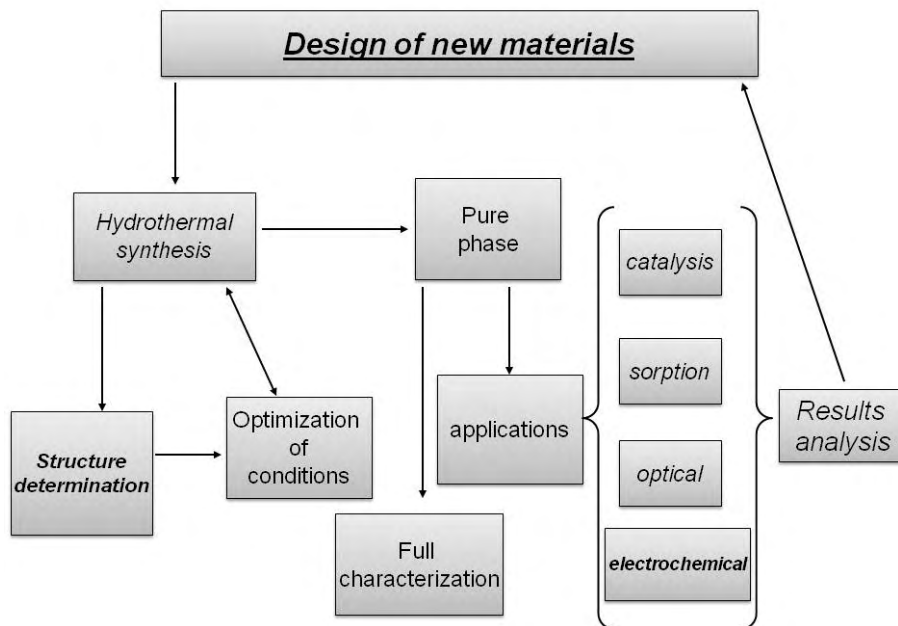


Figure I.2.01: Diagram showing the steps for the design of new materials, as those obtained in the present work.

Content

Four different ligands have been employed in combination with the rare earth metals. Up to forty compounds, belonging to nine different structural families have been obtained (table I.2.01). The first structural type, named RPF4 (RPF = Rare earth Polymeric Framework), has been obtained with 4,4'-(hexafluoroisopropylidene)bis(benzoic acid) ($H_2hfipbb$), the only carboxylate derivative ligand employed in this work. This is an aromatic ligand, consisting of two benzoic acids joined by a central atom, which is in sp^3 hybridization. This central atom is substituted with two CF_3 groups. The presence of the central sp^3 atom makes this molecule to have a bent geometry, having influence on the topology of the networks in which it is present. Bent ligands have been scarcely employed compared with linear ligands. In the case of $hfipbb$, it has been previously used in our group, in combination with zinc¹⁷⁴ and indium¹⁷⁵. The obtained frameworks exhibit unique unprecedented

topologies despite of being uninodal four-connected nets. The RPF4 family of compounds presents up to three different polymorphic phases that we have named α , β and γ phases. A structural and topological comparison of them has been made. The α polymorph has been obtained with the following metals of the rare-earth series: Y, La, Ce, Pr, Nd, Sm, Eu, Gd, Tb, Dy, Ho, Er, Yb. An evaluation of the catalytic and emitting properties has been made for RPF4- α family of compounds.

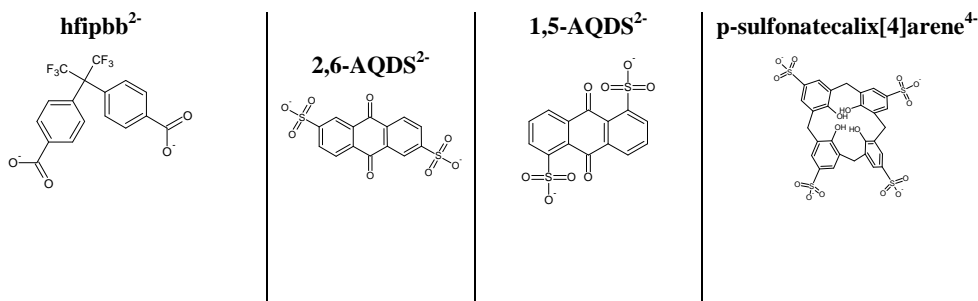
The rest of the new compounds have been prepared with sulfonate derivatives; in particular three different ligands have been employed. Two of them are two isomers of the anthraquinone disulfonate anion (AQDS), the 2,6 and the 1,5 isomers (2,6-AQDS and 1,5-AQDS). These ligands have been selected following previous work initiated in our laboratory with aromatic disulfonate ligands. In particular, naphthalene-2,6-disulfonate and naphthalene-1,5-disulfonate were previously employed to obtain three families of coordination polymers^{143, 144}. The differences between naphthalenedisulfonate, and anthraquinonedisulfonate are the length of the organic chains, with an additional ring in the case of anthraquinone, and the presence of the quinonic oxygen atom in the anthraquinone molecules. With the 2,6 isomer four families of compounds have been prepared. Three of them are polymeric frameworks, RPF5, RPF6 and RPF7; depending on the rare earth metal employed it is obtained one or another type. An evaluation of catalytic properties has been performed. Another family of compounds has been obtained with 2,6-AQDS, which we have named layered rare-earth hydroxides, LRHs. This family of compounds has been prepared with Dy, Ho, Er and Yb. Opposite to the RPFs compounds, in these compounds the metal atoms are not directly coordinated to sulfonate ligands. Evaluation of the catalytic properties of LRHs is presented.

On the other hand, with the 1,5-AQDS molecule, a family of polymeric compounds has been obtained, named RPF8. In this family, obtained with metals La, Pr, Nd, Sm, Eu, Gd, Tb, Dy, Ho, Er, the role of the organic part

will not be only that of a linker among metallic centers. In this case, the organic molecule is presented as an anionic radical, having therefore more influence on the properties of the materials. The magnetic properties of these compounds have been studied.

The last ligand employed in this thesis, is calix[4]arene p-sulfonic acid. This is a sulfonate derivative of the calix[4]arene molecule. Calixarenes are molecules widely employed in coordination chemistry. However, in the case of coordination polymers they have been scarcely employed. Compounds with La, Pr, Nd and Yb have been prepared, and are described in this thesis, next to an evaluation of their catalytic properties.

Table I.2.01: The combination of four different ligands and rare earth elements has resulted in the preparation of nine structural types, summarized in this table.



Y^{3+}	RPF4 α						
La ³⁺	RPF4 α	RPF4 β	RPF4 γ	RPF7	RPF8		RPF9
Ce ³⁺	RPF4 α						
Pr ³⁺	RPF4 α			RPF7	RPF8		RPF9
Nd ³⁺	RPF4 α			RPF6	RPF8		RPF9
Sm ³⁺	RPF4 α			RPF6	RPF8		
Eu ³⁺	RPF4 α				RPF8		
Gd ³⁺	RPF4 α			RPF6	RPF8		
Tb ³⁺	RPF4 α				RPF8		
Dy ³⁺	RPF4 α			RPF6	LRH	RPF8	
Ho ³⁺	RPF4 α			RPF6	LRH	RPF8	
Er ³⁺	RPF4 α			RPF6	LRH	RPF8	
Yb ³⁺	RPF4 α			RPF5	LRH		RPF9

3. References

1. K. V. Martin, *Journal of the American Chemical Society*, 1958, **80**, 233-236.
2. E. W. Berg and A. Alam, *Analytica Chimica Acta*, 1962, **27**, 459-464.
3. M. D. Glick and L. F. Dahl, *Inorganic Chemistry*, 1966, **5**, 289-293.
4. J. L. Atwood and G. D. Stucky, *Journal of Organometallic Chemistry*, 1968, **13**, 53-60.
5. J. L. C. Rowsell and O. M. Yaghi, *Microporous and Mesoporous Materials*, 2004, **73**, 3-14.
6. D. Venkataraman, G. B. Gardner, S. Lee and J. S. Moore, *Journal of the American Chemical Society*, 1995, **117**, 11600-11601.
7. O. M. Yaghi, G. Li and H. Li, *Nature*, 1995, **378**, 703-706.
8. M. Kondo, T. Yoshitomi, K. Seki, H. Matsuzaka and S. Kitagawa, *Angewandte Chemie International Edition in English*, 1997, **36**, 1725-1727.
9. H. K. Chae, D. Y. Siberio-Pérez, J. Kim, Y. Go, M. Eddaoudi, A. J. Matzger, M. O'Keeffe and O. M. Yaghi, *Nature*, 2004, **427**, 523-527.
10. G. Férey, C. Mellot-Draznieks, C. Serre, F. Millange, J. Dutour, S. Surble and I. Margiolaki, *Science*, 2005, **309**, 2040-2042.
11. S. S. Han and W. A. Goddard Iii, *Journal of Physical Chemistry C*, 2008, **112**, 13431-13436.
12. B. Schmitz, U. Müller, N. Trukhan, M. Schubert, G. Férey and M. Hirscher, *ChemPhysChem*, 2008, **9**, 2181-2184.
13. F. Salles, H. Jobic, G. Maurin, M. M. Koza, P. L. Llewellyn, T. Devic, C. Serre and G. Férey, *Physical Review Letters*, 2008, **100**.
14. A. G. Wong-Foy, A. J. Matzger and O. M. Yaghi, *Journal of the American Chemical Society*, 2006, **128**, 3494-3495.
15. S. S. Kaye, A. Dailly, O. M. Yaghi and J. R. Long, *Journal of the American Chemical Society*, 2007, **129**, 14176-14177.

16. Xiang Lin, J. Jia, X. Zhao, K. M. Thomas, A. J. Blake, G. S. Walker, N. R. Champness, P. Hubberstey and M. Schröder, *Angewandte Chemie - International Edition*, 2006, **45**, 7358-7364.
17. Y. Yan, X. Lin, S. Yang, A. J. Blake, A. Dailly, N. R. Champness, P. Hubberstey and M. Schroder, *Chemical Communications*, 2009, 1025-1027.
18. J. P. Zhang, S. Horike and S. Kitagawa, *Angewandte Chemie - International Edition*, 2007, **46**, 889-892.
19. S. Takamizawa, E. I. Nakata, H. Yokoyama, K. Mochizuki and W. Mori, *Angewandte Chemie - International Edition*, 2003, **42**, 4331-4334.
20. R. Banerjee, A. Phan, B. Wang, C. Knobler, H. Furukawa, M. O'Keeffe and O. M. Yaghi, *Science*, 2008, **319**, 939-943.
21. B. Wang, A. P. Côté, H. Furukawa, M. O'Keeffe and O. M. Yaghi, *Nature*, 2008, **453**, 207-211.
22. R. Babarao and J. Jiang, *Langmuir*, 2008, **24**, 6270-6278.
23. I. Senkovska and S. Kaskel, *Microporous and Mesoporous Materials*, 2008, **112**, 108-115.
24. X. Lin, A. J. Blake, C. Wilson, X. Z. Sun, N. R. Champness, M. W. George, P. Hubberstey, R. Mokaya and M. Schro?der, *Journal of the American Chemical Society*, 2006, **128**, 10745-10753.
25. S. I. Noro, S. Kitagawa, M. Kondo and K. Seki, *Angewandte Chemie - International Edition*, 2000, **39**, 2082-2084.
26. D. Tanaka, M. Higuchi, S. Horike, R. Matsuda, Y. Kinoshita, N. Yanai and S. Kitagawa, *Chemistry - An Asian Journal*, 2008, **3**, 1343-1349.
27. Y. E. Cheon and M. P. Suh, *Chemistry - A European Journal*, 2008, **14**, 3961-3967.
28. S. Horike, D. Tanaka, K. Nakagawa and S. Kitagawa, *Chemical Communications*, 2007, 3395-3397.

-
29. S. Hasegawa, S. Horike, R. Matsuda, S. Furukawa, K. Mochizuki, Y. Kinoshita and S. Kitagawa, *Journal of the American Chemical Society*, 2007, **129**, 2607-2614.
 30. K. Yamada, H. Tanaka, S. Yagishita, K. Adachi, T. Uemura, S. Kitagawa and S. Kawata, *Inorganic Chemistry*, 2006, **45**, 4322-4324.
 31. K. Uemura, R. Matsuda and S. Kitagawa, *Journal of Solid State Chemistry*, 2005, **178**, 2420-2429.
 32. T. K. Maji, K. Uemura, H. C. Chang, R. Matsuda and S. Kitagawa, *Angewandte Chemie - International Edition*, 2004, **43**, 3269-3272.
 33. J. Y. Lu and A. M. Babb, *Chemical Communications*, 2002, 1340-1341.
 34. K. Biradha and M. Fujita, *Angewandte Chemie - International Edition*, 2002, **41**, 3392-3395.
 35. H. J. Park and M. P. Suh, *Chemistry - A European Journal*, 2008, **14**, 8812-8821.
 36. M. P. Suh, J. W. Ko and H. J. Choi, *Journal of the American Chemical Society*, 2002, **124**, 10976-10977.
 37. K. Barthelet, J. Marrot, D. Riou and G. Férey, *Angewandte Chemie - International Edition*, 2002, **41**, 281-284.
 38. K. T. Thuy, P. Trens, N. Tanchoux, S. Bourrelly, P. L. Llewellyn, S. Loera-Serna, C. Serre, T. Loiseau, F. Fajula and G. Férey, *Journal of the American Chemical Society*, 2008, **130**, 16926-16932.
 39. F. Salles, A. Ghoufi, G. Maurin, R. G. Bell, C. Mellot-Draznieks and G. Férey, *Angewandte Chemie - International Edition*, 2008, **47**, 8487-8491.
 40. C. Serre, C. Mellot-Draznieks, S. Surble, N. Audebrand, Y. Filinchuk and G. Férey, *Science*, 2007, **315**, 1828-1831.
 41. Y. S. Bae, K. L. Mulfort, H. Frost, P. Ryan, S. Punnathanam, L. J. Broadbelt, J. T. Hupp and R. Q. Snurr, *Langmuir*, 2008, **24**, 8592-8598.

42. P. Horcajada, C. Serre, M. Vallet-Regí, M. Sebban, F. Taulelle and G. Férey, *Angewandte Chemie - International Edition*, 2006, **45**, 5974-5978.
43. P. Horcajada, C. Serre, G. Maurin, N. A. Ramsahye, F. Balas, M. Vallet-Regí, M. Sebban, F. Taulelle and G. Férey, *Journal of the American Chemical Society*, 2008, **130**, 6774-6780.
44. A. C. McKinlay, B. Xiao, D. S. Wragg, P. S. Wheatley, I. L. Megson and R. E. Morris, *Journal of the American Chemical Society*, 2008, **130**, 10440-10444.
45. P. S. Wheatley, A. C. McKinlay, R. E. Morris, P. M. Antoine Gédéon and B. Florence, in *Studies in Surface Science and Catalysis*, Elsevier, 2008, pp. 441-446.
46. J. A. R. Navarro, E. Barea, A. Rodriguez-Dieguez, J. M. Salas, C. O. Ania, J. B. Parra, N. Masciocchi, S. Galli and A. Sironi, *Journal of the American Chemical Society*, 2008, **130**, 3978-3984.
47. F. Gándara, B. Gómez-Lor, M. Iglesias, N. Snejko, E. Gutiérrez-Puebla and A. Monge, *Chemical Communications*, 2009, 2393-2395.
48. S. Neeraj, M. L. Noy, C. N. R. Rao and A. K. Cheetham, *Solid State Sciences*, 2002, **4**, 1231-1236.
49. H. Hayashi, A. P. Côté, H. Furukawa, M. O'Keeffe and O. M. Yaghi, *Nature Materials*, 2007, **6**, 501-506.
50. L. Zhang, X. Qu, M. Bi, S. Wang, S. Gong, Q. Huo and Y. Liu, *Microporous and Mesoporous Materials*, 2009, **119**, 344-348.
51. H. Wu, W. Zhou and T. Yildirim, *Journal of the American Chemical Society*, 2007, **129**, 5314-5315.
52. I. A. Baburin, S. Leoni and G. Seifert, *Journal of Physical Chemistry B*, 2008, **112**, 9437-9443.
53. Y. Q. Tian, Y. M. Zhao, Z. X. Chen, G. N. Zhang, L. H. Weng and D. Y. Zhao, *Chemistry - A European Journal*, 2007, **13**, 4146-4154.
54. T. K. Maji, G. Mostafa, H. C. Chang and S. Kitagawa, *Chemical Communications*, 2005, 2436-2438.

55. Y. Liu, V. C. Kravtsov, R. Larsen and M. Eddaoudi, *Chemical Communications*, 2006, 1488-1490.
56. Y. Q. Tian, C. X. Cai, Y. Ji, X. Z. You, S. M. Peng and G. H. Lee, *Angewandte Chemie - International Edition*, 2002, **41**, 1384-1386.
57. Y. Liu, V. C. Kravtsov and M. Eddaoudi, *Angewandte Chemie - International Edition*, 2008, **47**, 8446-8449.
58. X. C. Huang, Y. Y. Lin, J. P. Zhang and X. M. Chen, *Angewandte Chemie - International Edition*, 2006, **45**, 1557-1559.
59. C. Janiak, *Dalton Transactions*, 2003, 2781-2804.
60. F. X. Llabrás i Xamena, A. Abad, A. Corma and H. Garcia, *Journal of Catalysis*, 2007, **250**, 294-298.
61. Y. M. A. Yamada, Y. Maeda and Y. Uozumi, *Organic Letters*, 2006, **8**, 4259-4262.
62. D. N. Dybtsev, A. L. Nuzhdin, H. Chun, K. P. Bryliakov, E. P. Talsi, V. P. Fedin and K. Kim, *Angewandte Chemie - International Edition*, 2006, **45**, 916-920.
63. L. Alaerts, E. Seguin, H. Poelman, F. Thibault-Starzyk, P. A. Jacobs and D. E. De Vos, *Chemistry - A European Journal*, 2006, **12**, 7353-7363.
64. T. Uemura, K. Kitagawa, S. Horike, T. Kawamura, S. Kitagawa, M. Mizuno and K. Endo, *Chemical Communications*, 2005, 5968-5970.
65. N. V. Maksimchuk, M. N. Timofeeva, M. S. Melgunov, A. N. Shmakov, Y. A. Chesalov, D. N. Dybtsev, V. P. Fedin and O. A. Kholdeeva, *Journal of Catalysis*, 2008, **257**, 315-323.
66. M. V. Kirillova, A. M. Kirillov, M. F. C. Guedes Da Silva and A. J. L. Pombeiro, *European Journal of Inorganic Chemistry*, 2008, 3423-3427.
67. T. Hirayama, T. Manako and H. Imai, *e-Journal of Surface Science and Nanotechnology*, 2008, **6**, 237-240.
68. A. Bordoloi, F. Lefebvre and S. B. Halligudi, *Journal of Molecular Catalysis A: Chemical*, 2007, **270**, 177-184.

69. W. Mori, S. Takamizawa, C. N. Kato, T. Ohmura and T. Sato, *Microporous and Mesoporous Materials*, 2004, **73**, 31-46.
70. S. K. Yoo, J. Y. Ryu, J. Y. Lee, C. Kim, S. J. Kim and Y. Kim, *Dalton Transactions*, 2003, 1454-1456.
71. M. Abrantes, A. Valente, M. Pillinger, I. S. Goncalves, J. Rocha and C. C. Romao, *Journal of Catalysis*, 2002, **209**, 237-244.
72. M. Fujita, Y. J. Kwon, S. Washizu and K. Ogura, *Journal of the American Chemical Society*, 1994, **116**, 1151-1152.
73. W. Lin, *Journal of Solid State Chemistry*, 2005, **178**, 2486-2490.
74. Y. Li, Z. X. Zhang, F. Y. Fang, W. D. Song, K. C. Li, Y. L. Miao, C. S. Gu and L. Y. Pan, *Journal of Molecular Structure*, 2007, **837**, 269-273.
75. R. G. Xiong, X. Xue, H. Zhao, X. Z. You, B. F. Abrahams and Z. Xue, *Angewandte Chemie - International Edition*, 2002, **41**, 3800-3803.
76. H. Hou, Y. Song, Y. Fan, L. Zhang, C. Du and Y. Zhu, *Inorganica Chimica Acta*, 2001, **316**, 140-144.
77. S. D. Huang, R. G. Xiong, J. Han and B. R. Weiner, *Inorganica Chimica Acta*, 1999, **294**, 95-98.
78. O. R. Evans, R. G. Xiong, Z. Wang, G. K. Wong and W. Lin, *Angewandte Chemie - International Edition*, 1999, **38**, 536-538.
79. J. Yang, Q. Yue, G. D. Li, J. J. Cao, G. H. Li and J. S. Chen, *Inorganic Chemistry*, 2006, **45**, 2857-2865.
80. K. L. Wong, G. L. Law, Y. Y. Yang and W. T. Wong, *Advanced Materials*, 2006, **18**, 1051-1054.
81. B. Zhao, X. Y. Chen, P. Cheng, D. Z. Liao, S. P. Yan and Z. H. Jiang, *Journal of the American Chemical Society*, 2004, **126**, 15394-15395.
82. C. D. Wu, H. L. Ngo and W. Lin, *Chemical Communications*, 2004, **10**, 1588-1589.
83. D. M. Ciurtin, N. G. Pschirer, M. D. Smith, U. H. F. Bunz and H. C. Zur Loye, *Chemistry of Materials*, 2001, **13**, 2743-2745.

-
84. E. Coronado, J. R. Galán-Mascarós, C. J. Gómez-García and V. Laukhin, *Nature*, 2000, **408**, 447-449.
 85. Y. Liang, R. Cao, W. Su, M. Hong and W. Zhang, *Angewandte Chemie - International Edition*, 2000, **39**, 3304-3307.
 86. Y. Liang, M. Hong, W. Su, R. Cao and W. Zhang, *Inorganic Chemistry*, 2001, **40**, 4574-4582.
 87. S. R. Batten and K. S. Murray, *Coordination Chemistry Reviews*, 2003, **246**, 103-130.
 88. N. Snejko, E. Gutiérrez-Puebla, J. L. Martínez, M. A. Monge and C. Ruiz-Valero, *Chemistry of Materials*, 2002, **14**, 1879-1883.
 89. S. A. Cotton, *Lanthanide and Actinide Chemistry*, John Wiley & sons, Ltd, 2006.
 90. K. A. Gschneidner and L. Eyring, *Handbook on the Physics and Chemistry of Rare Earths*, North-Holland Publishing Company, 1978.
 91. L. Carlucci, G. Ciani and D. M. Proserpio, in *Making crystal by design*, Wiley-WCH, Weinheim, 2007.
 92. A. F. Wells, *Structural Inorganic Chemistry*, Oxford University Press, Oxford, 1984.
 93. A. F. Wells, *Three-dimensional Nets and Polyhedra*, Wiley, New York, 1977.
 94. A. F. Wells, *Further Studies of Three-dimensional Nets*, ACA Monograph 8, 1979.
 95. J. V. Smith, *Chemical Reviews*, 1988, **88**, 149-182.
 96. J. V. Smith, *Tetrahedral Frameworks of Zeolites, Clathrates and Related Materials*, Springer, Berlin, 2000.
 97. M. M. J. Treacy, K. H. Randall, S. Rao, J. A. Perry and D. J. Chadi, *Zeitschrift für Kristallographie*, 1997, **212**, 768-791.
 98. M. M. J. Treacy, I. Rivin, E. Balkovsky, K. H. Randall and M. D. Foster, *Microporous and Mesoporous Materials*, 2004, **74**, 121-132.
 99. M. O'Keeffe and B. G. Hyde, *Crystal Structures I: Patterns and Symmetry*, Mineralogical Society of America, Washington, 1996.

100. M. O'Keeffe, M. A. Peskov, S. J. Ramsden and O. M. Yaghi, *Accounts of Chemical Research*, 2008, **41**, 1782-1789.
101. C. Baerlocher, W. M. Meier and D. H. Olson, *Atlas of Zeolite Framework Types*, Elsevier, Amsterdam, 2001.
102. B. F. Hoskins and R. Robson, *Journal of the American Chemical Society*, 1990, **112**, 1546-1554.
103. H. Li, M. Eddaoudi, M. O'Keeffe and O. M. Yaghi, *Nature*, 1999, **402**, 276-279.
104. M. Eddaoudi, J. Kim, N. Rosi, D. Vodak, J. Wachter, M. O'Keeffe and O. M. Yaghi, *Science*, 2002, **295**, 469-472.
105. F. Serpaggi and G. Férey, *Journal of Materials Chemistry*, 1998, **8**, 2737-2741.
106. T. M. Reineke, M. Eddaoudi, M. Fehr, D. Kelley and O. M. Yaghi, *Journal of the American Chemical Society*, 1999, **121**, 1651-1657.
107. T. Devic, C. Serre, N. Audebrand, J. Marrot and G. Férey, *Journal of the American Chemical Society*, 2005, **127**, 12788-12789.
108. X. Guo, G. Zhu, Q. Fang, M. Xue, G. Tian, J. Sun, X. Li and S. Qiu, *Inorganic Chemistry*, 2005, **44**, 3850-3855.
109. R. J. Hill, D.-L. Long, P. Hubberstey, M. Schröder and N. R. Champness, *Journal of Solid State Chemistry*, 2005, **178**, 2414-2419.
110. C. C. Evans, L. Sukarto and M. D. Ward, *Journal of the American Chemical Society*, 1999, **121**, 320-325.
111. M. J. Horner, K. T. Holman and M. D. Ward, *Journal of the American Chemical Society*, 2007, **129**, 14640-14660.
112. V. A. Russell, C. C. Evans, W. J. Li and M. D. Ward, *Science*, 1997, **276**, 575-579.
113. V. A. Russell and M. D. Ward, *Journal of Materials Chemistry*, 1997, **7**, 1123-1133.
114. J. A. Swift and M. D. Ward, *Chemistry of Materials*, 2000, **12**, 1501-1504.

115. A. P. Cote and G. K. H. Shimizu, *Coordination Chemistry Reviews*, 2003, **245**, 49-64.
116. J. Cai, *Coordination Chemistry Reviews*, 2004, **248**, 1061-1083.
117. J. Cai, C.-H. Chen, C.-Z. Liao, J.-H. Yao, X.-P. Hu and X.-M. Chen, *Journal of the Chemical Society, Dalton Transactions*, 2001, 1137-1142.
118. S. Gao, L.-H. Huo, Z.-B. Zhu and S. W. Ng, *Acta Crystallographica Section E-Structure Reports Online*, 2005, **61**, m476-m477.
119. L. Wang, X. L. Yu, J. W. Cai and J. W. Huang, *Journal of Chemical Crystallography*, 2005, **35**, 481-486.
120. J. Cai, C.-H. Chen, X.-L. Feng, C.-Z. Liao and X.-M. Chen, *Journal of the Chemical Society, Dalton Transactions*, 2001, 2370-2375.
121. C. H. Chen, J. W. Cai, C. Z. Liao, X. L. Feng, X. M. Chen and S. W. Ng, *Inorganic Chemistry*, 2002, **41**, 4967-4974.
122. Z.-B. Zhu, S. Gao, L.-H. Huo and S. W. Ng, *Acta Crystallographica Section E-Structure Reports Online*, 2005, **61**, m288-m289.
123. R. Fu, S. Xiang, S. Hu, L. Wang, Y. Li, X. Huang and X. Wu, *Chemical Communications*, 2005, 5292-5294.
124. S. Gao, Z.-Z. Lu, L.-H. Huo, Zhi-Biao and Z. H. Zhao, *Acta Crystallographica Section C-Crystal Structure Communications*, 2005, **61**, m22-m24.
125. D. J. Hoffart, S. A. Dalrymple and G. K. H. Shimizu, *Inorganic Chemistry*, 2005, **44**, 8868-8875.
126. A. P. Cote and G. K. H. Shimizu, *Inorganic Chemistry*, 2004, **43**, 6663-6673.
127. D. J. Hoffart, S. A. Dalrymple and G. K. H. Shimizu, *Inorganic Chemistry*, 2005, **44**, 8868-8875.
128. Z.-X. Lian, J. Cai, C.-H. Chen and H.-B. Luo, *Crystengcomm*, 2007, **9**, 319-327.
129. J. Chen and Y. Z. Ruan, *Acta Crystallographica Section E-Structure Reports Online*, 2007, **63**, M2964-U2947.

130. J. F. Ma, J. Yang, S. L. Li, S. Y. Song, H. J. Zhang, H. S. Wang and K. Y. Yang, *Crystal Growth & Design*, 2005, **5**, 807-812.
131. J. Cai, C.-H. Chen, C.-Z. Liao, X.-L. Feng and X.-M. Chen, *Acta Crystallographica Section B-Structural Science*, 2001, **57**, 520-530.
132. S. Gao, Z. B. Zhu, L. H. Huo and S. W. Ng, *Acta Crystallographica Section E-Structure Reports Online*, 2005, **61**, M528-M530.
133. L.-H. Huo, S. Gao, S.-X. Xu, H. Zhao and S. W. Ng, *Acta Crystallographica Section E-Structure Reports Online*, 2004, **60**, m1240-m1241.
134. G. K. H. S. Adrien P. Côté, *Chemistry - A European Journal*, 2003, **9**, 5361-5370.
135. A. P. Cote and G. K. H. Shimizu, *Chemical Communications*, 2001, 251-252.
136. G. Smith, U. D. Wermuth and P. C. Healy, *Acta Crystallographica Section E-Structure Reports Online*, 2007, **63**, M3056-U1792.
137. J. Yang, L. Li, H. F. Ma, Y. Y. Liu and J. C. Ma, *Journal of Molecular Structure*, 2006, **796**, 41-46.
138. S. M. Downer, P. J. Squattrito, N. Bestaoui and A. Clearfield, *Journal of Chemical Crystallography*, 2006, **36**, 487-501.
139. B. J. Gunderman and P. J. Squattrito, *Acta Crystallographica Section C-Crystal Structure Communications*, 1996, **52**, 1896-1901.
140. G. B. Deacon, A. Gitlits, G. Zelesny, D. Stellfeldt and G. Meyer, *Zeitschrift Fur Anorganische Und Allgemeine Chemie*, 1999, **625**, 764-772.
141. B. D. Chandler, J. O. Yu, D. T. Cramb and G. K. H. Shimizu, *Chemistry of Materials*, 2007, **19**, 4467-4473.
142. B. D. Chandler, D. T. Cramb and G. K. H. Shimizu, *Journal of the American Chemical Society*, 2006, **128**, 10403-10412.
143. N. Snejko, C. Cascales, B. Gómez-Lor, E. Gutiérrez-Puebla, M. Iglesias, C. Ruiz-Valero and M. A. Monge, *Chemical Communications*, 2002, 1366-1367.

-
144. F. Gándara, A. García-Cortés, C. Cascales, B. Gómez-Lor, E. Gutiérrez-Puebla, M. Iglesias, A. Monge and N. Snejko, *Inorganic Chemistry*, 2007, **46**, 3475-3484.
145. J.-P. Zhao, B.-W. Hu, F.-C. Liu, X. Hu, Y.-F. Zeng and X.-H. Bu, *Crystengcomm*, 2007, **9**, 902-906.
146. Z. P. Deng, S. Gao, Z. B. Zhu and L. H. Huo, *Zeitschrift Fur Anorganische Und Allgemeine Chemie*, 2008, **634**, 593-596.
147. G. B. Deacon, R. Harika, P. C. Junk, B. W. Skelton and A. H. White, *New Journal of Chemistry*, 2007, **31**, 634-645.
148. R.-G. Xiong, J. Zhang, Z.-F. Chen, X.-Z. You, C.-M. Che and H.-K. Fun, *Journal of the Chemical Society, Dalton Transactions*, 2001, 780-782.
149. Z. Wang, M. Ströbele, K.-L. Zhang, H. J. Meyer, X.-Z. You and Z. Yu, *Inorganic Chemistry Communications*, 2002, **5**, 230-234.
150. M.-L. Hu, Q. Miao, Q. Shi and M.-D. Ye, *Acta Crystallographica Section C-Crystal Structure Communications*, 2004, **60**, m460-m464.
151. S. J. Dalgarno and C. L. Raston, *Chemical Communications*, 2002, 2216-2217.
152. S. J. Dalgarno, M. J. Hardie and C. L. Raston, *Crystal Growth & Design*, 2004, **4**, 227-234.
153. S. J. Dalgarno, J. L. Atwood and C. L. Raston, *Crystal Growth & Design*, 2007, **7**, 1762-1770.
154. J. L. Atwood, L. J. Barbour, S. Dalgarno, C. L. Raston and H. R. Webb, *Journal of the Chemical Society-Dalton Transactions*, 2002, 4351-4356.
155. F. Hohn, H. Billetter, I. Pantenburg and U. Ruschewitz, *Zeitschrift für Naturforschung*, 2002, **57**, 1375-1381.
156. L. Liu, S. Duraj, P. E. Fanwick, M. T. Andras and A. F. Hepp, *Journal of Coordination Chemistry*, 2003, **56**, 647-653.
157. Y. Q. Zheng and Z. P. Kong, *Zeitschrift für anorganische und allgemeine Chemie*, 2003, **629**, 1469-1471.

158. D. Braga, S. L. Giuffreda, F. Grepioni and M. Polito, *Crystengcomm*, 2004, **6**, 458-462.
159. Y. H. Wang, K. L. Chu, H. C. Chen, C. W. Yeh, Z. K. Chan, M. C. Suen, J. D. Chen and J. C. Wang, *Crystengcomm*, 2006, **8**, 84-93.
160. K. A. Brylev, N. G. Naumov, A. V. Virovets, S. J. Kim and V. E. Fedorov, *Journal of Cluster Science*, 2008, 1-12.
161. V. P. Fedin, A. V. Virovets, I. V. Kalinina, V. N. Ikorskii, M. R. J. Elsegood and W. Clegg, *European Journal of Inorganic Chemistry*, 2000, 2341-2343.
162. O. S. Jung, Y. J. Kim, Y. A. Lee, J. K. Lee and K. H. Yoo, *Bulletin of the Korean Chemical Society*, 2000, **21**, 39-43.
163. S. Mintova, S. Mo and T. Bein, *Chemistry of Materials*, 1998, **10**, 4030-4036.
164. K. J. Rao, B. Vaidhyanathan, M. Ganguli and P. A. Ramakrishnan, *Chemistry of Materials*, 1999, **11**, 882-895.
165. G. A. Tompsett, W. C. Conner and K. S. Yngvesson, *ChemPhysChem*, 2006, **7**, 296-319.
166. C. S. Cundy, *Collection of Czechoslovak Chemical Communications*, 1998, **63**, 1699-1723.
167. M. Park and S. Komarneni, *Microporous and Mesoporous Materials*, 1998, **20**, 39-44.
168. A. Arafat, J. C. Jansen, A. R. Ebaid and H. van Bekkum, *Zeolites*, 1993, **13**, 162-165.
169. S. H. Jung, T. Jin, Y. K. Hwang and J. S. Chang, *Chemistry - A European Journal*, 2007, **13**, 4410-4417.
170. E. R. Parnham and R. E. Morris, *Accounts of Chemical Research*, 2007, **40**, 1005-1013.
171. R. E. Morris, *Angewandte Chemie - International Edition*, 2008, **47**, 442-444.
172. E. R. Parnham and R. E. Morris, *Journal of the American Chemical Society*, 2006, **128**, 2204-2205.

173. R. E. Morris, P. M. Antoine Gédéon and B. Florence, in *Studies in Surface Science and Catalysis*, Elsevier, 2008, pp. 33-42.
174. A. Monge, N. Snejko, E. Gutiérrez-Puebla, M. Medina, C. Cascales, C. Ruiz-Valero, M. Iglesias and B. Gómez-Lor, *Chemical Communications*, 2005, 1291-1293.
175. F. Gándara, B. Gómez-Lor, E. Gutiérrez-Puebla, M. Iglesias, M. A. Monge, D. M. Proserpio and N. Snejko, *Chemistry of Materials.*, 2008, **20**, 72-76.

II.

Experimental

1. Experimental details

Hydrothermal Synthesis

The term hydrothermal reaction usually refers to any heterogeneous reaction in the presence of aqueous solvents or mineralizers under high pressure and temperature conditions to dissolve and recrystallize materials that are relatively insoluble under ordinary conditions¹. When non aqueous solvent are employed, the more general term *solvothermal* can also be applied. The hydro- and solvo- thermal techniques have been successfully employed in the preparation of zeolites and related materials. This synthetic procedure is a way to imitate the zeolites natural synthesis conditions, and it has been successfully applied for decades, first for synthetic zeolites^{2, 3}, and then for another related inorganic molecular sieves⁴⁻⁷. Natural zeolites are formed in the nature at basic pH values with temperatures below 100 °C and during long periods of times. In the laboratory, higher temperatures are utilized (120 – 200 °C), and the crystallization processes usually take periods of time from hours to several weeks. The hydrothermal methods have been modified and improved for years, introducing different elements in the system, such as structure directing agents, stirring, or different mineralizing agents like fluorine⁸⁻¹¹

In the case of coordination polymers, the use of the hydrothermal techniques is more recent, but it has demonstrated to be a very useful approach for the preparation of these materials. In fact, the compounds prepared under solvothermal conditions may present interesting features that make them different to those prepared at lower pressure and temperature, for example lower solubility in most common solvents or the presence of different coordination modes.

The syntheses are carried out in sealed recipients. Sealed glass tubes can be used¹², but it is more common the use of Teflon lined autoclaves. The mixtures are prepared and placed into Teflon lined vessels, which are then sealed and introduced into the stainless steel autoclaves. They are then heated at the selected temperature and for the required period of time, and after cooling, the product is recovered. The reaction mixture is found under an autogenous pressure, which will depend on the temperature and type of solvent employed, as well as on the presence of other compounds that can decompose during the process, increasing therefore the pressure in the system.

Due to the characteristics of this technique, in which the reactions take place in sealed recipients, the synthesis procedure may be considered as a *black box*, since the only information is the initial mixture composition and the final products obtained. The optimization of a synthesis procedure is therefore based on combinatorial approaches with variations of all the synthesis conditions (temperature, reagents, heating time, cooling time, solvents...) and analysis of the obtained products, generally with X-ray diffraction methods. It is quite usual that mixtures of products are obtained during the synthesis experiments, and the conditions must then be tuned until the desired product appears as unique phase, and also with a good yield that allow the characterization of the product, as well as its use in selected applications.

In recent years, the optimization processes have been automated¹³⁻¹⁷ with the use of the high-throughput processes, so that a higher number of experiments can be carried out and analyzed simultaneously. In these processes, robots are used to prepare a great number of mixtures with different composition and to analyze the resulting products. However, these methods are still too expensive and their use is not very extended, so they represent a clear advantage for the research groups that can dispose of them.

All the materials presented in this report have been hydro-solvothermally prepared. All the reagents are commercial, and are used as received, without

further purification. Details of the employed reagents for each material are given in their corresponding chapters. In a typical synthesis procedure, the corresponding amounts of the solid reagents (in the range of approximately a hundred milligrams) are weighted and placed into the Teflon lined vessel. The correct amount of solvents is then added, as well as the required pH controlling species, like triethylamine or a sodium hydroxide solution. This mixture is magnetically stirred at room temperature, and then the Teflon vessel is introduced into the autoclave, which is sealed and placed into an oven, preheated at the chosen temperature. After the heating time passes, the autoclave is cooled to room temperature, and then it is opened and the mixture is filtered with vacuum. The solid is washed with deionized water and acetone, and dried at room temperature. The recovered solid is first evaluated with the help of an optic microscope. If suitable single crystals are found, they are selected and collected. The bulk of the reaction is analyzed with powder X-ray diffraction to identify the products as well as to determine the purity of the obtained phases. Once the X-ray powder pattern indicates that the product is obtained purely, chemical elemental and thermogravimetric analysis are carried out to fully characterize them.



Figure II.1.01: Autoclaves employed in the hydrothermal synthesis.

X-ray diffraction

Due to the crystalline nature of the materials here presented, the X-ray diffraction techniques have been the characterization techniques mainly employed during the development of this work. The crystal structures of all materials have been determined by means of single crystal X-ray diffraction, while the use of the X-ray powder diffraction was essential during the optimization of the synthesis procedures and for the evaluation of the purity of the products.

Single crystal X-ray diffraction:

In 1912 Max von Laue showed that crystals are based on a three dimensional lattice which scatters radiation with a wavelength in the vicinity of interatomic distances, i.e. X- rays with $\lambda = 0.5\text{-}3.0 \text{ \AA}$. The process by which the X-ray radiation, without changing its wavelength, is converted through interference by the lattice to a vast number of observable “reflections” with characteristic directions in the space is called X-ray diffraction.

The solution of a crystal structure involves the determination of the precise spatial arrangements of all the atoms in a chemical compound in its crystalline state. In order to describe the structure of a crystal, it is only necessary to know the simplest repeating motif and the lengths and directions of the three vectors which together describe its repetition in space. The smallest repeating volume of the lattice is called the unit cell. It is characterized by three lattice constants a , b , c (the lengths of the basis vectors) and by the three angles which separate these vectors from one another. The positions of the atoms are described in terms of the crystallographic axes defined by the three basis vectors. The process in which the positions of all the atoms are correctly determined involves several steps:

The first step is naturally the obtaining of a suitable crystal. The development of a crystal depends on the relative rates of nucleation and growth. A rate of nucleation larger than the rate of growth results in the formation of agglomerates of small crystallites. On the other hand, too rapid a rate of growth may result in the inclusion of many faults in the crystal. For a new compound, the optimum conditions for the growth of a crystal cannot readily be predicted. When single crystals are obtained, one of them must be selected. The quality of the collected data will highly depend on the quality of the crystal, and therefore the selection of the appropriate single crystal must be carefully made. The crystals are selected with the help of an optical microscope. An ideal crystal must be free of defects, with well defined faces and edges. The use of polarized light helps to discard multiple crystals (individual parts normally extinguish at different angles when rotated) and to reveal the presence of cracks in a crystal (they appear as bright lines against the dark background). The size of the crystal is also important. To ensure a good statistics in the diffracted X-rays, one or two hundred micrometers are desired in every one of the crystal dimension. Once the best available single crystal has been selected, it is mounted on the extreme of a glass fiber, fixed with contact adhesive; typically a two-component glue is employed for this purpose. The glass fiber has been previously attached to a metal base, adapted to be mounted on a goniometric head.

When the crystal has been selected and mounted, the subsequent study will be carried out with the single crystal diffractometer. The equipment used in this work is a Bruker-Siemens Smart CCD diffractometer. This diffractometer is equipped with a normal focus, 4 kW sealed tube X-ray source, with a primary monochromator, using the Mo K α radiation, $\lambda = 0.71069 \text{ \AA}$. A charge coupled device (CCD) area detector is used to collect the diffracted reflections. This diffractometer has a 3 circles goniometer, in the center of which the crystal must be precisely centered. The preliminary study of the crystal includes a partial exploration of the reciprocal space. It usually takes less than one hour,

and it will give us an estimation of the quality of the crystal, which will determine if the whole data collection is being carried out. With the crystal correctly centered, the unit cell parameters and their orientation to the goniometer axes will be determined. This is given by the orientation matrix, which is a 3x3 matrix which gives the components of the three reciprocal axes in the three directions of the goniometer's axial system. A random search for reflections is made, and an indexing program will define a lattice onto which all the observed reflections will fit. Indexing programs are based on a peak search for scattering vectors over the first exposures. On the basis of the differences between these vectors, reciprocal base vectors are sought, which can describe all found peaks as reciprocal lattice points. A reduced cell is then obtained for that originally found, and the corresponding orientation matrix is determined.

If the cell parameters are not known and the crystal is of quality enough, a complete data collection is carried out. This consists on successive exposures of the crystal to the incident radiation at a rotation angle range. The angle range is selected based upon the symmetry of the crystal, and it must contain at least one full set of independent data for the relevant Laue group. The data collection will take several hours, depending on the exposure time and the size of the observed portion of the Ewald sphere.

After the data collection is over, the intensity of the observed reflexions are integrated in the volume of the observed reciprocal space, in the predicted positions calculated with the orientation matrix. This is made with the SAINT¹⁸ program, and to obtain good output data, a good accuracy in the orientation matrix is necessary, as well as that the crystal has not been displaced from the goniometer centre during the collection. The data integration is a feedback process, and the orientation matrix and the geometrical parameters of the diffractometer are also refined while the process is going on. The observed intensities are corrected with the polarization and Lorentz factors, and the Miller indices are assigned. Finally,

a semiempirical absorption correction based on equivalent reflections is made, using the SADABS software¹⁹.



Figure II.1.02: The SMART CCD diffractometer employed during the work here presented.

The final data set includes the cell parameters and the intensity data given as square structure factors F^2_{hkl} . This set of data will be used for the structure solution and refinement. The software package SHELXTL 6.10²⁰ includes programs for the structure solution and refinement of crystal structures from X-ray diffraction data. Using this software, and after the space group determination, direct methods have been used to the initial phase assignment, and a first model is obtained. This initial model is refined, and the subsequent Fourier syntheses give the electronic density maps in which the atoms are located. The structure is refined with a full-matrix least square refinement on square structure factors, F^2 , initially with isotropic thermal factors. Once all the non hydrogen atoms are located, a refinement is made with anisotropic thermal factors. The hydrogen atoms are finally located on the residual electronic density maps or geometrically calculated.

Once the crystal structure has been solved, and the positions for all the atoms are known, the graphical representations are made with software like XSHELL (included in the SHELXTL package), ATOMS²¹ or isocryst. This latter is included in the software package TOPOS²², which has been used for the topological analysis of the networks presented by the new materials.

A schematic representation of the crystal structure determination procedure is found in figure II.1.03.

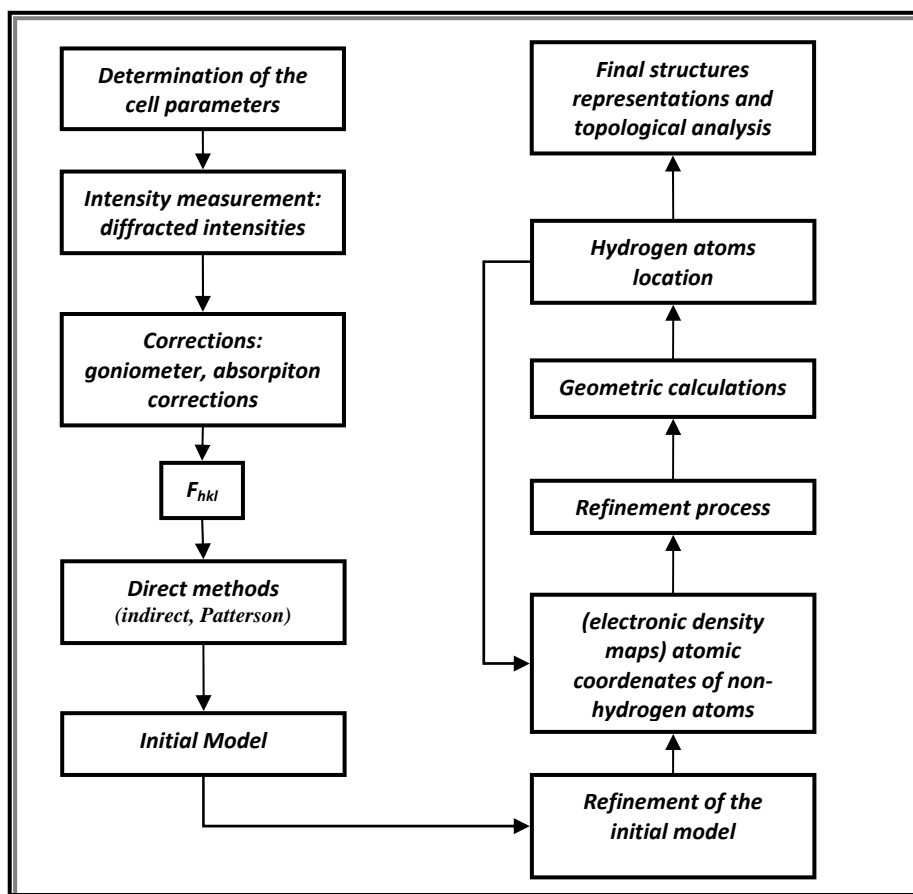


Figure II.1.03: Schematic chart showing the steps involved in a crystal structure solution.

Powder X-ray diffraction:

With the powder X-ray diffraction (PXRD) it is possible to analyze the crystalline phases of a microcrystalline sample. During the development of this research, PXRD has been used as routine technique, since it allows the purity testing of the prepared compounds.

Each crystalline phase exhibits a characteristic powder pattern, in which the 2θ positions of the diffracted peaks depend on the unit cell parameters and space group, and their relative intensities are function of the composition and atomic positions. They are also influenced by others factors such as textural features of the microcrystallines of the sample. Knowing a crystal structure, its powder pattern can be simulated, and then compared with the experimental pattern to determine the purity of the samples. The most suitable way to do this is the Rietveld method. The Rietveld method was first developed²³ for the refinement of crystalline structures using neutron diffraction data. Its use has been extended to the field of X-ray diffraction, and it is employed in, for example, the refinement of crystalline structures, the quantitative analysis of mixed crystalline phases, ab initio structure determination from powder data or estimation of the size and shape of crystallites.

The refinement of a crystalline structure by the Rietveld method consists in the minimization of the differences between an experimental powder pattern and one simulated with a structural model and with parameters that allows the distribution of the reflections intensities in the whole pattern. The function to be minimized is $S_y = \sum_i \omega w_i |y_i(o) - y_i(c)|^2$, where $y_i(o)$ and $y_i(c)$ are the observed and calculated intensities for each i point, and w_i is the assigned weight to each point. The calculated intensities are a function of two types of parameters: the atomic parameters allows the calculation of the intensity of the reflections, and they include the lattice parameters, space group, atomic positions, thermal agitation parameters and occupancy factors for the atoms in each crystalline phase. On the other hand, there also exist the global

parameters, which affect the whole pattern, and allow the distribution of the reflections intensities in each point of the pattern where they affect. Within these parameters there are included: the scale factor of the pattern, the background function, zero displacement, peaks shape parameters, scale factor for each crystalline phase and preferred orientation parameters.

For the refinements carried out with the materials presented in this report, the employed atomic factors are those determined with single crystal X-ray diffraction. The refinements have therefore mainly concerned to the global parameters.

The experimental powder patterns have been collected in two Bruker-AXS d8 advance diffractometers, the both of them operating with the Cu K_{α} radiation, at 40 kV and 30 mA. One of them is equipped with a position sensitive detector (PSD detector). With this diffractometer the powder patterns were collected in a 2θ range 5-60°, with a step size of 0.02°, and at exposure time of 2.5 s. The configuration of the PSD detector does not allow the collection of data at angles below 5°, and because of this, for the materials that presented Bragg positions at lower angles, the powder patterns were collected in a diffractometer equipped with a radiation sensitive detector (solX detector). The 2θ range was 3-60°, and step size of 0.02° was used, with an exposure time of 4 seconds per step. The Rietveld refinements have been carried out using the FULLPROF²⁴ software package.

Thermal analysis

The thermal analysis involves a set of experimental techniques in which the changes in a physical property of a substance and/or its products are measured in function of the temperature, under a controlled temperature program. The thermal analysis techniques are extensively used for the characterization of many different kinds of materials, including oxides, silicates, clays, ceramics

or polymers, among others. The processes that take place during the temperature variations are measured, like decomposition, desolvation, melting, solid state reactions, etc.

Among the techniques included in the thermal analysis, differential thermal and thermogravimetric analyses are widely employed, and in the case of polymeric frameworks, they give information about the temperature of decomposition of the materials, as well as about loss of solvent molecules, or possible phase transitions related to temperature changes.

More specifically, in the differential thermal analysis (DTA), the differences in temperature between a substance and a reference material are measured in function of the temperature, with both the substance and the reference under a controlled temperature program. This difference in temperature is represented versus the temperature, and it is related to the consumption or production of heat by the reactions taking place in the sample at a given temperature.

In a thermogravimetric analysis (TG), the mass of the sample is continuously measured in function of the temperature, under a controlled atmosphere. The percentage of the mass change is represented versus the temperature to give a thermogravimetric curve. This gives information of the changes that are taking place in the sample composition as the temperature varies.

The thermal analyses carried out in this work have been made with a SEIKO TG/DTA 320 equipment. Under the standard conditions, the analyses were carried out in a nitrogen atmosphere, with a N₂ flow of 50 ml/min, in a temperature range from room temperature to 800 °C, and with a heating rate of 10 °C / min.

Catalytic experiments and gas chromatography

Nowadays, catalysis has become one of the most significant areas of the chemistry, due to its great importance in the chemical industry. Catalysis is present in most of the chemical processes, from the fine chemistry to the petrochemical industry. In the homogeneous catalysis, the catalyst is in the same phase as the reactants, while in the heterogeneous catalysis, catalyst and reactants are in different phases. Whereas homogeneous catalysts usually present higher activity, the recyclability and easy separation of the heterogeneous catalysts make them as preferred in the industrial processes. Microporous and mesoporous inorganic materials are traditionally good candidates to be support for catalysts. Once the catalyst is supported on such porous materials, the system is heterogeneous, and a high number of active centers are also available. In the case of polymeric frameworks, its use as catalysts still remains less studied. However, the fact that they can have catalytically active elements in the framework makes them as a good alternative to other traditional heterogeneous catalyst types. Many of the materials prepared for this work have been evaluated as heterogeneous catalysts, testing their activity in test reactions, such as the oxidation of sulfides or the oxidation of linalool. In a typical catalytic activity experiment, a suspension containing a solution of the reactants and the catalyst at the adequate rate is heated under stirring. Specific details on catalytic experiments carried out are given in the corresponding chapter. The grade of conversion achieved at a selected period of time is measured by gas chromatography (GC). With the GC, compounds that can be vaporized without decomposition are analyzed and the different components of a mixture are separated. The compounds in gaseous form are carried by an inert gas, like helium or N_2 , in what is known as mobile phase. This phase is transported through a stationary phase, which usually is a microscopic layer of liquid or polymer on an inert solid support, inside a column. The compounds interact with the stationary

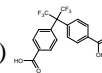
phase, and each different compound elute at a different time, known as the retention time. The GC experiments of this work have been carried out employing a Konik HRGC 4000 B Gas chromatograph, equipped with a flame ionization detector (FID), and a methyl silicone column as stationary phase.

2. References

1. K. Byrappa and M. Yoshimura, *Handbook of Hydrothermal Technology*, William Andrew Publishing, LLC, Norwich, 2001.
2. C. S. Cundy and P. A. Cox, *Chemical Reviews*, 2003, **103**, 663-701.
3. R. M. Barrer, *Hydrothermal Chemistry of Zeolites.*, 1982.
4. A. Rabenau, *Angewandte Chemie - International Edition in English*, 1985, **24**, 1026-1040.
5. P. Feng, X. Bu and G. D. Stucky, *Nature*, 1997, **388**, 735-741.
6. S. Feng and R. Xu, *Accounts of Chemical Research*, 2001, **34**, 239-247.
7. C. Cascales, E. Gutiérrez-Puebla, M. A. Monge and C. Ruíz-Valero, *Angewandte Chemie - International Edition*, 1998, **37**, 129-131.
8. T. Blasco, M. A. Camblor, A. Corma, P. Esteve, J. M. Guil, A. Martínez, J. A. Perdigón-Melón and S. Valencia, *Journal of Physical Chemistry B*, 1998, **102**, 75-88.
9. G. D. Price, J. J. Pluth, J. V. Smith, J. Michael Bennett and R. Lyle Patton, *Journal of the American Chemical Society*, 1982, **104**, 5971-5977.
10. G. D. Price, J. J. Pluth, J. V. Smith, T. Araki and J. M. Bennett, *Nature*, 1981, **292**, 818-819.
11. M. A. Camblor, L. A. Villaescusa and M. J. Díaz-Cabañas, *Topics in Catalysis*, 1999, **9**, 59-76.
12. D. Venkataraman, G. B. Gardner, S. Lee and J. S. Moore, *Journal of the American Chemical Society*, 1995, **117**, 11600-11601.
13. S. Bauer, C. Serre, T. Devic, P. Horcajada, J. Marrot, G. Férey and N. Stock, *Inorganic Chemistry*, 2008, **47**, 7568-7576.
14. W. F. Maier, K. Stowe and S. Sieg, *Angewandte Chemie - International Edition*, 2007, **46**, 6016-6067.

15. P. M. Forster, N. Stock and A. K. Cheetham, *Angewandte Chemie - International Edition*, 2005, **44**, 7608-7611.
16. N. Stock and T. Bein, *Angewandte Chemie - International Edition*, 2004, **43**, 749-752.
17. J. M. Newsam, T. Bein, J. Klein, W. F. Maier and W. Stichert, *Microporous and Mesoporous Materials*, 2001, **48**, 355-365.
18. Bruker, SAINT, Bruker AXS Inc., Madison, Wisconsin, USA, 2007.
19. Bruker, SADABS, Bruker AXS Inc., Madison, Wisconsin, USA, 2001.
20. G. M. Sheldrick, *Acta Crystallographica Section A-Foundations of Crystallography*, 2008, **64**, 112-122.
21. E. Dowty, 2000, p. ATOMS v. 5.10.
22. V. A. Blatov, *IUCr Comppcomm Newsletter*, 2006, **7**, 4.
23. H. M. Rietveld, *Journal of Applied Crystallography*, 1969, **2**, 65-&.
24. J. Rodríguez-Carvajal, *Physica B: Physics of Condensed Matter*, 1993, **192**, 55-69.

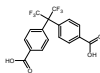
III. Results



1. RPF4: Rare earth + 4,4'-(hexafluoroisopropylidene)bis(benzoic acid)

Introduction:

As it was explained in the introduction section, dicarboxylate are probably the most employed type of ligands in the synthesis of coordination polymers. On the other hand, among the reported coordination polymers the aromatic ligands are more abundant than aliphatic. The aromaticity in the organic backbone provides robustness and a certain degree of rigidity to the ligand (and therefore to the framework), and the use of completely aromatic ligands is quite adequate especially when a specific topology is expected for the coordination polymer to be prepared, since this rigidity avoid angles variation in the molecule which is expected to coordinate to the metal centers in a linear way. In most of the cases, linear rigid ligands are employed, normally consisting on the fusion of benzene rings, with the carboxylate groups in their extremes. An alternative to the linear ligands is the use of molecules with other specific geometries that can provide the framework with structural features and topologies only achievable with the use of non-linear molecules. An example of this molecule is the 4,4'-(hexafluoroisopropylidene)bis(benzoic acid) ($H_2hfipbb$) (figure III.1.01). This molecule is formed by two benzoic acids joined by a central sp^3 carbon atom, which provides the molecule with a free rotation of the aromatic rings. Usually, the molecule adopts a V shaped configuration. The use of this molecule for the construction of metal-organic framework was previously evaluated by our group^{1, 2} and others^{3, 4}, employing transition metals. In particular, its use in the preparation of a Zn-MOF¹ gave rise to a new compound which exhibited very interesting structural features, with a chiral and porous structure with unprecedented topology, only possible due to the presence of this bent ligand. In this structure, Zn atoms in tetrahedral



coordination are forming chains through carboxylate bridges, and these chains being joined each other by the whole ligand molecules give rise to a three dimensional framework with a structure in which two kinds of channels are present, one of them with a shape imposed by the geometry of the ligand. In this new network, the tetrahedral Zn atoms are 4 connected nodes. When we employed another metal with a higher coordination number we found a different structure, which was also topologically unique. For example, in the In-MOF² prepared with hfipbb, the indium atoms appear in octahedral coordination, and again they are forming chains but in this case by sharing hydroxyl groups. These chains are also connected by the ligand molecules and here a two-periodic structure is formed, with 3D-layers (layers that cannot be flattened on a plane, since they have volume) in which square channels are present. Despite zinc and indium can vary their coordination number, both of them usually have preference for a particular coordination sphere, and as expected they appear tetrahedrally and octahedrally coordinated in these MOFs. When using rare earth elements it is harder to predict a coordination environment of the metals, especially because they very commonly appear coordinated to solvent molecules. Because of this, we consider that the use of rare earth elements with hfipbb acid, would probably produce structures with unexpected topologies, which should also bear the interesting properties coming from the use of these cations. With these ideas in mind, we started to evaluate the preparation of a rare-earth polymeric framework with hfipbb acid as ligand, finally obtaining the RPF4 family.

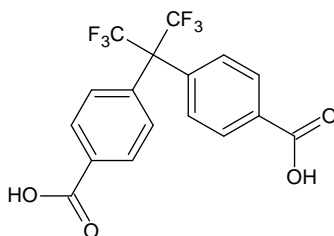
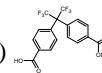


Figure III.1.01: 4,4'-(hexafluoroisopropylidene)bis(benzoic acid), (H₂hfipbb), the ligand employed in the preparation of the compounds presented in this chapter



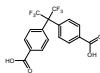
Synthesis:

During the first attempts to synthesize the new Ln³⁺-based materials with lanthanum and the H₂hfipbb (H₂hfipbb = 4,4'-(hexafluoroisopropylidene)bis(benzoic acid)) ligand, a mixture of three phases with different crystal structures was obtained. Only after determining their crystal structure it was found the same formula Ln₂(hfipbb)₃ for the three phases, being, thus, three polymorphs for the RPF4 family, named from now on as α, β and γ polymorphs.

The optimization of the synthesis procedure was carried out employing lanthanum as R³⁺, and adjusting the synthesis conditions, the RPF4-α and RPF4-β phases were obtained as pure phases.

As the number of reaction experiments carried out during the optimization process is about one hundred, only the final conditions in which we achieved our target are shown.

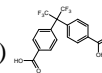
To obtain the RPF4-α phase, in a typical synthesis, 0.100 g of La(NO₃)₃·6H₂O and 0.138 g of H₂hfipbb (H₂L) are mixed in 12 ml of water and 2ml of ethyleneglycol (eg). The molar composition of the mixture is Ln : 1,5 L : 2140 H₂O : 115 eg. The mixture is stirred at room temperature for 5 minutes, and then placed into a Teflon lined stainless steel autoclave, which is sealed and placed in a preheated oven at 170 °C, and then heated for 2 days. After the heating time, the autoclave is cooled to room temperature and the mixture is filtered and washed with deionized water and acetone. This phase is also obtained with Y, La, Ce, Pr, Nd, Sm, Eu, Gd, Tb, Dy, Ho, Er, Yb. Similar synthesis procedures are carried out employing the corresponding amounts of the Ln(NO₃)₃ salts to obtain the corresponding products. The yield of the obtained products is in the range 60% - 70%.



The pure RPF4- β (R = La) was obtained from the mixture of $\text{La}(\text{NO}_3)_3 \cdot 6\text{H}_2\text{O}$ (0.043 g), H_2hfipbb acid (0.065 g), triethylamine (0,3 ml) and H_2O (5 ml). The molar composition of this mixture is La : 1,5 L : 20 Et_3N : 2775 H_2O . Heating this mixture in a Teflon-lined acid digestion bomb at 170 °C for 5 days, followed by cooling to room temperature result in pure white crystalline product of La-RPF4- β .

The RPF4- γ ($\text{Ln} = \text{La}$), polymeric framework was obtained from the mixture of $\text{La}(\text{NO}_3)_3 \cdot 6\text{H}_2\text{O}$ (0.043g), H_2hfipbb acid (0.065 g), 4,4'-Bipyridyl (0,016 g) and H_2O (5 ml). molar composition of this mixture is La : 1,5 L : bipy : 2775 H_2O . Heating this mixture in a Teflon-lined acid digestion bomb at 180 °C for 4 days, followed by cooling to room temperature result in a mixture of crystalline powder of La-RPF4- α and colourless large crystals of La-RPF4- γ . All attempts to obtain La-RPF4- γ as a pure phase were not successful. It's worth noting that if we use the synthesis conditions that lead to the obtaining of RPF4- α , but augmenting the time of the reaction (up to 5 days), a mixture of RPF4- α and RPF4- β is obtained.

The RPF4- α phase can also be obtained under different synthesis conditions. With a mixture of molar composition Ln : 1,5 L : 2500 H_2O heated at 160 °C for 18 hours result in the pure RPF4- α obtained as fine microcrystalline powder. When using a mixture of solvents the size of the crystals could be improved. With a molar composition of Ln : 1,5 L : 2500 H_2O : 885 acetone, small needle like crystals were obtained. These crystals, however, were not of enough quality for X-ray crystallography except for the case of lanthanum. A single crystal suitable for X-ray diffraction was obtained and used to solve the crystal structure. The data collection was carried out in Kappa Apex II diffractometer. Crystals of the monoclinic polymorph La-RPF4- β and orthorhombic polymorph La-RPF4- γ are quite good and the structures can be easily determined. The data collections were carried out in a SMART



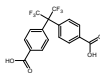
diffractometer. The main details of the data collection are given in table III.1.01.

Before start describing the procedure of the crystal structure solution for RPF4- α , it's worth giving some details about the Zn-MOF previously prepared with this same ligand. This information needed to be taken into account for the structure solution of the RPF4- α compound. This Zn-MOF crystallizes in the hexagonal space group $P6_422$ with cell parameters $a = b = 21.232 \text{ \AA}$ and $c = 7.708 \text{ \AA}$, and cell volume = 3009.4 \AA^3 . During the first attempts to solve the structure of RPF4- α , the same cell parameters were obtained. In fact RPF4- α polymorph owns an almost identical XRPD pattern than that of Zn-MOF. This made us think that the new series of Ln-hfipbb MOFs were isostructural to the Zn-MOF. However, the attempts to solve the crystal structure with this unit cell were unsuccessful. An analyses of the diffraction pattern gave us another hexagonal cell unit with double a and b parameters and quadruple volume. This fact makes us believe in some twin problem in this structure. A careful study on the X-ray diffraction spectra spots led us to think of the kind of twin that usually accompanies the NiSr hexagonal perovskites⁵, and to start calculating a possible matrix to apply to the initial fake parameters.

Only by applying the matrix

$$\begin{vmatrix} 0 & 0 & 1 \\ 1 & 0 & 0 \\ 1 & 2 & 0 \end{vmatrix}$$

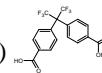
to this latest hexagonal cell, the structure could be solved in the orthorhombic space, with final cell parameter $a = 7.791 \text{ \AA}$, $b = 21.37 \text{ \AA}$, $c = 37.00 \text{ \AA}$ and volume = 6160.2 \AA^3 , in the space group $Pnan$. Subsequently the presence of three orthorhombic components in the twinned crystal was confirmed. and assigned 872 reflections were assigned into three domains⁶ (662:106:103). The second and third domains appear rotated from the first by 180° about the



III.1 RPF4 Rare earth + 4,4'-(hexafluoroisopropylidene)bis(benzoic acid)

Table III.1.01: Crystallographic and refinement data for the La-RPF4 crystals.

Identification code	La-RPF4- α	La-RPF4- β	La-RPF4- β
Empirical formula	$C_{51}H_{24}F_{18}La_2O_{12} [La_2(C_{17}H_8F_6O_4)_3]$		
Formula weight	1448.52		
Temperature	296(2) K		
Wavelength	0.71073 Å		
Crystal system, space group	<i>Orthorhombic, Pnan</i>	<i>Monoclinic, P2₁/n</i>	<i>Orthorhombic, C222₁</i>
Unit cell dimensions	$a = 7.7910(9)$ Å $\alpha = 90^\circ$ $b = 21.372(3)$ Å $\beta = 90^\circ$ $c = 36.997(3)$ Å $\gamma = 90^\circ$	$a = 7.5600(3)$ Å $\alpha = 90^\circ$ $b = 25.8914(1)$ Å $\beta = 90.8540(1)^\circ$ $c = 29.6752(1)$ Å $\gamma = 90^\circ$	$a = 7.4919(8)$ Å $\alpha = 90^\circ$ $b = 31.083(3)$ Å $\beta = 90^\circ$ $c = 22.483(2)$ Å $\gamma = 90^\circ$
Volume	$6160.2(13)$ Å ³	$5583.6(4)$ Å ³	$5235.7(10)$ Å ³
Z, Calculated density	4, 1.562 Mg/m ³	4, 1.723 Mg/m ³	4, 1.838 Mg/m ³
Absorption coefficient	1.057 mm ⁻¹	1.628 mm ⁻¹	1.736 mm ⁻¹
F(000)	2808	2808	2808
Crystal size	0.06 x 0.04 x 0.02 mm	0.20 x 0.10 x 0.06 mm	0.12 x 0.10 x 0.07
Theta range for data collection	1.10 to 28.62° 0<=h<=10	1.07 to 25.68° -9<=h<=9	1.31 to 26.48° -9<=h<=9
Limiting indices	0<=k<=28 0<=l<=48	-30<=k<=30 -35<=l<=36	-38<=k<=38 -27<=l<=28
Reflections collected / unique	22622 / 7622	36747 / 10356	21371 / 5360
Completeness to	$\theta = 25^\circ = 99.6\%$	$\theta = 26.02^\circ = 97.5\%$	$\theta = 26.48^\circ = 99.0\%$
Absorption correction	Semi-empirical from equivalents		
Max. and min. transmission	0.9711 and 0.9167	0.9087 and 0.7367	0.8882 and 0.8188
Refinement method	Full-matrix least-squares on F ²		
Data / restraints / parameters	22866 / 160 / 293	10356 / 355 / 748	5360 / 0 / 376
Goodness-of-fit on F ²	0.863	1.130	1.264
Final R indices [I>2 σ (I)]	R ₁ = 0.1385, wR ₂ = 0.2388	R ₁ = 0.0892, wR ₂ = 0.1691	R ₁ = 0.0898, wR ₂ = 0.2019
R indices (all data)	R ₁ = 0.4358, wR ₂ = 0.3620	R ₁ = 0.1547, wR ₂ = 0.1979	R ₁ = 0.0973, wR ₂ = 0.2114
Largest diff. peak and hole	2.454 and -3.197 e.Å ⁻³	0.946 and -2.283 e.Å ⁻³	2.050 and -5.090 e.Å ⁻³



real axis $[0 -1 1]$ and $[0 -1 -1/3]$, respectively. With this information, the whole data were integrated using SAINT⁷ which allows to split the overlapped reflections into their different components. The scaling and absorption procedure were carried out with TWINABS⁸. Two different hkl files are generated. The structure was solved using the detwinned HKLF4 format file, and it was refined with the twinned HKLF5 file and the two BASF parameters refined to a final composition of the twins equal to 47%:29%:24%.

Crystal structure description

Upon determining the crystal structures, the composition of the three compounds was found to be $[\text{La}_2(\text{C}_{17}\text{H}_8\text{F}_6\text{O}_4)_3]$.

In La-RPF4- α and La-RPF4- γ , the asymmetric unit comprises one half of the formula, while in La-RPF4- β there are two independent La atoms, and therefore one molecular formula per unit cell (figure III.1.02). In all cases the La ions are nine-coordinated forming distorted tricapped trigonal prims. (table III.1.02, figure III.1.03).

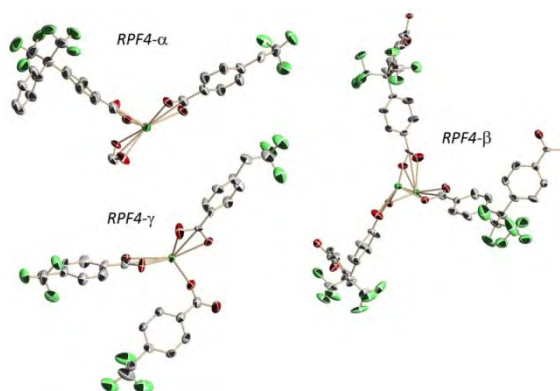
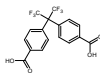


Figure III.1.02: ORTEP representation (50% probability) of the asymmetric units of the three La-RPF4 polymorphs. Green: La atoms. Red: O atoms. Grey: C atoms. Light green: F atoms.



III.1 RPF4 Rare earth + 4,4'-(hexafluoroisopropylidene)bis(benzoic acid)

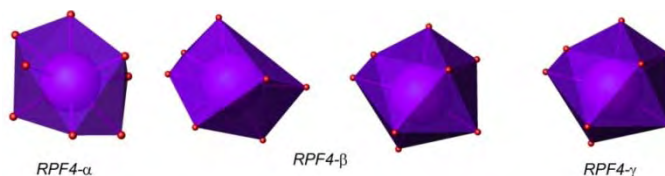
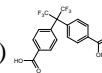


Figure III.1.03: The four coordination polyhedra of the three RPF4 polymorphs. The four are distorted tricapped trigonal prisms.

Table III.1.02: Interatomic distances in the coordination spheres of the metals in the La-RPF4 compound.

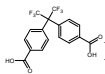
<i>La-RPF4-α</i>		<i>La-RPF4-β</i>			<i>La-RPF4-γ</i>		
Bond	Distance (Å)	Bond	Distance (Å)	Bond	Distance (Å)	Bond	Distance (Å)
La(1)-O(1)	2.443(12)	La(1)-O(1)	2.501(8)	La(2)-O(2)	2.536(7)	La(1)-O(1)	2.521(10)
La(1)-O(2)	2.712(13)	La(1)-O(2)	2.658(7)	La(2)-O(3)	2.539(7)	La(1)-O(1) ²	2.675(11)
La(1)-O(2) ¹	2.456(14)	La(1)-O(4) ¹	2.501(7)	La(2)-O(4)	2.612(7)	La(1)-O(2) ²	2.545(12)
La(1)-O(3)	2.769(11)	La(1)-O(6)	2.491(7)	La(2)-O(5)	2.568(8)	La(1)-O(3)	2.533(11)
La(1)-O(3) ²	2.471(12)	La(1)-O(7)	2.526(8)	La(2)-O(6)	2.677(7)	La(1)-O(4)	2.878(11)
La(1)-O(4)	2.467(11)	La(1)-O(8)	2.803(7)	La(2)-O(8) ¹	2.487(8)	La(1)-O(4) ¹	2.505(11)
La(1)-O(5)	2.560(12)	La(1)-O(9)	2.499(8)	La(2)-O(10)	2.470(7)	La(1)-O(5)	2.578(10)
La(1)-O(6)	2.668(11)	La(1)-O(10)	2.622(7)	La(2)-O(12)	2.616(7)	La(1)-O(6)	2.637(10)
La(1)-O(6) ¹	2.443(12)	La(1)-O(12) ¹	2.473(7)	La(2)-O(11)	2.500(8)	La(1)-O(6) ²	2.505(10)
Symmetry operator to generate equivalent positions: 1: x-1/2,-y+1,z 2: x+1/2,-y+1,z		Symmetry operator to generate equivalent positions: 1: x+1,y,z			Symmetry operator to generate equivalent positions: 1: x-1/2,-y+1/2,-z 2: x+1/2,-y+1/2,-z		

In RPF4- α phase, the hfpbb linker coordinates to four R^{3+} ions in a $\eta^3\mu_2$ way. The polyhedra are disposed forming chains along the a axis by sharing faces, via the μ_2 oxygen atoms. The organic molecules link these chains giving rise to a 3D structure, with three parallel tunnels down the a axis. All these channels are empty and have a cylindrical free void space with a window of diameters 5.2-5.5 Å, as computed by Platon⁹ (cavity routine). Although the structure looks quite similar to that of the previously mentioned zinc MOF¹, they have networks with different topologies. In the Zn-MOF, chains of metals are also found, in this case formed by the tetrahedral Zn atoms, and disposed around a helical axis. This network is uninodal 4-connected (point symbol ($6^5.8$)), with the tetraconnected nodes linked by the ligands always in



a crossing way. The network of the RPF4- α compounds is a uninodal 5-connected net. Each node/La-ion is directly connected to other two La ions of the same chain via bridging carboxylate oxygen atoms of the ligand, and also to other three La ions from different chains via the whole ligand as linkers (figure III.1.04). The result is a new net with short symbol ($4^2.6^8$). This net that had been theoretically predicted and named hxg-d-5-Imma in a search for net relations¹⁰, has been for the first time experimentally obtained with this work. Looking again at the two structures, the RPF4- α and that of Zn-MOF, it can be seen that each chain is connected to other three ones, through two ligand molecules in each connection, giving rise to square shaped channels. The difference between the two structures lies in the way these connections are made. Thus, in the Zn compound all metallic chains are connected through the ligand anions in a crossing way; in the rare earth compounds, however, these connections are established in two different manners: two of them in a crossing way (for the channels of A-type), and one in a parallel way (for the channels of B-type) (figure III.1.05). The different distribution of the A and B channels breaks the hexagonal symmetry and explains the preference for triple twins. Due to the bent geometry of the ligand, the fluorine atoms are all pointing into the C hexagonal channels. Consequently, the walls of the hexagonal tunnel are formed by CF₃-groups giving rise to hydrophobic fluorolined Teflon-like channels.

The two other polymorphs (figure III.1.06) exhibit a more dense structure, with smaller cell volumes than the first structure: RPF4- α has a cell volume of 6160.2(13) Å³, with a 23.8% of free volume, while those for RPF4- β and RPF4- γ are 5583.6(4) Å³ and 5235.7(10) Å³, with a free volume of 15.9% and 3.7%. As in RPF4- α , in RPF4- β and RPF4- γ chains formed by sharing faces La polyhedra are also found. Their networks can be also simplified as rods of La atoms, running along the *a* axis. The ligand is then considered as a linker between two La nodes from different chains. Opposite to RPF4- α , where all



III.1 RPF4 Rare earth + 4,4'-(hexafluoroisopropylidene)bis(benzoic acid)

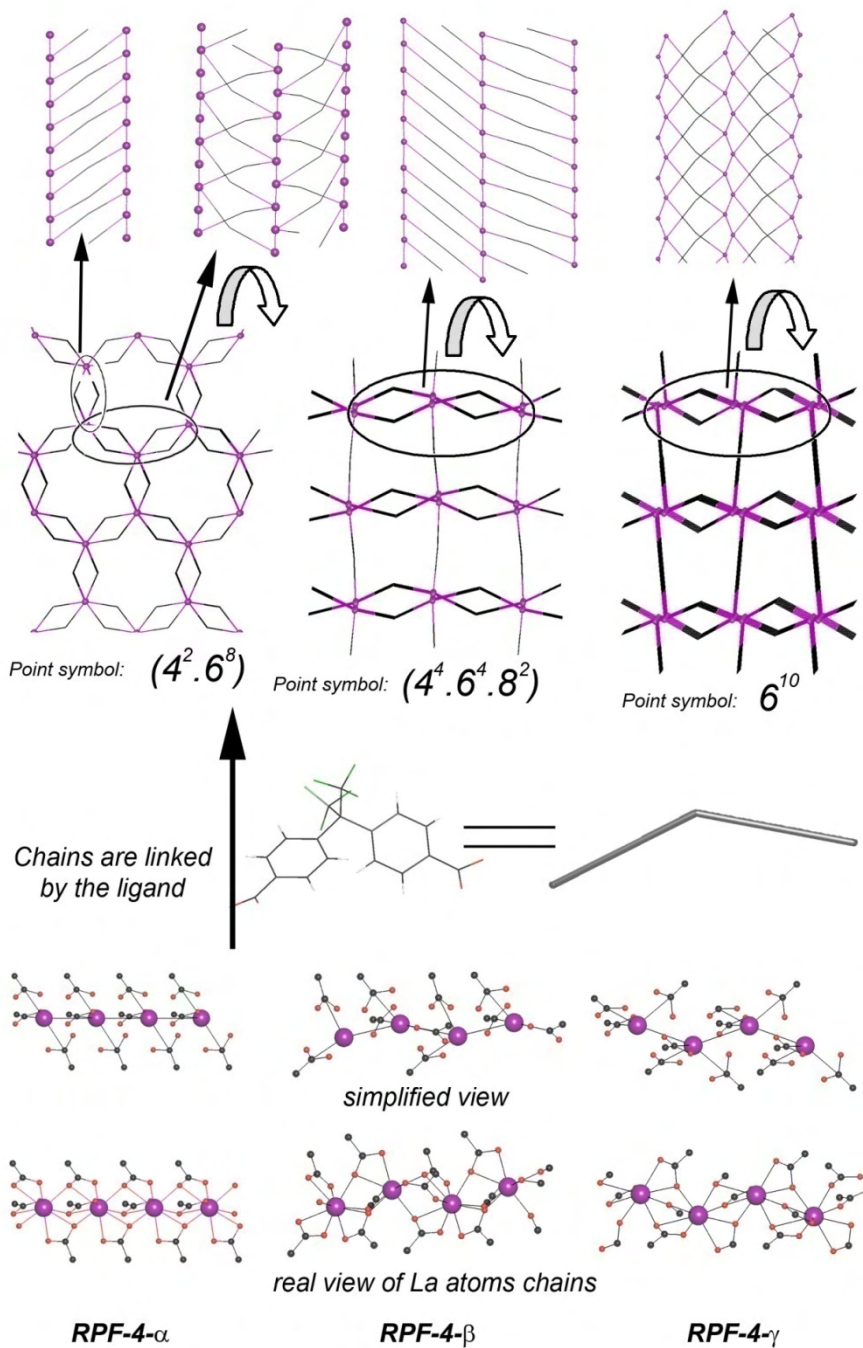


Figure III.1. 04: Topological analysis of the three RPF-4 polymorphs.

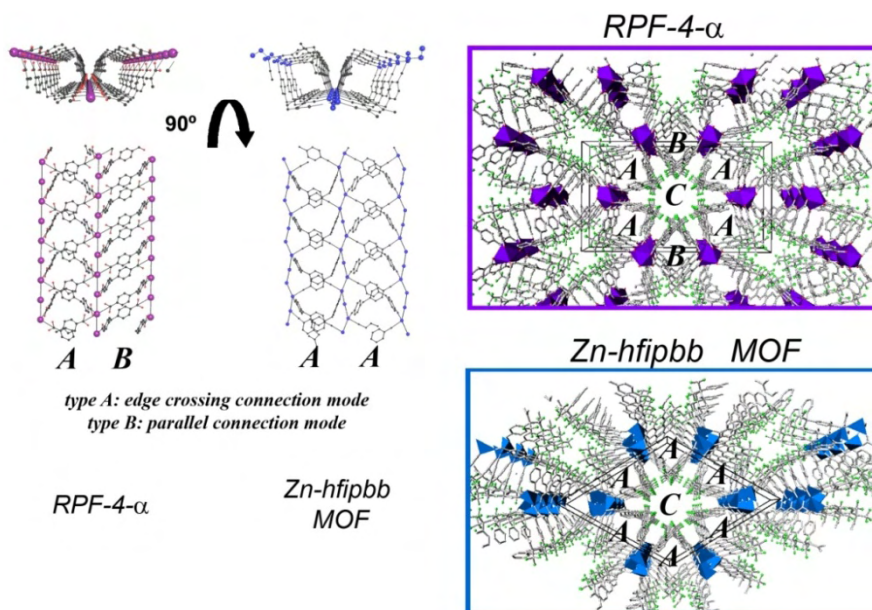
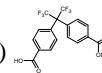


Figure III.1.05: A comparison of the two Zn-MOF and RPF4- α structures. Despite both look quite similar, the difference in the walls of the channels makes them to have different types of networks.

the interchains connections are made through two linkers, above and below the chains, in RPF4- β and RPF4- γ , there is a connection between chains which is made only by one ligand: in RPF4- β along the b axis, and in RPF4- γ along the c axis. The joining along the remaining direction is made by two linkers, above and below the chains. However, this connection is different in each case: in RPF4- β , they are all made in a parallel mode, with no edge-crossing presence, while in RPF4- γ , they are all in an edge-crossing manner (figure III.1.04 top). As a result, these two networks, also uninodal pentacoordinated, have different unprecedented topologies with a point symbol ($4^4.6^4.8^2$) for RPF4- β and (6^{10}) for RPF4- γ .

The three nets can also be compared in other way, describing layers of square (more or less deformed) channels, parallel to the ab plane for the α - and the β -, and to the ac plane in the case of γ -polymorph (figure III.1.07). Thus, both in α - and γ -polymorphs the layers are formed by crossed ligands; in the γ -polymorph, the layers stack on 010 joined by the remaining ligand; in the α -

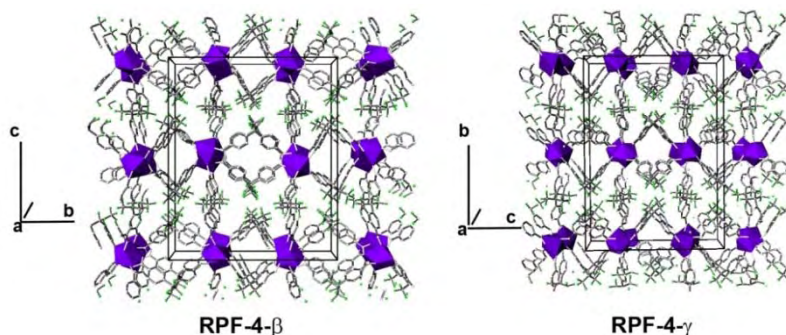
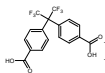


Figure III.1.06: Perspective view of the RPF4- β and RPF4- γ polymorphs.

polymorph the layers are undulated, stacking on 001 and joined by the no crossing ligands. Actually, in this α -polymorph, we can also find the undulated layers containing the square channels by rotating the cell $\pm 60^\circ$ over the a axis, but then the distribution of the crossing and no crossing ligands is different, which may be the cause of the triple twinning in this structure.

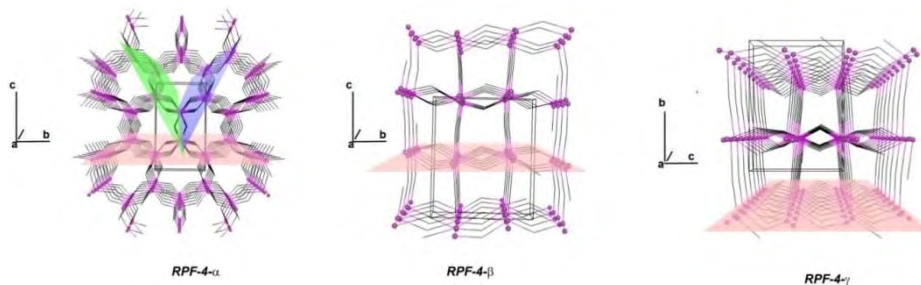
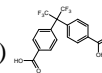


Figure III.1.07: Comparison of the three simplified networks. Layers containing the La atoms and the square channels are represented. In the case of the α -polymorph, there are two other possible orientations for these planes (shown with different colors), which is the cause of the twinning.

Table III.1.01.03 Point symbol, Vertex symbol, and Coordination sequence for each RPF4 polymorph network.

Polymorph	Point symbol	Vertex symbol	Coordination sequence
α	$(4^2.6^8)$	[4.4.6.6.6 ₂ .6 ₂ .6 ₄ .6 ₄ .6 ₄ .6 ₆]	(5,18,45,82,128,190,262,340,437,544)
β	$(4^4.6^4.8^2)$	[4.4.4.4.6.6.6.8 ₁₃ .8 ₁₃ .*]	(5,16,45,96,169,264,377,508,657,824)
γ	(6^{10})	[6 ₃ .6 ₃ .6 ₃ .6 ₃ .6 ₃ .6 ₃ .6 ₃ .6 ₃ .6 ₃ .6 ₃]	(5,20,52,112,188,284,391,516,653,808)



Characterization

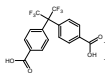
Among the three RPF4 polymorphs, the RPF4- α phase is that with most interesting structural features. The optimization of the synthesis procedure was focused to the obtaining of the α -polymorph as pure phase, to be then characterized, and its properties evaluated. The results presented from now on are referred exclusively to this phase compounds.

Powder X-ray diffraction

This phase was obtained with other rare-earth elements (Y, La, Ce, Pr, Nd, Sm, Eu, Gd, Tb, Dy, Ho, Er, Yb). A Rietveld refinement of the X-ray synchrotron data for the La compound was carried out, confirming the goodness of the solution obtained with the refinement of the twinned single crystal, and also demonstrating the purity of the prepared compound. All other compounds were found to be isostructural, and the Rietveld refinement with laboratory X-ray data were carried out too. The results shown in figure III.1.08 demonstrate the purity of all the compounds prepared. In figure III.1.09 the cell volume obtained from the refined parameters is represented, showing the variation in function of the radii of the rare earth element employed.

Elemental and thermal analyses

The RPF4- α compounds are thermally stable. The TG curves (figure III.1.10) show a similar thermal behavior for all series of compounds. The decomposition of the products starts at ~ 450 °C. Small mass loss are appreciated in the curves at low temperatures, which are attributed to the loss of adsorbed solvent molecules, present inside the channels, which is in concordance with the elemental analysis data. The experimental values (table III.1.04) are slightly higher than those expected for the empty framework,



III.1 RPF4 Rare earth + 4,4'-(hexafluoroisopropylidene)bis(benzoic acid)

indicating that solvent water and acetone molecules are present inside the channels.

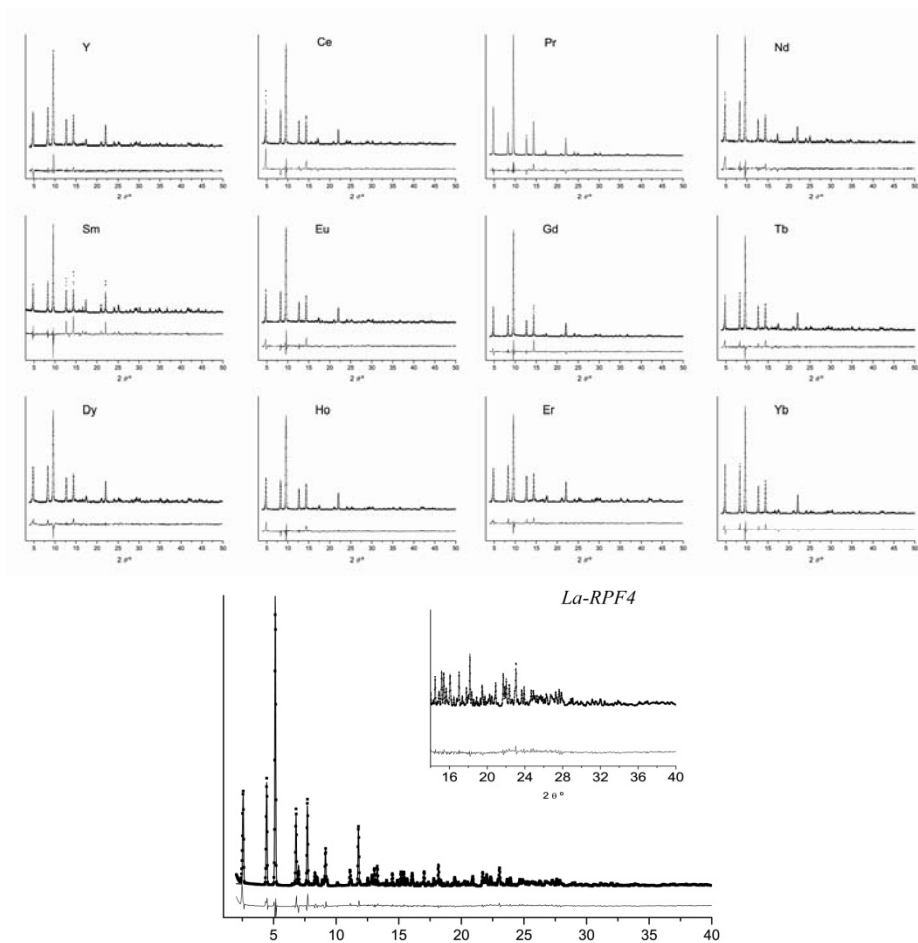


Figure III.1.08: Rietveld refinements for all the RPF4- α compounds, showing the experimental (dots) simulated (line) and difference patterns. For the refinement of La-RPF4- α , synchrotron radiation was employed. For the rest of the series, conventional laboratory X-ray data were used.

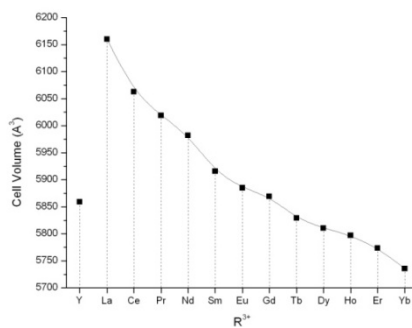
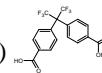


Figure III.1.09: Variation of the cell volume for each RPF4- α compound. The values of the cell volume are those obtained from the Rietveld refinements.

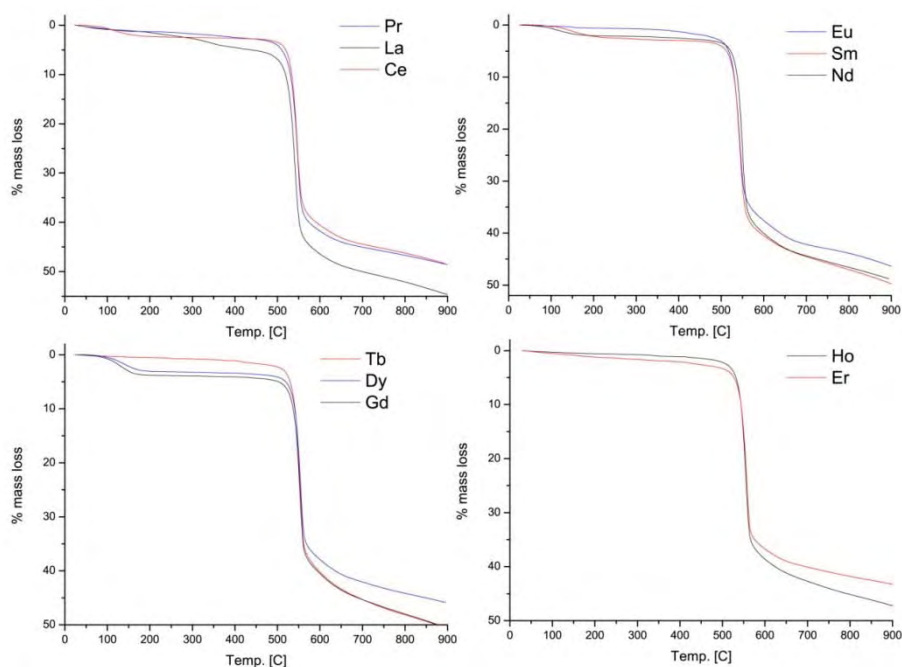
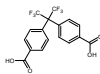


Figure III.1.10: TG curves of the RPF4- α compounds.

Table III.1.04: Experimental and calculated elemental analyses values for the RPF4- α compounds.

	R ³⁺	Y	La	Ce	Pr	Nd	Sm	Eu	Gd	Tb	Dy	Ho	Er	Yb
% C	Calc.	41.69	39.03	38.97	38.93	38.77	38.47	38.39	38.14	38.06	37.89	37.78	38.93	38.94
	Exp.	41.51	41.05	42.60	41.53	42.26	41.56	40.27	42.11	40.35	41.79	40.16	41.53	37.40
% H	Calc.	1.65	1.55	1.54	1.54	1.54	1.52	1.52	1.51	1.83	1.50	1.50	1.54	1.48
	Exp.	2.18	2.20	1.88	1.99	1.85	2.07	1.75	2.02	1.51	1.98	1.86	1.99	1.91

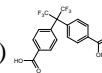


Evaluation of properties

Photoluminescence

As it was mentioned in the introduction section, the rare earth elements have interesting optical properties, and some lanthanide compounds exhibit luminescence coming from the f-f electronic transitions in the rare earth atoms. However, the extinction effects, which are due to high concentration of active cations in most of Ln-based solid compounds, have forced preparation of their non-active cations analogues, like yttrium, doped with active Ln cations. Another factor with negative influence on the Rare-Earth compounds emission is the presence of O–H bonds in the matrix, due to a vibrational energy transfer to water molecules^{11, 12}. In order to study the luminescence properties of these materials for possible future applications in optical devices, it is important to obtain water- and OH-free frameworks, in which long linkers provide enough separations between rare-earth cations. These two premises are true in the RPF4- α compounds: no water or hydroxyl groups are present in the coordination sphere of the Ln atoms, avoiding consequently the possible deactivation of the activated state of the rare-earth by transferring to the vibrational energy of the O-H bond. Besides, the organic linkers are long enough to separate the metallic atoms in two directions, at distances around 12.5 Å. In addition, the emission of the ligand may be used as the exciting light for the rare earth or, even, may directly transfer the energy to the Ln in a light emitting device (LED). Therefore, a photoluminescence study has been carried out with the compounds that include optically active atoms.

The emission and excitation spectra of the H₂hfipbb molecules have been obtained at room temperature from chloroform solution of H₂hfipbb, and from powder pressed into a pellet. Figure III.1.11 shows the emission of the molecule when excited at the 285 nm band of the absorption spectrum. The emission spectra for both, dissolution and pellet, are identical. The wide gap



of the molecules allows, in principle, to locate, in its transparency region, the localized levels of rare earths ions in order to obtain light of the desired wavelength. The wide emission of the molecules in the near UV (300-400 nm) may be transferred, radiatively or not, to the active ions (the rare earth) which present 4f-4f transitions in this energy range.

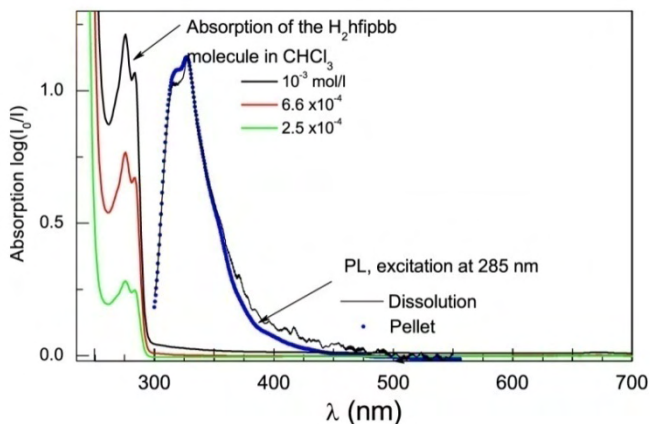
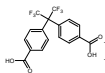


Figure III.1.11 Optical absorption of solutions of $H_2hfipbb$ for concentrations between 10^{-3} to 10^{-5} mol/l in chloroform. The solvent contribution has been subtracted. Photoluminescence of $H_2hfipbb$ in solution (line) and a pellet (dots). The excitation wavelength is 285 nm. The spectrum corresponding to the solution has been normalized to the pellet maximum.

For visible laser light excitation a microscope is used to select one single crystal, but, since the transmittance of the microscope optics is almost zero below 365 nm, the UV laser excitation (364 nm) is guided by external mirrors. In this case the spot of the incident light is much larger than the crystal size and the tested density varies strongly. It is therefore not possible to compare the intensities from different samples. Samples with a La matrix, doped with a small amount of optically active elements were prepared. A 95 % of lanthanum and a 5 % of Eu, Tb or Dy were employed, and the compounds are isostructural. These samples represent the diluted case where no concentration quenching of the luminescence is expected. In figure III.1.12 the photoluminescence of these samples is present, with the spectra normalized to the 380 nm value. The broad emission of the linking molecule



centered on 450 nm, when exciting at 364 nm, is detected in all samples. The 4f emissions of the rare earth ions are detected which cover the whole visible region, therefore, by combining them in the adequate ratio in the same crystal in principle it should be possible to obtain any color.

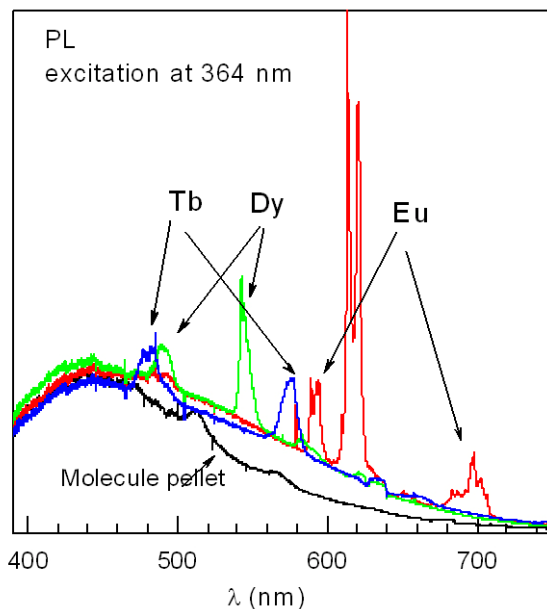


Figure III.1.12: Photoluminescence of crystals with 95% of La and 5% of Eu, Tb or Dy under laser excitation at 364 nm and room temperature. The arrows indicate the 4f transitions of the different rare-earth ions. The photoluminescence due to the ligand pellet is also presented. The spectra have been normalized at 380 nm.

When the excitation is far below the absorption of the ligand (454.4 nm in figure III.1.13), the broad background is very weak. In the present case the Eu compound shows the characteristic emission of Eu^{+3} in a low symmetry site where all the levels are non-degenerated. Tb and Dy ions also exhibit efficient emission in the blue to yellow wavelengths. The Eu, Dy and Tb crystal field transitions observed in the diluted samples are identified in figure III.1.13. The bands for Dy and Tb compounds are broad because of the splitting of both multiplets participating in the emission.

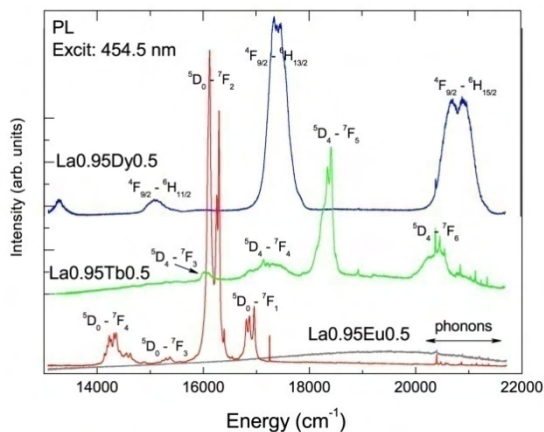
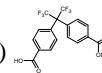


Figure III.1. 13: Photoluminescence under 454.4 nm excitation of the diluted crystals (95% La and 5% Dy, Tb or Eu). The spectra have been vertically shifted. The grey trace corresponds to the ligand molecule pellet. The very narrow peaks in the high energy region (close to the excitation energy) correspond to the phonons.

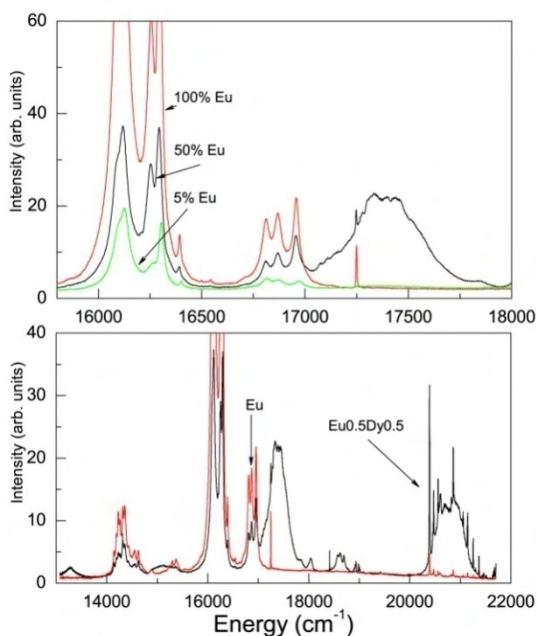
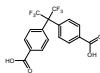


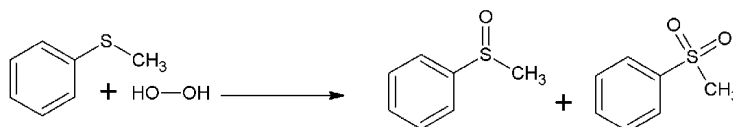
Figure III.1.14: Photoluminescence under 454.4 nm excitation for materials with different Eu content: Upper graph: visible Eu^{3+} emission range for three samples. Lower graph: Eu and Eu0.5Dy0.5 spectra evidencing the emission from both rare earth ions.



Finally, we have checked that in the case of Eu compounds there are no indications of quenching of the luminescence when increasing the Eu concentration. This would be useful in a LED device allowing an increase in the efficiency by increasing the density of active ions. In the upper part of figure III.1.14, the visible region of the Eu^{3+} emission of crystals containing 5%, 50% and 100% Eu is presented. The intensity of the different samples cannot be exactly compared since the sizes of the crystals are different and the tested crystal volumes are not identical. Nevertheless this allows concluding reliably that there is no concentration quenching of the luminescence, which is surely due to the structural features of the framework. Also, samples with 50% of Eu and 50% of Dy were prepared. The combination of Eu and Dy ions (lower part of figure III.1.14) may be of great interest for white emitters since they combine emissions in the blue (21000 cm^{-1}), yellow (17500 cm^{-1}) and red (16200 cm^{-1}).

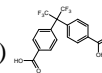
Catalytic experiments

Another dimension in exploring the obtained materials properties lies in the area of heterogeneous catalysis. Generally, Ln compounds are increasingly being used as catalysts in various organic transformations. The new materials obtained offer a possibility of combining the catalytic properties of rare-earth ions with the advantages of a heterogeneous catalyst. The capability of the RPF4- α compounds as redox catalysts has been tested in the reaction of oxidation of sulfides (scheme 01).



Scheme III.1.01: Oxidation of methyl phenyl sulfide with hydrogen peroxide to give the corresponding sulfoxide and the overoxidized sulfone.

In a general procedure, to a suspension containing 0.01 mmol of the catalyst in 5 ml of acetonitrile was added 1 mmol of substrate and then, 3 equivalents



of the oxidant (H_2O_2 30%) were added dropwise, under stirring. The catalysts were obtained from a mixture of composition Ln : 1,5 L : 2500 H_2O , and were used as prepared. Samples were taken at regular times and analyzed by gas chromatography. With this procedure, no activity was found after 8 hours of reactions. However, if previously an activation process of the catalysts is carried out, the reaction goes. Thus, if a suspension containing the as prepared catalysts was stirred overnight in presence of 3 equivalents of H_2O_2 , and after this the substrate and fresh oxidant was added, the reaction goes, being the methyl phenyl sulfide oxidized to sulfoxide or sulfone. This fact indicates that the active intermediate species is formed during the activation period. From a reaction mechanism viewpoint, the sulfoxidation reaction has to go through the corresponding peroxo species, as it happens in the hydrolysis of phosphodiester¹³ and RNA¹⁴, catalyzed by peroxide Ln complexes formed in Ln - H_2O_2 mixtures. In order to confirm the presence of this active species, IR spectrum of the catalyst was made before and after the activation period (figure III.1.15). A comparison of the spectra reveals the appearance of new bands at 1090 and 1448 cm^{-1} , which could be assigned to the new Ln - O bond in these active peroxide species. This same behavior has been later observed when employing different rare earth polymeric frameworks, allowing the proposal of a mechanism for the sulfide oxidation¹⁵.

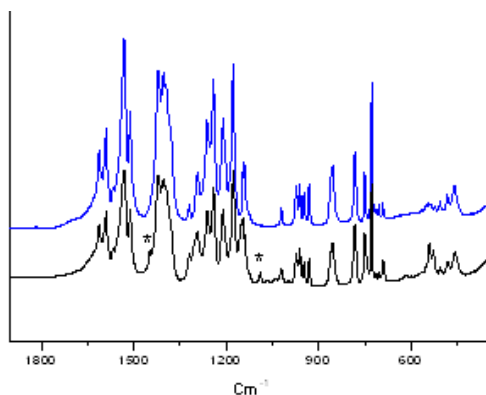
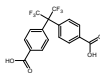


Figure III.1.15: Infrared spectra of the RPF-4- α catalyst before (blue) and after (black) the catalytic reaction. An asterisk indicates the changes in the spectra.



The same reaction was carried out with catalysts prepared with different metal atoms. Differences both in reactivity and selectivity are observed. Table III.1.05 shows that the activity increases in the series from lanthanum to ytterbium, while the selectivity goes in the opposite direction.

Table III.1.05: Values of conversion and selectivity employing different RPF4 compounds as heterogeneous catalyst in the oxidation of sulfides.

Rare-earth	t(min.)	Conv. (%)	% Sel. Sulfoxide	TOF(h ⁻¹)
Yb	180	92	30	60
Er	300	85	52	32
Gd	300	82	60	48
Sm	300	78	72	22
Nd	300	80	70	20
La	300	80	75	18

a = turnover frequency expressed as mol substrate converted per mol of active centre.

After the reaction cycles, the integrity of the framework was checked by means of powder X-ray diffraction. No change was observed in the structures, as it can be seen in figure III.1.16.

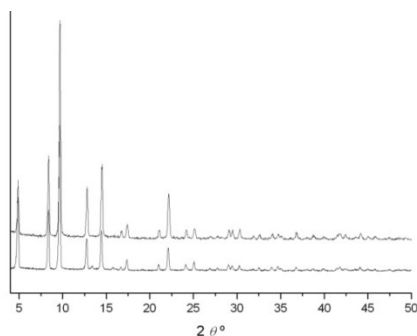


Figure III.1.16: Comparison of the X-ray powder pattern of the catalyst before (bottom) and after (top) the reaction cycle.

The results obtained in this chapter are collected in the papers n° 1 and 2 in the part VI of this report. They have been published in *Crystal Growth and Design*, 2008, 8, 378, and in *Inorganic Chemistry*, 2009, in press. Another paper with more optical and magnetic properties is currently being prepared.



2. Rare earth + Anthraquinone-2,6-disulfonate: RPF5, RPF6, RPF7 and LRH

Introduction:

In the preparation of Metal-organic frameworks, carboxylate derivatives are the most employed type of ligands. As it was explained in the introduction section, the chemistry of sulfonate derivatives still remains less studied within the field of coordination polymers^{16, 17}. There are few examples of compounds with sulfonate derivatives ligands¹⁸⁻²⁰, and many of them with mixed ligands, with another type of functional group apart from the sulfonate²¹.

In our group, we started to evaluate the possibilities that arenedisulfonate ligands offer in the construction of extended nets. Thus, with transition metal elements, nickel and cobalt, we obtained five compounds employing 1,5-naphthalendisulfonate and 2,6-naphthalenedisulfonate as ligands²². Four of these compounds have direct coordination of the sulfonate group to the metals. Three of them are complexes with supramolecular structures built up through hydrogen bonds and π - π stacking interactions and one of them is a monodimensional polymeric framework, the first reported with cobalt and a sulfonate ligand. In the case of transition metals, the presence of additional amine derivatives ligands results to be necessary to ease the coordination of the sulfonate group to the metal atoms. In the case of rare earth elements, and with the same naphthalenedisulfonate ligands, we prepared three families of compounds, which have polymeric frameworks²³. These three families demonstrated to be very robust compounds, with a variety of possible applications thanks to the incorporation of rare earth elements into the frameworks. Due to these good results, we proposed to extend the study on the preparation of rare-earth polymeric framework with arenedisulfonates ligands. This chapter deals with the utilization of anthraquinone-2,6-

disulfonate anion (2,6-AQDS, figure III.2.01) in the construction of rare-earth coordination polymers. Three families of polymeric framework, named RPF5, RPF6 and RPF7, and a family of layered hydroxides, named LRHs, have been obtained. Their structural characterization, together with an evaluation of their catalytic properties is here given. The structure of RPF5 was prepared with Yb as metal centre; RPF6 with Nd, Sm and Dy; RPF7 with La and Pr. The family of layered rare-earth hydroxides, LRHs, was prepared with Dy, Ho, Er and Yb.

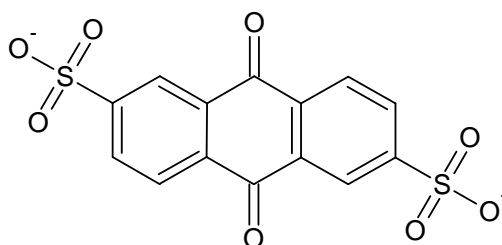


Figure III.2.01: The anthraquinone-2,6-disulfonate dianion.

Experimental

Synthesis

The synthesis conditions for all the compounds are quite similar, and the procedure is as described in chapter II.1, experimental section. In the case of the RPF compounds, the cation employed is decisive for the obtaining of one or another structural type. In the case of the LRH family, the correct choice of the pH controlling reagent is decisive to obtain them pure, as it is explained below. The optimized synthesis conditions for each compound are summarized in the table III.2.01



Table III.2 01: Optimized synthesis conditions

Compound	Molar composition of initial mixture	Temperature	pH	Time (h.)
Yb-RPF5	Yb ³⁺ : 2,6-AQDS ²⁻ : OH ⁻ : 1500 H ₂ O	175 °C	6.5	18
Dy-RPF6	Dy ³⁺ : 2,6-AQDS ²⁻ : OH ⁻ : 1500 H ₂ O	175 °C	6.5	18
Sm-RPF6	Sm ³⁺ : 2,6-AQDS ²⁻ : OH ⁻ : 1500 H ₂ O	175 °C	6.5	18
Nd-RPF6	Nd ³⁺ : 2,6-AQDS ²⁻ : OH ⁻ : 1500 H ₂ O	175 °C	6.5	18
Pr-RPF7	Pr ³⁺ : 2,6-AQDS ²⁻ : OH ⁻ : 1500 H ₂ O	175 °C	6.7	18
La-RPF7	La ³⁺ : 2,6-AQDS ²⁻ : OH ⁻ : 2500 H ₂ O	190 °C	6.9	18
Yb-LRH	4Yb ³⁺ : 2,6-AQDS ²⁻ : 9.5 Et ₃ N : 4000 H ₂ O	180 °C	6.5	18
Er-LRH	4Yb ³⁺ : 2,6-AQDS ²⁻ : 9.5 Et ₃ N : 4000 H ₂ O	180 °C	6.5	18
Ho-LRH	4Yb ³⁺ : 2,6-AQDS ²⁻ : 9.5 Et ₃ N : 4000 H ₂ O	180 °C	6.5	18
Dy-LRH	4Yb ³⁺ : 2,6-AQDS ²⁻ : 9.5 Et ₃ N : 4000 H ₂ O	180 °C	6.5	18

A 0.1 M solution of NaOH was used as a source of OH⁻. The Ln³⁺ cations were added as their corresponding hydrate nitrates. The AQDS²⁻ anion was added in form of its disodium salt. Commercial Et₃N was used as received.

Crystal structure determination

A suitable single crystal was carefully selected in each case. The crystal structure determinations were carried out as explained in chapter II.1, experimental section. The crystallographic and refinement data are found in tables III.2.02, III.2.04, III.2.08 and III.2.11. The RPF compounds crystallize as large single crystal, with the exception of Sm-RPF6, which was always obtained as microcrystalline powder, and crystals of good size could not be obtained. In the case of the LRH compounds, they crystallize as a fine crystalline powder, and only a few single crystals could be obtained for Dy and Yb LRH.

Following, the structural features and the characterization of each structural type are described.

RPF5 structural type

The Yb-RPF5 compound has a 3D structure, with the AQDS²⁻ anions coordinated to the Yb atoms. Its formula is [Yb(OH)(2,6-AQDS)(H₂O)] (figure III.2.02).

Table III.2. 02: Crystallographic and refinement data for Yb-RPF5

Identification code	Yb-RPF5
Empirical formula	$C_{14}H_9S_2YbO_{10}$
Formula weight	$[Yb (C_{14}H_9S_2O_8)(OH)(H_2O)]$ 574.37
Temperature	295(2) K
Wavelength	0.71073 Å
Crystal system, space group	Triclinic, <i>P</i> -1
Unit cell dimensions	$a = 7.3843(8) \text{ \AA}$ $a = 86.119(2)^\circ$ $b = 7.8665(8) \text{ \AA}$ $\beta = 86.097(2)^\circ$ $c = 13.737(1) \text{ \AA}$ $\gamma = 86.398(2)^\circ$
Volume	792.90 (15) Å ³
Z, Calculated density	2, 2.406 Mg/m ³
Absorption coefficient	6.219 mm ⁻¹
F(000)	550
Crystal size	0.20 x 0.15 x 0.10 mm
Theta range for data collection	1.49° to 28.27° -9<=h<=9
Limiting indices	-10<=k<=10 -17<=l<=17
Reflections collected / unique	7347/ 3717
Completeness to theta = 25.00°	98.5 %
Absorption correction	Semi-empirical from equivalents
Max. and min. transmission	0.5752 and 0.3693
Refinement method	Full-matrix least-squares on F ²
Data / restraints / parameters	3717 / 0 / 244
Goodness-of-fit on F ²	1.040
Final R indices [I>2σ(I)]	R ₁ = 0.00560, wR ₂ = 0.1291
R indices (all data)	R ₁ = 0.0678, wR ₂ = 0.1347
Largest diff. peak and hole	4.812 and -3.755 e.Å ⁻³

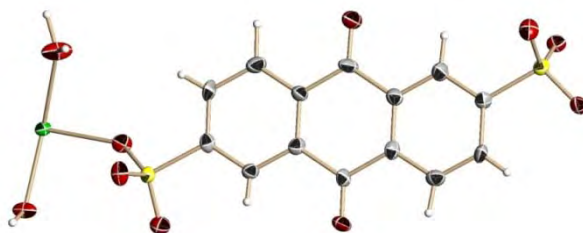


Figure III.2. 02: ORTEP drawing (50 % probability) of the asymmetric unit in Yb-RPF5. Green: Yb atom; red: O atoms; yellow: S atoms; grey: C atoms; white: H atoms

The lanthanide ion is heptacoordinated (table III.2.03) to two μ_2 -(OH) groups, one water molecule and four oxygen atoms, belonging to four different sulfonate groups in a YbO₇ monocapped trigonal prism (figure III.2.03).

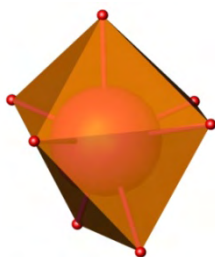


Figure III.2. 03: The coordination polyhedron in RPF5: a monocapped trigonal prism

Table III.2.03: Interatomic distances in the coordination sphere of Yb-RPF5

Bond	Distance (Å)
Yb(1)-O(2)	2.283(6)
Yb(1)-O(3)	2.299(6)
Yb(1)-O(5)	2.310(6)
Yb(1)-O(6)	2.282(6)
Yb(1)-O(9)	2.183(6)
Yb(1)-O(9) ¹	2.199(6)
Yb(1)-O(10)	2.325(7)
Yb(1)-Yb(1) ¹	3.5954(7)

Symmetry transformations used to generate equivalent atoms:

1: -x,-y+2,-z+1

Every two of these (YbO₇) polyhedra form Yb₂O₁₂ sharing edges dimeric units *via* two μ -OH⁻, which are isolated in the *b* direction and joined through S atoms of the sulfonate groups in the *a* direction. The SO₃ groups, with $\eta^2\mu_2$ coordination mode^{16, 17}, join the Yb₂(OH)₂ units, with the S atom acting as a bridge between every two dimeric units in a such way that an entirely inorganic layer is formed parallel to the *ab* plane (figure III.2.04, top). They are 10R (6Yb + 4S) containing layers with the coordinated water molecules pointing inside the rings. In the Yb-RPF-5 3D structure, the layers are connected along the *c* direction by $\eta^2\mu_2$ - $\eta^2\mu_2$ bonded AQDS²⁻ with a tilt angle of 66.27° between the *ab* plane, and that

involving the three aromatic rings (figure III.2.04, bottom left). These molecules are disposed along the [100] direction occupying two different position in the b axis, in an alternating configuration, and separated by 3.692 Å ($a/2$). Since the molecules in both position have the same slope trend, π - π stacking interactions between rings are not given. In figure III.2.04, bottom right, the projection of the bc plane is shown

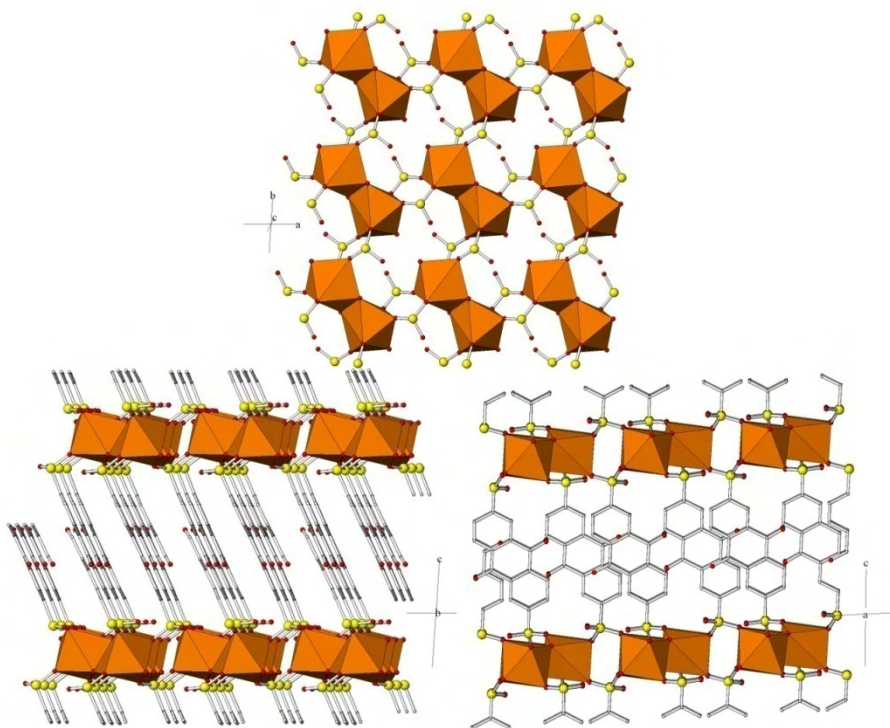


Figure III.2. 04: Top: representation of the inorganic layer formed in the RPF5 structure, projected in the ab plane. Bottom: a view of the structure along the b axis (left) and along the a axis (right)



Topological analysis:

From a topological point of view, we can describe an inorganic layer formed by the Yb atoms, where each atom is connected to the other three, one of them directly by hydroxyl groups and the other two through sulfonate bridges, resulting in a (6,3) honeycomb layer (figure III.2.05, top, left). The 3-dimensional real net, with these layers linked through the whole ligand, can be described as a binodal net, where the S atoms are 3 connected nodes, and the ytterbium atoms are 5 connected nodes (figure III.2.05, medium). This network, with point symbol $(4.6^2)_2(4^2.6^2.8^6)$ has maximum symmetry in the space group Fmmm and it is found with the code sqc707 in the EPINET database²⁴, where no previous examples of networks with this topology are described (figure III.2.05, top, right).

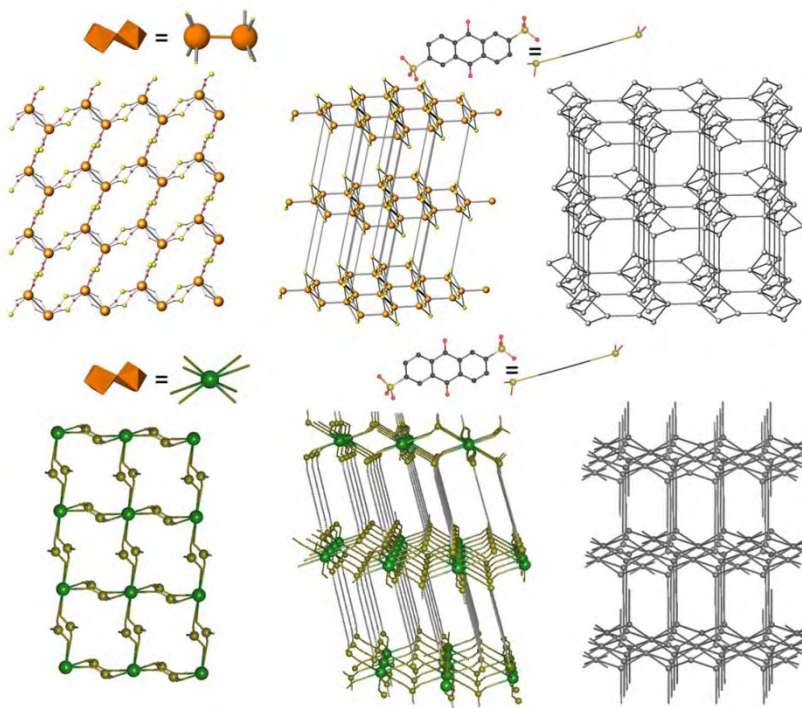


Figure III.2.05: Two possible topological simplifications of the RPF5 framework: Top: the 5- and 3-connected net, bottom: 8- and 3-connected net. For both top and bottom: Left: inorganic layer; middle: 3D real network; right: maximum symmetry embedding of the network

In an alternative depiction, we can consider the entire Yb_2OH_2 dimeric units as SBUs. Each SBU of this type is connected to eight SO_3 groups. In this depiction, the inorganic layer is a tetragonal one. The S atoms in the SO_3 groups are again 3 connected nodes, and as a result, the network is described as a binodal 3 connected and 8 connected net, with point symbol: $(4.6^2)_4(4^4.6^8.8^{12}.10^4)$, and maximum symmetry embedding in the space group $I4/mmm$. This network type can be found in the EPINET database with code sqc495.

X-ray powder diffraction:

The X-ray powder pattern of the compound indicates that the material can be obtained as a pure phase. In figure III.2.06 the Rietveld refinement of the X-ray powder pattern is shown.

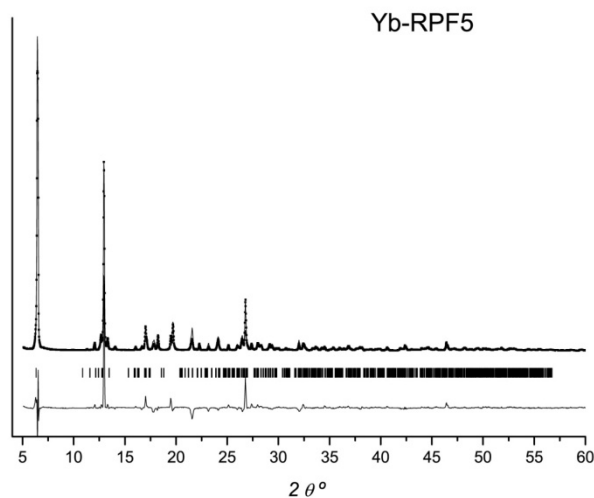


Figure III.2.06: The Rietveld refinement of the Yb-RPF5 compound, showing the experimental (dot) and simulated pattern (line), and the difference pattern.

Elemental analysis data: The chemical elemental analysis for Yb-RPF5 also confirms the purity of the sample prepared under the optimized conditions: %C, calculated 29.25 , found 28.90 ; %H, calculated 1.58 , found 1.57.



Thermogravimetric analysis: The thermogravimetric analysis carried out reveals that the framework remains without change until ~ 285 °C, temperature at which the only water molecule present in the structure is lost (mass loss: experimental 3%, calculated 3.1%) (figure III.2.07, left). There is an irreversible phase transition associated to this change, showing the PXRD pattern a different crystalline phase when the sample is heated above this temperature (see figure III.2.07 right). This dehydrated crystalline phase remains stable until the total decomposition of the product, which begins at ~ 485 °C. After an initial weight lost of ~ 21 % in a 80 degrees interval, the product decomposes gradually until a final mass loss of ~ 62 %, which indicates the almost total loss of the organic molecule (% calculated for Yb_2O_3 as residue = 69%; the difference in % of mass loss is probably due to the presence of coke residue).

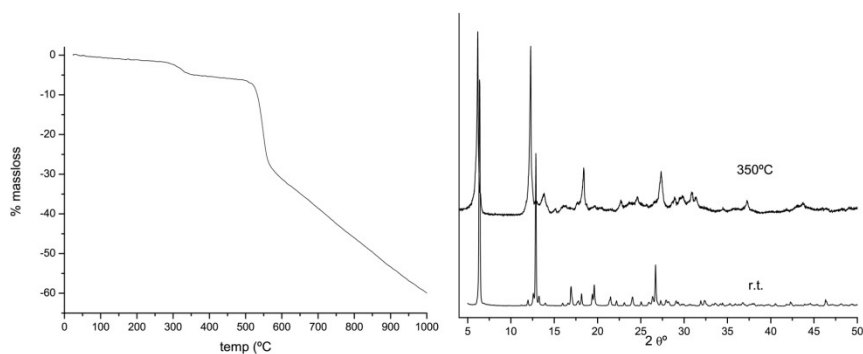


Figure III.2.07: Left: TG curve of the Yb-RPF5 compound. Right: the PXRD pattern of the Yb-RPF5 compound at room temperature and after being heated above 350 °C.

RPF6 structural type

The molecular formula of the RPF6 structural type, determined after the crystal structure solution, is $[\text{Ln}(\text{OH})(2,6\text{-AQDS})(\text{H}_2\text{O})_3]$. Single crystals could be obtained when employing Nd, Gd, Dy, Ho and Er. As it is explained below, only in the case of Nd, Sm and Dy the product was obtained with a good degree of purity, and therefore the characterization of the materials was carried out exclusively for these elements. Crystallographic details for the rest of the collected crystals can be found in chapter V.1, additional crystal structures. The ORTEP representation of the Nd-RPF6 and Dy-RPF6 asymmetric units are shown in figure III.2.08. In the case of Sm, the product was always obtained as a crystalline powder, and it was proved to be isostructural to the Nd and Dy compounds by means of powder X-ray diffraction.

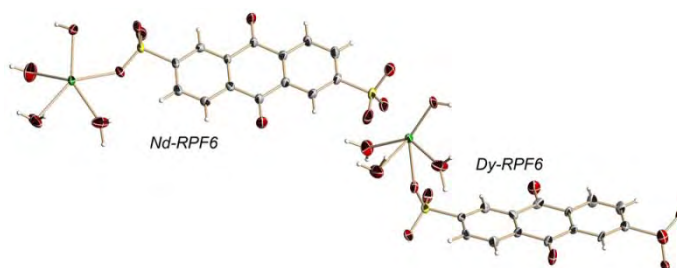


Figure III.2.08: ORTEP drawing (50 % probability) of the asymmetric units of the RPF6 compounds. Green: Ln atoms; red: O atoms; yellow: S atoms; grey: C atoms; white: H atoms.

In the RPF6 compounds, the Ln atoms are octacoordinated. Their coordination sphere is formed by 3 oxygen atoms from three SO_3^- groups, 2 hydroxyl groups, and three water molecules, forming a trigonal prism, square face biccapped (figure III.2.09, table III.2.05). As in RPF5, the Ln^{3+} cations are forming edge sharing dimeric units *via* two $\mu\text{-OH}^-$ groups. These $[\text{Ln}_2(\text{OH})_2(\text{H}_2\text{O})_6]$ units are placed parallel to the *ab* plane, and they are joined each other along the *c* axis by the anthraquinone molecules.



Table III.2.04: Crystallographic and refinement data for the RPF6 compounds

Identification code	Nd-RPF6	Dy-RPF6
Empirical formula	$C_{14}H_{13}S_2NdO_{12}$ [Nd(C ₁₄ H ₆ S ₂ O ₈)(OH)(H ₂ O) ₃]	$C_{14}H_{13}S_2DyO_{12}$ [Dy(C ₁₄ H ₆ S ₂ O ₈)(OH)(H ₂ O) ₃]
Formula weight	581.60	599.86
Temperature	296(2) K	295(2) K
Wavelength	0.71073 Å	
Crystal system, space group	Triclinic, P-1	
Unit cell dimensions	$a = 7.3086(3)$ Å $b = 7.9855(3)$ Å $c = 15.4179(6)$ Å	$a = 10.3582(7)$ Å $b = 10.3578(4)$ Å $c = 15.8213(11)$ Å
Volume	$889.71(6)$ Å ³	$867.3(2)$ Å ³
Z, Calculated density	2, 2.171 Mg/m ³	2, 2.297 Mg/m ³
Absorption coefficient	3.220 mm ⁻¹	4.617 mm ⁻¹
F(000)	570	582
Crystal size	0.30 x 0.22 x 0.18 mm	0.20 x 0.10 x 0.05 mm
Theta range for data collection	1.33° to 28.82°	1.34° to 29.16°
Limiting indices	-9<h<=9 -10<k<=10 -20<l<=20	-9<h<=9 -10<k<=10 -20<l<=20
Reflections collected / unique	7858 / 4131	7771 / 3979
Completeness to theta = 25.00°	96.9 %	96.4 %
Absorption correction	Semi-empirical from equivalents	
Max. and min. transmission	0.5949 and 0.4451	0.8200 and 0.4586
Refinement method	Full-matrix least-squares on F ²	
Data / restraints / parameters	4131 / 0 / 262	3979 / 0 / 262
Goodness-of-fit on F ²	1.106	0.948
Final R indices [I>2σ(I)]	R ₁ = 0.0400, wR ₂ = 0.1093	R ₁ = 0.0554, wR ₂ = 0.1012
R indices (all data)	R ₁ = 0.0465, wR ₂ = 0.1126	R ₁ = 0.1057, wR ₂ = 0.1336
Largest diff. peak and hole	1.218 and -1.672 e.Å ⁻³	1.734 and -2.087 e.Å ⁻³

The coordination mode of the sulfonate groups in the anthraquinone ligand are $\eta^2\mu_2$ and η^1 . They links every two dimeric units, giving rise to double chains running along the (001) direction. As there is not any covalent bond among [Ln₂(OH)₂(H₂O)₆] dimeric units in the ab plane, the coordination polymer is extended in just one direction, and the supramolecular 3D net is built up *via* hydrogen bonds. These are formed between the two non-coordinated oxygen atoms of the monocoordinated sulfonate group and the hydroxyl group and a water molecule in the coordination sphere of the rare earth atoms. The distances and angles of the hydrogen bonds are present in table III.2.06. The tilt angle between the ab plane and that involving the AQDS molecules is 64.37°. Despite in both RPF5 and RPF6 all the Ln atoms

are situated on a plane, the main difference between these two MOFs lies in the absence of bridge sulfonate groups between $\text{Ln}_2(\text{OH})_2$ dimeric units in the lanthanide containing plane of the latter. Thus, while RPF5 exhibits a 3D covalent network, in RPF6 the covalent net is 1D, and the 3D supramolecular one is only sustained by the H-bonds.

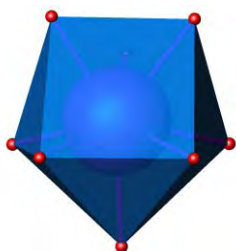


Figure III.2.09: LnO_8 .
The coordination polyhedron in RPF6; a bicapped trigonal prism

Table III.2.05: Interatomic distances in the coordination sphere of RPF6 compounds

Dy-RPF6		Nd-RPF6	
Bond	Distance (Å)	Bond	Distance (Å)
Dy(1)-O(1)	2.362(7)	Nd(1)-O(3)	2.431(3)
Dy(1)-O(5) ²	2.382(7)	Nd(1)-O(4)	2.495(4)
Dy(1)-O(6) ³	2.416(7)	Nd(1)-O(5)	2.469(4)
Dy(1)-O(9)	2.256(7)	Nd(1)-O(8)	2.485(4)
Dy(1)-O(9) ¹	2.268(7)	Nd(1)-O(11)	2.530(4)
Dy(1)-O(10)	2.390(7)	Nd(1)-O(12) ¹	2.342(4)
Dy(1)-O(11)	2.453(7)	Nd(1)-O(12)	2.357(3)
Dy(1)-O(12)	2.469(8)	Nd(1)-O(13)	2.551(5)
Dy(1)-Dy(1) ¹	3.6289(11)	Nd(1)-Nd(1) ¹	3.7630(5)

Symmetry operators codes:
1: -x,-y+2,-z; 2: x,y,z-1; 3: -x,-y+2,-z+1

Symmetry operators codes:
1: -x,-y+2,-z+1; 2: -x,-y+2,-z

Table III.2.06: Hydrogen bonds in the RPF6 compounds

D-H...A ¹	D-H ²	H...A ³	D...A ⁴	<D-H...A ⁵
Dy-RPF6				
O(10)w-H(81)w.....O(2)s ^[1]	0.98 Å	1.74 Å	2.72 Å	172°
O(10)w-H(82)w.....O(4)s ^[2]	1.12 Å	1.97 Å	2.81 Å	129°
O(12)w-H(111)w.....O(2)s ^[3]	0.87 Å	2.09 Å	2.90 Å	155°
O(9)h-H(121)h.....O(3)s ^[1]	0.84 Å	2.05 Å	2.88 Å	177°
Nd-RPF6				
O(8)w-H(81)w.....O(1)s ^[1]	0.96 Å	1.77 Å	2.72 Å	165°
O(8)w-H(82)w.....O(6)s ^[2]	1.05 Å	2.02 Å	2.83 Å	132°
O(11)w-H(111)w.....O(1)s ^[3]	0.84 Å	2.15 Å	2.92 Å	152°
O(12)h-H(121)h.....O(2)s ^[4]	0.83 Å	2.06 Å	2.88 Å	174°

D = donor atom; A = acceptor atom

1 = names of donor, hydrogen and acceptor atoms involved in the hydrogen bond; 2 = distance donor – acceptor; 3 = distance H – acceptor; 4 = distance donor – acceptor; 5 = angle donor – hydrogen – acceptor

Element(n)w = atom in a water molecule; Element(n)h = atom in a hydroxyl group; Element(n)s = atom in a SO_3^- group

Symmetry operators codes: [1] = -1+x,y,z [2] = -x,-1-y,1-z [3] = 1-x,1-y,-z

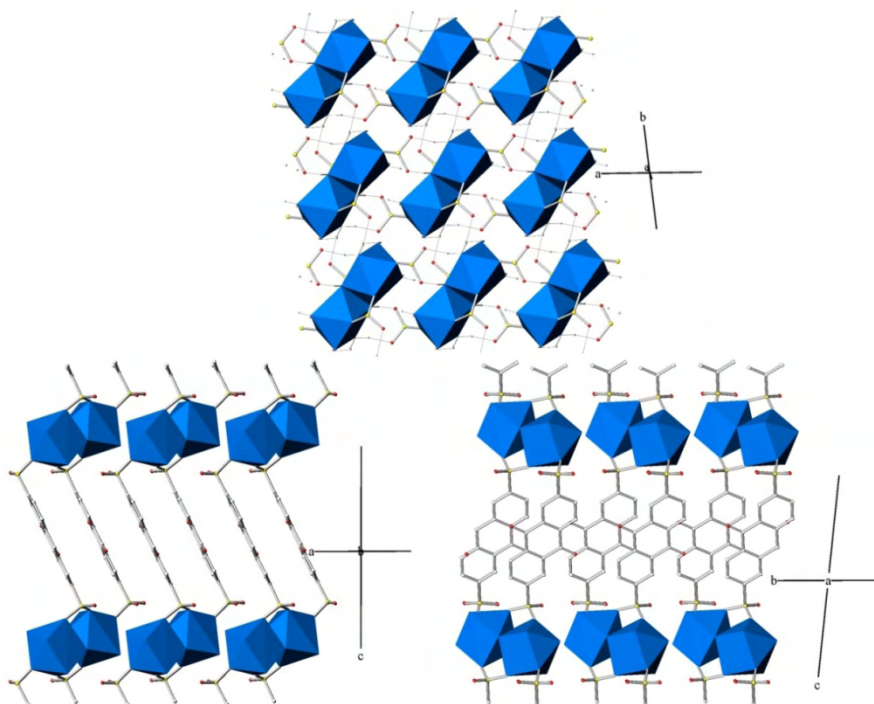


Figure III.2.10: Top: projection of the inorganic layer formed by hydrogen bonds in RPF6. Bottom: two views of the covalently bonded double chains present in the RPF6 compounds.

X-Ray powder diffraction: A Rietveld refinement of each prepared samples has been carried out. The results of the refinements for the three sample are shown in figure III.2.10, in which the simulated, experimental and difference patterns are presented, together with the Bragg positions. In the dysprosium and samarium samples, a small signal appears at about $2\theta = 10^\circ$, which is attributed to the presence of a small amount of LRH phase.

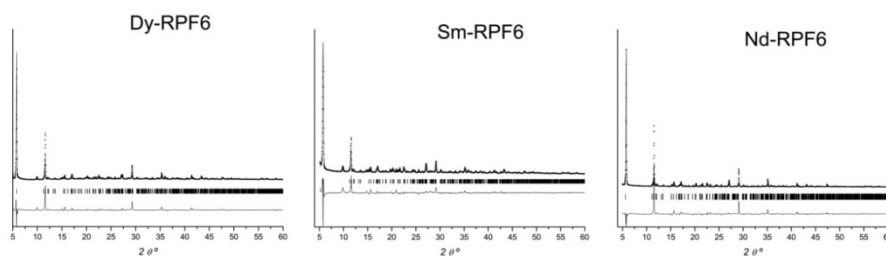


Figure III.2.11: Rietveld refinements of the RPF6 compounds, showing the experimental (dots) and simulated (line) powder pattern, and the difference pattern. The Bragg positions are shown as columns.

Elemental chemical analyses: the values of the elemental analyses demonstrate the purity of the obtained materials. In table III.2.07 the experimental and calculated values are compared.

Table III.2.07: Elemental chemical analysis data of the RPF6 compounds

		Dy-RPF6	Sm-RPF6	Nd-RPF6
%C	<i>calculated</i>	28.01	28.59	28.89
	<i>experimental</i>	26.90	27.68	27.97
%H	<i>calculated</i>	2.19	2.23	2.26
	<i>experimental</i>	2.20	2.33	2.16

Thermogravimetric analysis: Regarding to the thermal stability of the RPF6 structural type, a thermogravimetric analysis was carried out for the Nd, Sm and Dy samples. In the three of them, the total decomposition of the framework starts at ~ 460 °C. Previously, the coordinated water molecules have been lost. In the case of the Nd sample, this takes place in two steps. In the first, one molecule is lost (3.1% observed, 3.08 calculated), and the second step the other two molecules (6.3% observed, 6.16 calculated). In the Sm and Dy samples, the loss of the water molecules takes place more gradually, with a total mass loss of 9.9% and 8.8% at ~ 300 °C, for Sm and Dy respectively (calculated 9.19% for Sm and 9.01% for Dy).

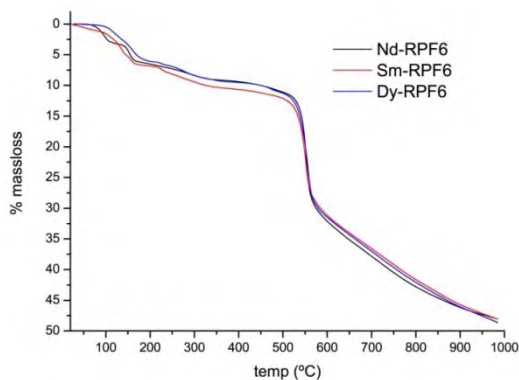


Figure III.2.12: TG curves for the three RPF6 compounds.



RPF7 structural type

Owning the same formula $[\text{Ln}(\text{OH})(2,6\text{-AQDS})(\text{H}_2\text{O})]$ that RPF5, RPF7 fits in the third structural type of coordination polymers built up from 2,6-AQDS and rare earth cations, and was obtained for lanthanum and praseodymium. These compounds crystallize in the triclinic P-1 space group, with twice the formula per asymmetric unit. The ORTEP views of La and PrRPF7 are shown in Figure III.2.13.

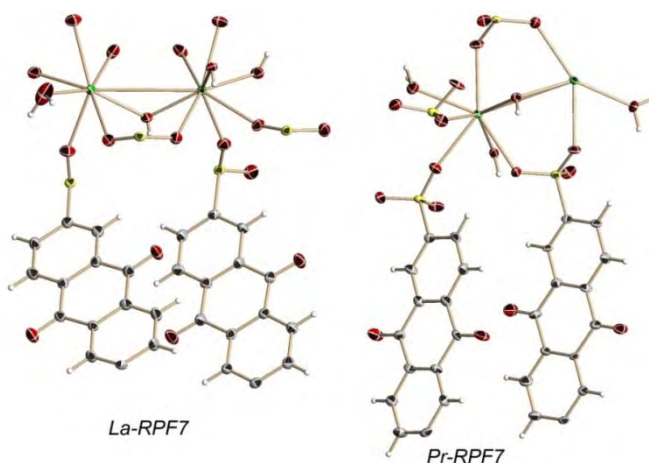


Figure III.2.13: ORTEP drawing (50% probability) of the two RPF7 compounds. Green: Ln atoms; red: O atoms; yellow: S atoms; grey: C atoms; white: H atoms.

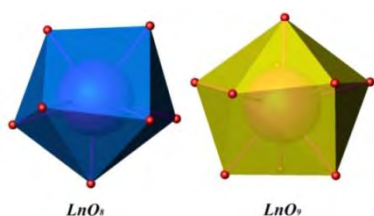


Figure 14: The two coordination polyhedra in the RPF7 compounds: a bicapped trigonal prism, and a tricapped trigonal prism.

There are, therefore, two crystallographically independent Ln atoms per asymmetric unit. One of them is octa-coordinated and forms a LnO_8 distorted trigonal prism, square face bicapped; the other, nine-coordinated, is in the centre of a LnO_9 tricapped trigonal prism. Four of these polyhedra (two of each class) are linked together via μ_2 and $\mu_3(\text{OH})$, in such a way

that two LnO_9 polyhedra share one edge among them, and another with a LnO_8 one. As in RPF5 and RPF6 metallic clusters lie on a plane parallel to the ab plane. Connections along the a direction are made via SO_3 bridging groups in a $\eta^3\mu_3$ coordination mode, with two oxygen atoms of each sulfonate group bonded to one tetrameric unit and the third to another one. This arrangement gives rise to chains parallel to that direction. There is no any covalent connection among tetramers along the b direction, but they are joined via hydrogen bonds between the coordinated water molecules and the uncoordinated oxygen atoms of the SO_3 groups. As a result of both type of

Table III.2.08: Crystallographic and refinement data for the RPF7 compounds

Identification code	La-RPF7	Pr-RPF7
Empirical formula	$C_{14}H_9S_2LaO_{10}$ [La($C_{14}H_9S_2O_8$)(OH)(H_2O)]	$C_{14}H_9S_2PrO_{10}$ [Pr($C_{14}H_9S_2O_8$)(OH)(H_2O)]
Formula weight	540.24	542.24
Temperature	296(2) K	295(2) K
Wavelength	0.71073 Å	
Crystal system, space group	Triclinic, $P-1$	
Unit cell dimensions	$a = 10.4039(4)$ Å $\alpha = 76.789(1)^\circ$ $b = 10.4239(4)$ Å $\beta = 76.311(1)^\circ$ $c = 15.8965(5)$ Å $\gamma = 78.084(1)^\circ$	$a = 10.3582(7)$ Å $\alpha = 76.675(1)^\circ$ $b = 10.3578(4)$ Å $\beta = 76.194(1)^\circ$ $c = 15.8213(11)$ Å $\gamma = 77.929(1)^\circ$
Volume	$1609.36(10)$ Å ³	$15282.54(19)$
Z, Calculated density	4, 2.230 Mg/m ³	4, 2.276
Absorption coefficient	2.972 mm ⁻¹	3.401
F(000)	1048	1056
Crystal size	0.18 x 0.18 x 0.08 mm	0.20 x 0.10 x 0.06
Theta range for data collection	1.37° to 29.17°	1.35° to 29.08°
Limiting indices	-14<= h <=13 -14<= k <=14 -21<= l <=21	-14<= h <=14 -13<= k <=13 -21<= l <=21
Reflections collected / unique	15023 / 7603	14056 / 7253
Completeness to theta = 25.00°	98.2 %	95.7 %
Absorption correction	Semi-empirical from equivalents	
Max. and min. transmission	0.7970 and 0.6168	0.8220 and 0.5495
Refinement method	Full-matrix least-squares on F ²	
Data / restraints / parameters	7403 / 0 / 487	7253 / 0 / 487
Goodness-of-fit on F ²	1.130	1.048
Final R indices [I>2σ(I)]	R ₁ = 0.0399, wR ₂ = 0.0869	R ₁ = 0.0503, wR ₂ = 0.0992
R indices (all data)	R ₁ = 0.0556, wR ₂ = 0.0919	R ₁ = 0.0849, wR ₂ = 0.1089
Largest diff. peak and hole	0.723 and -1.223 e-Å ⁻³	1.236 and -1.844 e-Å ⁻³



linkages, inorganic pseudo-layers appear, which are connected along the c direction by the whole organic molecule to give rise a 3D framework.

Table III.2.09: Interatomic distances in the coordination sphere of RPF7 compounds

La-RPF7				Pr-RPF7			
Bond	Distance (Å)	Bond	Distance (Å)	Bond	Distance (Å)	Bond	Distance (Å)
La(1)-O(6)	2.392(3)	La(2)-O(1)	2.476(3)	Pr(1)-O(1)	2.540(5)	Pr(1)-Pr(2)	3.9256(6)
La(1)-O(8)	2.666(3)	La(2)-O(2)	2.485(4)	Pr(1)-O(4)	2.539(5)	Pr(2)-O(2) ²	2.569(5)
La(1)-O(9)	2.626(3)	La(2)-O(3)	2.480(3)	Pr(1)-O(9)	2.627(5)	Pr(2)-O(5) ¹	2.446(5)
La(1)-O(10)	2.541(3)	La(2)-O(4)	2.616(3)	Pr(1)-O(10) ²	2.508(5)	Pr(2)-O(11)	2.576(5)
La(1)-O(11)	2.625(3)	La(2)-O(5)	2.612(3)	Pr(1)-O(12)	2.590(5)	Pr(2)-O(13)	2.565(5)
La(1)-O(12)	2.583(3)	La(2)-O(6)	2.360(3)	Pr(1)-O(17)	2.347(5)	Pr(2)-O(14) ¹	2.438(5)
La(1)-O(13)	2.645(3)	La(2)-O(7)	2.620(3)	Pr(1)-O(18)	2.624(5)	Pr(2)-O(17)	2.315(5)
La(1)-O(13) ¹	2.539(3)	La(2)-O(13) ¹	2.494(3)	Pr(1)-O(18) ²	2.502(4)	Pr(2)-O(18) ²	2.449(5)
La(1)-O(14)	2.578(3)	La(1)-La(2)	4.0011(4)	Pr(1)-O(20)	2.603(5)	Pr(2)-O(19)	2.431(5)

Symmetry operators codes:
 1: $-x+1, -y, -z+1$;

Symmetry operators codes:
 1: $-x-1, -y, -z+1$ 2: $-x, -y, -z+1$

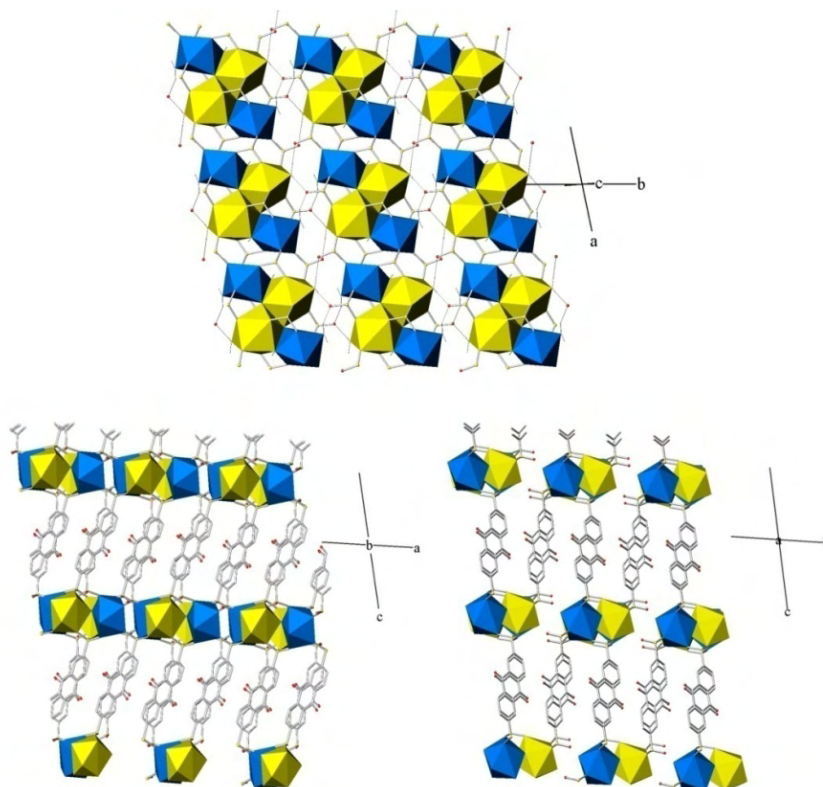


Figure III.2.15: Top: a view of the inorganic layer formed in the RPF7 compounds. Bottom: two views of the three dimensional structure of the RPF7 compounds.

Topology: Concerning to the AQDS²⁻ anions connectivity, even though there are two crystallographically different ligands, which coordinate in $\eta^3\mu_3$ - $\eta^3\mu_3$ and $\eta^2\mu_2$ - $\eta^2\mu_2$ modes, the overall connectivity with the tetrameric inorganic units is the same, since both of them are connected to one tetramer through one of their sulfonate groups and to two through the other one. All in all, in the topological simplification of the net work, the AQDS²⁻ anions are three connected nodes, while the tetrameric units are twelve connected nodes. The network is, thus, a bi-nodal net 3 and 12 connected of the Au_4Ho type, with point symbol $(4^{20}.6^{28}.8^{18}) (4^3)$. A topological representation of the RPF7 network is shown in figure III.2.16.

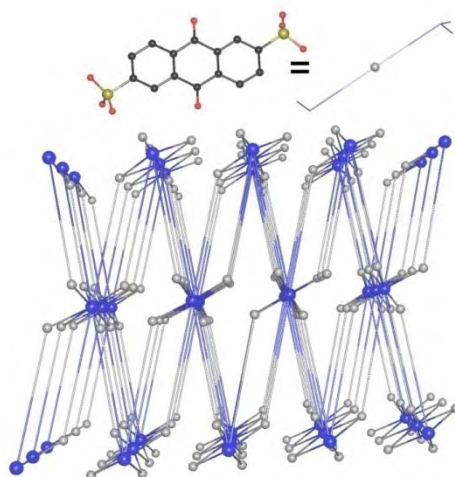


Figure III.2.16: Topological simplification of the RPF7 network: the blue balls represent the 12-connected tetrameric units, and the grey balls represent the 3-connected ligands.

X-ray powder diffraction and elemental chemical analysis. Both lanthanum and praseodymium materials are obtained purely, as demonstrated by the elemental analyses and the powder X-ray diffraction patterns. In the table III.2.10 the values of the elemental chemical analysis are shown, while in figure III.2.17, the Rietveld refinements of the two samples are shown.

Table III.2.10: elemental chemical analyses data for the RPF7 compounds

		Pr-RPF7	La-RPF7
%C	calculated	30.98	31.10
	experimental	30.50	30.76
%H	calculated	1.68	1.68
	experimental	1.78	1.77

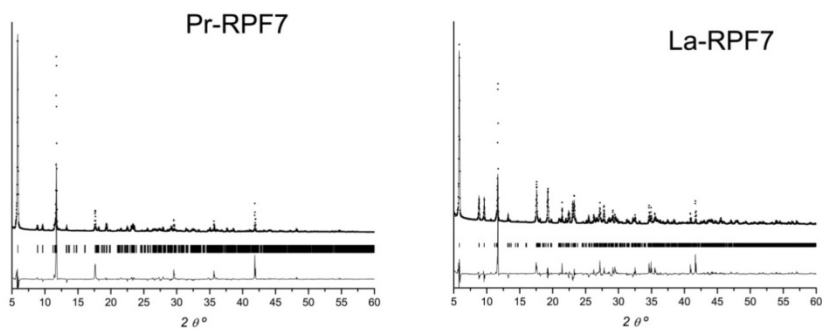


Figure III.2.17. Rietveld refinement of the two Ln-RPF7 compounds, showing the comparison of the experimental (dots) and calculated (line) X-ray powder patterns, together with the Bragg positions (columns) and difference pattern (bottom).

Thermal behavior. Thermogravimetric analyses of the products (figure III.2.18) indicate that the total decomposition of the framework, with the loss of the organic part starts above ~ 450 °C. Previously, the loss of the coordinated water molecules takes place at ~ 270 °C (% calculated mass loss = 3.3 %, experimental = 3.3%).

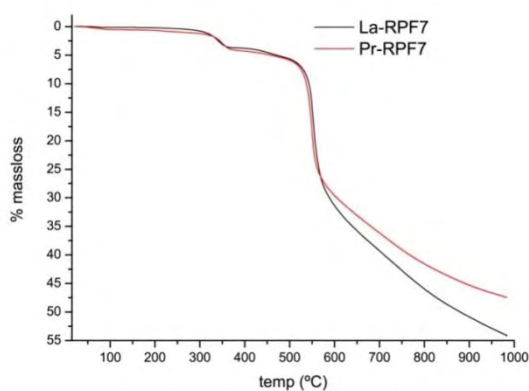


Figure III.2.18: TG curves for the two RPF7 compounds.

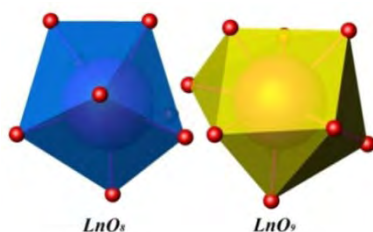
LRH structural type

This is the last family of compounds presented in this chapter, and we have named it as LRH, layered rare earth hydroxides, for its similitude with the LDHs, layered double hydroxides. Opposite to the previously described RPFs families, the LRH is a kind of layered materials, whose structure bears a clear analogy with that of the layered double hydroxides (LDHs). The LDHs are a well known family of compounds, with many applications as adsorbents, drug-delivery vehicles, polymer stabilizers, and catalysts²⁵. The structure of the LDHs derives from the brucite type, and consists of layers formed by hydroxides of divalent cations, generally transition metal cations, which are substituted by trivalent cations resulting in a positively charged layer. The charge of the layer is compensated by the presence of anions which are placed in the interlayer space, next to water molecules. Their general molecular formula is $[M^{II}_{1-x}M^{III}_x(OH)_2]^{x+} (A^{n-})_{x/n} \cdot yH_2O$, where M are transition metal cations, and A are generally inorganic anions. In the new LRHs compounds, the positive charge of the inorganic layer is created only by trivalent rare-earth hydroxo-cations, which arises from the high and variable coordinative capability of the rare-earth centers and the tendency of the hydroxide ion to form μ_n connections in structures that contain these rare-earth centers. The cationic charge is here neutralized with organic anions in the interlayer space, in this case anthraquinone-2,6-disulfonate. The general formula of this new type of compounds is $[R_4(OH)_{10}(H_2O)_4]^{2+}(AQDS^{2-})$ (R = rare-earth cation). They crystallize in the orthorhombic space group Ibam. Crystallographic and refinement details are given in table III.2.11. Interatomic distances in the coordination sphere of Yb-LRH and Dy-LRH are found in table III.2.12. Two kinds of differently coordinated rare-earth atoms are present in the structure. One of them is a dodecahedron, coordinated to seven OH⁻ groups, and to a water molecule. The other is a trigonal prism, square face tricapped, coordinated to eight OH⁻ groups and to a water molecule (figure. III.2.19).



Table III.2.11: Crystallographic and refinement data for the LRH compounds

Identification code	Yb-LRH		Dy-LRH	
Empirical formula	$C_7H_{12}SYb_2O_{11}$ $[Yb_2(C_7H_3SO_4)(OH)_5(H_2O)_2]$		$C_7H_{12}SDy_2O_{11}$ $[Dy_2(C_7H_3SO_4)(OH)_5(H_2O)_2]$	
Formula weight	650.31		629.23	
Temperature	295(2) K		295(2) K	
Wavelength	0.71073 Å			
Crystal system, space group	Orthorhombic, <i>Ibam</i>			
Unit cell dimensions	$a = 12.5401(6)$ Å	$\alpha = 90^\circ$	$a = 12.722(1)$ Å	$\alpha = 90^\circ$
	$b = 35.6519(3)$ Å	$\beta = 90^\circ$	$b = 35.453(4)$ Å	$\beta = 90^\circ$
	$c = 7.0347(6)$ Å	$\gamma = 90^\circ$	$c = 7.1836(11)$ Å	$\gamma = 90^\circ$
Volume	3145.1 (6) Å ³		3240.0(5) Å ³	
Z, Calculated density	8, 2.747 Mg/m ³		8, 2.580 Mg/m ³	
Absorption coefficient	12.000 mm ⁻¹		9.328 mm ⁻¹	
F(000)	2384		2320	
Crystal size	0.20 x 0.10 x 0.06 mm		0.30 x 0.08 x 0.06 mm	
Theta range for data collection	1.72° to 33.14°		1.15° to 29.15°	
	-19<= <i>h</i> <=8		-17<= <i>h</i> <=14	
Limiting indices	-30<= <i>k</i> <=47		-10<= <i>k</i> <=46	
	-9<= <i>l</i> <=10		-9<= <i>l</i> <=9	
Reflections collected / unique	7780 / 2606		8157 / 2144	
Completeness to theta = 25.00°	98.4 %		98.8 %	
Absorption correction	Semi-empirical from equivalents			
Max. and min. transmission	0.5329 and 0.1976		0.6045 and 0.1663	
Refinement method	Full-matrix least-squares on F ²			
Data / restraints / parameters	2606 / 12 / 105		2144 / 0 / 110	
Goodness-of-fit on F ²	1.024		1.090	
Final R indices [<i>I</i> >2σ(<i>I</i>)]	R ₁ = 0.0719, wR ₂ = 0.1883		R ₁ = 0.0547, wR ₂ = 0.1614	
R indices (all data)	R ₁ = 0.0947, wR ₂ = 0.2007		R ₁ = 0.0700, wR ₂ = 0.1678	
Largest diff. peak and hole	5.227 and -7.997 e·Å ⁻³		2.587 and -3.521 e·Å ⁻³	



Polyhedra of the same type are placed in alternated rows parallel to the [001] direction forming layers parallel to the ac plane. The AQDS²⁻ anions are located in the interlamellar space, linked to the layers

through hydrogen bonds. They are highly ordered, with a titling angle formed between the organic anion S-S axes and the normal of the respective

hydroxide layers of 30.86° . The value of the basal spacing is one half of the b parameter.

Table III.2.12: Interatomic distances in the coordination sphere of the LRH compounds

Yb-LRH				Dy-LRH			
Bond	Distance (Å)	Bond	Distance (Å)	Bond	Distance (Å)	Bond	Distance (Å)
Yb(1)-O(1)	2.536(11)	Yb(2)-O(1) ⁷	2.300(7)	Dy(1)-O(3)	2.294(7)	Dy(2)-O(4) ³	2.355(6)
Yb(1)-O(2)	2.271(11)	Yb(2)-O(1) ³	2.300(7)	Dy(1)-O(3) ²	2.294(7)	Dy(2)-O(4) ⁶	2.355(6)
Yb(1)-O(3)	2.325(8)	Yb(2)-O(2) ¹	2.390(7)	Dy(1)-O(1)	2.315(9)	Dy(2)-O(1)	2.419(6)
Yb(1)-O(3) ⁴	2.325(8)	O(2)-Yb(2)	2.390(7)	Dy(1)-O(2) ³	2.326(9)	Dy(2)-O(1) ⁷	2.419(6)
Yb(1)-O(3) ³	2.240(8)	O(3)-Yb(2)	2.427(8)	Dy(1)-O(3) ³	2.368(7)	Dy(2)-O(2) ⁷	2.450(6)
Yb(1)-O(3) ²	2.240(8)	Yb(2)-O(3) ¹	2.427(8)	Dy(1)-O(3) ⁴	2.368(7)	Dy(2)-O(2)	2.450(6)
Yb(1)-O(4) ³	2.269(11)	O(4)-Yb(2)	2.418(7)	Dy(1)-O(5)	2.471(11)	Dy(2)-O(3) ⁶	2.470(6)
Yb(1)-O(5)	2.385(14)	Yb(2)-O(4) ¹	2.418(7)	Dy(1)-O(4)	2.537(9)	Dy(2)-O(3) ³	2.470(6)
Yb(1)-O(5)	2.578(3)	Yb(1)-Yb(1) ⁶	3.7361(5)	Dy(1)-Dy(1) ³	3.8228(5)	Dy(2)-O(61)	2.790(16)
Yb(1)-Yb(2) ³	3.5221(6)	Yb(1)-Yb(1) ³	3.7361(5)	Dy(1)-Dy(1) ⁵	3.8228(5)	Dy(1)-Dy(2) ³	3.5926(6)
Yb(1)-Yb(2) ²	3.5221(6)	Yb(2)-Yb(2) ⁴	3.5173(2)	Dy(2)-Dy(2) ²	3.5918(3)	Dy(1)-Dy(2) ⁴	3.5926(6)
Yb(2)-Yb(1) ³	3.5221(6)	Yb(2)-Yb(2) ⁵	3.5173(2)	Dy(2)-Dy(2) ¹	3.5918(3)	Dy(2)-Dy(1) ⁶	3.5926(6)

Symmetry operators code: 1: -x+0,y+0,-z+1/2; 2: -x+1/2,-y+1/2,z+1/2; 3: -x+1/2,-y+1/2,-z+1/2; 4: x,y,-z+1; 5: x,y,-z; 6: -x+1/2,-y+1/2,-z+3/2; 7: x-1/2,-y+1/2,z;	Symmetry operators code: 1: x,y,-z+1; 2: x,y,-z; 3: -x+1/2,-y+1/2,-z+1/2; 4: -x+1/2,-y+1/2,z-1/2; 5: -x+1/2,-y+1/2,-z-1/2; 6: x+1/2,-y+1/2,z; 7: -x+1,y+0,-z+1/2;
---	---

The AQDS²⁻ anions are situated parallel to the *ab* plane in an alternated configuration, and separated 3.5 Å (*c*/2) and 12.5 Å (*a*) along the [001] and [100] directions, respectively. This arrangement gives rise to $\pi-\pi$, and O— π stacking interactions of the parallel type²⁶ among the AQDS²⁻ central rings and among one of the quinonic oxygen atoms and lateral aromatic rings, respectively, at a distance 3.52 Å. Thanks to this well ordered disposition of the anions in the interlayer space, this compound has a porous structure, with channels running along the *c* direction. The potential solvent area is 16.4 %, as computed by Platon⁹.

From a crystallographic point of view a direct relation exists between the brucite derived LDH hexagonal lattice and that of the LRHs. Given that in the later there are two independent well ordered Ln atoms by asymmetric unit, the ideal hexagonal superlattice would have an *a'* parameter twice that of the mineral. As the distances among R atoms are not uniform, this hexagonal superlattice is not real but it has a distortion that gives rise to an orthorhombic



larger cell for the LRH compound. Vectors of the LRH unit cell can be deduced from those of the LDH by roughly applying the transformation matrix $(2 \ -2 \ 0, \ 0 \ 0 \ -1, \ 2 \ 2 \ 0)$ (figure III.2.20).

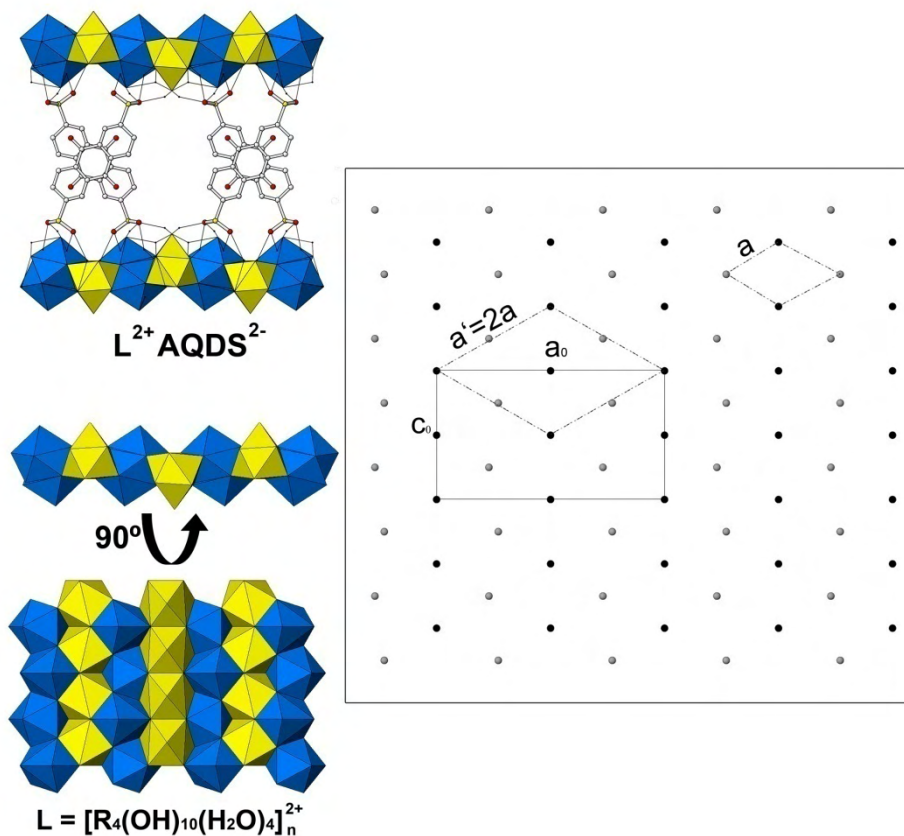


Figure III.2.20: Left: a representation of the LRH structure, formed by cationic layers with the AQDS molecules intercalated. Right: relationship between the hexagonal brucite type net of the LDH compounds, and the orthorhombic cell in the LRH compounds.

Topological analysis

In terms of topology, the cationic $[\text{Yb}_2(\text{OH})_{10}]^{2+}_n$ layer can be depicted as a pentanodal 3,7,8 connected net, with stoichiometry $(3c)_5(7c)(8c)$, where the 7c and 8c nodes are given by the ytterbium atoms, and the 3c by the hydroxylic oxygen atoms (figure III.2.20, top left). To study the 3D net formed through the hydrogen bonds, the model has been simplified as follow: First of all the oxygen atoms of the layer are omitted, giving rise to a (3,6) sheet of Yb atoms (figure III.2.20, top right). Secondly, the intercalated AQDS molecules are directly connected to the $[\text{Yb}_2(\text{OH})_{10}]^{2+}$ layers via hydrogen bonds (figure III.2.20, bottom left). The result is a trinodal, octa- and pentaconnected net with stoichiometry $(5-c)(8-c)_2$, and point symbol $(3^{10}.4^{12}.5^6)(3^3.4^3.6^2.7^2)(3^8.4^{11}.5^7.6^2)$ (Figure III.2.20, bottom right).

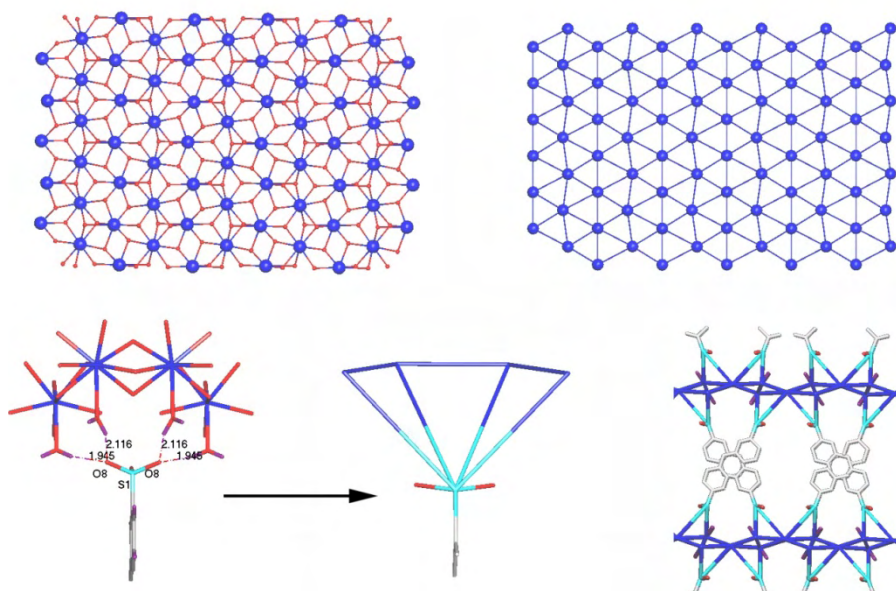


Figure III.2.21: Topological analysis of LRH framework. Top: ball-and-stick (left) and simplified without oxygen atoms (right) view of the Ln-O layer; down: depicting of LRH structure considering hydrogen bond.

Elemental analysis and X-ray powder diffraction

The LRHs family of compounds has been obtained as pure phases employing Yb, Er, Ho and Dy. Elemental analyses results are found in table III.2.13. Single crystals have been obtained only in the cases of Yb and Dy, and the erbium and holmium compounds were demonstrated to be isostructural by means of powder X-ray diffraction. Rietveld refinements were carried out for the four compounds, and their results are shown in figure III.2.22.

Table III.2.13: Elemental chemical analyses values for the LRH compounds

		Yb-LRH	Er-LRH	Ho-LRH	Dy-LRH
%C	calculated	12.92	13.69	13.25	13.35
	experimental	12.49	12.78	12.69	12.92
%H	calculated	1.85	1.96	1.89	1.91
	experimental	2.22	2.17	2.19	2.33

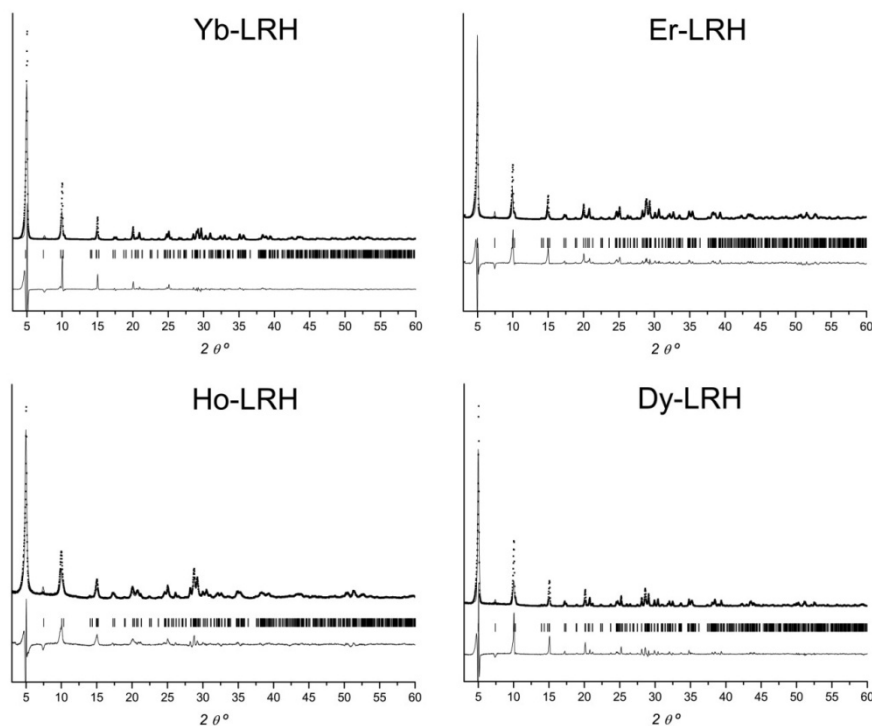


Figure III.2.22: Rietveld refinements of the LRH compounds, showing experimental (dots) and simulated (line) patterns, and the difference pattern. The Bragg positions are marked as columns.

Thermal behavior:

TGA-DTA analysis (figure III.2.23) shows a first mass loss (3.5 %) before 60 °C, which is due to the loss of adsorbed water molecules. In the temperature range of 100-400 °C, there are three steps in the TG curves, corresponding to a total mass loss of ~10 %. A mass detector was used for the Yb-LRH sample TG analysis, and the only signal corresponding to a mass of 18 was found in this temperature range. Consequently, a loss of 7 water molecules is assumed from the TG values (calculated value = 9.7%). Four of them, are the 4 coordinated water molecules, present in the initial structure. The remaining three molecules come from the inorganic layer, in such a way that the formula of this layer after the heating, should be $[R_4O_3(OH)_4]^{2+}$. An elemental analysis made to the Yb-LRH sample after being heated at 500 °C (under the same conditions than in the TG experiments) shows that all the organic components remain in the structure.

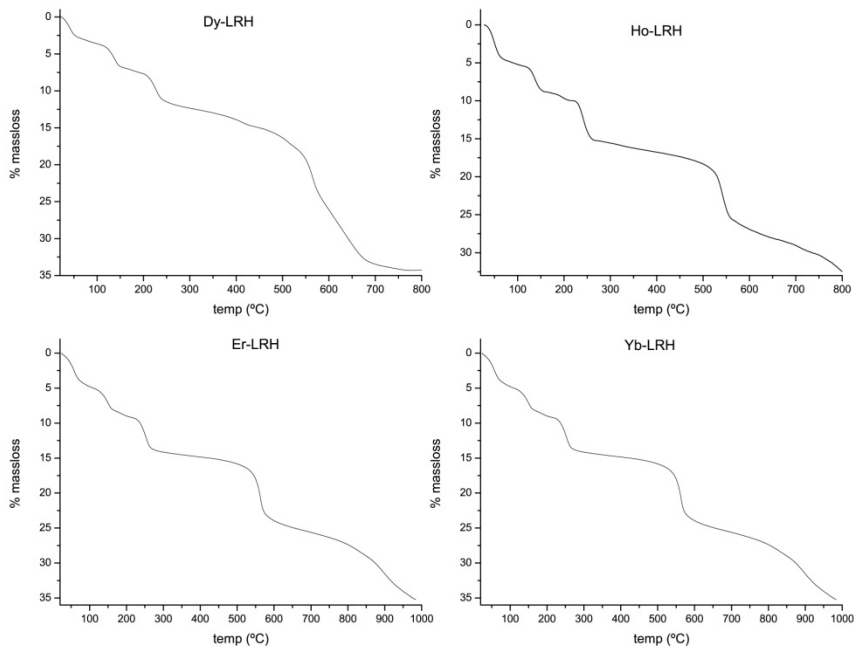


Figure III.2.23: TG curves for the four LRH compounds



The result of this analysis (14 % C, 0.6 %H, and 5.1 % S) demonstrates that the AQDS²⁻ anion remains intact in the structure (experimental C/S = 7.3, calculated = 7.0). To see the influence of these changes on the crystal structure, a variable temperature X-ray diffraction experiment was carried out with the Yb-LRH compound. The PXRD patterns of the heated samples show no changes in the peaks positions until 300 °C (figure III.2.24). At this temperature, a shift of the first peak to higher angle happens, and consequently, a diminution of the basal space to a value of 17.0 Å. Only the three first peaks are observed, indicating that the layered structure remains, but the layer is not so ordered. Finally, at 500 °C, a new diminution of the interlayer space takes place, with a final basal space of 16,5 Å, before the total decomposition of the structure begins.

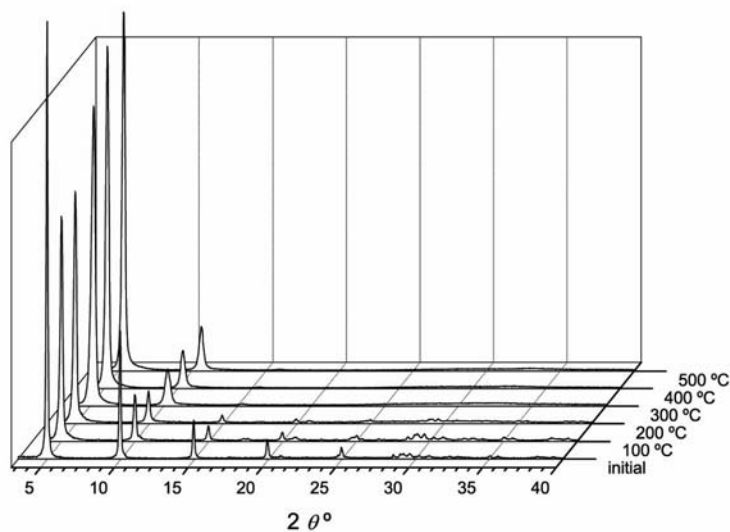


Figure III.2.24: Variable temperature powder X-ray diffraction patterns of the Yb-LRH compound.

Structural comparison

By adjusting the synthesis conditions, several structural types have been obtained with the use of anthraquinone-2,6-disulfonate and rare earth elements, with different structural characteristics that make them suitable to be used in different catalytic processes, as it is showed later. At the light of the results obtained in this chapter, some conclusion can be reached:

1. By using different rare earth cations as connectors and the AQDS²⁻ anion as linker, up to three new polymeric structural types were obtained.
2. As the synthesis conditions were kept invariable for the rare earth series compounds, and depending on the Ln atomic number: RPF5, RPF6 and RPF7 were obtained we can infer that the radius of the selected metal governs mainly the formation of each structural type. Considering only covalent interactions, two three dimensional nets are formed: one is RPF5, corresponding to the smallest radius element (Yb in seven coordination). The other is RPF7, obtained when involving the largest elements of the series La and Pr, both in eight and nine coordination. The mono dimensional net of RPF6 corresponds to elements of the central part of the series, Nd – Er, in eight coordination. If hydrogen bond interactions are taken into account, the three nets are three dimensional, and in doing this, some comparison can be made among them (figure III.2.24):
 - i) The primary building units are mono, two or three-capped trigonal prisms for RPF5, 6 and 7 respectively;
 - ii) The secondary building units are dimeric units for RPF5 and RPF6, and tetrameric units for RPF7,
 - iii) Inorganic (pseudo-) layers parallel to the *ab* plane are formed in the three structure types, by SBUs junctions through: covalent bonds



in RPF5, hydrogen bonds in RPF6, and mixed covalent and hydrogen bonds in RPF7,

- iv) The 2,6-AQDS linker acts as $\eta^2\mu_2-\eta^2\mu_2$ in RPF5, $\eta^2\mu_2-\eta^1$ in RPF-6 and in a double way as $\eta^3\mu_3-\eta^3\mu_3$ and $\eta^2\mu_2-\eta^2\mu_2$ in RPF7 to give three different frameworks.

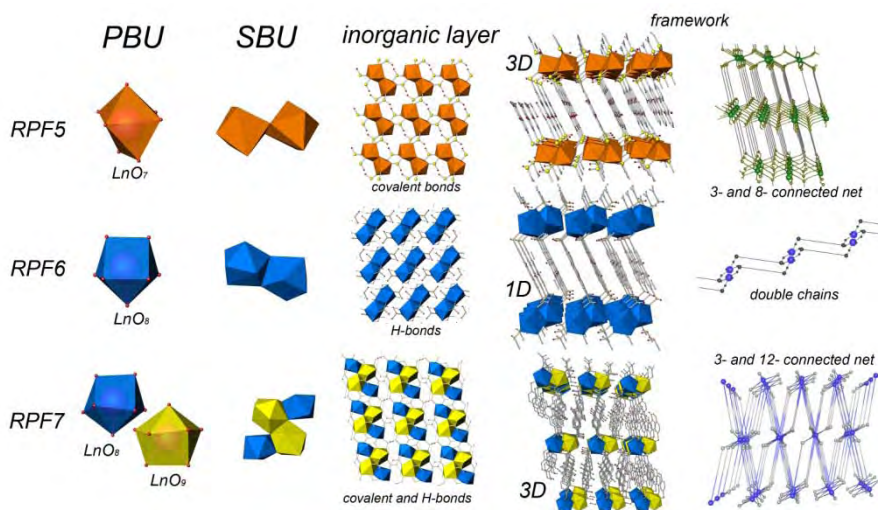


Figure III.2.25: Comparison of the three rare-earth polymeric framework presented in this chapter

LRHs: On the other hand, another type of structure can be prepared using 2,6-AQDS. In the LRHs, a more dense layer is formed, with the rare earth elements joined by μ_3 hydroxyl groups giving rise to an extended layer with formula $[\text{Ln}_4(\text{OH})_{10}]^{2+}$. The formation of this structural type seems to be kinetically favored. This fact can be understood taking into account that in this latter structural type, the sulfonate ligands are not coordinated to the rare-earth elements. The rare-earth elements are known to easily form diverse type of hydroxo aggregates in solution, and it can be expected that the formation of the $\text{SO}_3^- - \text{Ln}$ bonds is the most energetically demanding step in the synthesis procedure. Thus, during the preparation of the polymeric phases RPF5, RPF6 and RPF7, different results are observed, depending on the rare earth element used:

- With elements from Sm to Er, the presence of the LRH phase is detected even under the most favorable conditions for the formation of the RPF phases, with maximum amount in the case of Tb, and minimum for Dy and Sm (figure III.2.26).
- For the elements La, Pr, Nd, and Yb, their corresponding polymeric frameworks were obtained as pure phases.

It seems plausible that for the larger La, Pr and Nd, their higher ionic radii makes it difficult the formation of the dense hydroxide layer, with larger μ_n -OH – Ln bonds, and no presence of LRH was detected in any of the synthesis experiments carried out with these elements.

- In the case of ytterbium, it is possible to obtain its corresponding LRH phase. Indeed, it can be prepared purely, since its small ionic radius allows the formation of the layer. However, precisely being the rare earth element with the smallest ionic radius, the formation of a phase in which this element is in lower coordination number may also be favored, and the preparation of the RPF5 phase (Yb with CN 7) is possible with the adequate synthesis conditions.

In any case, a correct choice of the synthesis conditions is important to control the formation of one or another phase. The cases of ytterbium and dysprosium are representative for the optimization of the synthesis conditions, since both the RPF and LRH structures can be obtained with them. In table III.2.14 the syntheses experiments carried out with Yb and Dy are presented:

Despite of the fact that for all the experiments the pH value is 6.5, the source of OH⁻ anions seems to be a decisive factor: when using an amine the LRH phase is obtained, while with an inorganic base such as Na(OH), a mixture of 2D LRH and 3D RPF phases can appear independently of the reagents ratio. The only way to obtain the RPF material as single product is by adjusting its molecular formula with the equimolar amount of OH⁻ anions. It seems that the



Table III.2.14: Syntheses experiments carried out with Yb and Dy, illustrating the influence of the synthesis conditions on the obtained products.

Yb/AQDS ^a	H ₂ O/AQDS ^a	Base	Product
4	4400	Et ₃ N	Pure LRH phase
4	4400	Py	Pure LRH phase
1	1500	NaOH	Pure RPF phase
4	4400	NaOH	RPF majority phase + LRH presence
4	1500	NaOH	RPF + LRH
1	4400	Et ₃ N	Pure LRH phase
1	1500	Et ₃ N	Pure LRH phase
Dy/AQDS ^a	H ₂ O/AQDS ^a	Base	Product
4	4400	Et ₃ N	Pure LRH phase
4	4400	Py	Pure LRH phase
1	1500	NaOH	RPF phase with small presence of LRH
1	1500	Et ₃ N	Pure LRH phase
4	4400	NaOH	RPF majority phase + LRH presence

a: molar ratio

presence of any other different compound added to control pH, such as triethylamine or pyridine in the mixture, release more hydroxide anions as the reaction runs, so that the formation of the cationic layer with a higher OH/R³⁺ ratio (molecular formula [R₄(OH)₁₀]²⁺) is favoured, and the LRH product is obtained. This factor seems to be more important than the possible amine template effect, or the possible influence of the Brönsted/Lewis acid character of the used base.

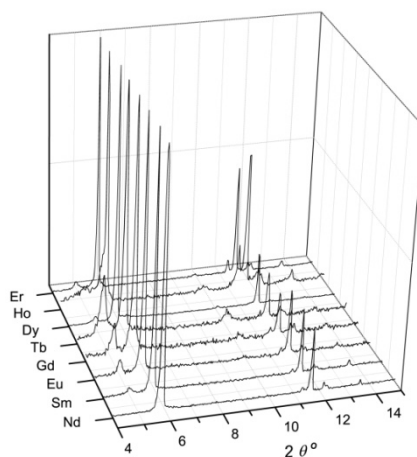


Figure III.2.26: PXRD patterns of the samples prepared under the synthesis conditions optimized for the obtaining of the RPF6 phase. The signals at $2\theta \sim 5^\circ$ and 10° correspond to the LRH phase. The signal at $2\theta \sim 6^\circ$ corresponds to the RPF6 phase.

Catalytic activity experiments:

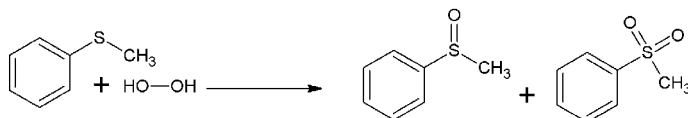
As it has been mentioned in previous chapters, the use of rare earth elements as catalyst is being increased. The use of the materials presented in this report combines the properties of the rare earth elements with the advantages of the heterogeneous catalysis. Traditional homogeneous catalysts consist of an active metal cation, and specific ligands which have influence on the activity. Generally, homogeneous catalysts present higher activity than their heterogeneous analogous, since being in solution there is a higher number of active centers accessible to the reactants. On the other hand, the recyclability and easy separation of the heterogeneous catalysts represent a clear advantage. The search for heterogeneous catalysts that present grade of activity similar to the homogeneous ones is a big challenge for the chemical industry.

The use of polymeric frameworks in which the active elements belong to the structure is an alternative to the traditional heterogeneous (or “heterogenized”) catalysts. When the conditions are optimized, they can easily be prepared in one step. In addition, and it has been explained in the introductory section, the number of possible combinations among metals and ligands is huge, allowing to introduce the most adequate elements for the reactions in which they will be used. In addition, the specific metal-ligand interactions are also present in these materials. All in all, the heterogeneous catalysis is a field in which the use of polymeric framework is very promising, and preliminary and comparative studies of catalytic activity are necessary.

The compounds presented in this chapter have been evaluated as heterogeneous catalysts, and the results offer some conclusions on the structure-properties relationship. As a first reaction test the oxidation of organic sulfides has been selected. Sulfides are oxidized to the corresponding sulfoxides and sulfones, and sulfoxides are known to have interesting and



useful biological and pharmacodynamic properties²⁷ as well as being the most widely used chiral auxiliaries^{28,29}. The selected substrate was methyl-phenyl sulfide (scheme III.2.01).



Scheme III.2.01: The oxidation of methyl-phenyl sulfide with hydrogen peroxide produces the corresponding sulfoxide or the overoxidized sulfone.

General procedure for oxidation reactions: Oxidation reactions were carried out in a 15 ml flask equipped with a magnetic stirrer. The flask was charged with: i) 5 ml of a suspension of the catalyst in acetonitrile. ii) a solution of substrate (methyl phenyl sulfide, 1 mmol). The oxidant, H₂O₂ 50 % was added dropwise while the overall suspension was heated at 353 K. Samples were taken at regular times and, after filtration, they were analyzed by means of gas chromatography. The ratio R³⁺ / substrate was 1 : 100 for the RPF6 and RPF7 compounds, and 1 : 1000 for the RPF5 and LRH materials.

Separation and recycling: After the reaction cycles, the catalyst was separated by decantation of the solution, and reused with fresh solvent and substrate, starting a new cycle of reaction when the oxidizing agent is added. While the oxidation of sulfide continued in presence of the catalyst, there was no further significant conversion when the catalyst was removed from the reaction system. The kinetic curves of three consecutive cycles of reaction are shown in figure III.2.27 and figure III.2.28.



The turnover frequency defines the molecules reacting per active site in unit time and it is a parameter that helps us to compare several catalysts. TOF values are shown in table III.2.15. The four families of compounds prepared with rare-earth cations and 2,6-anthraquinone-disulfonate anions are active as redox catalysts, showing good grade of conversions in three consecutive cycles of reaction. There is a great difference among the LRHs and the RPFs families, demonstrating the LRH compounds a higher grade of activity, with TOF values above 1150 h^{-1} . The structures of the RPFs families are quite dense, and diffusion of the reactants is not possible. The catalytic activity takes place on the surface and the number of accessible active sites is therefore low. This explains the lower TOF values exhibited by them. Among the three RPF families, the RPF6 and RPF7 families present lower TOF values than RPF5. This fact can be explained in terms of coordination number. In RPF5 the rare-earth cation is present with coordination number seven, while in RPF6 the CN is 8, and in RPF7, there are cations with CN 8 and 9. With a lower coordination number, the approximation of the reactants and the formation of the active species are easier, and the catalytic activity should therefore be higher. In the case of the LRHs, despite of the rare-earth cations are in coordination numbers 8 and 9, the compounds have a more open structure, allowing the diffusion of the reagents through the channels present in the framework. Due to this, there is a higher amount of accessible active sites. On the other hand, the selectivity to sulfoxide is quite good (table III.2.16). La-RPF7 and Ho-LRH show the lowest selectivity, which in any case is above 70 %. In contrast, the two Yb compounds, Yb-RPF5 and Yb-LRH, are able to oxidize the sulfide to almost exclusively sulfoxide. The high values of TOF and selectivity exhibited by the Yb-LRH compound make this compound as a very promising material as efficient redox heterogeneous catalyst.

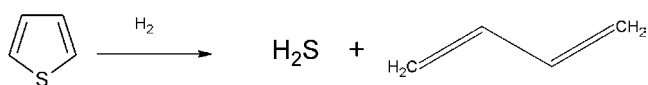
Table III.2. 15: TOF values presented by the compounds employed as catalysts in the oxidation of methyl-phenyl sulfide.

TOF (h ⁻¹)	La-RPF7	Pr-RPF7	Nd-RPF6	Sm-RPF6	Dy-RPF6	Yb-RPF5	Dy-LRH	Ho-LRH	Er-LRH	Yb-LRH
Run 1	19.8	24.6	33.0	16.5	31.3	268.6	1186.7	1133.3	1200.0	1200.0
Run 2	22.0	22.0	35.4	17.8	24.6	185.7	1560.0	1133.3	1460.0	1220.0
Run 3	21.2	21.7	22.7	19.3	31.6	270.0	946.7	1200.0	1066.7	1280.0
Average	21.0	22.8	30.4	17.9	29.1	241.4	1231.1	1155.6	1242.2	1233.3

Table III.2.16: Selectivity to sulfoxide, as % of sulfoxide in the products

Selectivity to sulfoxide	La-RPF7	Pr-RPF7	Nd-RPF6	Sm-RPF6	Dy-RPF6	Yb-RPF5	Dy-LRH	Ho-LRH	Er-LRH	Yb-LRH
Run 1	80	90	82	90	91	95	84	78	82	91
Run 2	80	86	87	90	88	98	85	71	87	93
Run 3	65	86	88	82	88	95	88	67	88	90
Average	75	87	86	87	89	96	86	72	86	91

The differences in the accessibility to the active centers between compounds can be an explanation of the substantial difference in activity among the RPF and LRH compounds. However, to go further inside the influence of the structure on the catalytic properties, another reaction was performed using the two Yb-AQDS structural types. Thus, the activity of Yb-LRH and Yb-RPF was also tested in the reaction of hydrodesulphurization of thiophene. The elimination of organic sulphur compounds is an important process in green chemistry, and of special interest for the petrochemical industry. With the hydrodesulphurization (HDS), the thiophene is decomposed under a hydrogen atmosphere to hydrogen sulfide and 1,3-butadiene, compounds easily separable. (Scheme III.3.02).



Scheme III.3.02: Scheme of the hydrodesulphurization of thiophene under hydrogen atmosphere.

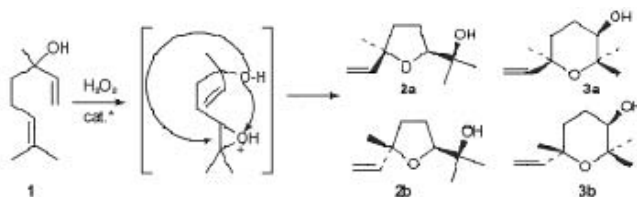


The reactions were carried out in a Parr reactor, under 6 bar of H₂. For thiophene decomposition, 10 ml (125 mmol) of substrate and 0.040 g of Yb-LRH or 0.072 g of Yb-RPF5 (0.125 mmol of Yb-catalyst) were mixed and heated at different temperatures, with stirring. After selected time intervals, the reactor was cooled, then opened and the remained amount of thiophene was measured.

The Yb-LRH under 6 bar of H₂ at only 343 K shows a conversion of 50% in 26 hours, with a ratio substrate/Yb = 1000. It is worth pointing out that these results are obtained under much milder conditions than those usually utilized (high pressure of H₂, i.e. 30-60 bar and at temperatures in the range 623-673 K)³⁰. For the Yb-RPF-5, a higher grade of conversion is obtained with the same rate of substrate vs. active centre and the total decomposition of the thiophene is achieved after 24 hours. By increasing the temperature, the reaction becomes faster in such a way that only 16 hours are needed at 373 K, and a conversion of 90% is found after only 4.3 hours at 393 K.

In contrast to the oxidation reaction tests, in the HDS reaction the RPF5 compounds demonstrate a higher activity, and therefore, in this case the porosity and accessibility of the active sites do not seem to be the most decisive factors. Reasons related to the reaction mechanism and the differences in the structures are of higher influence on the catalytic activity. From a reaction mechanism viewpoint, the sulfo-oxidation reaction has to go through the corresponding peroxy species, as it happens in the hydrolysis of phosphodiester³¹ and RNA¹⁴, catalyzed by peroxide rare earth complexes formed in rare earth - H₂O₂ mixtures. In the case of the use of rare-earths as catalysts in the oxidation of sulfides, spectroscopic evidences as the presented in chapter 1 have allowed us to recently propose a reaction mechanism involving the presence of a Ln – O – OH intermediate species¹⁵. Accordingly, the different catalytic behavior of the two kinds of compounds in sulfides oxidation is a consequence of the different charge density over the rare earth cation caused by the ligand nature: In the cationic layer of Yb-LRH, the

coordination sphere of the Yb atom is composed only by oxygen atoms of μ_3 -OH anions, and one water molecule. In the 3D Yb-RPF5, the charge density over the Yb cation is higher, since most oxygen atoms of the coordination sphere come from SO_3^- groups, and thus, the formation of the active peroxy complex is slower when using this latter system as catalyst. In the case of the HDS reaction, though the Yb-RPF5 structure is less open than that of Yb-LRH and thus, the catalytic reaction should take place only on surface, the activity of the former is higher. This is due to the low Yb coordination number in this compound, which allows an easier access of the substrate to the active centre. In addition, the acidity coming from the coordinated ligand favours the heterolytic rupture of the hydrogen molecule and the subsequent reaction with the substrate. To support the fact that the coordination of the ligand gives more acidity to the active metal centre, another catalytic reaction in which acid centres are needed, was also carried out. The two materials were then tested as bifunctional redox-acid catalyst in the transformation of 3,7-dimethylocta-1,6-dien-3-ol (linalool) to hydroxy ethers (furanoid and pyranoid forms, 2 and 3 in scheme III.3.03), in acetonitrile, at 353 K, with an excess of H_2O_2 . In the reaction scheme, shown below, the first step involves the epoxidation of the 2,3 double bond. In the second step, the presence of acid sites is needed for the intramolecular opening of the epoxide ring by the hydroxyl group at position 6 or 7.



Scheme III.3.03: Catalytic oxidation of linalool.

As it has been shown above, the Yb-LRH material is very active as redox catalyst, but acts poorly as acid catalyst, so that only 36% of conversion occurs after 28 hours, with a ratio 1 : 100 Yb : substrate. In the case of Yb-

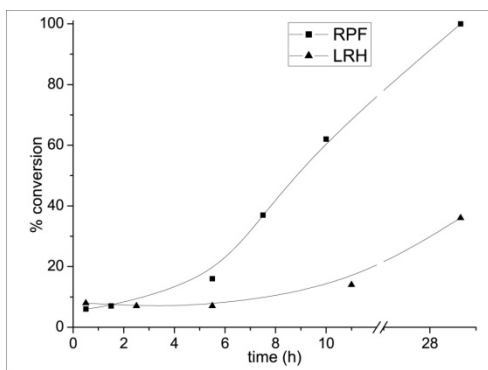


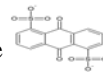
Figure 29: Kinetic profile for the epoxidation of linalool employing the Yb-RPF5 and the Yb-LRH compounds as catalysts

RPF5, a total conversion is achieved after 28 hours, with the same Yb to substrate ratio, and with a high selectivity to the furanoid *versus* pyranoid products (9:1 in the first run; 7:3 in the second run). Figure III.2.29 shows the activity of both products for the oxidation of linalool. These results support the fact that the coordination or its absence of the SO_3^- groups has a decisive

influence on the catalytic activity. Besides, it can also be concluded that the structural features related to the coordination environment of the metals are of high importance in the development of the catalytic reactions in which the materials are to be used, and employing the same components, a correct choice of the synthesis conditions allows the preparation of the most adequate framework.

The results presented in this chapter have been published in *Angewandte Chemie International Edition*, 2006, 45, 7998, and *Chemistry of Materials*, 2009, 21, 655. They can be found in part VI of this report.

The LRH materials have been patented, with number P200601422



3. RPF8: Rare earth + Anthraquinone-1,5-disulfonate

Introduction

In the previous chapter, the possibilities that anthraquinone-2,6-disulfonate anion (AQDS²⁻) offers for the construction of hybrid organo-inorganic materials have been described. In the four different structural types there presented, inorganic layers are joined by the organic molecules. The geometry of the 2,6 isomer of the anthraquinone molecule seems to be favorable for this type of construction. In the previous work²³ carried out in our group on rare-earth elements and arenedisulfonate ligands, the use of two isomers of the naphthalenedisulfonate (NDS) molecules led to the formation of different structural types defined by (among other factors) the different geometry of the ligand. In the case of the current study, the anthraquinonedisulfonate molecules differ from their NDS analogues not only in the length of the organic chain, but also in the presence of the quinonic oxygen atoms in the organic skeleton, giving these atoms an extra functionality to the organic ligand.

Quinones are one of the most important and well-studied examples of organic redox couples. Quinones and their derivatives are known to have a rich redox chemistry, as they are able to suffer redox processes, involving the formation of radical species³²⁻³⁹. Their transformation by gain or loss of electrons is an important natural process in biological energy conversion, and they are also used as electron shuttle intermediates⁴⁰⁻⁴². The formation and characterization of their radical species have been widely studied with different spectroscopic and electrochemical methods (UV, EPR, CV, etc). Their use as ligands in the formation of complexes with magnetic properties has also been evaluated⁴³⁻⁴⁶.

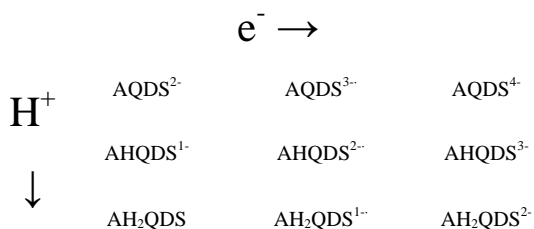
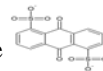


There are however only a few examples of reported crystal structures that include the radical species⁴⁷⁻⁴⁹.

As a quinone derivative, anthraquinone shows an electrochemically reversible apparent two-electron-two-proton reduction-oxidation. Like most other quinones, the electron exchanges are thought to take place in successive one-electron steps leading to one-electron radical intermediates known as semiquinones⁵⁰⁻⁵². In the case of their sulfonate derivatives, there are several reports dealing with the characterization of their different species in solution, and the study of the reduction and photoreduction processes that they suffer^{32, 34, 36, 53-58}.

On the other hand, the presence of organic radical species in metalorganic framework is not very extended yet. There are some examples of polymeric frameworks in which the organic ligand is a radical species, these materials exhibiting interesting magnetic properties⁵⁹⁻⁶³. In most cases, the radical species exist previous to their use in the formation of the extended network.

The formation of the anthraquinone radical species has been described in the literature, and it can be accomplished by means of electrochemical methods (electroreduction of the reactants) and photoreduction. In the case of the latter, different mechanisms of formation have been proposed, involving the excitation of the AQDS molecules to a triplet state and electron exchange processes^{32, 34, 36, 53, 54}. The general scheme of the AQDS electron and proton transfer system is a nine-member scheme as shown below. With protic solvents, the overall system is a two-electron-two-proton process. At high pH values, the disproportionation reactions between the radical anions can be neglected. At this pH conditions the radical lifetimes are known to be long⁶⁴. In the case of aprotic solvents, quinones are well known to undergo two successive one electron reductions, first to form the radical anion and then the dianion^{65, 66}.



Scheme III.3.01: The nine members in the two electron-two proton oxidation-reduction process of the anthraquinone-disulfonate molecule.

Following with our study on rare-earth disulfonate MOFs, in this chapter the use of the anthraquinone-1,5-disulfonate ligand to prepare a family of rare-earth polymeric frameworks, RPF-8, is presented. In this family of polymeric compounds the organic molecules are found as anion radicals, and their formation is achieved by an in situ reduction of the commercial Na₂AQDS reagents, this reduction taking place during the solvothermal reaction.

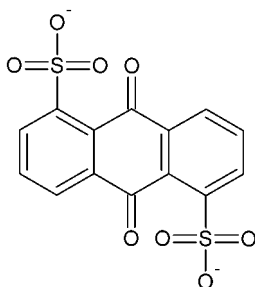


Figure III.3.01: the anthraquinone-1,5-disulfonate anion

Synthesis

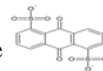
The solvothermal reaction of Na₂AQDS with a nitrate salt of Ln (Ln=La-Er) results in the formation of the new material. The optimized synthesis conditions are as follows: 0.260 g of Na₂AQDS and 0.130 g of La(NO₃)₃·6H₂O are solved in 5.4 ml of water, and then 16.4 ml of BuOH are added. The molar composition of this mixture is



0.5La:AQDS:500H₂O:300BuOH. The mixture is stirred at room temperature for 5 minutes, and then placed into a Teflon lined stainless steel autoclave. This is sealed and heated in an oven at 180 °C for 18 hours. After the heating time, the autoclave is cooled to room temperature and the product is filtered and washed with deionized water and acetone. An equal synthesis procedure was employed for the products prepared with the other rare earth elements.

The obtained product was a microcrystalline dark solid, which revealed to be formed by be green crystals. The mother liquor was orange, since it contained an excess of the anthraquinone salts. A single crystal suitable for X-ray crystallography was obtained in the case of the syntheses with lanthanum, praseodymium, samarium, and gadolinium, while all other compounds demonstrated to be isostructural by means of powder X-ray diffraction.

Regarding to the study of the synthesis conditions, the presence of both water and butanol, solvents is necessary for the formation of the product. The experiments carried out in water and in absence of butanol resulted in the formation of exclusively an amorphous red solid. A series of experiments were carried out with initial mixtures of molar composition of La : AQDS : 500 H₂O : x BuOH (x = 0, 10, 20, 100, 200, 300). As the amount of butanol in the initial mixture increases, more green crystals of the new material appear in the product. With x = 300, the product appear as major phase, but with low yield, and mixed with the red solid in the product. The only way to obtain the desired product as the only phase and in good yield is to adjust the initial mixture composition to a ratio of AQDS / Ln = 2. With this initial mixture, the green RPF8 product is obtained purely and in good yield. It is known that the AQDS molecules suffer self-exchange electron processes when the radical species are formed, and it seems plausible that during the synthesis procedure an excess of AQDS molecules is needed to somehow stabilize the presence of the radical species before they coordinate to the Ln ions, forming the new material.



Structure

With the obtained single crystals, the structure of the RPF8 compounds was determined. The product crystallizes in the orthorhombic system, space group $P2_12_12$. The formula of the compounds is $C_{14}H_{12}O_{11}S_2Ln$ which is equivalent to $LnL(H_2O)_3$, where $L = AQDS^{3-}$. The main crystallographic and refinement data are found in table III.3.01. The Ln atoms are octacoordinated to three water molecules, and to five oxygen atoms from the organic ligands. Three of them are oxygen of the SO_3^- groups, and two are quinonic oxygen atoms. Thus, opposite to the 2,6-AQDS compounds, in the RPF8 phase the quinonic oxygen atoms are coordinated to the Ln cations. The 1,5 disposition of the SO_3 groups makes possible that the AQDS molecule behaves as a chelating ligand, coordinating to the Ln cations through both the sulfonic and the quinonic oxygen atoms. There are two different SO_3^- groups regarding to their coordination modes. One of them is bonded to two Ln cations in a $\eta^2\mu_2$ mode, through two oxygen atoms, while the other is monocoordinated to a Ln cation, in a η^1 mode. The asymmetric units are represented in figure III.3.02. the coordination polyhedron of the Ln cations is represented in figure III.3.03.

The Ln atoms are forming zig-zag chains along the a direction, via the bridge $\eta^2\text{-}\mu_2$ sulfonate group. Two AQDS molecules join these chains along the b direction, giving rise to double layers, which stack in the c axes in an AA sequence. Hydrogen bonds are present between adjacent layers, formed by the coordinated water molecules and the uncoordinated oxygen atoms of the sulfonate groups.



Table III.3.01: Crystal and refinement data for the RPF8 compounds.

Identification code	La-RPF8	Pr-RPF8	Sm-RPF8	Gd-RPF8
Empirical formula	$C_{14}H_{12}S_2LaO_{11}$ [La($C_{14}H_6S_2O_8$) (H_2O) ₃]	$C_{14}H_{12}S_2PrO_{11}$ [Pr($C_{14}H_6S_2O_8$) (H_2O) ₃]	$C_{14}H_{12}S_2SmO_{11}$ [Sm($C_{14}H_6S_2O_8$) (H_2O) ₃]	$C_{14}H_{12}S_2GdO_{11}$ [Gd($C_{14}H_6S_2O_8$) (H_2O) ₃]
Formula weight	559.27	561.27	570.71	577.61
Temperature	295(2) K			
Wavelength	0.71073 Å			
Crystal system, space group	Orthorhombic, $P2_12_12$			
Unit cell dimensions	$a = 11.5258(7)$ Å $b = 21.0639(12)$ Å $c = 7.1175(4)$ Å	$a = 11.4498(17)$ Å $b = 20.923(2)$ Å $c = 7.1043(9)$ Å	$a = 11.465(3)$ Å $b = 20.956(5)$ Å $c = 7.1395(16)$ Å	$a = 11.3486(17)$ Å $b = 20.756(3)$ Å $c = 7.0785(11)$ Å
Volume	$1727.97(17)$ Å ³	$1702.0(4)$ Å ³	$1715.3(7)$ Å ³	$1667.4(4)$ Å ³
Z, Calculated density	4, 2.150 Mg/m ³	4, 2.190 Mg/m ³	4, 2.210 Mg/m ³	4, 2.301 Mg/m ³
Absorption coefficient	2.776 mm ⁻¹	3.170 mm ⁻¹	3.729 mm ⁻¹	4.292 mm ⁻¹
F(000)	1092	1100	1112	1120
Crystal size	0.10 x 0.05 x 0.05 mm	0.30 x 0.06 x 0.02 mm	0.30 x 0.02 x 0.02 mm	0.30 x 0.02 x 0.02 mm
Theta range for data collection	1.93° to 29.25°	2.03° to 26.37°	2.01° to 25.67°	2.66° to 26..6°
Limiting indices	-8<=h<=15 -27<=k<=27 -6<=l<=9	-8<=h<=14 -21<=k<=26 -8<=l<=8	-13<=h<=13 -25<=k<=21 -8<=l<=8	-14<=h<=13 -25<=k<=25 -8<=l<=8
Reflections collected / unique	9259 / 4052	6516 / 3213	8913 / 3091	12311 / 3392
Completeness to theta = 25.00°	98.4 %	97.7 %	97.1 %	99.4 %
Absorption correction		Semi-empirical from equivalents		
Max. and min. transmission	0.8737 and 0.7688	0.9393 and 0.4497	0.9637 and 0.4009	0.9583 and 0.3592
Refinement method		Full-matrix least-squares on F ²		
Data / restraints / parameters	4052 / 0 / 253	3213 / 132 / 253	3091 / 84 / 242	3392 / 0 / 247
Goodness-of-fit on F ²	1.030	0.977	0.975	0.976
Final R indices [I>2σ(I)]	R ₁ = 0.0558, wR ₂ = 0.1270	R ₁ = 0.0539, wR ₂ = 0.0795	R ₁ = 0.0589, wR ₂ = 0.0977	R ₁ = 0.0493, wR ₂ = 0.0787
R indices (all data)	R ₁ = 0.0759, wR ₂ = 0.1394	R ₁ = 0.0820, wR ₂ = 0.0867	R ₁ = 0.1003, wR ₂ = 0.1083	R ₁ = 0.0812, wR ₂ = 0.0864
Flack parameter	-0.02(3)	0.01(3)	0.42(3)	0.02(2)
Largest diff. peak and hole	1.481 and -3.038 e·Å ⁻³	0.940 and -0.945 e·Å ⁻³	0.878 and -1.153 e·Å ⁻³	0.854 and -1.270 e·Å ⁻³

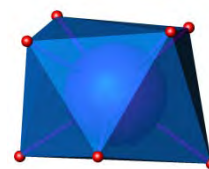
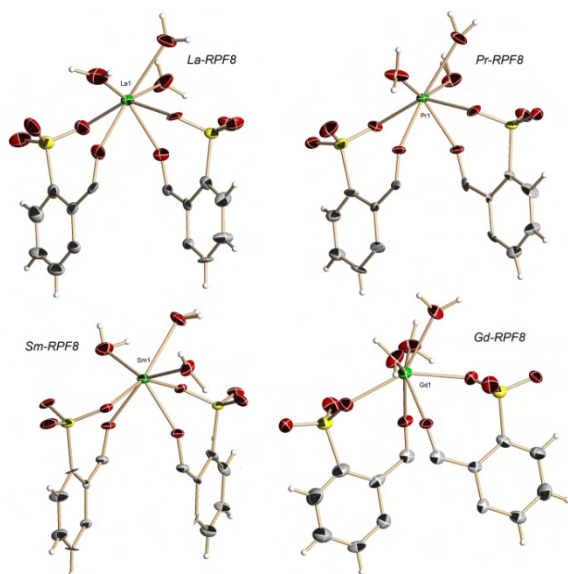
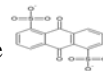


Figure III.3.03: the coordination polyhedron in RPF8: a distorted tricapped trigonal prims

Figure III.3.02: ORTEP representation (50% probability) of the asymmetric units of the RPF8 compounds. Green: Ln atoms; Red: O atoms; Yellow: S atoms; Grey: C atoms; White: H atoms.

Table III.3.02: Interatomic distances in the coordination spheres of the metal atoms in the RPF8 compounds.

La-RPF8		Pr-RPF8		Sm-RPF8		Gd-RPF8	
Bond	Distance (Å)	Bond	Distance (Å)	Bond	Distance (Å)	Bond	Distance (Å)
La(1)-O(1)	2.529(6)	Pr(1)-O(3)	2.487(7)	Sm(1)-O(1)	2.459(8)	Gd(1)-O(1)	2.425(6)
La(1)-O(2)	2.519(7)	Pr(1)-O(4)	2.476(7)	Sm(1)-O(4)	2.481(8)	Gd(1)-O(3) ²	2.431(6)
La(1)-O(4)	2.526(7)	Pr(1)-O(5) ¹	2.489(6)	Sm(1)-O(5) ¹	2.449(8)	Gd(1)-O(4) ¹	2.411(6)
La(1)-O(7)	2.383(7)	Pr(1)-O(7)	2.328(7)	Sm(1)-O(7)	2.323(9)	Gd(1)-O(7)	2.285(6)
La(1)-O(8)	2.367(7)	Pr(1)-O(8)	2.343(6)	Sm(1)-O(8)	2.316(8)	Gd(1)-O(8)	2.278(6)
La(1)-O(9)	2.485(8)	Pr(1)-O(9)	2.551(7)	Sm(1)-O(9)	2.424(9)	Gd(1)-O(9)	2.374(6)
La(1)-O(10)	2.625(7)	Pr(1)-O(10)	2.442(7)	Sm(1)-O(10)	2.540(9)	Gd(1)-O(10)	2.481(6)
La(1)-O(11)	2.536(8)	Pr(1)-O(11)	2.494(7)	Sm(1)-O(11)	2.464(8)	Gd(1)-O(11)	2.414(6)
		Symmetry operator to generate equivalent positions: 1: x-1/2,-y+3/2,-z+2		Symmetry operators to generate equivalent positions: 1: x+1/2,-y+1/2,-z+2		Symmetry operators to generate equivalent positions: 1: -x+1,-y+2,z 2: x-1/2,-y+3/2,-z+1	

The disposition of the Ln atoms in the layers, and their connection through the ligands gives rise to a 6^3 honeycomb topology of the double layers, with the Ln atoms as the three connected nodes, joined by ligand molecules (figure III.3.03). The coordinated water molecules and the uncoordinated oxygen



atoms from the sulfonate group form hydrogen bonds, and if they are taken into account, the Ln atoms of adjacent layers become connected among them, giving rise to the three-dimensional bnn hexagonal network.

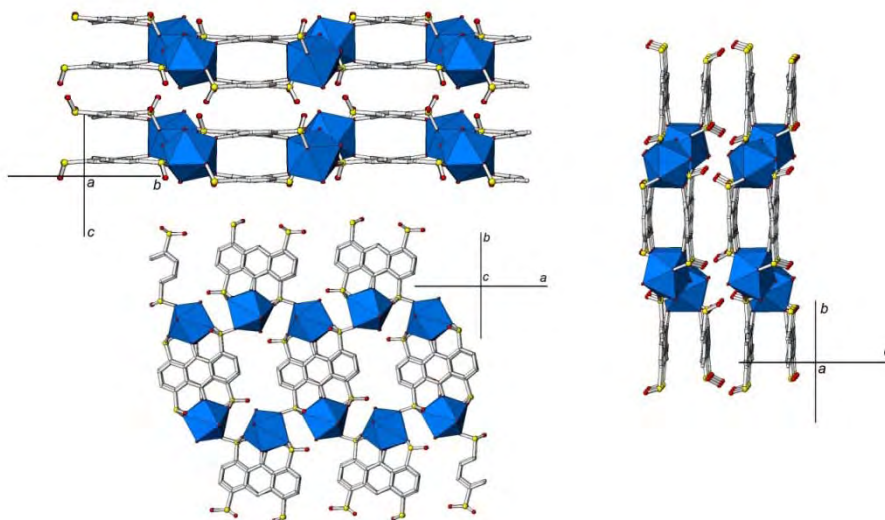


Figure III.3.04: Three views of the RPF8 structural type: The LnO8 polyhedra are disposed forming chains along the a axis. The joining of these chains is made by two AQDS molecules to give rise to double layers, stacking along the c direction.

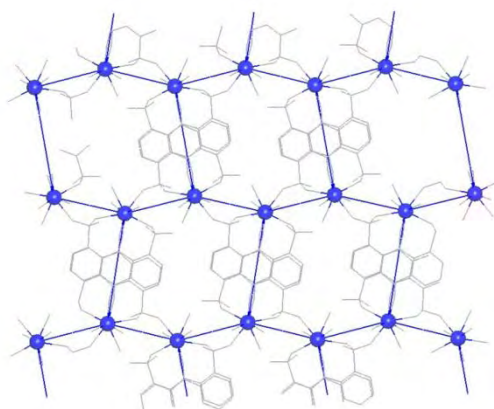
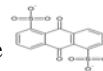


Figure III.3.05: The topological simplification of the double layers. The Ln nodes are disposed forming a 6^3 layer.



In the RPF8 structural type, the anthraquinone molecules are present as AQDS³⁻ anion radical. There are not many examples of semiquinones crystal structures reported, and to the best of our knowledge this is the first case of an anthraquinone radical species crystallographically characterized and also the first example of a radical species in MOFs, formed in situ during the synthesis.

In the semiquinone species, the additional charge is delocalized over the anthraquinone molecule central ring and the quinonic oxygen atoms. The bond distances of these O atoms with their corresponding C atoms suffer then an elongation, since this bond has a partial single component in the radical species. The C – C bonds in the central ring are also affected by the presence of an additional electron. Thus, bond 2, as numerated in figure xx, suffers a decrease in its length, since the electronic delocalization implies a partial aromatic component in this central ring, while bond 3 is elongated.

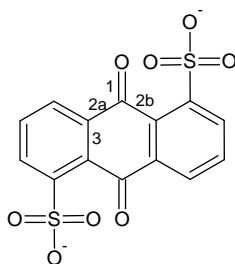


Figure III.3.06: numeration of the bonds that experiment changes in their length as result of the reduction of the anthraquinone molecule.

In the four crystal structure here reported, the values of the C – O bonds lie in the range 1.260(15) to 1.302(13) Å, clearly demonstrating the partially single bond nature in this bond, due to the reduction of the molecule.. For each crystal, there are two C – O bonds, corresponding to the two different AQDS molecules in each case (the asymmetric units comprises two halves AQDS molecules). The values of these bond lengths are compared in Table III.3.03 together with those corresponding to the oxidized form of AQDS.



To obtain the radical species, several factors are decisive: as mentioned above, the presence of BuOH as a co-solvent is necessary. In addition, the presence of the rare-earth element in the system also has influence not only in the structural type obtained, but also in the formation of the radical species during the synthesis procedure. To prove this fact, several synthesis experiments were performed: first, a synthesis procedure in absence of rare earth salt was carried out. A mixture with the same amounts of Na₂AQDS, water and butanol was heated for the same time at the same temperature. Orange large crystals were obtained. The structure of one of them was solved, revealing to be a sodium salt of AQDS, isostructural to that found in the Cambridge Structural Database (CSD), with reference HAPXOL⁶⁷. In this crystal structure, the AQDS molecules also behave as chelating ligands, with coordination to the Na ions through the sulfonic and the quinonic O atoms. There is another Na₂AQDS crystal structure deposited in the CSD database, with code YIWYAE⁶⁸. In these two crystal structures, the C – O bond distances are 1.216 and 1.217 Å respectively, typical of the double C–O bond of quinonic group

On the other hand, synthesis experiments employing transition metals were also carried out. Mixtures of molar composition equivalent to the optimized for the rare-earth elements were prepared, now with transition metal salts instead of the rare-earth salts. CoCl₂ and FeCl₂ were used. A same structural type was obtained in both cases, with the M²⁺ cations hexacoordinated to two water molecules and to four O atoms from four sulfonate groups. In this case, the anthraquinone molecules appear as AQDS²⁻ dianion, with no presence of the radical species. The C – O bonds are those expected for the C–O double bond typical in the not reduced form of the AQDS anion. Details of the crystal structures of the Fe and Co AQDS compounds can be found in the supplementary material, chapter V.1. These experiments demonstrated that the presence of the rare-earth elements is necessary to obtain the semiquinone species in a crystalline solid.

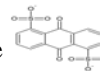


Table III.3.03: Interatomic distances in the AQDS molecules of different compounds

Compound	HAPXOL (ref. 67)	YIWYAE (ref. 68)	Co- AQDS	Fe- AQDS	LaRPF8	PrRPF8	SmRPF8	GdRPF8
Bond^a	<i>quinones</i>				<i>Semiquinones^b</i>			
1	1.217	1.216	1.211(4)	1.213(3)	1.302(11)	1.282(11)	1.260(15)	1.277(10)
					1.301(12)	1.270(11)	1.302(13)	1.271(11)
2a	1.487	1.482	1.505(4)	1.500(3)	1.441(14)	1.450(13)	1.458(16)	1.464(13)
					1.426(14)	1.454(14)	1.426(16)	1.464(13)
2b	1.498	1.496	1.498(4)	1.492(3)	1.451(15)	1.455(12)	1.508(17)	1.438(12)
					1.447(12)	1.461(14)	1.426(17)	1.435(13)
3	1.410	1.404	1.396(3)	1.399(3)	1.402(13)	1.417(12)	1.453(17)	1.430(12)
					1.418(12)	1.453(14)	1.426(17)	1.459(13)

a: bonds are numerated according to figure III.3.06
b: in the RPF8 compounds, two values are given for each bond, since there are two independent molecules in the asymmetric unit.

On the other hand, the formation of the radical species, and the coordination to the metals in a chelating manner, makes the AQDS molecules to be disposed in a parallel way. This gives rise to the presence of $\pi - \pi$ stacking interactions between the anthraquinone molecules. They stack along the c axis, in a perfect face-to-face disposition, with interactions among the three rings of the molecules. This type of disposition is not common in anthraquinone crystals, and in the RPF9 structural type, this is achieved thanks to the formation of the semiquinone species, allowing a higher interactions among the central rings. Besides, the chelating coordination to the metals, also forces the molecules to be parallel and perfectly aligned.

Two distances among planes are found, one between molecules belonging to a same double-layer, and the other between adjacent layers. The values of the distances are shown in Table III.3.04:

Table III.3.04: Distances between AQDS molecules planes

	La-RPF8	Pr-RPF8	Sm-RPF8	Gd-RPF8
Intra-layer distance (Å)	3.43	3.42	3.43	3.39
Inter-layer distance (Å)	3.69	3.67	3.71	3.68



Characterization

X-ray powder diffraction

The X-ray powder patterns of the RPF8 compounds demonstrate that the materials can be obtained as pure phases. A Rietveld refinement was carried out for each compound, and the results are shown in figure III.3.07.

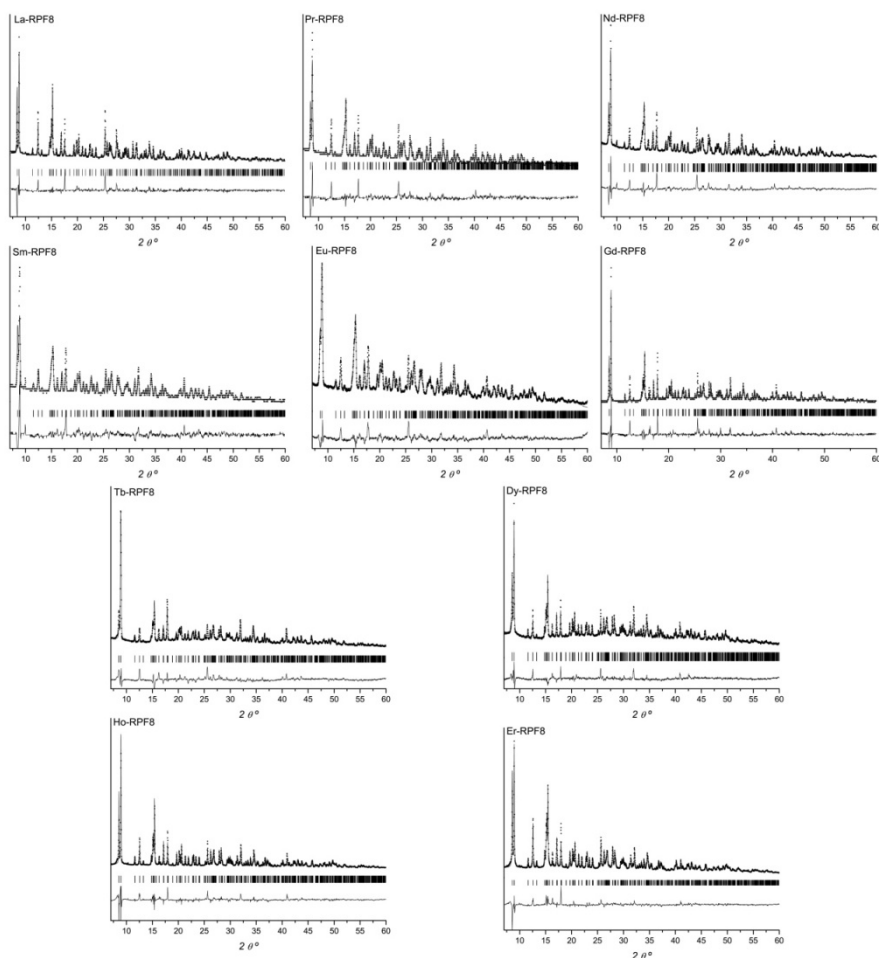
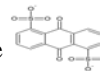


Figure III.3.07: Rietveld refinements of the RPF8 compounds, showing experimental (dots), simulated (line) and difference patterns. The Bragg positions are marked as columns.



Thermal and elemental chemical analysis:

The results of the elemental analyses for the RPF8 compounds are presented in table III.3.05, compared with their calculated values.

Table III.3.05: Elemental analysis results of the RPF8 compounds

Rare earth		La	Pr	Nd	Sm	Eu	Gd	Tb	Dy	Ho	Er
%C	calculated	30.04	29.93	29.76	29.44	29.35	29.00	28.82	28.70	28.59	29.09
	experimental	30.28	30.25	29.21	29.30	28.90	26.46	26.89	27.09	25.04	28.06
%H	calculated	2.17	2.16	2.15	2.12	2.12	2.09	2.08	2.07	2.06	2.10
	experimental	2.22	2.16	2.09	2.11	2.09	2.09	2.12	2.09	2.10	2.08

The lower values of %C in some of the compounds might be due to the presence of water molecules, coming from the synthesis

The TG curves of the RPF8 compounds are shown in Figure III.3.07. Under heating, the compounds gradually decompose, first losing the coordinated water molecules in a temperature range ~ 150 – 310 °C (calculated mass loss for La-RPF8, 9.4%, observed 9.5%), followed by the loss of the organic component of the framework, and the subsequent total decomposition.

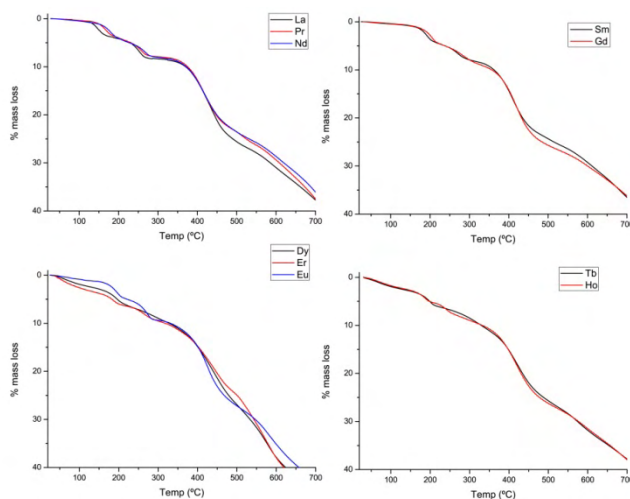


Figure III.3.07: TG curves of the RPF8 compounds



Conductivity measurements

Conductivity is a property not much studied in coordination polymers. There are some examples of coordination polymers exhibiting electrical conductivity⁶⁹⁻⁷². In general, they are transition metal compounds, in which there are short distance contacts between the metal atoms and the π electrons of the ligands, and / or with π - π stacking interaction at very low distances.

In RPF8 compounds, where the metallic cations are those of the rare earth elements, the possible conductivity could be a consequence of the interactions among the anthraquinone molecule π systems. As it was described above, the anthraquinone radical molecules are arranged in a perfect face-to-face disposition at two different distances between their planes. The intralayer distance is short, ~ 3.4 Å while the interlayer one is around 3.7 Å. (with small variation depending on the R cation)

Conductivity measurements were carried out in a single crystal of the La-RPF8 compound with dimensions 0.420 x 0.055 x 0.055 mm. The contacts were fixed with silver coated glue at the extremes of the crystal. The current intensity was measured *versus* the applied voltage, in the range 0-100 V. In

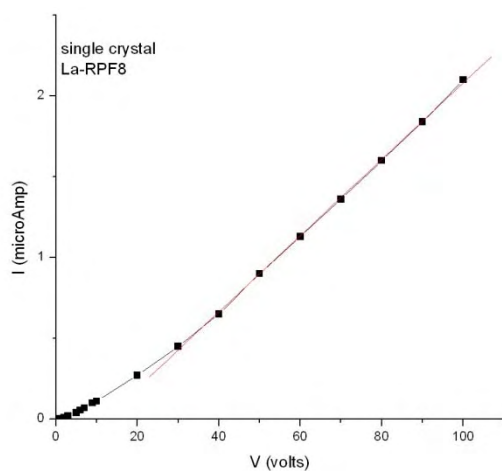
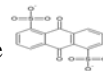


Figure III.3.08: *I* vs. *V* measured in a La-RPF8 crystal

figure III.3.08, the values of the measured current intensity are represented.

Calculated room temperature conductivity for La-RPF8 crystal is $3.3 \cdot 10^{-3} \text{ S cm}^{-1}$. This value is within the range of other compounds with π - π stacking interaction with shorter distances among



aromatic rings⁶⁹, or even that caused by interactions among transition metals in 1D net⁷⁰. This seems to indicate that the presence of a delocalized electron in the anthraquinone radical improves the conducting properties of the materials.

Magnetic measurements:

Although it is known that most Rare-earth containing compounds are paramagnetic, and reach the magnetic order, if any, at very low temperatures, we performed magnetic susceptibility measurement on RPF8 compounds, to see the influence of the radical in the compounds magnetism.

The magnetization measurements were performed as a function of temperature and field using a Quantum Design superconducting quantum interference device SQUID magnetometer in the range 2 to 300 K and fields up to 50 kOe. The samples in the form of powder (typically 20 mg) were closed in diamagnetic polycarbonate capsules. The background signal from the straw and capsule were measured separately and subtracted from the data to give the pure magnetic signal of the samples. For each sample, the susceptibility have been measured in a field of 10 kOe, first decreasing the temperature down to 2 K and then increasing it up to 300 K. Additionally, a magnetization curve a function of field has been measured at $T = 10$ K. Finally, for the Dy and Ho based samples, we used a Quantum Design PPMS extraction magnetometer to get $M(H)$ curves up to 85 kOe at several temperatures down to 2 K.

As it was expected, all those compounds of the RPF8 series with unpaired f electrons resulted to be paramagnetic, and with a Curie-Weiss temperature $\Theta < 0$ in all cases, indicating the presence of antiferromagnetic exchange interactions, except for Gd-RPF8 compound.



Magnetic moment values were higher than those corresponding to the free Ln^{3+} cations in all the cases. In order to prove that this increase is due to the radical semiquinone species, we performed the same measurement in the La-RPF8 compound, with none unpaired f electron. The result was a paramagnetic material, with an effective magnetic moment μ of 0.39.

To rule out the possibility of a contamination in the $\text{La}(\text{NO}_3)_3$ reagent, a magnetic susceptibility measurement was also carried out on La-RPF7 compound (synthesized with the same $\text{La}(\text{NO}_3)_3$ reagent and 2,6-AQDS, in which no radical is formed). As expected for a La^{3+} compound, the value of the magnetic moment in La-RPF7 resulted to be null ($\mu = 0$). All together indicates the presence of the radical species. In figure III.3.09 the variation of the atomic magnetic moment for the La-RPF7 and La-RPF8 compounds is compared, showing the magnetic contribution of the radical in RPF8.

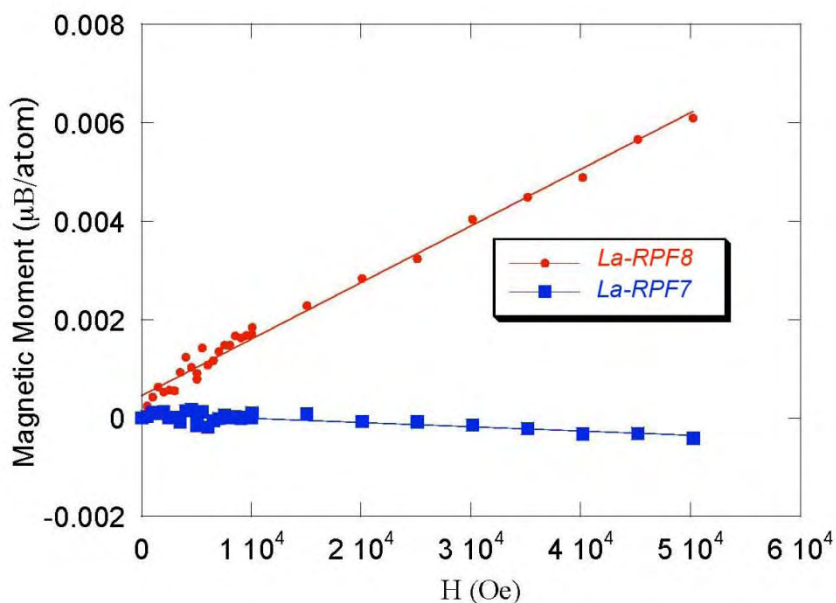


Figure III.3.10: Comparison of the atomic magnetic moment for the La-RPF7 and La-RPF8 compounds.

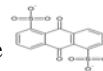


Table III.3.06 shows the experimental and calculated magnetic moment for the different Ln free ions. Figure III.3.10 shows the temperature dependence of the magnetic susceptibility and of the inverse susceptibility at 10 kOe.

Table III.3.06 Magnetic moment of the RPF8 compounds

Compound	μ_{eff}	θ_p (K)	Free Ln ³⁺ ion	μ_{eff}
La-RPF7	0	-	La	0
La-RPF8	0.39	-47.54	La	0
Pr-RPF8	3.63	-32.72	Pr	3,58
Nd-RPF8	3.72	-38.55	Nd	3,62
Sm-RPF8	3.31	-595.25	Sm	0.85
Eu-RPF8	4.63	-315.61	Eu	0
Gd-RPF8	8.1	0.1	Gd	7,94
Tb-RPF8	10.65	-5.65	Tb	9,72
Dy-RPF8	10.97	-1.94	Dy	10,65
Ho-RPF8	10.82	-6.48	Ho	10,61
Er-RPF8	9.94	-6.6	Er	9,58

As it can be seen in the graphics, the Gd, Tb, Dy, Ho and Er RPF8 compounds follow the Curie-Weiss law, and with small deviations the La, Pr, and Nd compounds. The behavior of the Sm and Eu RPF8 compounds do not fit with the Curie-Weiss law, since there is a contribution of the Van Vleck paramagnetism.



III.3: RPF8: Rare earths + Athraquinone-1,5-disulfonate

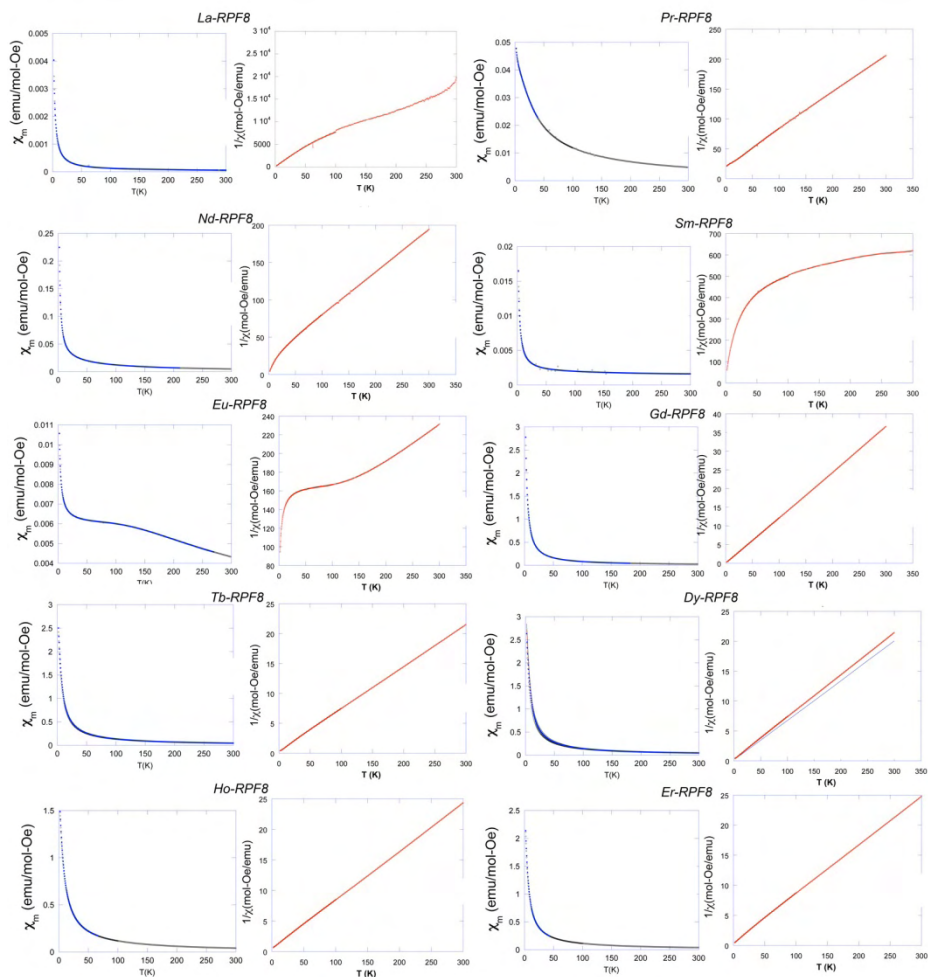
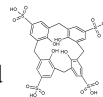


Figure III.3.09: representation of the molar magnetic susceptibility (blue graphics) and its inverse (red graphics) vs. temperature for the RPF8 compounds.



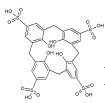
4. RPF9: Rare earth + calix[4]arene-*p*-sulfonic acid

Introduction

This chapter deals with the preparation of the RPF9 family of compounds, which is the last family of compounds here presented. These compounds have been prepared with a sulfonate derivative ligand, calix[4]arene-*p*-sulfonic acid, and their structure exhibits the especial structural features characteristic of the calixarene molecules.

Calixarenes and their analogues are fascinating basket-shaped compounds that possess the ability to hold metal ions, as well as molecules, in their interior⁷³⁻⁷⁵. In the solid state, the cone shapes of the calixarenes give bowl cavities that can encapsulate some small molecules, both charged and neutral, by weak interactions including H-bonding, H-aromatic, etc., so that these compounds have been widely regarded as important macrocyclic host molecules in host-guest chemistry⁷⁶⁻⁸⁰. As a result of their considerably easy synthesis from phenols and aldehydes⁸¹⁻⁸³, they are receiving increasingly wide attention. Water-soluble calixarenes have been exploited in all areas of supramolecular chemistry over the past two decades⁸⁴⁻⁹⁰. Some reports deal with complexes or coordination polymers of *p*-sulfonatocalix[*n*]arenes with transition metals⁹¹⁻¹⁰⁰; when dealing with rare-earth elements, not many reports can be found, being most of them dedicated to isolated or linked, through weak interactions (H-bond or π - π interactions), complexes.

In the new compounds presented in this chapter, *p*-sulfonatocalix[4]arene has been employed to give rise to a new family of polymeric frameworks. As in the previous sulfonate RPF families, the rare earth elements are found forming hydroxo aggregates, but in this case, the number of Ln atoms in the cluster is six. The synthesis of inorganic clusters continues attracting considerable



attention, due to the interesting properties of the metallic aggregates^{101, 102}. Rare earth element clusters still remain less studied than those of transition metals. The control of the hydrolysis of the lanthanide salts in presence of appropriate ligands appears as a common strategy for the synthesis of the hydroxo lanthanide clusters. However, the cluster-forming ability of *p*-sulfonatocalix[*n*]arenes as multidentate and multi-nucleating ligands has not been described up to now. Such ability has been discovered for thiacalix[*n*]arenes¹⁰³, in which the introduction of S heteroatom enforces significantly a coordinative capacity of the ligand molecule. Only tri- and tetra-nuclear clusters were found to be supported by thiacalix[4]arenes, and only up to penta-nuclear clusters, by a larger and more flexible thiacalix[6]arene. Octalanthanide and dodecalanthanide wheels were reported supported by *p*-tert-butylsulfonylcalix[4]arene^{104, 105}.

Among the lanthanide clusters, the hexanuclear hydroxo lanthanide cluster of the M6X8 type appears as a common unit, both as an independent cluster and as a core of a larger aggregate. In this M6X8 hydroxo lanthanide cluster, the Ln atoms are disposed octahedrally, linked by μ_3 -OH groups, and in most cases, with a central μ_6 oxygen atom. This latter has been suggested to have an influence on the stability of the Ln₆ units, but some examples of octahedral Ln₆ aggregates can be found without it¹⁰⁶⁻¹⁰⁹. Despite in the most of the examples the hydroxo lanthanide clusters are discrete units, a great effort is being done to incorporate these types of lanthanide aggregates into polymeric frameworks¹¹⁰⁻¹¹³, and in many cases they are in combination with transition metals in the framework^{111, 114-116}. The synthesis, crystal structure and catalytic activity study of the first example of rare earth polymeric framework composed by hexanuclear hydroxo-lanthanide clusters and *p*-sulfonatocalix[4]arene (H₅L, figure III.4.01) are here discussed.

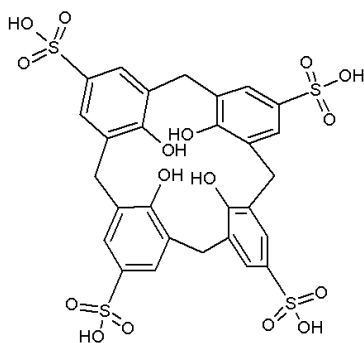
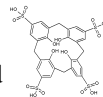
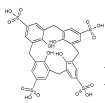


Figure III.4.01: calix[4]arene-p-sulfonic acid

Synthesis

The products were obtained under hydrothermal conditions. The molar composition of the initial mixture was $3\text{Ln} : \text{H}_5\text{L} : 5300 \text{H}_2\text{O} : 9.5 \text{Et}_3\text{N}$ ($\text{pH} = 8$). The Ln^{3+} ions were added in their hydrate nitrate form. H_5L is the calix[4]arene-p-sulfonic acid. In a typical synthesis, 0.197 g of $\text{La}(\text{NO}_3)_3 \cdot 6\text{H}_2\text{O}$ and 0.117 g of H_5L are solved in 13.5 ml of water. 0.18 ml of Et_3N are then added, and the solution is magnetically stirred at room temperature for 5 minutes. After this, the solution is placed into a Teflon lined stainless steel autoclave, and heated at 160°C for 10 hours. After cooling to room temperature, the product is filtered, then washed with water and acetone, and dried in air. Equivalent synthesis procedures are carried out employing $\text{Pr}(\text{NO}_3)_3 \cdot 6\text{H}_2\text{O}$ and $\text{Nd}(\text{NO}_3)_3 \cdot 6\text{H}_2\text{O}$ to obtain the corresponding products. The pH control seems to be critical: experiments with pH values lower or higher than 8 were unsuccessful, and no product was obtained. The product appears with good yield after only 5 hours of heating. With heating times longer than 10 hours the yield decreases significantly (36% yield after 20h), suggesting that the product decomposes in the reaction media.

Under this synthesis conditions, the obtaining of the products with smaller lanthanides was unsuccessful. Only in the case of ytterbium, a few crystals were obtained and with slightly modified conditions: Mixture of molar



composition $10\text{Yb} : \text{H}_5\text{L} : 10000 \text{H}_2\text{O}$ heated at $160\text{ }^\circ\text{C}$ for 24 hours. For the La, Pr and Nd preparations, only a few single crystals were obtained in the case of Pr and Nd, and in all cases they were very small crystals.

Structural description

The RPF9 crystal structure was solved in the tetragonal system, space group $I4/m$ (table III.4.01). In the figure III.4.02 the asymmetric units of the Pr- and Nd-RPF9 crystals are shown.

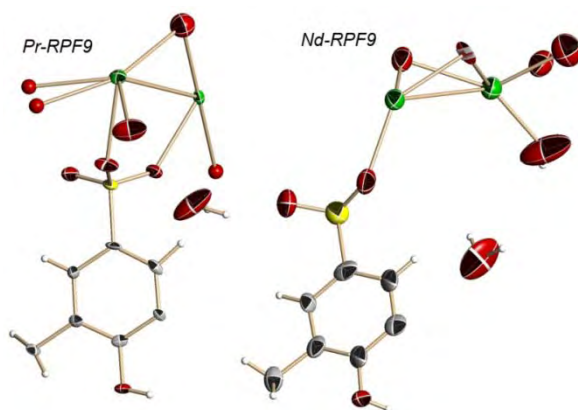


Figure III.4.02: ORTEP representation (50% probability) of the asymmetric units of Pr and Nd RPF9. Green: Ln atoms; Red: O atoms; Grey: C atoms; Yellow: S atoms; White: H atoms.

There are two crystallographically independent Ln atoms: one of them (Ln1) is on a four-fold axis and coordinated to four $\mu_3\text{-OH}^-$ groups, four O atoms from SO_3^- groups, and in the case of the Pr crystals, to a water molecule with occupancy factor lower than one. The other lanthanide atom (Ln2) coordinates to four $\mu_3\text{-OH}^-$ groups, two oxygen atoms from two SO_3^- groups, and to two water molecules, one of them disordered in two positions in Pr crystals.

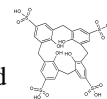


Table III.4.01: Main crystallographic and refinement data for Pr- and Nd-RPF9 compounds.

Identification code	Pr-RPF9	Nd-RPF9
Empirical formula	$C_{28}H_{40}O_{29}Pr_3S_4$	$C_{28}H_{40}Nd_3O_{28.50}S_4$
Formula weight	1391.61	1393.56
Temperature	296(2) K	296(2) K
Wavelength (Å)	1.54178 Å	1.54178 Å
Crystal system, space group	Tetragonal, $I4/m$	Tetragonal, $I4/m$
Unit cell dimensions	$a = 11.9761(3)$ Å $\alpha = 90^\circ$ $b = 11.9761(3)$ Å $\beta = 90^\circ$ $c = 31.399(1)$ Å $\gamma = 90^\circ$	$a = 11.9612(6)$ Å $\alpha = 90^\circ$ $b = 11.9612(6)$ Å $\beta = 90^\circ$ $c = 31.373(3)$ Å $\gamma = 90^\circ$
Volume	4503.5(2) Å ³	4488.5(6) Å ³
Z	4	4
Calculated density	2.035 Mg/m ³	2.062 Mg/m ³
Absorption coefficient	27.075 mm ⁻¹	28.650 mm ⁻¹
F(000)	2676	2720
Crystal size (mm)	0.04 x 0.03 x 0.03	0.02 x 0.02 x 0.01
Theta range for data collection	3.95 to 60.29 deg.	2.82 to 59.66 deg.
Limiting indices	-13 <= h <= 9 -9 <= k <= 13, -35 <= l <= 35	-13 <= h <= 13 -13 <= k <= 12 -27 <= l <= 34
Reflections collected / unique	6560 / 1623	6704 / 1660
Completeness to	$\theta^\circ = 58.00$ 96.0 %	$\theta^\circ = 59.66$ 97.6 %
Absorption correction	Semi-empirical from equivalents	
Max. and min. transmission	0.6140 and 0.4111	0.7626 and 0.5981
Refinement method	Full-matrix least-squares on F ²	
Data / restraints / parameters	1623 / 0 / 153	1660 / 0 / 141
Goodness-of-fit on F ²	1.047	0.892
Final R indices [I > 2σ(I)]	$R_1 = 0.0399$, $wR_2 = 0.11186$	$R_1 = 0.1002$, $wR_2 = 0.1989$
R indices (all data)	$R_1 = 0.0461$, $wR_2 = 0.1205$	$R_1 = 0.2309$, $wR_2 = 0.2363$
Largest diff. peak and hole	1.129 and -0.872 e.Å ⁻³	1.932 and -1.880 e.Å ⁻³

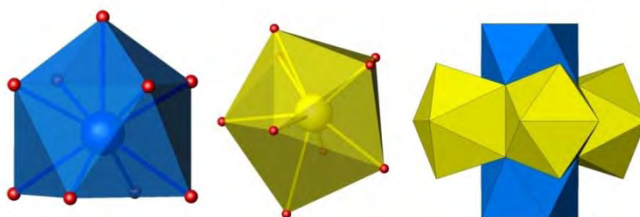


Figure III.4.03: The two types of coordination polyhedra formed by the Ln atoms (in blue a mon capped square antiprism, and in yellow a tricapped trigonal prism) and their disposition in the cluster that they form.

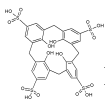


Table III.4.02: Interatomic distances in the coordination spheres of the metal atoms in the RPF9 compounds

Pr-RPF9				Nd-RPF9			
Bond	Distance (Å)	Bond	Distance (Å)	Bond	Distance (Å)	Bond	Distance (Å)
Pr(1)-O(5)		Pr(2)-O(5)		Nd(1)-O(5)		Nd(2)-O(5)	
Pr(1)-O(5) ¹	2.483(5)	Pr(2)-O(5) ¹	2.417(5)	Nd(1)-O(5) ²	2.453(11)	Nd(2)-O(5) ¹	2.410(12)
Pr(1)-O(5) ⁵		Pr(2)-O(5) ²		Nd(1)-O(5)		Nd(2)-O(5) ⁵	
Pr(1)-O(5) ⁶		Pr(2)-O(5) ³		Nd(1)-O(5) ³		Nd(2)-O(5) ⁶	
Pr(1)-O(2)		Pr(2)-O(81)		Nd(1)-O(2)		Nd(2)-O(1)	
Pr(1)-O(2) ¹	2.497(5)	Pr(2)-O(82)	2.61(4)	Nd(1)-O(2) ¹	2.484(15)	Nd(2)-O(1) ⁶	2.664(16)
Pr(1)-O(2) ⁵		Pr(2)-O(7)		Nd(1)-O(2) ²		Nd(2)-O(7)	
Pr(1)-O(2) ⁶		Pr(2)-O(1)		Nd(1)-O(2) ³		Nd(2)-O(6)	
Pr(1)-O(11)		Pr(2)-O(1) ³		Nd(1)-O(11)		Nd(2)-O(11)	
Pr(1)-O(6)	2.6548(8)	Pr(2)-O(11)	2.631(5)	Nd(1)-Nd(2)	2.567(3)	Nd(2)-Nd(1) ⁷	2.6778(18)
Pr(1)-O(6)	2.74(6)	Pr(2)-Pr(1)	2.7509(7)	Nd(1)-Nd(2) ¹	3.710(2)	Nd(2)-Nd(1) ¹	3.710(2)
Pr(1)-Pr(2) ⁷	3.8230(7)	Pr(2)-Pr(1) ⁴	3.8230(7)	Nd(1)-Nd(2) ⁴			

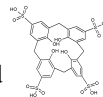
Symmetry operators code:

1: -y+1,x-1,z ; 2: -y+1,x-1,-z+1; 3: x,y,-z+1; 4: -x+2,-y,-z+1; 5: y+1,-x+1,z ; 6: -x+2,-y,z ; 7: y+1,-x+1,-z+1

Symmetry operators code:

1: -y+1,x-1,z ; 2: y+1,-x+1,z ; 3: -x+2,-y,z ; 4: y+1,-x+1,-z+1; 5: -y+1,x-1,-z+1; 6: x,y,-z+1; 7: -x+2,-y,-z+1

This arrangement gives rise to the formation of hexameric clusters, in which the octahedrally disposed lanthanide atoms are joined through 8 μ_3 -OH groups to give rise rhombic dodecahedra (Figure III.4.04). This type of cluster, which has been already reported in other lanthanide compounds, is depicted in most of cases, with a central oxygen atom coordinated to the six 6 Ln atoms¹¹⁷⁻¹²⁰. There are also some examples in which this central atom does not appear in the cluster^{107, 114}. In the present MOFs, a high electronic density was located at the centre of the cluster, which was effectively assigned to an oxygen atom. The structure of three different Pr crystals and one of Nd were refined, finding this atom in all of them, and its thermal parameters showed in all cases relatively high values, which is unexpected for a hexacoordinated O atom (see Figure III.4.04, left). The population factors refinement indicated total occupation for this atom in all cases. In order to allow differences in the Ln-O distances, and at the same time to study the possibility of that the high thermal parameter values for the central oxygen is due to pseudosymmetry effects (they are positioned on a fourfold centre), the crystal structure for the compounds was also refined in P1, in the primitive cell with parameters $a = 17839 \text{ \AA}$, $b = 17.839 \text{ \AA}$, $c = 11.988 \text{ \AA}$, $\alpha = 109.63^\circ$, $\beta = 109.63^\circ$, $\gamma = 123.26^\circ$ and volume 2255.7 \AA^3 resulting from applying the matrix $(-0.5a-0.5b-0.5c, -$



0.5a-0.5b+0.5c, b) to the tetragonal cell. The results of these refinements confirmed the occupancy obtained for this atom in I4/m space group, and showed that effectively this oxygen atom position is slightly shifted from the rhombic dodecahedra centre, bearing a considerable anisotropy in the direction in which, (as we will see later), the hydrogen atom could be situated.

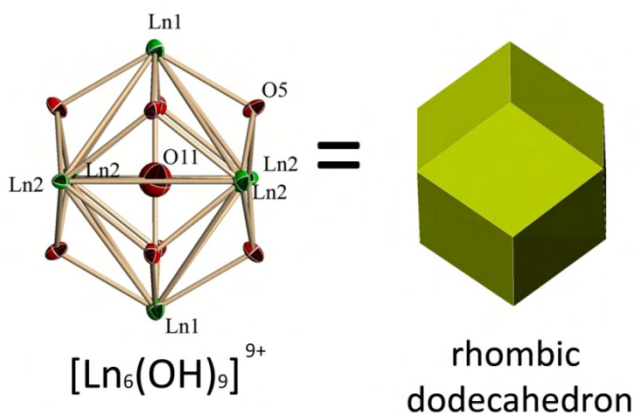
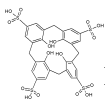


Figure III.4.04: ORTEP representation (50% probability) of the Ln_6O_9 units formed by the Ln atoms and the hydroxyl group. Note the higher values of the thermal parameters of the central O11 atom. The geometry of this aggregate is that of a rhombic dodecahedron (right).

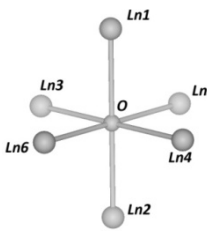
Oxygen or Hydroxyl group? Another matter related to the presence of central oxygen in the hydroxo cluster is the chemical nature of this atom. All papers reporting this type of hexanuclear Ln cluster with a central oxygen atom indicate that this is an O^{2-} anion. An exception is RPF3²³, a MOF previously prepared in our group, where the oxygen atom is clearly identified as OH^- not only on the base of the structural data but also on the electrical neutrality. Regarding to the charge balancing in RPF9, in the H_5L ligand there are five acidic hydrogen atoms, four of them coming from the sulfonate groups and the fifth from one phenolic group¹²¹. If the central oxygen atom were an O^{2-} , all the ligands should be HL^4 , if it were a hydroxyl group, there should coexist HL^4 and L^{5-} species, and in the case of no existence of this atom all the ligands should be in L^{5-} form.

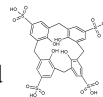


Under our synthesis conditions (pH ~ 8) the major protonation state of the ligand is L^{5-} , being difficult to find all the ligand as HL^{4-} species. This makes it possible the presence of a hydroxyl group instead of an O^{2-} ion. We therefore consider that the obtained compound composition could be $[Ln_6(OH)_9(HL)(L)(H_2O)_y]$ ($Ln = La, Pr$ and Nd ; $8 < y < 9$), with one half of the calixarene molecules monoprotonated.

The presence of a hydrogen atom of the OH^- central group is also sterically feasible. In RPF3²³ the hydrogen atom is positioned along one of the $Ln-O$ longest distance, (table III.4.03). In the RPF9 case, the interatomic $Ln-\mu_6O$ distances are symmetrically related in the tetragonal cell. However, the results of the P1 refinements of all the crystals demonstrate that a hydrogen atom could be accommodated inside the cluster and placed along one of these $O-Ln$ longest distances, which also could justify the high anisotropy of this oxygen atom.

Table III.4.03: Comparison of the interatomic μ_6O-Ln distances in the $I4/m$ and $P1$ refinements, and those of the $LnPF3$ compound²³. In bolds the pairs of distances with a higher variation in the $P1$ refinement are marked, as well as the one along which the H atom is found in the $LnPF3$ compound.

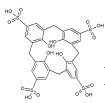
	Pr-RPF9 (crystal a)		Pr-RPF9 (crystal b)		Pr-RPF9 (crystal c)		Nd-RPF9		Nd-RPF3
	$I4/m$	$P1$	$I4/m$	$P1$	$I4/m$	$P1$	$I4/m$	$P1$	
O-Ln1	2.691	2.656	2.655	2.624	2.669	2.449	2.567	2.562	2.645
O-Ln2	2.691	2.755	2.655	2.692	2.669	2.901	2.567	2.600	2.645
O-Ln3	2.769	2.701	2.751	2.886	2.756	2.779	2.678	2.440	2.764
O-Ln4	2.769	2.860	2.751	2.620	2.756	2.771	2.678	2.917	3.174
O-Ln5	2.769	3.051	2.751	2.790	2.756	2.627	2.678	2.588	2.688
O-Ln6	2.769	2.489	2.751	2.719	2.756	2.902	2.678	2.800	2.688



Additionally, bond valences calculations also support the assignment of the central O atom as a hydroxyl group. With the bond valence method¹²⁹ the formal oxidation state of an atom in a crystal is calculated according to valence-sum rule: $V_i = \sum_j v_{ij}$. v_{ij} is the bond valence value and it is related to the bond length between nearest-neighbouring atoms $i - j$ (d_{ij}). It has the expression: $v_{ij} = e^{(R_{ij}-d_{ij})/b}$. b is a constant¹³⁰ with value 0.37\AA , R_{ij} is known as the bond-valence parameter, and it is calculated for each element in a given oxidation state. We have performed the calculations with the R_{ij} values calculated for lanthanides compounds by Breese and O'Keeffe¹²³, and by Trzesowska et al.¹²². We have carried out the bond valence sum calculations of the central oxygen atom with the RPF9 crystal data, as well as with other reported compounds in which an μ_n -O atom is present, either as O^{2-} or as OH^- . The bond valence sum values of the RPF9 compound are in the same range than those of the RPF3 compound and other reported μ_n OH^- groups, lower than those corresponding to other reported μ_6-O^{2-} atoms (see table III.4.04)

Table III.4.04: Comparison of the bond valence sum of the μ_n O atoms, calculated with the R_{ij} bond-valence parameters reported by Trzesowska et al.¹²² and by Breese and O'Keeffe¹²³

Compound		μ_n -O atom bond valence sum	
		R_{ij} by Trzesowska et al.	R_{ij} by Breese and O'Keeffe
Nd-RPF3[Ref. 23]		1.006(1)	1.094(1)
Eu-RPF3[Ref. 23]		0.994(9)	1.102(10)
Nd-RPF9	I4/m	1.353(3)	1.471(4)
	P1	1.305(124)	1.420(135)
Pr-RPF9 crystal_a	I4/m	1.056(2)	1.167(2)
	P1	1.060(103)	1.171(114)
Pr-RPF9 crystal_b	I4/m	1.129(1)	1.248(1)
	P1	1.087(33)	1.201(37)
Pr-RPF9 crystal_c	I4/m	1.105(3)	1.221(4)
	P1	1.177(247)	1.301(273)
[(Nd(NO ₃) ₂) ₃ (Nd(L)) ₂ (μ_5 -OH)] L = 1-Aziridineethanol Nd compound including a μ_5 -OH ⁻ group [Ref. 124]		1.006(1)	1.094(1)
Eu ^(III) ₅ (OH) ₉ (H ₂ O) ₆ (O ₂ C-C ₂ H ₄ -CO ₂) ₃ Eu compound including a μ_5 -OH ⁻ group [Ref. 125]		1.163(14)	1.289(16)
[Yb ₆ (CH ₂ O ₆ S ₂) ₄ O(OH) ₈ (H ₂ O) ₆] Yb compound including a μ_6 -O atom [Ref. 126]		1.634(0)	1.685(2)
[(DMF) ₁₆ Yb ₆ (μ_6 -O)(μ_3 -OH) ₈ (μ -NC)Pd(μ -CN)(CN) ₂][Pd(CN) ₄] ₃ Yb compound including a μ_6 -O atom [Ref. 127]		1.662(3)	1.807(4)
[(C ₅ Me ₅)Sm] ₆ O ₉ H ₆ Sm compound including a μ_6 -O atom [Ref. 128]		1.752(8)	1.874(9)



On the other hand, attempts to obtain RPF9 with smaller lanthanides under the current synthesis conditions only gave a few crystals of the Yb compound. The crystal structure showed that the Yb compound belongs also to the RPF9 family, but in this case without any electron density at the centre of the cluster, being the formula thus, $[\text{Yb}_6(\text{OH})_8\text{L}_2(\text{H}_2\text{O})_8]$ with all the ligand molecules completely deprotonated (L^{5-}). All in all, we do not rule out the possible existence of an O^{2-} anion, but we opt for the presence of a hydroxyl group inside the RPF9 clusters, as it is in LnPF3 , or even the coexistence of both, depending on a narrow pH value synthesis range.

The asymmetric unit and the hydroxo-lanthanide cluster of the Yb-RPF9 compound are shown in Figure III.4.05. The main crystallographic and refinement data for the collected Yb-RPF9 crystal are presented in table III.4.05

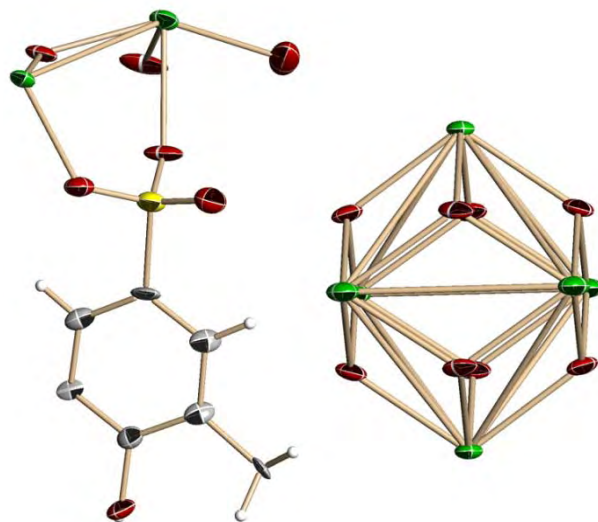


Figure III.4.05 ORTEP representation (50% probability) of the YbRPF9 asymmetric unit, and the $\text{Ln}_6(\text{OH})_8$ cluster. Note the absence of the central oxygen atom inside the cluster.

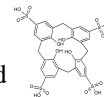
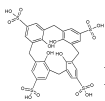


Table III.4.05: Main crystallographic and refinement data for Yb-RPF9

Identification code	Yb-RPF9
Empirical formula	C ₂₈ H ₂₀ O ₂₄ Yb ₃ S ₄
Formula weight	1387.80
Temperature	296(2) K
Wavelength (Å)	0.71073 Å
Crystal system, space group	Tetragonal, I4/m
Unit cell dimensions	a = 11.9660 Å α = 90°
	b = 11.9660 Å β = 90°
	c = 30.539(3) Å γ = 90°
Volume	4372.7(6) Å ³
Z,	4
Calculated density	2.108 Mg/m ³
Absorption coefficient	6.636 mm ⁻¹
F(000)	2616
Crystal size (mm)	0.10 x 0.02 x 0.02
Theta range for data collection	1.33 to 25.68 deg. -14 ≤ h ≤ 14
Limiting indices	-14 ≤ k ≤ 14
	-37 ≤ l ≤ 35
Reflections collected / unique	16326 / 2146
Completeness to θ° = 25.00	100.0 %
Absorption correction	Semi-empirical from equivalents
Max. and min. transmission	0.8787 and 0.5566
Refinement method	Full-matrix least-squares on F ²
Data / restraints / parameters	2146 / 53 / 141
Goodness-of-fit on F ²	1.341
Final R indices [I > 2σ(I)]	R ₁ = 0.1258, wR ₂ = 0.2218
R indices (all data)	R ₁ = 0.1486, wR ₂ = 0.2311
Largest diff. peak and hole	4.230 and -3.359 e.Å ⁻³

In the new RPF9 MOFs the usual for calixarenes up–down ‘bi-layer’ arrangement is maintained, and the calixarene molecules are bonded each other through the hexanuclear Ln clusters. Each [Ln₆(OH)₉] cluster joins eight sulfonatocalixarene ligands through the SO₃⁻ groups. Thus, one sulfonate oxygen atom is bonded to the axial Ln1 atom, another to an equatorial Ln2, and the third remains uncoordinated. The hydroxo-lanthanide clusters located in the *ab* plane, are joined each other through the calixarene anions, up and down this plane.



This arrangement gives rise to the formation of double layers with intersecting channels (Figure III.4.06), forming cavities with a maximum height of 11.87 Å (distance between calixarene molecules) and maximum width of 8.32 Å (distance between clusters). The double layers stacks along the c direction in an AB sequence, not allowing any channel along this direction. The topology of the double layers is of the Al_2O_3 type, binodal 8 and 4 connected, being the clusters the 8 connected centres, and the calixarene anions the 4 connected nodes. The point symbol of this network is $(4^{20}.6^8)(4^6)_2$, (Figure III.4.07).

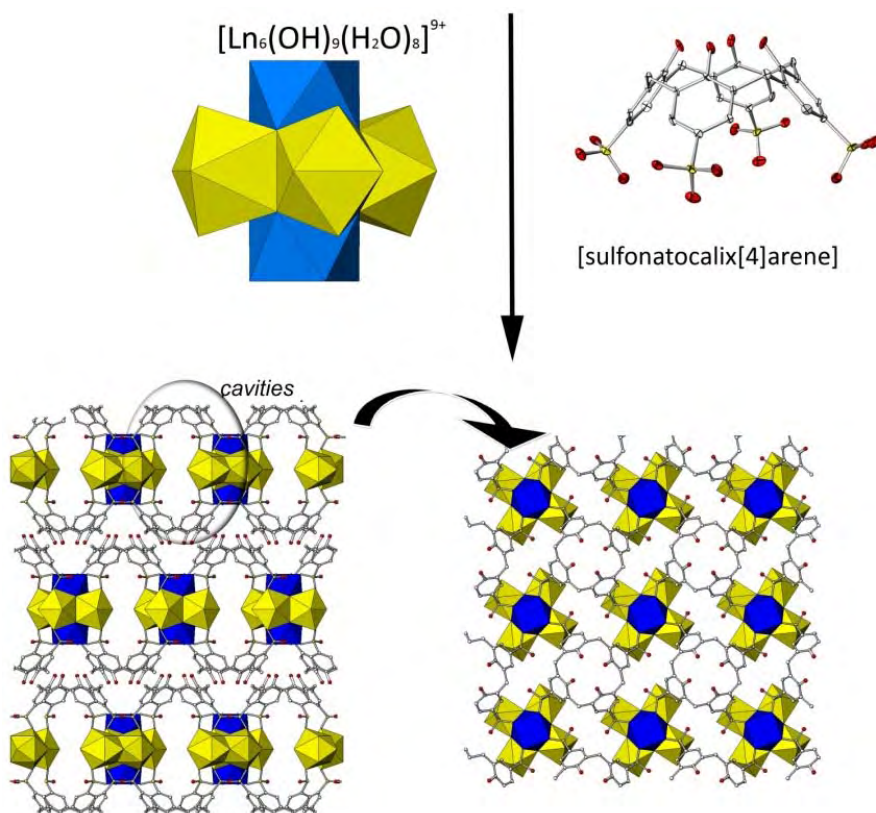


Figure III.4.06: The polymeric framework in RPF9 is formed by the joining of the Ln clusters through the sulfonatocalix[4]arene molecules, giving rise to the formation of double layers with channels running within them along two directions. Uncoordinated water molecules are here omitted for clarity. The coordinated water molecules are represented as part of the coordination polyhedra of the Ln atoms.

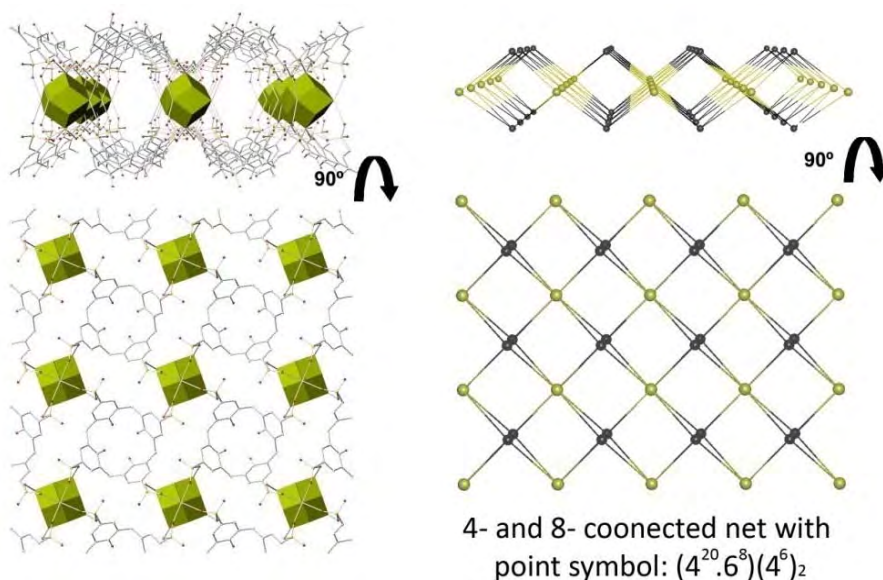
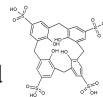
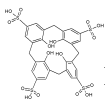


Figure III.4.07: The $\text{Ln}_6(\text{OH})_8$ clusters are the SBUs in the topological depicting of the structure. In the left, the perspective view of a double layer is presented, as well as its projection in the ab plane. In the right, the topological simplification of a double layer is presented (same views as in the left).

X-ray powder diffraction and thermal analysis

The La, Pr and Nd RPF9 compounds were obtained as pure phases. In Figure III.4.08, the Rietveld refinements for these compounds are shown. The differences in the intensity of the experimental patterns might be attributed to the presence of adsorbed water molecules inside the channels of the structure. These water molecules are the responsible of the first mass loss observed in the TG curves (Figure III.4.09). The loss of these water molecules has an influence on the structure. A variable temperature X-ray powder diffraction study was carried out with the NdRPF9 sample. As it can be seen in Figure III.4.10, while the sample is heated, the relative intensity of the peaks varies, due to the progressive loss of the adsorbed molecules.



III.4: RPF9: Rare earths + calix[4]arene-p-sulfonic acid

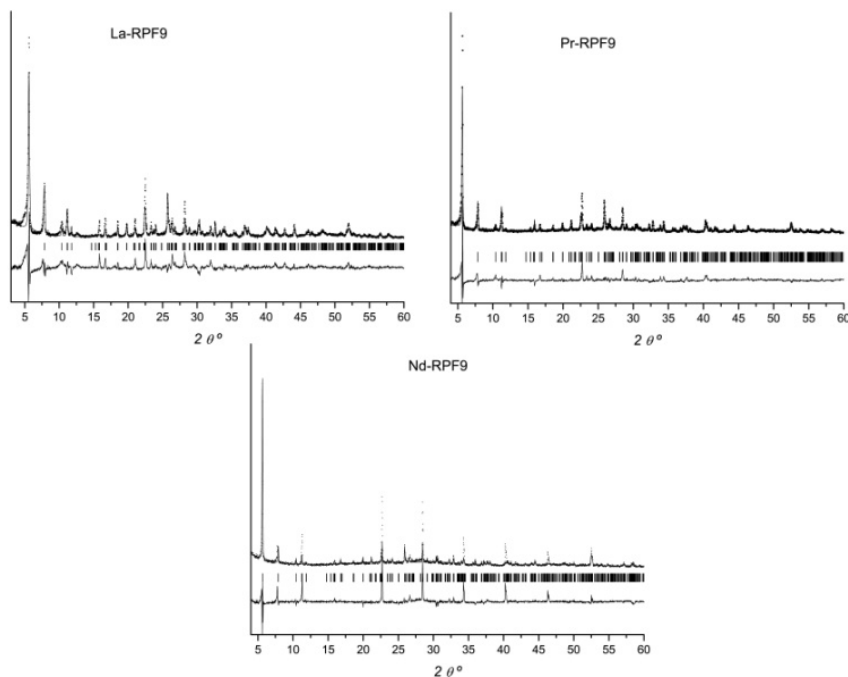


Figure III.4.08: Rietveld refinements of the La- Pr- and Nd-RPF9 compounds, showing the experimental (dot) and simulated (line) patterns, as well as the difference pattern. The Bragg positions are marked as columns.

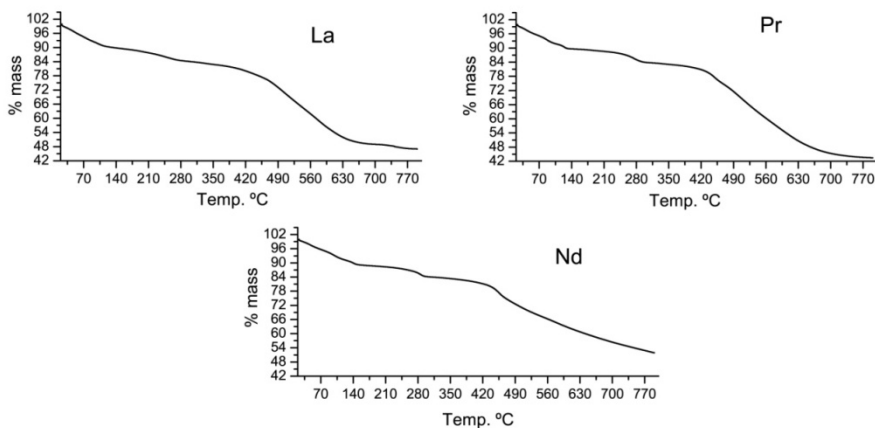
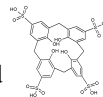


Figure III.4.09: Thermogravimetric curves for the La-, Pr- and Nd-RPF9 compounds.

Finally, a phase transition is observed when the sample is heated above 125 °C. The high temperature powder pattern could be indexed in the tetragonal system with the following parameters: $a = b = 11.600 \text{ \AA}$, $c = 28.276 \text{ \AA}$, cell



volume = 3793.8 Å³. These parameters are quite similar to those of the original structure, suggesting that after the water molecules evaporation, the rest of the framework should remain without significant changes. The powder pattern of the new crystalline phase, however, is not of quality enough to refine the atomic positions in the new cell. The second step in the TG curve at ~ 240 °C corresponds to the loss of the coordinated water molecules. The total decomposition of the framework, with the loss of the organic part begins above 350 °C.

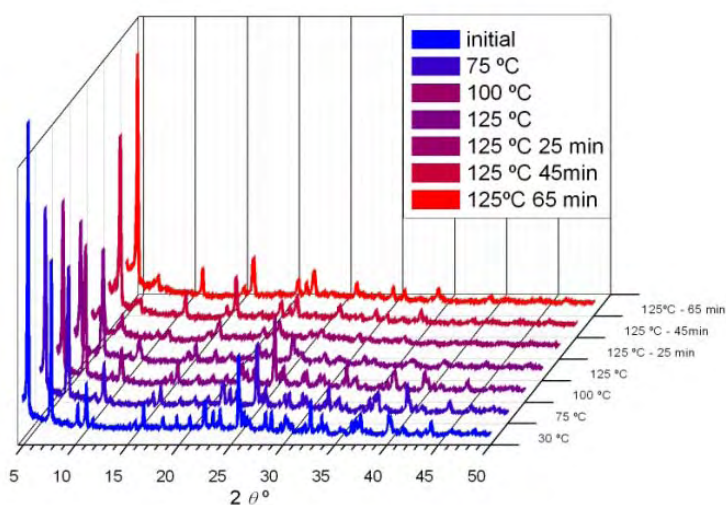
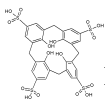


Figure III.4.10: Variable temperature powder X-ray diffraction of the Nd-RPF9 compound, showing the phase transitions suffered by the structure.

Catalytic properties

As the 2,6-AQDS families of compounds, the RPF9 new materials have been evaluated as heterogeneous catalysts. The open frameworks that they exhibit, together with the high nuclearity of the inorganic SBUs make the RPF9



materials as good candidates for being used as heterogeneous catalysts. Thus, the three La, Pr and Nd RPF9 compounds have been tested in the catalytic oxidation of methyl-phenyl sulphide. The experiments were carried out as follow: one mmol of methyl phenyl sulphide was added to a suspension containing the corresponding amount of catalyst (ratio Ln : substrate = 1:1000), in 5 ml of acetonitrile. The suspension was heated to 80 °C under stirring, and then hydrogen peroxide (H₂O₂ 50%, 3mmol) was added dropwise. At selected intervals of time, the grade of conversion was measured in a gas chromatographer. *Separation and recycling*: After the reaction cycles, the catalyst was separated by decantation of the solution, and reused with fresh solvent and substrate, starting a new cycle of reaction when the oxidizing agent is added. While the oxidation of sulfide continued in presence of the catalyst, there was no further significant conversion when the catalyst was removed from the reaction system. The blank experiments, carried out in absence of catalyst, showed no conversion after 4 hours.

In all cases an increase in the activity was observed after the first cycle of reaction. As in RPF4, this is attributed to the need of an induction period for the formation of the active species, which probably is an Ln peroxo derivative. Thus, in the subsequent cycles, the activity was enhanced, achieving high values of conversion in short periods of time, especially for the Pr compound. It is worth pointing out the low amount of the catalyst needed, with a high ratio of substrate to metal (1000:1), and therefore, high values of TOF are obtained, reaching a grade of conversion similar to other similar rare-earth polymeric frameworks, and better than those of the corresponding oxides¹³¹. In Figure III.4.11 the kinetic curves for the three cycles of reactions are shown for each catalyst. On the other hand, the catalysts also exhibit a good grade of selectivity. In table III.4.06, the % of selectivity to sulfoxide is shown, together with the TOF values reached by the RPF9 compounds. After the reaction cycle, the integrity of the catalysts was checked by PXRD. The material was confirmed to be intact (Figure III.4.12).

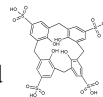


Table III.4.06: TOF values and selectivity expressed as % of sulfoxide in the products for the three reaction cycles carried out with the three RPF9 compounds as heterogeneous catalyst.

Run	La-RPF9			Pr-RPF9			Nd-RPF9		
	1	2	3	1	2	3	1	2	3
TOF (h ⁻¹) ^a	108	193	509	150	195	212	83	286	870
% sulfoxide	87	95	92	85	86	86	90	92	89

a = turnover frequency expressed as mol substrate converted per mol of active centre.

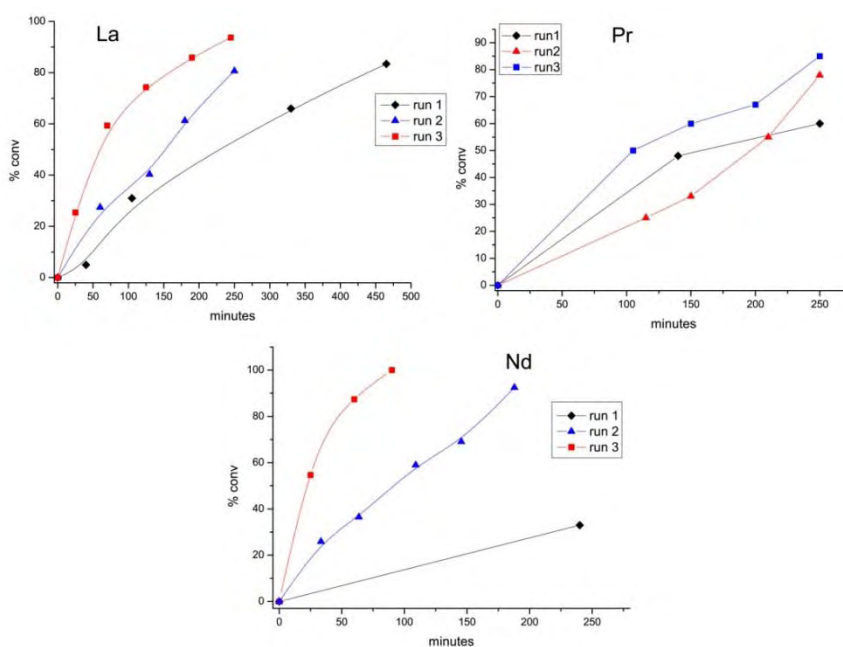


Figure III.4.11: Kinetic curves for the oxidation of methyl-phenyl sulfide for the three RPF9 compounds

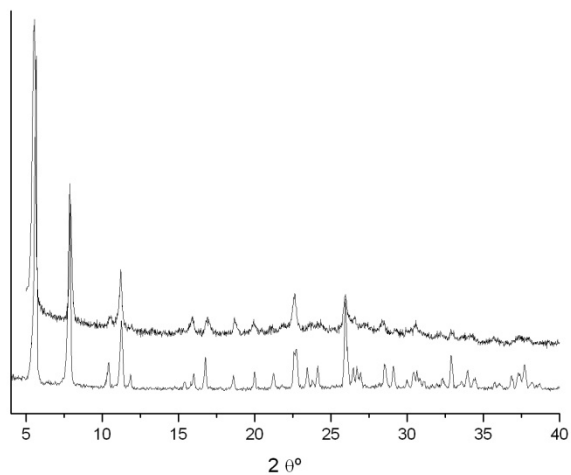
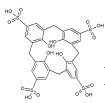


Figure III.4. 12: PXRD pattern of the Pr-RPF9 compound after the catalytic reaction.

With the results presented in this chapter, a publication for *Chemical Communication* has been prepared. It can be found in the part VI of the current report.

5. References

1. A. Monge, N. Snejko, E. Gutiérrez-Puebla, M. Medina, C. Cascales, C. Ruiz-Valero, M. Iglesias and B. Gómez-Lor, *Chemical Communications*, 2005, 1291-1293.
2. F. Gándara, B. Gómez-Lor, E. Gutiérrez-Puebla, M. Iglesias, M. A. Monge, D. M. Proserpio and N. Snejko, *Chemistry of Materials.*, 2008, **20**, 72-76.
3. L. Pan, D. H. Olson, L. R. Ciemmolonski, R. Heady and J. Li, *Angewandte Chemie - International Edition*, 2006, **45**, 616-619.
4. L. Pan, M. B. Sander, X. Huang, J. Li, M. Smith, E. Bittner, B. Bockrath and J. K. Johnson, *Journal of the American Chemical Society*, 2004, **126**, 1308-1309.
5. J. Campá, E. Gutiérrez-Puebla, A. Monge, I. Rasines and C. Ruíz-Valero, *Journal of Solid State Chemistry*, 1996, **126**, 27-32.
6. G. M. Sheldrick, 2003.
7. , Bruker-Siemens Analytical X-ray Instrument Inc., Madison, WI, 2004.
8. Bruker, TWINABS, Bruker AXS Inc., Madison, Wisconsin, USA, 2001.
9. A. L. Spek, 2007.
10. V. A. Blatov, *Acta Crystallographica Section A-Foundations of Crystallography*, 2007, **63**, 329-343.
11. F. Serpaggi, T. Luxbacher, A. K. Cheetham and G. Férey, *Journal of Solid State Chemistry*, 1999, **145**, 580-586.
12. S. A. Cotton, *Lanthanide and Actinide Chemistry*, John Wiley & sons, Ltd, 2006.
13. Y. Mejia-Radillo and A. K. Yatsimirsky, *Inorganica Chimica Acta*, 2003, **351**, 97-106.
14. J. Kamitani, J. Sumaoka, H. Asanuma and M. Komiyama, *Journal of the Chemical Society. Perkin Transactions 2*, 1998, 523-527.

15. M. C. Bernini, F. Gándara, M. Iglesias, N. Snejko, E. Gutiérrez-Puebla, Elena V. Brusau, Griselda E. Narda and M. A. Monge, *Chemistry - A European Journal*, 2009.
16. A. P. Cote and G. K. H. Shimizu, *Coordination Chemistry Reviews*, 2003, **245**, 49-64.
17. J. Cai, *Coordination Chemistry Reviews*, 2004, **248**, 1061-1083.
18. A. P. Cote and G. K. H. Shimizu, *Inorganic Chemistry*, 2004, **43**, 6663-6673.
19. D. Sun, R. Cao, W. Bi, X. Li, Y. Wang and M. Hong, *European Journal of Inorganic Chemistry*, 2004, 2144-2150.
20. D. J. Hoffart, S. A. Dalrymple and G. K. H. Shimizu, *Inorganic Chemistry*, 2005, **44**, 8868-8875.
21. J. F. Ma, J. Yang, S. L. Li, S. Y. Song, H. J. Zhang, H. S. Wang and K. Y. Yang, *Crystal Growth & Design*, 2005, **5**, 807-812.
22. F. Gándara, C. Fortes-Revilla, N. Snejko, E. Gutiérrez-Puebla, M. Iglesias and M. Angeles Monge, *Inorganic Chemistry*, 2006, **45**, 9680-9687.
23. F. Gándara, A. García-Cortés, C. Cascales, B. Gómez-Lor, E. Gutiérrez-Puebla, M. Iglesias, A. Monge and N. Snejko, *Inorganic Chemistry*, 2007, **46**, 3475-3484.
24. S. T. Hyde, O. Delgado Friedrichs, S. J. Ramsden and V. Robins, *Solid State Sciences*, 2006, **8**, 740-752.
25. V. Rives, *Layered Double Hydroxides: Present and Future*, Nova Science Publishers, New York, 2001.
26. C. Janiak, *Journal of the Chemical Society, Dalton Transactions*, 2000, 3885-3896.
27. A. G. Renwick, *Sulfur-containing Drugs and Related Organic Compounds*, 1989.
28. M. Mikolajczyk, J. Drabowicz and P. Kielbasinski, *Asymmetric and Stereoselective Synthesis*, CRC Press, Boca Raton, 1997.
29. M. C. Carreno, *Chemical Reviews*, 1995, **95**, 1717-1760.

30. K. R. Sharma and E. S. Olson, *Catalytic hydrodesulfurization with hydrotalcites, Processing and utilization of high-sulfur coals IV*, Elsevier Science Publisher, Amsterdam, 1991.
31. Y. Mejia-Radillo and A. K. Yatsimirsky, *Inorganica Chimica Acta*, 2002, **328**, 241-246.
32. K. Akiyama and S. Tero-Kubota, *Journal of Physical Chemistry B*, 2002, **106**, 2398-2403.
33. A. Babaei, P. A. Brooksby, A. Flood and A. J. McQuillan, *Applied Spectroscopy*, 2000, **54**, 496-501.
34. D. Beckert and R. W. Fessenden, *Journal of Physical Chemistry*, 1996, **100**, 1622-1629.
35. Y. Kobori and J. R. Norris, *Journal of the American Chemical Society*, 2006, **128**, 4-5.
36. I. Loeff, J. Rabani, A. Treinin and H. Linschitz, *Journal of the American Chemical Society*, 1993, **115**, 8933-8942.
37. J. Säuberlich, O. Brede and D. Beckert, *Journal of Physical Chemistry A*, 1997, **101**, 5659-5665.
38. J. R. Tobias Johnsson Wass, E. Ahlberg, I. Panas and D. J. Schiffrin, *Journal of Physical Chemistry A*, 2006, **110**, 2005-2020.
39. R. C. White, V. Gorelik, E. G. Bagryanskaya and M. D. E. Forbes, *Langmuir*, 2007, **23**, 4183-4191.
40. D. K. Newman and R. Kolter, *Nature*, 2000, **405**, 94-97.
41. M. A. Glaus, C. G. Heijman, R. P. Schwarzenbach and J. Zeyer, *Applied and Environmental Microbiology*, 1992, **58**, 1945-1951.
42. J. T. Nurmi and P. G. Tratnyek, *Environmental Science and Technology*, 2002, **36**, 617-624.
43. S. Bin-Salamon, S. H. Brewer, E. C. Depperman, S. Franzen, J. W. Kampf, M. L. Kirk, R. K. Kumar, S. Lappi, K. Peariso, K. E. Preuss and D. A. Shultz, *Inorganic Chemistry*, 2006, **45**, 4461-4467.
44. E. Evangelio and D. Ruiz-Molina, *European Journal of Inorganic Chemistry*, 2005, **2005**, 2957-2971.

45. A. Caneschi, A. Dei, H. Lee, D. A. Shultz and L. Sorace, *Inorganic Chemistry*, 2001, **40**, 408-411.
46. D. Ruiz-Molina, J. Veciana, K. Wurst, D. N. Hendrickson and C. Rovira, *Inorganic Chemistry*, 2000, **39**, 617-619.
47. J.-M. Lu, S. V. Rosokha, I. S. Neretin and J. K. Kochi, *Journal of the American Chemical Society*, 2006, **128**, 16708-16719.
48. V. Ganesan, S. V. Rosokha and J. K. Kochi, *Journal of the American Chemical Society*, 2003, **125**, 2559-2571.
49. H. Bock, A. John and C. Näther, *Journal of the Chemical Society, Chemical Communications*, 1994, 1939-1940.
50. W. M. Clark, *Oxidation-Reduction Potentials of Organic Systems*, The Williams & Wilkins Co., Baltimore, MD, 1960.
51. J. Q. Chambers, in *The Chemistry of Quinonoid Compounds*, eds. S. Patai and Z. Rappoport, Wiley, New York, 1988, pp. 719-757.
52. D. Meisel and R. W. Fessenden, *Journal of the American Chemical Society*, 1976, **98**, 7505-7510.
53. J. Geimer and D. Beckert, *Chemical Physics Letters*, 1998, **288**, 449-458.
54. K. M. Rosso, D. M. A. Smith, Z. Wang, C. C. Ainsworth and J. K. Fredrickson, *The Journal of Physical Chemistry A*, 2004, **108**, 3292-3303.
55. R. S. K. A. Gamage, A. J. McQuillan and B. M. Peake, *Journal of the Chemical Society, Faraday Transactions*, 1991, **87**, 3653-3660.
56. J. Geimer and D. Beckert, *Applied Magnetic Resonance*, 2000, **18**, 505-513.
57. J. Geimer, K. Hildenbrand, S. Naumov and D. Beckert, *Physical Chemistry Chemical Physics*, 2000, **2**, 4199-4206.
58. J. M. Lü, L. M. Wu, J. Geimer and D. Beckert, *Physical Chemistry Chemical Physics*, 2001, **3**, 2053-2058.
59. H. Zhao, M. J. Bazile-Jr, J. R. Galán-Mascarós and K. R. Dunbar, *Angewandte Chemie - International Edition*, 2003, **42**, 1015-1018.

60. D. Maspoch, D. Ruiz-Molina, K. Wurst, N. Domingo, M. Cavallini, F. Biscarini, J. Tejada, C. Rovira and J. Veciana, *Nature Materials*, 2003, **2**, 190-195.
61. D. Maspoch, D. Ruiz-Molina, K. Wurst, C. Rovira and J. Veciana, *Chemical Communications*, 2004, **10**, 1164-1165.
62. N. Roques, D. Maspoch, I. Imaz, A. Datcu, J. P. Sutter, C. Rovira and J. Veciana, *Chemical Communications*, 2008, 3160-3162.
63. N. Roques, D. Maspoch, F. Luis, A. Camon, K. Wurst, A. Datcu, C. Rovira, D. Ruiz-Molina and J. Veciana, *Journal of Materials Chemistry*, 2008, **18**, 98-108.
64. E. Laviron, *Journal of Electroanalytical Chemistry*, 1983, **146**, 15-36.
65. K. Sasaki, T. Kashimura, M. Ohura, Y. Ohsaki and N. Ohta, *Journal of the Electrochemical Society*, 1990, **137**, 2437-2443.
66. M. Namazian and M. L. Coote, *Journal of Physical Chemistry A*, 2007, **111**, 7227-7232.
67. J. Karolak-Wojciechowska, W. Kwiatkowski and A. Socha, *Polish Journal of Chemistry*, 1993, **67**, 1159.
68. E. Gamag, B. M. Peake and J. Simpson, *Australian Journal of Chemistry*, 1993, **46**, 1595-1604.
69. S. Q. Liu, T. Kuroda-Sowa, H. Konaka, Y. Suenaga, M. Maekawa, T. Mizutani, G. L. Ning and M. Munakata, *Inorganic Chemistry*, 2005, **44**, 1031-1036.
70. S. Delgado, P. J. Sanz Miguel, J. L. Priego, R. Jiménez-Aparicio, C. J. Gómez-García and F. Zamora, *Inorganic Chemistry*, 2008, **47**, 9128-9130.
71. M. Tadokoro, S. Yasuzuka, M. Nakamura, T. Shinoda, T. Tatenuma, M. Mitsumi, Y. Ozawa, K. Toriumi, H. Yoshino, D. Shiomi, K. Sato, T. Takui, T. Mori and K. Murata, *Angewandte Chemie International Edition*, 2006, **45**, 5144-5147.
72. C. Janiak, *Dalton Transactions*, 2003, 2781-2804.

73. G. W. Orr, L. J. Barbour and J. L. Atwood, *Science*, 1999, **285**, 1049-1052.
74. J. L. Atwood, L. J. Barbour, A. Jerga and B. L. Schottel, *Science*, 2002, **298**, 1000-1002.
75. J. L. Atwood, L. J. Barbour and A. Jerga, *Science*, 2002, **296**, 2367-2369.
76. D. B. Qin, F. B. Xu, Q. S. Li, H. B. Song and Z. Z. Zhang, *Synlett*, 2005, 2987-2989.
77. C. D. Gutsche, *Calixarenes: Monographs in Supramolecular Chemistry*, The Royal Society of Chemistry, 1989.
78. B. Masci, S. L. Mortera, D. Persiani and P. Thuéry, *Journal of Organic Chemistry*, 2006, **71**, 504-511.
79. A. Saha, S. K. Nayak, S. Chottopadhyay and A. K. Mukherjee, *Journal of Physical Chemistry B*, 2004, **108**, 7688-7693.
80. B. Turner, A. Shterenberg, M. Kapon, K. Suwinska and Y. Eichen, *Chemical Communications*, 2001, 13-14.
81. C. D. Gutsche and J. A. Levine, *Journal of the American Chemical Society*, 1982, **104**, 2652-2653.
82. C. D. Gutsche, B. Dhawan, K. H. No and R. Muthukrishnan, *Journal of the American Chemical Society*, 1981, **103**, 3782-3792.
83. J. L. Atwood, A. W. Coleman, H. Zhang and S. G. Bott, *Journal of Inclusion Phenomena*, 1989, **7**, 203-211.
84. P. K. Thallapally, P. B. McGrail, S. J. Dalgarno and J. L. Atwood, *Crystal Growth & Design*, 2008, **8**, 2090-2092.
85. M. Makha, Y. Alias, C. L. Raston and A. N. Sobolev, *New Journal of Chemistry*, 2008, **32**, 83-88.
86. M. Makha, Y. Alias, C. L. Raston and A. N. Sobolev, *New Journal of Chemistry*, 2007, **31**, 662-668.
87. J. A. Ripmeester, G. D. Enright, C. I. Ratcliffe, K. A. Udachin and I. L. Moudrakovski, *Chemical Communications*, 2006, 4986-4996.

88. P. J. Nichols and C. L. Raston, *Dalton Transactions*, 2003, 2923-2927.
89. Z. Asfari and V. Bohmer, *Calixarenes*, Kluwer Academic Publishers, Dordrecht, The Netherlands, 2001.
90. L. Mandolini and R. Ungaro, *Calixarenes in action*, London, U.K., 2000.
91. W. Liao, Y. Bi, S. Gao, D. Li, H. Zhang and R. Dronskowski, *European Journal of Inorganic Chemistry*, 2008, 2959-2962.
92. D. S. Guo and Y. Liu, *Crystal Growth & Design*, 2007, **7**, 1038-1041.
93. S. J. Dalgarno, J. L. Atwood and C. L. Raston, *Crystal Growth & Design*, 2007, **7**, 1762-1770.
94. C. B. Smith, L. J. Barbour, M. Makha, C. L. Raston and A. N. Sobolev, *Chemical Communications*, 2006, 950-952.
95. S. J. Dalgarno, J. L. Atwood and C. L. Raston, *Crystal Growth & Design*, 2006, **6**, 174-180.
96. J. L. Atwood, T. Ness, P. J. Nichols and C. L. Raston, *Crystal Growth & Design*, 2002, **2**, 171-176.
97. M. Selkti, A. W. Coleman, I. Nicolis, N. Douteau-Guével, F. Villain, A. Tomas and C. De Rango, *Chemical Communications*, 2000, 161-162.
98. A. Drljaca, M. J. Hardie, C. L. Raston and L. Spiccia, *Chemistry - A European Journal*, 1999, **5**, 2295-2299.
99. A. Drljaca, M. J. Hardie, J. A. Johnson, C. L. Raston and H. R. Webb, *Chemical Communications*, 1999, 1135-1136.
100. J. L. Atwood, G. William Orr, F. Hamada, R. L. Vincent, S. G. Bott and K. D. Robinson, *Journal of the American Chemical Society*, 1991, **113**, 2760-2761.
101. G. Schmidt, *Cluster and Colloids: From Theory to Applications*, VCH, Weinheim, 1994.
102. L. J. de Jongh, *Physics and Chemistry of Metal Cluster Compounds*, Kluwer, Dordrecht, 1994.

103. T. Kajiwara, N. Iki and M. Yamashita, *Coordination Chemistry Reviews*, 2007, **251**, 1734-1746.
104. T. Kajiwara, K. Katagiri, S. Takaishi, M. Yamashita and N. Iki, *Chemistry - An Asian Journal*, 2006, **1**, 349-351.
105. T. Kajiwara, H. Wu, T. Ito, N. Iki and S. Miyano, *Angewandte Chemie - International Edition*, 2004, **43**, 1832-1835.
106. M. R. Burgstein, M. T. Gamer and P. W. Roesky, *Journal of the American Chemical Society*, 2004, **126**, 5213-5218.
107. R. Wang, D. Song and S. Wang, *Chemical Communications*, 2002, 368-369.
108. R. Wang, H. D. Selby, H. Liu, M. D. Carducci, T. Jin, Z. Zheng, J. W. Anthis and R. J. Staples, *Inorganic Chemistry*, 2002, **41**, 278-286.
109. P. W. R. Markus R. Bürgstein, *Angewandte Chemie - International Edition*, 2000, **39**, 549-551.
110. D. Weng, X. Zheng and L. Jin, *European Journal of Inorganic Chemistry*, 2006, 4184-4190.
111. X.-J. Zheng, L.-P. Jin and S. Gao, *Inorganic Chemistry*, 2004, **43**, 1600-1602.
112. Z. Zheng, *Chemical Communications*, 2001, 2521-2529.
113. Bao-Qing Ma, D.-S. Zhang, S. Gao, T.-Z. Jin, Chun-Hua and Y. G.-X. Xu, *Angewandte Chemie - International Edition*, 2000, **39**, 3644-3646.
114. S. Xiang, S. Hu, T. Sheng, R. Fu, X. Wu and X. Zhang, *Journal of the American Chemical Society*, 2007, **129**, 15144-15146.
115. X. Gu and D. Xue, *Inorganic Chemistry*, 2007, **46**, 5349-5353.
116. M. B. Zhang, J. Zhang, S. T. Zheng and G. Y. Yang, *Angewandte Chemie - International Edition*, 2005, **44**, 1385-1388.
117. I. A. Charushnikova and C. Den Auwer, *Crystallography Reports*, 2007, **52**, 226-229.
118. A. V. Mudring and A. Babai, *Zeitschrift für anorganische und allgemeine Chemie*, 2005, **631**, 261-263.

119. N. Mahe, O. Guillou, C. Daiguebonne, Y. G erault, A. Caneschi, C. Sangregorio, J. Y. Chane-Ching, P. E. Car and T. Roisnel, *Inorganic Chemistry*, 2005, **44**, 7743-7750.
120. D.-S. Zhang, B.-Q. Ma, T.-Z. Jin, S. Gao, C.-H. Yan and T. C. W. Mak, *New Journal of Chemistry*, 2000, **24**, 61-62.
121. J.-P. Scharff and M. Mahjoubi, *New Journal of Chemistry*, 1991, **15**, 883-887.
122. A. Trzesowska, R. Kruszynski and T. J. Bartczak, *Acta Crystallographica Section B-Structural Science*, 2004, **60**, 174-178.
123. N. E. Bresse and M. O'Keeffe, *Acta Crystallographica Section B-Structural Science*, 1991, **47**, 192-197.
124. M. K. Thompson, A. J. Lough, A. J. P. White, D. J. Williams and I. A. Kahwa, *Inorganic Chemistry*, 2003, **42**, 4828-4841.
125. C. Serre, F. Pelle, N. Gardant and G. F erey, *Chemistry of Materials*, 2004, **16**, 1177-1182.
126. Z.-C. Zhang, *Acta Crystallographica Section C-Crystal Structure Communications*, 2008, **64**, m381-m383.
127. J. Liu, E. A. Meyers and S. G. Shore, *Inorganic Chemistry*, 1998, **37**, 5410-5411.
128. W. J. Evans, N. T. Allen, M. A. Greci and J. W. Ziller, *Organometallics*, 2001, **20**, 2936-2937.
129. I. D. Brown, *The Chemical Bond in Inorganic Chemistry: The Bond Valence Model*, Oxford Science Publications, Oxford, 2002.
130. I. D. Brown and D. Altermatt, *Acta Crystallographica Section B-Structural Science*, 1985, **41**, 244-247.
131. J. Perles, M. Iglesias, C. Ruiz-Valero and N. Snejko, *Journal of Materials Chemistry*, 2004, **14**, 2683-2689.

IV. Discussion and Conclusions

1. Comparative analysis

A deep study on the synthetic factors that address the formation of one or another framework has led us to the construction of different architectures for tailored materials. Careful design of several reactions using rare earth elements in combination with different ligands has allowed the obtaining of 40 new metal-organic framework compounds belonging to nine novel structural types. Structural characterization, together with evaluation of properties is presented in this thesis. At this point, an overview of the results is necessary to extract some conclusions on the properties and features of the new materials.

Structural considerations

In their compounds, rare earth elements manifest a variable coordination number, which allows extra-coordination to water or other solvent molecules. Among the nine obtained structural types, the rare earth elements have coordination numbers from seven to nine. Five different types of coordination polyhedra are found. They are represented in figure IV.1.01, bottom right. All over this work, we have played with the possibility of controlling the presence of coordinated hydroxyl groups in the frameworks, going from the three RPF4 polymorphs, without any OH⁻ group, to the LRH materials, in which the inorganic layer is exclusively formed by OH and water molecules coordinated to the Ln³⁺ ions.

The three polymorphic forms in which RPF4 may appear have as a common feature the absence of any coordinated solvent molecules. This is due to the formation of sharing edges polyhedra chains. With a ratio $L^{2-} / Ln^{3+} = 1.5$ (which avoids the presence of OH⁻ groups) there are six oxygen atoms per Ln atom. The Ln atoms being nine-coordinated exclusively by ligands oxygen atoms, forces the existence of μ_2 bridge mode in one half of them.

In the case of the other polymeric frameworks, water molecules are always found coordinated to the metal atoms, and different types of aggregates are formed.

In RPF5, RPF6, RPF7, and RPF9 families, rare earth atoms form diverse types of hydroxo clusters with $\mu_n\text{-OH}^-$ groups, finding $\text{Ln}_2(\text{OH})_2$, $\text{Ln}_4(\text{OH})_4$ and $\text{Ln}_6(\text{OH})_9$ aggregates. Similar aggregates were also found in previous rare earth polymeric frameworks prepared in our group, named as RPF1, RPF2 and RPF3. A comparison of those structural types with the new ones is made as follows:

The SO_3^- group appears with a wide variation of coordination modes linked to the hydroxo-metal aggregates, through one, two or three sulfonate oxygen atoms. Regarding the connection with the aggregates, it can be coordinated just to one hydroxo cluster, or behave as a short bridge among two clusters. In figure IV.1.02 the ways in which the SO_3^- is connected to the hydroxo clusters are shown, which will give rise to the inorganic SBUs, as described later.

In the light of these results, it seems likely that during the water-based synthesis procedure, the aqua hydroxo aggregates are readily formed. The sulfonate ligands can then coordinate to the metal atoms, varying their coordination mode to the most favorable conformation. In the extreme case of the LRH compounds (probably kinetically controlled), the hydroxo-lanthanide layer would be quickly formed, saturating the lanthanide coordination sphere, and avoiding, thus, the coordination to the ligand SO_3^- groups.

In any case, these examples demonstrate that the sulfonate ligands are suitable to be employed in the construction of polymeric framework, with a high variability in the coordination mode.

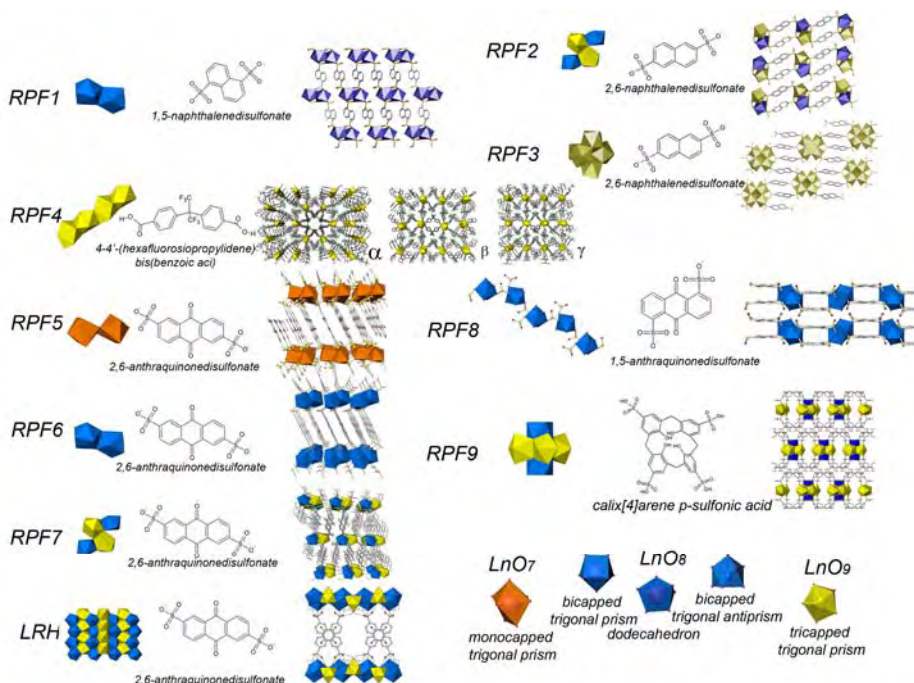


Figure IV.1.01: A summary of the nine new structural types prepared in this work, together with the three first families of rare earth polymeric frameworks prepared in our group. In the left corner, the different rare earth coordination polyhedra are shown.

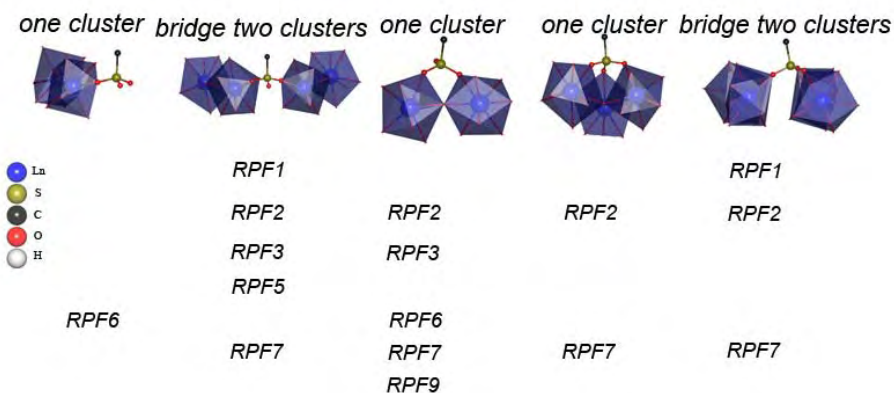


Figure IV.1.02: Different coordination modes of the sulfonate group, and the structural types in which they are found.

Topological comparison of sulfonate containing frameworks

For this comparison, the topological simplification of the real structures is made as indicated below:

- In all the structural types, with exception of RPF8, the SBUs (Secondary Building Units) are formed by coordination of the sulfonate oxygen atoms to the inorganic hydroxo aggregates (Figure IV.1.03, left column).
- The sulfonate group represented as a (CSO₃) tetrahedron, is joined to the ligand organic part by one vertex, and to the inorganic SBUs either as a bridge between two of them, (tri-connected node) or only to one unit (total connectivity equal to two) being therefore a linker. In the case of RPF9, the sulfonatocalixarene molecule behaves as a tetra-connected node. The simplified coordination modes of the sulfonate ligands are shown in figure IV.1.03, top middle.
- Simplified SBUs are built by introduction of a pseudo atom whose coordinates are those of the Ln atom positions centroid, and the vertexes are the connections with the SO₃ groups.

The obtained networks according to these simplifications and their topological classification are represented in Figure IV.1.03, right column. They are commented as follows.

In RPF1, RPF5 and RPF6 the SBUs are formed by dimeric units. In RPF1 and RPF5, we find 8 connected SBUs nodes, and 3 connected SO₃ nodes. Nevertheless, due to the different geometry of the ligands (1,5-NDS in RPF1, and 2,6-AQDS in RPF5), they have different topologies (see figure).

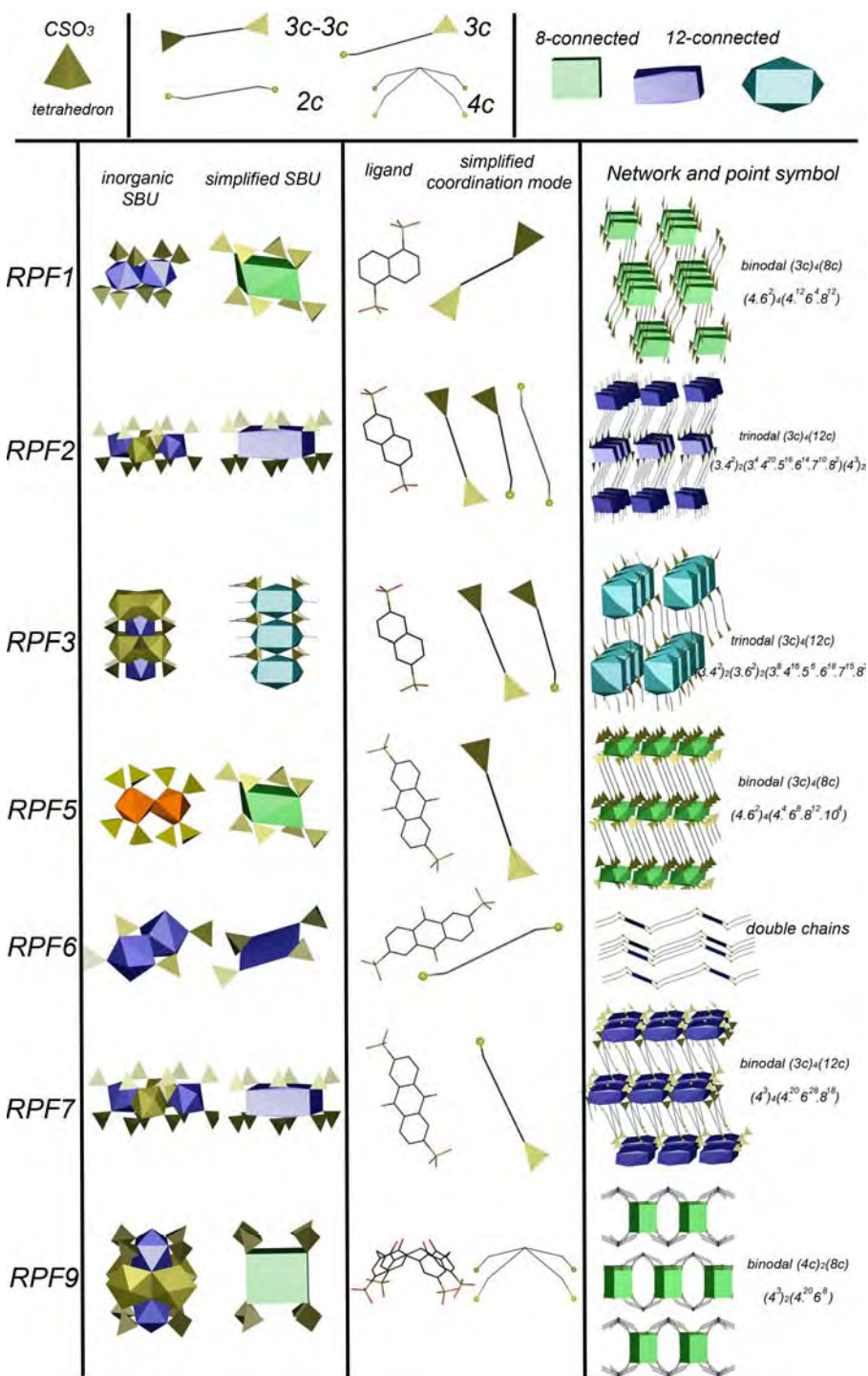


Figure IV.1.03: Results of the topological analysis of the rare earth polymeric framework prepared with sulfonate ligands

In RPF6, the dimeric units give rise to 4-connected square shaped SBUs. The ligands are merely linkers among the squares, and the structure is mono dimensional, with double chains. The presence of three water molecules coordinated to the metal atoms avoids a higher coordination of the inorganic cluster, and explains the different connectivity in this structure type.

RPF2 and RPF7 exhibit tetrameric aggregates, and in both structures there is just one coordinated water molecule, allowing thus, a high connectivity of the SBUs (12 connected).

In RPF2, the SBUs are linked in three different ways, as represented in figure IV.1.03, middle column. RPF2 owns a two-periodic network, formed by rows of inorganic SBUs joined by the ligands to give 3-nodal layers. In RPF7, there is only one way to link the SBUs, giving rise to a binodal 12- and 3-connected 3-dimensional network.

In RPF3 and RPF9, the SBUs consist of hexameric clusters, with the Ln atoms octahedrally disposed. In RPF3, these SBUs, which are 12-connected, are joined among them *via* shared axial Ln atoms to give rise to inorganic backbone associations. These are linked through the ligands in a 12- and 3-connected 3D network. In RPF9, the hexameric clusters are isolated, and they give rise to eight connected SBUs with cubic geometry. In this structure type, formed by calixarene ligands, the special geometry of the ligands imposes the formation of an 8- and 4- connected two-periodic net.

Comparison of the catalytic activity.

Several factors have influence on the catalytic activity of a given material. For a reaction with a certain mechanism, the achieved final grade of conversion will depend, among other factors, on the accessibility of the substrate to the active centers, and on the coordination sphere of the active centre.

For the catalytic oxidation of methyl phenyl sulfide, carried out in this work with several structural types, a comparison of the different employed materials can be made. During this redox process, no change in the oxidation state of the Ln metal is expected, and the mechanism has to go through the formation of an Ln-O intermediate species, with changes in the coordination sphere of the metal. The formation of this species is traditionally the slowest step of the reaction, and this explains the need of an induction period.

The LRH, RPF9 and RPF4 compounds have open structures, and in principle they can display a higher number of accessible sites, which favors the catalytic activity. However, the activity of the RPF4 compounds is clearly lower than that of the LRH and RPF9.

This is due, in our opinion, because in the RPF4 compounds, the coordination sphere of the metal atoms is formed exclusively by O atoms from the carboxylate groups. Therefore, a change in the coordination sphere of the Ln cation is expected to be difficult. In fact, for the reactions with RPF4 as catalysts, an activation period is required previous to the reaction goes. After this activation period, a change in the infrared spectra of the catalyst was observed, which allowed us proposing an Ln-O-O peroxy species as active intermediate. The formation of the peroxy species is more difficult in RPF4 coordination sphere, but it implies a change easier to be detected by spectroscopic methods.

In all other evaluated compounds, hydroxo groups and water molecules are found coordinated to the metallic atoms. In principle, these aqua ligands should be more easily displaced by the substrate molecules in the coordination sphere to form the intermediate species.

Thus, the LRH compounds, with the Ln atoms exclusively coordinated to OH⁻ groups and water molecules, are those with the highest activity. In these compounds, the active species are rapidly formed, and the kinetic curves show no induction period. Besides, the open structure of these compounds, with presence of channels, favors the diffusion of the reactants, and excellent values of conversion are obtained with a very low amount of catalyst, and in short period of time.

With the RPF9 compounds, high conversion values are also obtained, with a high substrate to catalyst ratio. The open structure of these compounds also favors the conversion. When using RPF9 compounds as catalyst, the activity increases after the first cycle of reaction, indicating that the formation of the active species is slower than in the LRH compounds. In this case, two different Ln atoms are present, with coordination spheres composed by five OH⁻ groups and 4 sulfonate oxygen atoms and by four OH⁻ groups, two water molecules, and two sulfonate oxygen atoms, respectively. The presence of coordinated oxygen atoms from the sulfonate groups probably makes more difficult the formation of the peroxo intermediate species, which is reflected in the increase of activity after the first cycle of reaction.

In the case of the RPF6 and RPF7 compounds, coordinated sulfonate groups are present. The two structures are dense, and the catalytic activity will only take place on the surface. The sum of these factors explains the lower values of activity demonstrated by these compounds, even with a higher amount of catalyst (substrate / catalyst = 100)

RPF5 has a dense structure, but the coordination number of the Ln cation is seven. This low coordination number allows the easier formation of the active

species. The substrate molecules will find an unhindered active centre, and good values of activity are also obtained.

For a reaction involving a different mechanism, other results are found. Thus, for the hydrodesulphurization (HDS) of thiophene, the RPF5 compounds exhibit the highest activity. In this case, the sum of the extra acidity coming from the coordinated sulfonate groups and the low Ln coordination number results in a very active material, even with a dense structure. The obtained values for this compound in the HDS are better than those of the LRH compound.

Table IV.1.01: Average TOF values (h^{-1}) shown by different catalysts in the oxidation of methyl-phenyl sulfide

Ln³⁺	La	Nd	Yb
Family (C.N.)			
RPF4 (9)	18	20	60
RPF5 (7)	-	-	241
RPF6 (8)	-	30	-
RPF7 (8,9)	21	-	-
RPF9 (8,9)	200	413	-
LRH (8,9)	-	-	1233

2. Conclusions

- By hydrothermal reaction of rare earth elements and organic ligands, 40 new compounds have been obtained, belonging to nine structural types. Eight structural types are coordination polymers, while the ninth is a new type of crystalline layered material.
- The use of a dicarboxylic ligand with a bent geometry (hfipbb) has allowed the obtaining of a new family of rare earth polymeric frameworks, RPF4. This new family of compounds, with formula Ln_2L_3 presents three polymorphic phases, α , β , and γ . The crystal structure for the three of them has been determined for the corresponding La compounds.
- The structure of the RPF4- α phase has been solved from twinned crystals. With the subsequent analysis of the crystal structure, the intrinsically triple twinned nature of this structure has been explained.
- The three polymorphic phases of RPF4 have networks with unique topologies: The three of them are uninodal pentacoordinated, derived from rod-shaped secondary building units. Such topologies can only be reached by using bent ligands.
- RPF4- α structural type has been obtained for the following rare earth elements: Y, Ce, Pr, Nd, Sm, Eu, Gd, Tb, Dy, Ho, Er, and Yb. X-ray powder diffraction Rietveld refinements demonstrate the purity of all these compounds.
- Compounds of the RPF4- α phase have proven to have interesting properties: they are luminescent materials with high emission efficiency. The combination of different rare earth elements in a same framework makes these compounds promising materials for their use in light emitting devices. They also present catalytic activity as

heterogeneous redox catalysts, in the oxidation of methyl phenyl sulfide. During the catalytic experiments, the need of an activation period for the formation of an active intermediate has been observed. The presence of this active species has been detected by spectroscopic methods, and it has been identified as a Ln-peroxo species.

- The use of anthraquinone-2,6-disulfonate with rare earth elements has resulted in the obtaining of three polymeric structural types: RPF5 for Yb, RPF6 for Nd, Sm, Gd, Dy, Ho and Er, and RPF7 for La and Pr.
- A new class of pillared crystalline material for intercalation chemistry, named as LRH, Layered Rare-Earth Hydroxides, has been prepared. They have an ordered and tuneable porous structure and gather the interest of layered double hydroxide (LDH) and the chemical and physical properties of the rare earth cations. Furthermore, they can be employed as materials for anion exchange, intercalation, catalysis and two dimensionally confined space reactions, LRH are also a promising way to get organic-inorganic nanocomposite devices.
- The formation of LRH structural type seems to be kinetically controlled over the polymeric frameworks, especially for the smallest rare earth cations. Compounds with this structure type have been prepared with Dy, Ho, Er and Yb.
- All the rare earth–anthraquinone-2,6-disulfonate materials show catalytic activity in the oxidation of methyl phenyl sulfide. Among them, those belonging to the LRH family are the most active materials. The YbRPF5 compound is also a good catalyst for the hydrodesulphurization of thiophene. Structural features explain the differences in the activity among the materials.

- A new structural type, RPF8, has been prepared with anthraquinone-1,5-disulfonate anion radical. With the adequate synthesis conditions, the in situ formation of the radical form has been achieved. For the first time, this semiquinone species of an anthraquinone derivative has been crystallographically characterized.
- A series of isostructural RPF8 compounds has been prepared with elements La, Pr, Nd, Sm, Eu, Gd, Tb, Dy, Ho, and Er. X-ray powder diffraction Rietveld refinements demonstrate the purity of all these compounds.
- The semireduction of the 1,5-AQDS molecule and its coordination with the rare earth atoms in a chelating way results in a structure type with π - π stacking interactions in a perfect face-to-face fashion.
- Physical properties of RPF8 have been studied, showing the radical species influence on the new material behavior. Variations on the magnetic moment as well as conductivity values evidence the presence of a free electron in the AQDS radical species.
- A rare earth polymeric framework, RPF9, based on p-sulfonatocalix[4]arene and hexanuclear hydroxo-lanthanide aggregates has been for the first time prepared. This structure type has been obtained with La, Pr, Nd, and Yb.
- In the RPF9 compounds the central O atom is identified as belonging to a hydroxyl group, on the basis of interatomic distances and bond valence calculations. This is in contrast to most of the reported examples of this type of clusters, where the central atom is identified as an O^{2-} anion. In RPF9 compounds, the hydroxyl nature of this oxygen atom implies that the calixarene molecules are in an acid-base equilibrium during the formation of the product.

- RPF9 compounds are good heterogeneous redox catalysts in the oxidation of methyl phenyl sulfide.
- Finally, from the comparison of the rare earth – sulfonate compounds it can be concluded that rare earth elements tend to form different types of hydroxo-aggregates. These hydroxo-aggregates form the secondary building units in the construction of the polymeric frameworks. They have a high connectivity degree, and diverse geometries. The joining of these SBUs through the sulfonate ligands results in the formation of extended networks with uncommon topologies. The sulfonate ligands have demonstrated to be able to coordinate to the inorganic SBUs in many different ways.

3. Conclusiones

- Con el uso de elementos de las tierras raras y diversos ligandos orgánicos, 40 nuevos compuestos han sido preparados, pertenecientes a nueve tipos estructurales. Seis de ellos son polímeros de coordinación, mientras que el séptimo es un nuevo tipo de material laminar cristalino.
- El uso de un ligando dicarboxílico que coordina en una disposición en forma de V, ha dado lugar a la obtención de una nueva familia de polímeros de coordinación de tierras raras, RPF4. Esta nueva familia de compuestos, con fórmula Ln_2L_3 , presenta tres posibles polimorfos, α , β y γ . Sus tres estructuras cristalinas han sido resueltas para el correspondiente compuesto de lantano.
- La estructura de la fase RPF4- α se ha resuelto a partir de cristales maclados. El consiguiente análisis de la estructura cristalina ha permitido explicar la naturaleza intrínseca triplemente maclada de esta estructura.
- Los tres posibles RPF4 polimorfos presentan redes con topologías únicas. Las tres son redes uninodales, pentacoordinadas, que derivan de unidades secundarias de construcción con forma de cadenas. Estas topologías sólo son posibles gracias a la utilización de un ligando con una disposición doblada.
- Compuestos isoestructurales del tipo RPF4- α han sido obtenidos con Y, Ce, Pr, Nd, Sm, Eu, Gd, Tb, Dy, Ho, Er, e Yb. Así lo demuestran los refinamientos de Rietveld de los patrones de difracción de rayos X de polvo, que indican que han sido obtenidos de forma pura.
- Los compuestos con esta fase RPF4- α ha demostrado tener propiedades ópticas interesantes, siendo materiales luminiscentes con alta eficiencia de emisión. La combinación de distintos metales dentro

de un mismo compuesto, hace de ellos materiales prometedores para su uso en dispositivos emisores de luz.

- Los compuestos del tipo estructural RPF4- α presentan además actividad como catalizadores heterogéneos redox, en la oxidación de metil fenil sulfuro. Durante los experimentos de actividad catalítica, se ha observado la necesidad de un periodo de activación que es atribuido a la formación la especie activa. Dicha especie activa ha sido detectada en estos compuestos con métodos espectroscópicos, identificándola como un especie peroxo-Ln.
- El uso de antraquinona-2,6-disulfonato ha resultado en la obtención de tres polímeros de coordinación, RPF5, RPF6, y RPF7. Los estudios de síntesis demuestran que cada catión lantánido tiene preferencia por la formación de uno u otro tipo estructural, en función del tamaño del catión: La y Pr forman RPF7; Nd, Sm, Gd, Dy, Ho y Er forman RPF6; Yb forma RPF5
- Una nueva clase de materiales cristalinos apilados para la química de intercalación ha sido preparada. Llamados LRHs, (Layered Rare earth Hydroxides), poseen una estructura porosa que reúne el interés de los hidróxidos dobles laminares (HDL) y las interesantes propiedades físicas y químicas de los elementos de las tierras raras. Estos materiales pueden ser utilizados para intercambio iónico, química de intercalación o catálisis.
- La formación del tipo estructural LRH parece estar cinéticamente controlada sobre la de las estructuras poliméricas, especialmente con los cationes lantánidos de menor radio iónico. Este tipo estructural ha sido preparado empleando Dy, Ho, Er e Yb.
- Todos los materiales formados con tierras raras y antraquinona-2,6-disulfonato muestran actividad catalítica en la oxidación de metil fenil sulfuro. Entre todos ellos, lo materiales pertenecientes al tipo LRH son los más activos. El compuesto Yb-RPF5 es también un buen catalizador heterogéneo en la hidrodeshidrosulfurización de tiofeno. Las

características estructurales de cada compuesto explican las diferencias en actividad catalítica entre cada material.

- Un nuevo tipo estructural, RPF8, ha sido preparado con antraquinona-1,5-disulfonato. Con las condiciones de síntesis adecuadas se ha conseguido la formación in situ de la especie semireducida (anión radical) de la molécula de antraquinona. Por primera vez, esta especie semiquinona de un derivado de antraquinona ha sido cristalográficamente caracterizada.
- El hecho de que la molécula de 1,5-AQDS esté en forma semireducida y su coordinación a los cationes de tierras raras en modo quelato, resulta en una estructura con presencia de interacciones del tipo apilamiento π - π . Estas interacciones tienen lugar entre las moléculas de antraquinona, con los anillos aromáticos perfectamente alineados.
- Propiedades físicas de los compuestos RPF8 han sido estudiadas, mostrando la influencia de la especie radical en el comportamiento del nuevo material. Las variaciones en el momento magnético o los valores de conductividad obtenidos evidencian la presencia del electrón libre en la especie semiquinona.
- Un nuevo polímero de coordinación, RPF9, ha sido obtenido a partir del ácido p-sulfocalix[4]areno y clústeres hexanucleares hidroxolantánidos. Este tipo estructural se ha obtenido con La, Pr, Nd e Yb.
- En el clúster presente en RPF9, el átomo de oxígeno central se ha identificado como perteneciente a un grupo hidróxido, en base a diferencias en distancias interatómicas y a cálculos de valencia de enlace. En la mayoría de compuestos en los que este tipo de clúster ha sido publicado, el átomo de oxígeno central se ha identificado como un anión O^{2-} . En los compuestos RPF9, la presencia de un grupo OH-central implica que las moléculas de sulfocalixareno estén en un equilibrio ácido-base durante la formación de los productos.

- Los compuestos RPF9 también presentan actividad catalítica como catalizadores heterogéneos redox, en la oxidación de metil fenil sulfuro.
- De la comparación de los diferentes materiales formados con elementos de las tierras raras y ligandos sulfonato, se puede concluir que los cationes lantánidos presentan tendencia a formar distintos tipos de hidroxos agregados durante los procedimientos de síntesis. Estos agregados son las unidades de construcción secundarias en la formación de los polímeros de coordinación. Tienen un alto grado de conectividad y diversas geometrías. La unión de estas SBU a través de los ligandos sulfonato derivados resulta en la formación de polímeros de coordinación con topologías poco habituales. Los ligandos sulfonatos se han mostrado capaces de coordinar a las SBUs inorgánicas de diferentes maneras.

V.

Supplementary
material

1. Additional crystal structures

Gd, Ho and Er RPF6 crystals

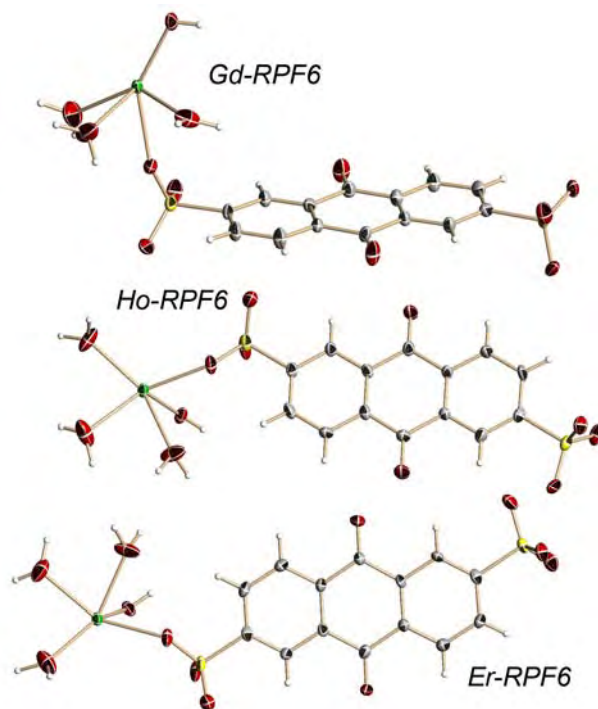


Figure V.1.01: ORTEP representation (50% probability) of the asymmetric units of the Gd, Ho and Er RPF6 compounds. Green: Ln atoms; Yellow: S atoms; Red: O atoms; Grey: C atoms; White: H atoms.

Table V.1.01: Main crystallographic and refinement data for the Gd, Ho and Er RPF6 crystals.

Identification code	Gd-RPF6	Ho-RPF6	Er-RPF6	
Empirical formula	$C_{14}H_{13}S_2GdO_{12}$ [Gd($C_{14}H_6S_2O_8$)(OH)(H ₂ O) ₃]]	$C_{14}H_{13}S_2HoO_{12}$ [Ho($C_{14}H_6S_2O_8$)(OH)(H ₂ O) ₃]]	$C_{14}H_{13}S_2ErO_{12}$ [Er($C_{14}H_6S_2O_8$)(OH)(H ₂ O) ₃]]	
Formula weight	594.61	602.29	604.62	
Temperature	295(2) K	295(2) K	295(2) K	
Wavelength		0.71073 Å		
Crystal system, space group		Triclinic, <i>P</i> -1		
Unit cell dimensions	$a = 7.260(1) \text{ \AA}$ $\alpha = 83.882(2)^\circ$ $b = 7.943(1) \text{ \AA}$ $\beta = 89.104(2)^\circ$ $c = 15.352(2) \text{ \AA}$ $\gamma = 83.924(2)^\circ$	$a = 7.2571(5) \text{ \AA}$ $b = 7.9321(5) \text{ \AA}$ $c = 15.3101(1) \text{ \AA}$	$\alpha = 83.858(1)^\circ$ $\beta = 88.954(1)^\circ$ $\gamma = 82.405(1)^\circ$	$a = 7.2517(7) \text{ \AA}$ $b = 7.9243(7) \text{ \AA}$ $c = 15.293(1) \text{ \AA}$ $\alpha = 83.842(2)^\circ$ $\beta = 88.931(2)^\circ$ $\gamma = 82.171(2)^\circ$
Volume	873.7 (2) Å ³	868.9(1) Å ³	865.6(1) Å ³	
Z, Calc. density	2, 2.260 Mg/m ³	2, 2.303 Mg/m ³	2, 2.320 Mg/m ³	
Absorption coefficient	4.103 mm ⁻¹	4.864 mm ⁻¹	5.158 mm ⁻¹	
F(000)	578	584	586	
Crystal size	0.18 x 0.08 x 0.04 mm	0.20 x 0.10 x 0.08 mm	0.20 x 0.16 x 0.04 mm	
Theta range for data collection	1.33° to 29.22°	2.61° to 29.15°	2.61° to 29.41°	
Limiting indices	-9<=h<=9 -10<=k<=10 -20<=l<=20	-9<=h<=9 -10<=k<=10 -20<=l<=20	-9<=h<=9 -10<=k<=10 -20<=l<=20	
Reflections collected / unique	7299 / 4193	8368 / 4177	8406 / 4258	
Completeness to theta = 25.00°	98.5 %	98.5 %	98.5 %	
Absorption correction		Semi-empirical from equivalents		
Max. and min. transmission	0.8531 and 0.5255	0.6970 and 0.4429	0.8203 and 0.4252	
Refinement method		Full-matrix least-squares on F ²		
Data / restraints / parameters	4193 / 0 / 262	4177 / 2 / 262	4258 / 0 / 262	
Goodness-of-fit on F²	1.113	1.030	1.033	
Final R indices [I>2σ(I)]	R ₁ = 0.0437, wR ₂ = 0.0873	R ₁ = 0.0412, wR ₂ = 0.0745	R ₁ = 0.0426, wR ₂ = 0.0815	
R indices (all data)	R ₁ = 0.0602, wR ₂ = 0.1036	R ₁ = 0.0578, wR ₂ = 0.0789	R ₁ = 0.0552, wR ₂ = 0.0853	
Largest diff. peak and hole	0.873 and -1.530 e·Å ⁻³	1.331 and -1.506 e·Å ⁻³	1.576 and -1.317 e·Å ⁻³	

Fe and Co 1,5-AQDS compounds

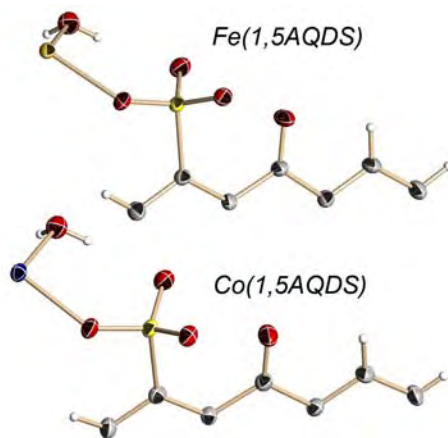


Figure V.1.02: ORTEP representation (50% probability) of the asymmetric units of the Fe(1,5-AQDS) and Co(1,5-AQDS) compounds. Orange: Fe atom; Blue: Co atom; Yellow: S atoms; Red: O atoms; Grey: C atoms; White: H atoms.

The two compounds of 1,5-AQDS and Fe or Co are isostructural. The transition metal atoms are in octahedral environment, coordinated to two water molecules and to four oxygen atoms from four different sulfonate groups. Chains of octahedra are formed, through the bridge SO_3 groups. These chains run along the a axis, and are joined by the whole ligand molecules which is coordination mode $\eta^2\mu_2\text{-}\eta^2\mu_2$. A two dimensional structure is formed, with layers parallel to the (1,1,1) plane.

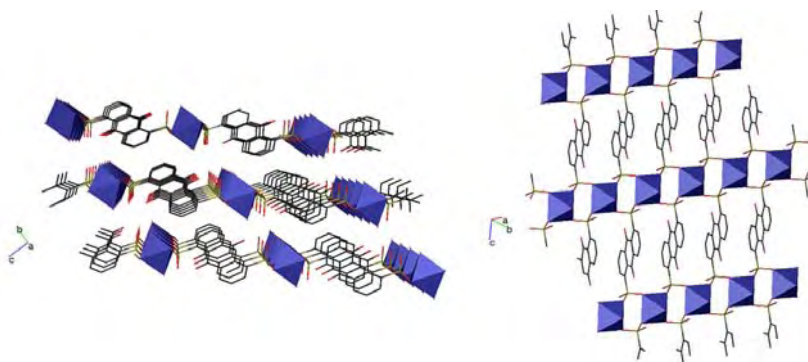


Figure V.1.03: Polyhedral representation of the Fe(1,5AQDS) structure.

Table V.1.02: Main crystallographic and refinement data for the Fe(1,5AQDS) and Co(1,5AQDS) compounds

Identification code	Fe-1,5AQDS	Co-1,5AQDS
Empirical formula	$C_{14}H_{10}S_2FeO_{10}$ [Fe($C_{14}H_3S_2O_8$)(H_2O)]	$C_{14}H_{10}S_2CoO_{10}$ [Fe($C_{14}H_3S_2O_8$)(H_2O)]
Formula weight	458.19	461.27
Temperature	296(2) K	295(2) K
Wavelength	0.71073 Å	
Crystal system, space group	Triclinic, <i>P</i> -1	
Unit cell dimensions	$a = 5.3050(5)$ Å $\alpha = 89.263(2)^\circ$ $b = 7.8643(7)$ Å $\beta = 87.850(2)^\circ$ $c = 9.1073(8)$ Å $\gamma = 75.895(2)^\circ$	$a = 5.3039(8)$ Å $\alpha = 89.378(2)^\circ$ $b = 7.8339(12)$ Å $\beta = 87.591(2)^\circ$ $c = 9.0947(14)$ Å $\gamma = 75.950(2)^\circ$
Volume	368.24 (6) Å ³	366.26 (10)
Z, Calculated density	1, 2.066 Mg/m ³	1, 2.091
Absorption coefficient	1.370 mm ⁻¹	1.520
F(000)	232	1056 mm ⁻¹
Crystal size	0.20 x 0.20 x 0.10 mm	0.20 x 0.08 x 0.06
Theta range for data collection	2.24° to 28.28°	2.24° to 26.36°
Limiting indices	-7 ≤ h ≤ 6 -10 ≤ k ≤ 10 -11 ≤ l ≤ 11	-6 ≤ h ≤ 6 -9 ≤ k ≤ 9 -11 ≤ l ≤ 11
Reflections collected / unique	3308 / 1686	2767 / 1408
Completeness to theta = 25.00°	95.7 %	95.5 %
Absorption correction	Semi-empirical from equivalents	
Max. and min. transmission	0.8751 and 0.7712	0.9143 and 0.7509
Refinement method	Full-matrix least-squares on F ²	
Data / restraints / parameters	1686 / 0 / 144	1408 / 0 / 144
Goodness-of-fit on F²	1.065	1.061
Final R indices [I > 2σ(I)]	R ₁ = 0.0327, wR ₂ = 0.0863	R ₁ = 0.0350, wR ₂ = 0.0847
R indices (all data)	R ₁ = 0.0364 wR ₂ = 0.0887	R ₁ = 0.0459, wR ₂ = 0.0881
Largest diff. peak and hole	0.382 and -0.370 e·Å ⁻³	0.378 and -0.440 e·Å ⁻³

Additional Pr-RPF9 collected crystals

Table V.1.03 Main crystallographic and refinement data for the PR-RPF9 compounds

Identification code	Pr-RPF9 crystal b	Pr-RPF9 crystal c
Empirical formula	C ₂₈ H ₂₀ O ₂₉ Pr ₃ S ₄	C ₂₈ H ₂₄ O ₂₉ Pr ₃ S ₄
Formula weight	1371.41	1375.44
Temperature	296(2) K	296(2) K
Wavelength (Å)	1.54178 Å	0.71073 Å
Crystal system, space group	Tetragonal, I4/m	Tetragonal, I4/m
Unit cell dimensions	a = 11.9878(8) Å α = 90° b = 11.9878(8) Å β = 90° c = 31.393(2) Å γ = 90°	a = 11.9923(19) Å α = 90° b = 11.9923(19) Å β = 90° c = 31.387(8) Å γ = 90°
Volume	4511.4(5) Å ³	4513.9(15) Å ³
Z,	4,	4,
Calculated density	2.019 Mg/m ³	2.024 Mg/m ³
Absorption coefficient	27.027 mm ⁻¹	3.466 mm ⁻¹
F(000)	2644	2660
Crystal size (mm)	0.04 x 0.02 x 0.02	0.04 x 0.02 x 0.02
Theta range for data collection	2.82 to 58.89 deg.	1.82 to 25.65 deg.
Limiting indices	-12<=h<=11 -13<=k<=13, -34<=l<=24	-12<=h<=8 -14<=k<=13 -16<=l<=37
Reflections collected / unique	6650 / 1639	6803 / 1686
Completeness to	θ° = 58.89 98.4 %	θ° = 25.00 78.9 %
Absorption correction	Semi-empirical from equivalents	
Max. and min. transmission	0.6140 and 0.4111	0.9339 and 0.8738
Refinement method	Full-matrix least-squares on F ²	
Data / restraints / parameters	1639 / 15 / 153	1686 / 9 / 149
Goodness-of-fit on F ²	1.036	1.276
Final R indices [I>2σ(I)]	R ₁ = 0.0813, wR ₂ = 0.1955	R ₁ = 0.1382, wR ₂ = 0.2398
R indices (all data)	R ₁ = 0.1729, wR ₂ = 0.2250	R ₁ = 0.1693, wR ₂ = 0.2531
Largest diff. peak and hole	1.812 and -2.157 e.Å ⁻³	1.852 and -2.870 e.Å ⁻³

P1 refinement of the RPF9 crystals

Table V.1.04 Main crystallographic and refinement data for the RPF9 compounds refined in P1

Identification code	Pr-RPF9 crystal a	Pr-RPF9 crystal b	Pr-RPF9 crystal c	Nd-RPF9
Empirical formula	C ₅₆ H ₄₀ O ₅₀ Pr ₆ S ₈	C ₅₆ H ₄₀ O ₅₀ Pr ₆ S ₈	C ₅₆ H ₄₀ O ₅₀ Pr ₆ S ₈	C ₅₆ H ₃₈ O ₅₀ Pr ₆ S ₈
Formula weight	2662.82	2662.82	2662.82	2648.78
Temperature	296(2) K	296(2) K	296(2) K	296(2) K
Wavelength (Å)	1.54178 Å	1.54178 Å	0.71073	1.54178 Å
Crystal system, space group	Triclinic, P1	Triclinic, P1	Triclinic, P1	Triclinic, P1
Unit cell dimensions	a = 11.9784(5) Å α = 109.620(2)° b = 11.9801(5) Å β = 109.624(2)° c = 17.8515(8) Å γ = 90.050(2)°	a = 17.839(1) Å α = 109.63° b = 17.839(1) Å β = 109.63° c = 11.988(5) Å γ = 123.26°	a = 17.839(4) Å α = 109.65° b = 17.836(4) Å β = 109.63° c = 11.993(3) Å γ = 123.23°	a = 11.961(1) Å α = 109.61° b = 11.961(1) Å β = 109.61° c = 17.821(2) Å γ = 90°
Volume	2251.70(12) Å ³	2255.7(2) Å ³	2256.9(9)	2244.3(3)
Z, Calculated density	1 2.003 Mg/m ³	1 1.925 Mg/m ³	1 1.959 Mg/m ³	1 1.960 Mg/m ³
Absorption coefficient	27.032 mm ⁻¹	26.920 mm ⁻¹	3.458 mm ⁻¹	28.567 mm ⁻¹
F(000)	1306	1258	1282	1270
Crystal size (mm)	0.04 x 0.04 x 0.02	0.04 x 0.02 x 0.02	0.04 x 0.02 x 0.02	0.02 x 0.02 x 0.01
Theta range for data collection	2.81 to 64.76 deg.	2.82 to 58.89 deg.	1.82 to 26.37 deg.	2.82 to 59.66 deg.
Limiting indices	-10<=h<=13 -12<=k<=14, -20<=l<=18	-17<=h<=19 -19<=k<=12 -13<=l<=13	-19<=h<=15 -2<=k<=22 -14<=l<=13	-13<=h<=13 -12<=k<=13 -16<=l<=18
Reflections collected / unique	8237 / 5928 [R(int) = 0.0745]	6650 / 5863 [R(int) = 0.0689]	7018 / 3870 [R(int) = 0.0043]	6729 / 5953 [R(int) = 0.0904]
Completeness to	θ° = 60.00 92.5 %	θ° = 58.89 68.2 %	θ° = 25.00 45.9 %	θ° = 59.66 67.9 %
Max. and min. transmission	0.4111 and 0.2210	0.6150 and 0.4123	0.9341 and 0.8741	0.7632 and 0.5988
Refinement method	Full-matrix least-squares on F ²			
Data / restraints / parameters	8237 / 3 / 540	5863 / 3 / 420	3870 / 3 / 344	5953 / 3 / 384
Goodness-of-fit on F ²	1.080	1.005	1.071	1.000
Final R indices [I>2σ(I)]	R ₁ = 0.0518, wR ₂ = 0.1389	R ₁ = 0.0999, wR ₂ = 0.2174	R ₁ = 0.0963, wR ₂ = 0.1902	R ₁ = 0.1123, wR ₂ = 0.2325
R indices (all data)	R ₁ = 0.0601, wR ₂ = 0.1437	R ₁ = 0.2158, wR ₂ = 0.2532	R ₁ = 0.1124, wR ₂ = 0.2006	R ₁ = 0.2961, wR ₂ = 0.2846
Largest diff. peak and hole	1.506 and -1.401 e.Å ⁻³	1.870 and -1.974 e.Å ⁻³	2.419 and -1.213	2.010 and -2.353

2. Atomic coordinates

Atomic coordinates ($\times 10^4$) and equivalent isotropic displacement parameters ($\text{\AA}^2 \times 10^3$) for the collected crystals. $U(\text{eq})$ is defined as one third of the trace of the orthogonalized U^{ij} tensor.

<i>La-RPF4-α</i>					<i>La-RPF4-γ</i>				
	x	y	z	U(eq)		x	y	z	U(eq)
C(1)	-1070(20)	3781(9)	3412(6)	48(2)	C(1)	4620(20)	3367(6)	-48(7)	40(4)
C(2)	-350(20)	3155(11)	3449(7)	49(2)	C(2)	5450(20)	3796(5)	48(6)	36(3)
C(3)	1280(20)	3032(8)	3335(5)	49(2)	C(3)	4800(20)	4148(5)	-254(7)	41(4)
C(4)	2140(20)	2472(9)	3384(6)	49(2)	C(4)	5670(20)	4535(5)	-256(7)	37(3)
C(5)	1170(20)	1991(9)	3580(5)	49(2)	C(5)	7300(20)	4581(6)	66(6)	43(4)
C(6)	-560(20)	2096(10)	3690(5)	49(2)	C(6)	7910(30)	4243(5)	396(7)	45(4)
C(7)	-1240(20)	2693(9)	3637(5)	51(2)	C(7)	6990(20)	3844(5)	382(6)	41(3)
C(8)	2080(30)	1329(10)	3626(5)	56(3)	C(8)	8400(30)	5000	0	45(6)
C(9)	830(30)	838(11)	3737(8)	72(5)	C(9)	9680(30)	4931(8)	-552(15)	87(9)
C(10)	3540(30)	1435(12)	3949(6)	68(5)	C(10)	10640(20)	3002(6)	980(6)	35(4)
C(11)	3080(30)	1122(9)	3269(5)	55(5)	C(11)	11800(20)	3272(6)	1367(6)	37(4)
C(12)	2050(30)	1181(10)	2961(5)	59(6)	C(12)	11040(20)	3633(7)	1626(9)	50(5)
C(13)	2720(20)	967(9)	2628(5)	46(5)	C(13)	12070(30)	3924(6)	1979(7)	46(4)
C(14)	4420(20)	734(10)	2616(6)	48(2)	C(14)	13821(19)	3836(6)	2093(6)	31(3)
C(15)	5250(20)	675(10)	2938(5)	44(2)	C(15)	14590(20)	3501(6)	1815(7)	42(4)
C(16)	4700(20)	879(11)	3270(6)	44(2)	C(16)	13580(30)	3229(7)	1463(7)	44(5)
C(17)	-4930(19)	4460(11)	2728(6)	44(2)	C(17)	15000	4131(8)	2500	35(5)
C(18)	-1080(20)	5693(9)	3953(5)	44(2)	C(18)	13900(20)	4397(8)	2918(8)	57(6)
C(19)	-160(20)	6124(12)	4220(7)	44(2)	C(19)	4897(19)	2114(4)	1057(6)	28(3)
C(20)	-910(20)	6639(9)	4360(5)	51(2)	C(20)	3650(20)	1866(6)	1386(6)	35(4)
C(21)	-120(20)	7025(12)	4603(7)	48(2)	C(21)	3200(20)	2002(7)	1978(7)	49(5)
C(22)	1530(20)	6866(9)	4728(5)	44(2)	C(22)	1980(30)	1773(5)	2311(6)	42(4)
C(23)	2290(20)	6346(9)	4586(5)	49(2)	C(23)	1250(20)	1399(6)	2099(6)	41(4)
C(24)	1480(20)	5949(9)	4354(5)	51(2)	C(24)	1720(20)	1259(6)	1521(7)	45(4)
C(25)	2500	7291(13)	5000	32(4)	C(25)	2850(30)	1507(6)	1187(6)	44(4)
C(26)	1330(30)	7699(10)	5248(6)	56(4)	C(26)	0	1104(8)	2500	43(6)
F(1)	492(18)	785(7)	3527(4)	85(4)	C(27)	-1180(30)	832(8)	2149(9)	62(6)
F(2)	190(17)	915(9)	4078(4)	103(5)	F(1)	10340(20)	4546(5)	-562(8)	111(6)
F(3)	1619(17)	275(5)	3733(3)	92(4)	F(2)	8670(20)	4963(5)	-1055(6)	97(5)
F(4)	4739(16)	1811(8)	3840(4)	77(4)	F(3)	10977(17)	5193(5)	-595(9)	116(7)
F(5)	2668(15)	1742(6)	4221(3)	91(4)	F(4)	12649(14)	4173(3)	3208(4)	55(3)
F(6)	4160(20)	928(7)	4066(4)	105(5)	F(5)	13038(17)	4716(3)	2646(5)	61(3)
F(7)	580(18)	8134(8)	5038(4)	89(5)	F(6)	14924(15)	4592(4)	3330(5)	59(3)
F(8)	2205(15)	7971(6)	5512(3)	85(4)	F(7)	-2123(19)	1077(4)	1723(5)	77(4)
F(9)	30(9)	7343(9)	5388(4)	62(4)	F(8)	-440(20)	519(4)	1863(5)	82(5)
La(1)	2960(1)	-4995(1)	3374(1)	36(1)	F(9)	-2530(20)	643(4)	2470(6)	83(4)
O(1)	-2626(13)	3881(6)	3503(4)	57(3)	La(1)	7877(1)	2473(1)	295(1)	26(1)
O(2)	-236(13)	4234(8)	3258(4)	39(3)	O(1)	5485(13)	3030(4)	126(4)	33(2)
O(3)	-5715(15)	4445(6)	3025(3)	45(3)	O(2)	3164(17)	3342(4)	-284(7)	72(4)
O(4)	-3366(15)	4670(6)	2740(3)	65(3)	O(3)	9016(14)	3043(4)	1004(5)	47(3)
O(5)	-2597(12)	5842(6)	3857(3)	44(2)	O(4)	11405(15)	2718(3)	671(5)	41(3)
O(6)	-273(13)	5228(7)	3801(4)	44(2)	O(5)	6171(17)	2302(6)	1262(4)	72(5)
					O(6)	4704(13)	2124(4)	453(4)	34(2)

La-RPF4-β

	x	y	z	U(eq)		x	y	z	U(eq)
C(1)	8038(17)	7392(5)	-799(4)	32(2)	C(26)	11525(18)	4320(7)	1834(5)	55(4)
C(2)	6840(15)	7410(5)	-1182(4)	32(3)	C(27)	13460(20)	5119(7)	1980(5)	55(4)
C(3)	7349(16)	7662(6)	-1562(4)	53(4)	C(28)	13755(15)	4537(4)	1265(4)	28(3)
C(4)	6277(17)	7656(6)	-1943(4)	53(4)	C(29)	13037(15)	4330(5)	866(4)	35(3)
C(5)	4674(15)	7386(5)	-1951(4)	30(3)	C(30)	14057(16)	4077(5)	556(4)	37(3)
C(6)	4128(17)	7145(6)	-1559(4)	42(3)	C(31)	15826(15)	4022(5)	631(4)	29(3)
C(7)	5144(16)	7148(5)	-1181(4)	36(3)	C(32)	16576(16)	4230(6)	1028(5)	48(4)
C(8)	3546(15)	7392(5)	-2391(4)	33(3)	C(33)	15569(16)	4490(5)	1340(4)	42(3)
C(9)	2282(18)	7889(6)	-2353(4)	44(4)	C(34)	12953(17)	6300(5)	-339(4)	32(3)
C(10)	2438(17)	6868(6)	-2433(4)	40(3)	C(35)	9191(14)	8181(5)	402(4)	28(3)
C(11)	4692(16)	7413(5)	-2817(4)	36(3)	C(36)	8768(16)	8672(5)	671(4)	31(3)
C(12)	6161(17)	7087(6)	-2845(4)	43(4)	C(37)	9413(19)	9167(5)	525(5)	51(4)
C(13)	7283(17)	7114(6)	-3210(4)	44(4)	C(38)	9030(20)	9623(6)	763(5)	54(4)
C(14)	6877(13)	7444(5)	-3569(4)	24(3)	C(39)	8100(20)	9599(5)	1150(4)	50(4)
C(15)	5335(16)	7756(5)	-3547(4)	41(3)	C(40)	7450(20)	9113(5)	1305(5)	55(4)
C(16)	4282(16)	7731(6)	-3176(4)	39(3)	C(41)	7784(18)	8654(6)	1053(4)	43(3)
C(17)	3099(17)	7499(5)	1046(4)	32(2)	C(42)	7920(20)	10128(6)	1427(4)	57(4)
C(18)	7921(16)	6359(5)	704(4)	32(3)	C(43)	9730(30)	10236(6)	1665(6)	80(5)
C(19)	9059(15)	5957(4)	936(4)	25(3)	C(44)	6550(30)	10086(6)	1791(5)	80(5)
C(20)	10783(16)	5857(5)	795(4)	44(4)	C(45)	7360(20)	10596(5)	1115(5)	52(4)
C(21)	11792(16)	5487(5)	1021(5)	40(3)	C(46)	8000(20)	11119(6)	1185(5)	57(4)
C(22)	11210(15)	5197(5)	1373(4)	27(3)	C(47)	7496(17)	11527(5)	896(4)	40(3)
C(23)	9492(17)	5292(6)	1515(5)	49(4)	C(48)	6369(15)	11437(5)	546(4)	32(3)
C(24)	8449(15)	5676(5)	1301(4)	42(4)	C(49)	5659(19)	10925(6)	492(5)	55(4)
C(25)	12484(15)	4797(5)	1614(4)	32(3)	C(50)	6140(20)	10511(5)	771(5)	52(4)
F(1)	1468(11)	7894(4)	-1954(3)	66(3)	C(51)	4114(16)	8136(5)	-224(4)	30(3)
F(2)	3175(12)	8340(3)	-2392(3)	61(2)	F(10)	14473(12)	4811(5)	2246(3)	88(3)
F(3)	1013(11)	7880(4)	-2667(3)	68(3)	F(11)	12338(11)	5379(4)	2236(3)	79(3)
F(4)	1053(10)	6862(4)	-2149(3)	64(3)	F(12)	14508(11)	5486(4)	1789(3)	71(3)
F(5)	3389(12)	6443(4)	-2358(3)	66(2)	F(13)	10431(18)	9773(4)	1847(4)	115(5)
F(6)	1698(11)	6826(4)	-2850(3)	67(3)	F(14)	10980(17)	10386(5)	1364(4)	107(4)
F(7)	10360(11)	4090(4)	1549(3)	69(3)	F(15)	9743(19)	10595(4)	1983(3)	119(5)
F(8)	12631(11)	3942(4)	1967(3)	73(3)	F(16)	7140(20)	9760(4)	2133(3)	129(5)
F(9)	10622(13)	4467(4)	2195(3)	82(3)	F(17)	6330(20)	10570(4)	1997(4)	143(6)
La(1)	10630(1)	7214(1)	-25(1)	22(1)	F(18)	5001(16)	9924(4)	1624(4)	97(4)
La(2)	5669(1)	7258(1)	328(1)	22(1)	O(7)	11360(12)	6349(4)	-426(3)	53(3)
O(1)	9669(11)	7459(4)	-809(3)	54(3)	O(8)	13677(11)	6571(3)	-16(3)	36(2)
O(2)	7409(9)	7244(3)	-397(2)	32(2)	O(9)	10192(13)	8197(4)	104(3)	48(2)
O(3)	4641(11)	7654(4)	1067(3)	43(2)	O(10)	8463(10)	7730(3)	505(3)	30(2)
O(4)	2517(10)	7285(3)	673(2)	27(2)	O(11)	5296(12)	8207(3)	67(3)	48(2)
O(5)	6429(12)	6471(4)	855(3)	52(3)	O(12)	3396(9)	7665(3)	-250(2)	23(2)
O(6)	8504(10)	6614(3)	366(3)	33(2)					

Yb-RPF5

	x	y	z	U(eq)
Yb(1)	1707(1)	8287(1)	4856(1)	15(1)
C(1)	5361(12)	11504(11)	2424(6)	22(2)
C(2)	5739(12)	13033(11)	1924(7)	21(2)
C(3)	6604(12)	13024(11)	991(7)	21(2)
C(4)	7070(14)	11492(11)	568(7)	26(2)
C(5)	6687(17)	9950(12)	1073(8)	37(3)
C(6)	5816(16)	9970(12)	2021(7)	32(2)
C(7)	8003(15)	11436(11)	-421(7)	28(2)
C(8)	218(12)	5368(11)	2361(6)	20(2)
C(9)	652(14)	6912(12)	1865(7)	27(2)
C(10)	1530(13)	6888(11)	948(7)	23(2)
C(11)	2029(12)	5345(11)	533(6)	21(2)
C(12)	1576(13)	3819(11)	1033(7)	25(2)
C(13)	679(13)	3818(11)	1939(7)	23(2)
C(14)	3014(13)	5300(11)	-452(6)	21(2)
O(1)	3295(10)	13117(9)	3709(5)	30(2)
O(2)	3215(9)	10039(8)	3728(5)	26(1)
O(3)	4168(9)	8711(9)	5730(5)	26(1)
O(4)	8388(16)	10123(10)	-808(6)	66(3)
O(5)	420(8)	6134(8)	4126(5)	22(1)
O(6)	1277(9)	6318(8)	6136(5)	24(1)
O(7)	-2496(9)	6551(9)	3453(5)	29(2)
O(8)	3522(12)	3973(9)	-798(5)	41(2)
O(9)	747(9)	10416(8)	5734(5)	25(1)
O(10)	3939(9)	6378(9)	4221(6)	36(2)
S(1)	4333(3)	11515(3)	3632(2)	16(1)
S(2)	-889(3)	5439(3)	3540(2)	18(1)

Nd-RPF6

	x	y	z	U(eq)
C(1)	4152(7)	8111(6)	3423(3)	25(1)
C(2)	4531(7)	6735(6)	2950(3)	24(1)
C(3)	4037(7)	5149(7)	3266(3)	29(1)
C(4)	-3196(8)	15058(6)	5921(3)	27(1)
C(5)	-642(7)	12645(6)	3272(3)	24(1)
C(6)	-221(7)	11243(6)	2809(3)	23(1)
C(7)	-648(7)	9641(6)	3147(3)	26(1)
C(8)	-1511(7)	9447(6)	3951(3)	26(1)
C(9)	-2869(7)	10594(6)	5282(3)	24(1)
C(10)	-1933(7)	13952(6)	4565(3)	22(1)
C(11)	-1955(7)	10829(6)	4422(3)	22(1)
C(12)	-1505(7)	12437(6)	4072(3)	20(1)
C(13)	-3296(7)	12084(6)	5772(3)	22(1)
C(14)	-2828(7)	13699(6)	5438(3)	21(1)
Nd(1)	1756(1)	8141(1)	307(1)	21(1)
O(1)	7067(5)	5601(5)	1910(3)	38(1)
O(2)	6346(6)	8646(5)	1859(3)	42(1)
O(3)	4271(5)	6919(5)	1265(2)	32(1)
O(4)	1626(6)	9856(4)	1573(2)	34(1)
O(5)	745(6)	7818(5)	-1181(2)	37(1)
O(6)	2133(6)	12735(5)	1793(3)	38(1)
O(8)	588(6)	6147(5)	1481(3)	47(1)
O(9)	-3249(6)	9193(5)	5592(3)	40(1)
O(10)	-1578(6)	15348(5)	4252(2)	38(1)
O(11)	2750(8)	5197(6)	-106(3)	59(2)
O(12)	1405(5)	10986(4)	-310(2)	29(1)
O(13)	4723(8)	8419(8)	-565(4)	68(2)
S(1)	5644(2)	7005(2)	1926(1)	24(1)
S(2)	796(2)	11527(2)	1761(1)	26(1)

Dy-RPF6

	x	y	z	U(eq)
C(1)	4490(13)	6761(13)	2929(6)	20(2)
C(2)	4142(14)	8131(13)	3418(6)	21(2)
C(3)	3267(13)	7919(12)	4228(6)	20(2)
C(4)	2849(14)	9416(12)	4735(6)	22(2)
C(5)	1949(14)	9173(12)	5606(6)	20(2)
C(6)	1516(15)	10564(13)	6081(7)	27(3)
C(7)	651(14)	10344(14)	6891(7)	27(3)
C(8)	253(14)	8742(13)	7228(7)	24(2)
C(9)	649(14)	7363(13)	6747(6)	23(2)
C(10)	1517(13)	7572(12)	5945(6)	18(2)
C(11)	1947(14)	6060(13)	5438(6)	22(2)
C(12)	2823(14)	6324(12)	4561(6)	20(2)
C(13)	3188(14)	4955(13)	4051(7)	25(2)
C(14)	4021(14)	5171(12)	3243(6)	22(2)
Dy(1)	1724(1)	8170(1)	305(1)	19(1)
O(1)	4219(9)	6937(9)	1232(4)	26(2)
O(2)	7076(9)	5625(10)	1873(5)	33(2)
O(3)	6267(11)	8699(9)	1834(5)	35(2)
O(4)	-2087(10)	7233(9)	8247(5)	34(2)
O(5)	779(11)	7801(10)	8862(4)	37(2)
O(6)	-1629(11)	10152(9)	8463(4)	33(2)
O(7)	3218(11)	10825(9)	4430(5)	37(2)
O(8)	1580(12)	4649(9)	5743(5)	37(2)
O(9)	-1353(9)	9079(9)	316(5)	29(2)
O(10)	597(11)	6225(10)	1430(6)	45(2)
O(11)	4601(11)	8416(13)	-539(6)	56(3)
O(12)	2778(12)	5253(11)	-79(5)	52(3)
S(1)	5595(3)	7045(3)	1889(2)	21(1)
S(2)	-788(4)	8464(3)	8281(2)	24(1)

Gd-RPF6

	x	y	z	U(eq)
C(1)	4506(8)	6765(8)	2936(4)	20(1)
C(2)	4030(9)	5172(8)	3247(4)	26(1)
C(3)	3196(9)	4947(8)	4060(4)	26(1)
C(4)	2830(8)	6333(8)	4557(4)	19(1)
C(5)	1955(9)	6047(8)	5436(4)	21(1)
C(6)	1523(8)	7572(7)	5939(4)	18(1)
C(7)	675(9)	7363(8)	6747(4)	21(1)
C(8)	251(8)	8784(8)	7212(4)	19(1)
C(9)	662(9)	10362(8)	6880(4)	23(1)
C(10)	1534(9)	10571(8)	6070(4)	23(1)
C(11)	1965(8)	9168(8)	5603(4)	20(1)
C(12)	2857(9)	9438(8)	4729(4)	22(1)
C(13)	3292(8)	7922(8)	4231(4)	19(1)
C(14)	4135(9)	8137(8)	3419(4)	21(1)
Gd(1)	1733(1)	8154(1)	306(1)	17(1)
O(1)	1594(8)	4654(6)	5747(3)	36(1)
O(2)	3220(8)	10839(6)	4418(3)	36(1)
O(3)	4239(6)	6940(6)	1240(3)	28(1)
O(4)	6270(7)	8701(6)	1840(3)	36(1)
O(5)	7084(6)	5634(7)	1892(3)	33(1)
O(6)	793(7)	7824(6)	8843(3)	34(1)
O(7)	-2077(7)	7265(6)	8232(3)	33(1)
O(8)	-1609(7)	10161(6)	8456(3)	29(1)
O(9)	-1399(6)	9037(6)	299(3)	25(1)
O(10)	592(7)	6195(6)	1448(4)	41(1)
O(11)	2746(9)	5254(7)	-91(4)	53(2)
O(12)	4654(8)	8404(8)	-538(4)	53(2)
S(1)	5611(2)	7042(2)	1903(1)	21(1)
S(2)	-769(2)	8479(2)	8266(1)	23(1)

V.2 Atomic coordinates

<i>Ho-RPF6</i>					<i>Er-RPF6</i>				
	x	y	z	U(eq)		x	y	z	U(eq)
C(1)	10245(8)	-1225(7)	7227(3)	20(1)	C(1)	-232(8)	1239(7)	2764(4)	20(1)
C(2)	10667(8)	-2647(7)	6763(3)	21(1)	C(2)	-671(8)	2652(7)	3235(4)	19(1)
C(3)	11523(8)	-2436(6)	5944(3)	20(1)	C(3)	-1523(8)	2442(7)	4053(4)	19(1)
C(4)	11941(8)	-3938(7)	5437(3)	21(1)	C(4)	-1952(8)	3952(7)	4566(4)	22(1)
C(5)	12831(8)	-3682(6)	4557(3)	19(1)	C(5)	-2839(8)	3682(7)	5443(4)	20(1)
C(6)	13189(8)	-5053(7)	4048(4)	25(1)	C(6)	-3185(9)	5051(8)	5950(4)	26(1)
C(7)	14022(8)	-4835(7)	3238(4)	25(1)	C(7)	-4021(9)	4838(7)	6774(4)	26(1)
C(8)	14490(7)	-3230(7)	2930(3)	19(1)	C(8)	-4484(7)	3224(7)	7075(4)	20(1)
C(9)	14122(8)	-1863(7)	3409(4)	24(1)	C(9)	-4129(8)	1856(7)	6590(4)	20(1)
C(10)	13288(7)	-2079(6)	4235(3)	17(1)	C(10)	-3291(8)	2087(7)	5763(4)	19(1)
C(11)	12848(8)	-568(7)	4737(4)	23(1)	C(11)	-2865(8)	564(7)	5268(4)	20(1)
C(12)	11956(7)	-834(7)	5608(3)	20(1)	C(12)	-1959(8)	831(7)	4395(4)	21(1)
C(13)	11527(8)	576(7)	6079(4)	24(1)	C(13)	-1530(8)	-567(7)	3905(4)	25(1)
C(14)	10662(8)	354(7)	6895(4)	25(1)	C(14)	-647(8)	-362(7)	3092(4)	26(1)
Ho(1)	8278(1)	1827(1)	9695(1)	18(1)	Er(1)	1718(1)	-1821(1)	304(1)	18(1)
O(1)	8358(6)	167(5)	8473(2)	28(1)	O(1)	2091(6)	2741(6)	1736(3)	34(1)
O(2)	7913(6)	-2739(5)	8255(3)	34(1)	O(2)	-798(6)	2188(5)	1127(3)	32(1)
O(3)	10785(6)	-2187(5)	8866(3)	35(1)	O(3)	1632(6)	-166(5)	1519(3)	28(1)
O(4)	5797(5)	3048(5)	8771(2)	27(1)	O(4)	4207(5)	-3054(5)	1219(3)	26(1)
O(5)	2917(6)	4359(5)	8134(3)	34(1)	O(5)	7086(5)	-4363(6)	1861(3)	31(1)
O(6)	3765(6)	1285(5)	8174(3)	33(1)	O(6)	6225(6)	-1276(6)	1816(3)	33(1)
O(7)	11600(7)	-5352(5)	5742(3)	36(1)	O(7)	-1602(7)	5356(5)	4258(3)	34(1)
O(8)	13214(7)	829(5)	4426(3)	38(1)	O(8)	-3211(7)	-835(5)	5570(3)	36(1)
O(9)	11370(5)	940(5)	9690(2)	25(1)	O(9)	-1356(5)	-928(5)	307(3)	25(1)
O(10)	9412(6)	3769(6)	8578(3)	46(1)	O(10)	585(6)	-3744(6)	1413(4)	45(1)
O(11)	7229(8)	4709(6)	10076(3)	50(1)	O(11)	2773(8)	-4706(6)	-75(3)	49(1)
O(12)	5410(7)	1593(7)	10353(3)	51(1)	O(12)	4579(7)	-1591(7)	-525(3)	51(1)
S(1)	9227(2)	-1533(2)	8288(1)	23(1)	S(1)	775(2)	1529(2)	1707(1)	23(1)
S(2)	4406(2)	2945(2)	8114(1)	21(1)	S(2)	5587(2)	-2939(2)	1883(1)	20(1)

La-RPF7

	x	y	z	U(eq)		x	y	z	U(eq)
C(1)	4956(5)	1518(5)	-1711(3)	21(1)	C(15)	1811(5)	4921(5)	2085(3)	20(1)
C(2)	271(5)	-727(5)	2379(3)	18(1)	C(16)	2865(5)	824(5)	578(3)	20(1)
C(3)	1819(5)	0(4)	1053(3)	17(1)	C(17)	1358(5)	-806(4)	620(3)	17(1)
C(4)	2982(5)	-27(4)	-804(3)	17(1)	C(18)	4390(5)	1561(5)	-830(3)	23(1)
C(5)	3915(5)	5841(5)	-2170(3)	19(1)	C(19)	190(5)	3467(5)	2270(3)	21(1)
C(6)	4526(4)	697(4)	-2125(3)	15(1)	C(20)	2088(5)	4969(5)	1175(3)	19(1)
C(7)	2744(5)	5034(4)	-718(3)	18(1)	C(21)	3534(5)	-60(5)	-1689(3)	20(1)
C(8)	1912(5)	-855(5)	-327(3)	18(1)	C(22)	3083(5)	5805(5)	591(3)	20(1)
C(9)	1256(5)	27(5)	1935(3)	20(1)	C(23)	1739(5)	4218(5)	-135(3)	22(1)
C(10)	1426(5)	4233(5)	826(3)	19(1)	C(24)	4611(5)	6552(5)	-1836(3)	23(1)
C(11)	876(5)	4169(5)	2622(3)	18(1)	C(25)	4354(5)	6504(5)	-932(3)	22(1)
C(12)	478(5)	3500(5)	1374(3)	22(1)	C(26)	3005(5)	5062(5)	-1621(3)	21(1)
C(13)	380(5)	-1577(5)	1078(3)	23(1)	C(27)	3406(5)	5764(4)	-362(3)	18(1)
C(14)	3429(5)	775(5)	-370(3)	19(1)	C(28)	-174(5)	-1536(5)	1955(3)	23(1)
La(1)	3446(1)	1683(1)	4828(1)	12(1)	La(2)	2092(1)	-1728(1)	5050(1)	14(1)
O(1)	656(3)	-1478(3)	3965(2)	25(1)	O(11)	2677(3)	3820(3)	5544(2)	22(1)
O(2)	3314(5)	-3807(4)	4532(3)	53(1)	O(12)	1846(3)	3548(3)	4036(2)	23(1)
O(3)	420(4)	-3201(4)	5842(2)	27(1)	O(13)	6055(3)	825(3)	4650(2)	17(1)
O(4)	2905(3)	-3234(3)	6445(2)	26(1)	O(14)	4685(3)	3485(3)	3738(2)	21(1)
O(5)	674(4)	-695(3)	6397(2)	28(1)	O(15)	5755(4)	5454(3)	3424(2)	27(1)
O(6)	1799(3)	608(3)	4561(2)	20(1)	O(17)	1521(4)	-1539(4)	-708(2)	29(1)
O(7)	3566(3)	-1250(3)	3465(2)	21(1)	O(18)	3281(4)	1501(4)	955(2)	29(1)
O(8)	4534(3)	749(3)	3346(2)	21(1)	O(19)	1195(4)	3545(4)	-441(2)	37(1)
O(9)	1587(3)	1325(4)	6262(2)	26(1)	O(20)	3590(4)	6511(4)	894(2)	34(1)
O(10)	4211(3)	1462(3)	6266(2)	25(1)	O(21)	72(4)	5438(3)	3919(2)	28(1)
S(1)	4776(1)	-654(1)	3253(1)	15(1)	S(3)	-396(1)	-709(1)	3514(1)	15(1)
S(2)	5880(1)	4077(1)	3318(1)	17(1)	S(4)	566(1)	4097(1)	3779(1)	16(1)

Pr-RPF7

	x	y	z	U(eq)		x	y	z	U(eq)
C(1)	1067(7)	4153(7)	2179(4)	15(2)	C(15)	488(7)	-698(7)	2132(5)	16(2)
C(2)	385(7)	3441(7)	1836(5)	18(2)	C(16)	51(7)	-1529(7)	1723(5)	19(2)
C(3)	664(7)	3483(7)	932(5)	21(2)	C(17)	602(7)	-1562(7)	841(5)	20(2)
C(4)	1589(7)	4233(7)	367(5)	20(2)	C(18)	1573(7)	-788(7)	365(4)	16(2)
C(5)	1928(7)	4202(7)	-594(5)	17(2)	C(19)	2125(7)	-817(7)	-586(5)	20(2)
C(6)	2916(7)	5048(7)	-1184(5)	17(2)	C(20)	3187(7)	12(7)	-1066(4)	14(1)
C(7)	3190(7)	5098(7)	-2081(5)	20(2)	C(21)	3722(7)	-12(7)	-1951(5)	19(2)
C(8)	4142(7)	5851(7)	-2624(5)	19(2)	C(22)	4711(7)	744(7)	-2399(4)	14(2)
C(9)	4828(8)	6556(8)	-2272(5)	23(2)	C(23)	5181(8)	1550(7)	-1980(5)	21(2)
C(10)	4530(7)	6527(7)	-1370(5)	20(2)	C(24)	4616(7)	1580(8)	-1102(5)	23(2)
C(11)	3572(7)	5773(7)	-810(5)	18(2)	C(25)	3645(7)	812(7)	-630(5)	17(2)
C(12)	3263(7)	5791(7)	137(5)	18(2)	C(26)	3097(7)	854(7)	323(5)	19(2)
C(13)	2257(7)	4986(7)	719(5)	17(2)	C(27)	2029(7)	31(7)	801(5)	15(2)
C(14)	1986(7)	4924(7)	1626(5)	20(2)	C(28)	1477(7)	54(7)	1688(4)	17(2)
Pr(1)	-1559(1)	1660(1)	4825(1)	12(1)	Pr(2)	-2876(1)	-1718(1)	5054(1)	13(1)
O(1)	-343(5)	3468(5)	3760(3)	21(1)	O(11)	-1407(5)	-1277(5)	3487(3)	20(1)
O(2)	2082(5)	3215(5)	3568(3)	24(1)	O(12)	-3434(5)	1359(5)	6235(3)	23(1)
O(3)	731(5)	5440(5)	3449(3)	24(1)	O(13)	-4310(5)	-685(5)	6371(3)	26(1)
O(4)	-3164(5)	3492(5)	4051(3)	22(1)	O(14)	-5679(5)	1467(5)	6004(3)	22(1)
O(5)	-5445(5)	3160(5)	4172(3)	24(1)	O(15)	1705(5)	-1496(5)	-966(3)	27(1)
O(6)	-4937(5)	5411(5)	3931(3)	27(1)	O(16)	3492(5)	1545(5)	699(4)	30(1)
O(7)	1422(6)	3488(6)	-895(3)	31(1)	O(17)	-3164(5)	588(5)	4556(3)	16(1)
O(8)	3797(6)	6459(6)	448(4)	34(2)	O(18)	1046(5)	829(4)	4654(3)	16(1)
O(9)	-465(5)	753(5)	3353(3)	19(1)	O(19)	-1741(6)	-3781(5)	4538(4)	45(2)
O(10)	825(5)	-1450(5)	3742(3)	24(1)	O(20)	-2308(5)	3810(5)	5522(3)	22(1)
S(1)	858(2)	4064(2)	3336(1)	15(1)	S(3)	-204(2)	-665(2)	3269(1)	13(1)
S(2)	-4453(2)	4056(2)	3793(1)	15(1)	S(4)	-4619(2)	726(2)	6454(1)	14(1)

Yb-LRH

	x	y	z	U(eq)
C(1)	1739(17)	4159(6)	5000	29(4)
C(2)	730(17)	4243(6)	5000	32(4)
C(3)	397(17)	4607(5)	5000	28(4)
C(4)	1111(16)	4902(6)	5000	31(4)
C(5)	2229(18)	4818(7)	5000	41(5)
C(6)	2560(19)	4443(7)	5000	47(6)
C(7)	-753(17)	4700(6)	5000	33(5)
O(1)	4684(9)	2210(3)	5000	13(1)
O(2)	1008(9)	2105(3)	5000	13(1)
O(3)	1685(6)	2711(2)	2976(11)	13(1)
O(4)	1166(9)	2169(3)	0	13(1)
O(5)	2915(11)	1673(4)	5000	25(3)
O(6)	0	1608(7)	2500	61(6)
O(7)	1298(14)	3446(5)	5000	69(6)
O(8)	2897(11)	3653(4)	3285(19)	59(4)
O(9)	-1438(15)	4455(5)	5000	50(5)
S(1)	2223(4)	3691(2)	5000	33(1)
Yb(1)	2694(1)	2337(1)	5000	11(1)
Yb(2)	0	2389(1)	2500	17(1)

Dy-LRH

	x	y	z	U(eq)
C(1)	4235(15)	5308(5)	0	42(4)
C(2)	3910(14)	4900(5)	0	41(4)
C(3)	2813(16)	4826(5)	0	58(6)
C(4)	2487(14)	4444(5)	0	49(5)
C(5)	3248(14)	4165(5)	0	39(4)
C(6)	4269(14)	4239(4)	0	36(4)
C(7)	4613(14)	4609(4)	0	33(4)
Dy(1)	2295(1)	2331(1)	0	14(1)
Dy(2)	5000	2366(1)	2500	20(1)
O(1)	3986(7)	2089(3)	0	19(1)
O(2)	3832(7)	2153(3)	5000	19(1)
O(3)	1670(5)	2292(2)	2988(10)	19(1)
O(4)	325(7)	2220(3)	0	22(2)
O(5)	2045(9)	1640(3)	0	36(3)
O(7)	3650(12)	3448(3)	0	73(5)
O(8)	2130(8)	3658(3)	1647(16)	65(3)
O(9)	3614(11)	5566(4)	0	69(5)
O(61)	5000	1579(4)	2500	50(4)
S(1)	2778(4)	3688(1)	0	42(1)

V.2 Atomic coordinates

<i>La-RPF8</i>				<i>Pr-RPF8</i>					
	x	y	z	U(eq)		x	y	z	U(eq)
C(1)	8060(9)	9132(5)	3527(13)	22(2)	C(1)	2656(10)	9491(5)	6493(16)	24(3)
C(2)	9055(8)	9542(4)	3651(13)	18(2)	C(2)	1755(10)	9905(5)	6398(17)	30(3)
C(3)	10232(8)	9339(4)	3795(14)	18(2)	C(3)	1924(10)	10565(5)	6453(17)	29(3)
C(4)	11165(8)	9796(4)	3671(13)	19(2)	C(4)	3017(10)	10800(5)	6598(15)	24(3)
C(5)	12306(9)	9561(4)	3628(15)	26(3)	C(5)	3984(9)	10404(5)	6684(16)	22(3)
C(6)	13234(9)	9973(5)	3524(17)	35(3)	C(6)	3815(9)	9716(5)	6666(14)	17(3)
C(7)	13042(9)	10625(5)	3480(16)	33(3)	C(7)	4857(10)	9316(5)	6824(15)	19(3)
C(8)	7673(9)	10517(5)	8512(14)	26(3)	C(8)	6981(8)	9135(4)	11491(14)	13(3)
C(9)	8827(8)	10271(5)	8385(13)	22(2)	C(9)	8074(9)	9370(5)	11547(16)	29(3)
C(10)	9002(9)	9612(5)	8329(15)	25(2)	C(10)	8255(9)	10028(5)	11487(17)	28(3)
C(11)	10154(9)	9339(5)	8177(14)	22(2)	C(11)	7340(9)	10448(5)	11387(16)	23(3)
C(12)	8032(11)	9201(5)	8431(16)	36(3)	C(12)	6177(8)	10206(5)	11333(15)	15(3)
C(13)	6943(10)	9432(5)	8545(16)	34(3)	C(13)	5965(8)	9538(4)	11355(16)	13(3)
C(14)	6754(10)	10091(5)	8621(15)	37(3)	C(14)	4762(8)	9329(5)	11195(16)	18(2)
La(1)	10656(1)	7838(1)	6031(1)	20(1)	O(1)	992(6)	8662(3)	5920(12)	33(2)
O(1)	11960(6)	6927(3)	6977(11)	32(2)	O(2)	2925(7)	8382(4)	4793(10)	42(2)
O(2)	8573(6)	8029(3)	5114(11)	27(2)	O(3)	2473(6)	8358(3)	8143(10)	22(2)
O(3)	8893(6)	8138(3)	1739(11)	38(2)	O(4)	6422(6)	8024(3)	9866(9)	24(2)
O(4)	12538(6)	8383(3)	6870(11)	35(2)	O(5)	8064(6)	8062(3)	11944(9)	24(2)
O(5)	6026(6)	11334(3)	9136(12)	43(2)	O(6)	6116(6)	8125(3)	13267(10)	30(2)
O(6)	7933(8)	11608(4)	10169(13)	52(2)	O(7)	4778(5)	8717(3)	7087(10)	21(2)
O(7)	10496(5)	8744(3)	4041(10)	26(1)	O(8)	4503(6)	8738(3)	10949(11)	22(2)
O(8)	10223(6)	8728(3)	7937(10)	31(2)	O(9)	5239(7)	6802(3)	10215(11)	41(2)
O(9)	9580(8)	7418(4)	8789(12)	51(2)	O(10)	5385(6)	7415(3)	6253(11)	40(2)
O(10)	9753(7)	6777(3)	4763(14)	49(2)	O(11)	3281(6)	7572(3)	11938(10)	37(2)
O(11)	11748(8)	7558(4)	3050(11)	51(2)	Pr(1)	4356(1)	7841(1)	8990(1)	17(1)
S(1)	8152(2)	8284(1)	3303(4)	24(1)	S(1)	2239(2)	8661(1)	6293(4)	24(1)
S(2)	7247(2)	11330(1)	8713(4)	30(1)	S(2)	6865(2)	8275(1)	11695(4)	18(1)

<i>Sm-RPF8</i>				<i>Gd-RPF8</i>					
	x	y	z	U(eq)		x	y	z	U(eq)
C(1)	9830(11)	694(7)	6870(20)	18(2)	C(1)	4751(8)	9318(4)	3797(14)	23(2)
C(2)	8806(11)	286(6)	6677(17)	14(3)	C(2)	5976(8)	9532(4)	3648(13)	20(3)
C(3)	7647(11)	529(6)	6505(19)	17(3)	C(3)	6986(9)	9123(4)	3531(12)	23(2)
C(4)	6695(11)	107(6)	6420(20)	30(4)	C(4)	8102(10)	9372(5)	3423(14)	34(3)
C(5)	6926(12)	-554(7)	6500(20)	28(4)	C(5)	8277(9)	10045(5)	3491(14)	37(3)
C(6)	8011(11)	-810(6)	6607(18)	21(3)	C(6)	7329(9)	10447(5)	3577(13)	28(3)
C(7)	8980(11)	-392(6)	6723(19)	16(3)	C(7)	6176(8)	10212(4)	3647(12)	19(2)
C(8)	9797(10)	681(6)	11190(20)	18(2)	C(8)	4856(9)	9308(5)	8131(14)	23(2)
C(9)	8827(10)	212(6)	11353(17)	13(3)	C(9)	6027(9)	9596(5)	8325(14)	25(3)
C(10)	7653(11)	435(7)	11390(20)	27(4)	C(10)	6999(10)	9193(5)	8376(13)	28(3)
C(11)	6723(12)	34(7)	11515(18)	24(4)	C(11)	8124(11)	9437(5)	8506(15)	42(3)
C(12)	6899(11)	-624(7)	11581(17)	21(3)	C(12)	8286(10)	10108(5)	8557(16)	43(3)
C(13)	8008(11)	-875(6)	11512(18)	19(3)	C(13)	7355(10)	10527(5)	8479(15)	33(3)
C(14)	9032(11)	-459(6)	11381(19)	15(3)	C(14)	6173(9)	10294(5)	8317(13)	26(3)
Sm(1)	9373(1)	2157(1)	9007(1)	19(1)	Gd(1)	4380(1)	7846(1)	5990(1)	24(1)
O(1)	7501(7)	1660(4)	8172(12)	20(1)	O(1)	6424(5)	8012(3)	5115(9)	30(2)
O(2)	7913(9)	1632(4)	4784(12)	33(2)	O(2)	6159(6)	8113(3)	1710(10)	39(2)
O(3)	5986(7)	1357(4)	6015(15)	36(2)	O(3)	8114(5)	8048(3)	3119(8)	28(2)
O(4)	8088(7)	3057(4)	8090(12)	26(2)	O(4)	7476(5)	11671(3)	6856(9)	28(2)
O(5)	6410(7)	3019(4)	10102(11)	20(1)	O(5)	9014(5)	11363(3)	9005(11)	38(2)
O(6)	6148(7)	3114(4)	6732(13)	31(2)	O(6)	7076(7)	11631(3)	10229(10)	47(2)
O(7)	9787(7)	1290(4)	7090(12)	20(2)	O(7)	4506(6)	8724(2)	4051(9)	26(1)
O(8)	9499(7)	1274(3)	10948(13)	21(2)	O(8)	4801(5)	8702(3)	7888(9)	27(2)
O(9)	10365(8)	2570(4)	6266(13)	37(2)	O(9)	5331(6)	7429(3)	8715(10)	41(2)
O(10)	10237(8)	3204(4)	10140(13)	34(2)	O(10)	5268(6)	6826(3)	4845(10)	42(2)
O(11)	8303(8)	2444(4)	11879(11)	34(2)	O(11)	3328(6)	7561(3)	3147(8)	37(2)
S(1)	7242(3)	1356(2)	6316(5)	23(1)	S(1)	6890(2)	8264(1)	3310(3)	25(1)
S(2)	6883(3)	3267(2)	8312(5)	17(1)	S(2)	7753(2)	11360(1)	8688(4)	30(1)

Pr-PRF9

	x	y	z	U(eq)
C(1)	6946(6)	3986(6)	2762(2)	15(2)
C(2)	7709(6)	4739(6)	2935(2)	14(2)
C(3)	7409(6)	2606(6)	3273(2)	17(2)
C(4)	8354(6)	4379(6)	3278(2)	16(2)
C(5)	7883(6)	5883(6)	2752(2)	15(2)
C(6)	8218(7)	3301(6)	3438(2)	17(2)
C(7)	6759(6)	2933(6)	2933(2)	11(2)
Pr(1)	10000	0	4155(1)	16(1)
Pr(2)	9008(1)	2072(1)	5000	20(1)
O(1)	8504(5)	2954(5)	4257(2)	32(2)
O(2)	9292(4)	1651(4)	3751(2)	24(1)
O(3)	10109(5)	3483(5)	3831(2)	36(2)
O(4)	6396(5)	4304(4)	2398(2)	24(1)
O(5)	10612(4)	1700(4)	4542(2)	19(1)
O(6)	10000	0	3282(19)	130(20)
O(7)	6946(8)	2598(10)	5000	61(3)
O(81)	9940(30)	4040(30)	5000	95(11)
O(82)	9137(16)	4162(15)	5000	54(5)
O(9)	5567(7)	1827(9)	4342(3)	94(3)
O(11)	10000	0	5000	53(5)
S(1)	9109(2)	2824(2)	3848(1)	19(1)

Nd-PRF9

	x	y	z	U(eq)
C(1)	1763(7)	3331(7)	3452(2)	21(2)
C(2)	2563(7)	2613(7)	3290(2)	18(2)
C(3)	3222(7)	2928(6)	2945(2)	14(2)
C(4)	5593(7)	1630(7)	3291(2)	18(2)
C(5)	5247(7)	2281(7)	2949(2)	16(2)
C(6)	4086(7)	2125(7)	2764(2)	17(2)
C(7)	6002(7)	3044(6)	2772(2)	16(2)
Nd(1)	0	0	4107(1)	15(1)
Nd(2)	1003(1)	2214(1)	5000	20(1)
O(1)	705(5)	1671(5)	3761(2)	31(2)
O(2)	1495(5)	2955(5)	4269(2)	37(2)
O(3)	-131(5)	3514(6)	3856(2)	39(2)
O(4)	5686(5)	3596(5)	2414(2)	29(2)
O(5)	590(4)	-1569(4)	4572(2)	19(1)
O(7)	390(17)	4153(11)	5000	128(7)
O(8)	3045(10)	2554(12)	5000	79(4)
O(9)	0	0	3292(7)	46(8)
O(10)	4390(9)	1984(11)	4318(3)	116(4)
S(1)	891(2)	2854(2)	3864(1)	23(1)

Yb-PRF9

	x	y	z	U(eq)
C(1)	1790(20)	3170(20)	1547(7)	22(4)
C(2)	2460(20)	2320(20)	1723(8)	24(5)
C(3)	2130(20)	1695(19)	2071(8)	18(3)
C(4)	1070(20)	1920(20)	2243(8)	17(4)
C(5)	320(20)	2723(19)	2055(8)	18(3)
C(6)	710(20)	3355(19)	1709(8)	22(5)
C(7)	-810(20)	2910(20)	2254(8)	21(5)
O(1)	3503(15)	4236(15)	1254(6)	26(3)
Yb(1)	5000	5000	877(1)	17(1)
Yb(2)	3012(1)	3909(1)	0	23(1)
O(2)	2262(17)	3423(16)	716(6)	33(4)
O(3)	1664(16)	5051(17)	1140(6)	36(4)
O(4)	735(16)	1384(16)	2603(6)	31(4)
O(5)	5448(15)	6535(15)	430(5)	25(4)
O(6)	2720(30)	1990(20)	0	43(7)
O(7)	1160(30)	4370(40)	0	62(8)
O(10)	3390(30)	460(30)	623(10)	102(13)
S(1)	2332(6)	4039(6)	1130(2)	25(1)

VI. Published articles

With the results of the present thesis, the following articles have been published:

1. “Layered Rare-Earth Hydroxides: A Class of Pillared Crystalline Compounds for Intercalation Chemistry”, F. Gándara, J. Perles, N. Snejko, M. Iglesias, B. Gómez-Lor, E. Gutiérrez-Puebla, M. A. Monge, *Angewandte Chemie - International Edition*, **2006**, 45, 7998-8001
2. “Rare Earth Arenedisulfonate Metal-Organic Frameworks: An Approach toward Polyhedral Diversity and Variety of Functional Compounds”. F. Gándara, A. García-Cortés, C. Cascales, B. Gómez-Lor, E. Gutiérrez-Puebla, M. Iglesias, M. A. Monge, *Inorganic Chemistry*, **2007**, 46, 3475-2484
3. “A Rare-Earth MOF Series: Fascinating Structure, Efficient Light Emitters, and Promising Catalysts” F. Gándara, A. de Andrés, B. Gómez-Lor, E. Gutiérrez-Puebla, M. Iglesias, M. A. Monge, D. M. Proserpio and N. Snejko. *Crystal Growth & Design* **2008** , 8, 378–380
4. “Controlling the Structure of Arenedisulfonates toward Catalytically Active Materials”, F. Gándara, E. Gutierrez-Puebla, M. Iglesias, D. M. Proserpio, N. Snejko, M. A. Monge, *Chemistry of Materials*, **2009**, 21, 665-661
5. “Three Lanthanum MOF polymorphs: Insights into Kinetically and Thermodynamically Controlled Phases” F. Gándara, V. de la Peña-O’shea, F. Illas, N. Snejko, D. M. Proserpio, E. Gutiérrez-Puebla, M. A. Monge, *Inorganic Chemistry*, **2009**, in press, DOI: 10.1021/ic801779j
6. “Isolated Hexanuclear Hydroxo Lanthanide Secondary Building Units in a Rare-Earth Polymeric Framework Based on p-Sulfonatocalix[4]arene” F. Gándara, E. Gutierrez-Puebla, M. Iglesias, N. Snejko, M. A. Monge *Crystal Growth & Design*, **2010**, in press, DOI: 10.1021/cg900704x

Communications

Layered Compounds

DOI: 10.1002/anie.200602502

Layered Rare-Earth Hydroxides: A Class of Pillared Crystalline Compounds for Intercalation Chemistry**

Felipe Gándara, Josefina Perles, Natalia Snejko, Maria Iglesias, Berta Gómez-Lor, Enrique Gutiérrez-Puebla,* and M. Angeles Monge*

The well-known layered double hydroxides (LDHs) and their thermal-treatment products, which are used as adsorbents, drug-delivery vehicles, polymer stabilizers, and catalysts,^[1–7] are generally based on brucite-like materials doped with d-block elements, although studies on a Li⁺–Al³⁺ LDH^[8] and on ionic europium and gadolinium complexes intercalated in pillared LDHs have recently been reported.^[9] Compounds of the type presented herein, which are formed by pure cationic rare-earth hydroxide layers, have not yet been reported; they represent a new generation of pillared materials, in which the properties of intercalation materials are combined with those of rare-earth elements. [R₃(OH)₆(H₂O)₆]_nA_n (R = rare-earth ions, A = intercalated organic anions, 2,6-naphthalenedisulfonate (NDS²⁻) and 2,6-anthraquinonedisulfonate (AQDS²⁻)) is the first family of layered rare-earth hydroxides (LRHs). In these LRHs, the positive charge of the inorganic layer is created only by trivalent rare-earth hydroxocations, which arises from the high and variable coordinative capability of the rare-earth centers and to the tendency of the hydroxide ion to form μ₆ connections in structures that contain these rare-earth centers. Rigid organic anions are intercalated to neutralize the positive charge. Apart from their potential as ion exchangers, these new materials contain a great number of active metal centers with the capability of varying the coordination number in catalytic processes, which confers to them great possibilities in the field of green chemistry. In fact, the performed tests in hydrodesulfurization (HDS), sulfide oxidation, and redox reactions reveal these new LRHs to be high-quality heterogeneous catalysts. Other interesting physical properties emerging from both the f–f interactions and those of intercalated organic anions are also to be expected.

[*] F. Gándara, J. Perles, Dr. N. Snejko, Dr. M. Iglesias, Dr. B. Gómez-Lor, Prof. Dr. E. Gutiérrez-Puebla, Prof. Dr. M. A. Monge
Instituto de Ciencia de Materiales de Madrid
Cartoblanco, 20849-Madrid (Spain)
fax: (+34) 91-3720623
E-mail: amonge@icmm.csic.es

[**] F.G. and J.P. acknowledge their FPI fellowship from Spanish Ministry for Education and Science (MEC) co-funded by Fondo Social Europeo. This work was supported by the Spanish MCYT projects MAT 2007-02001, CTQ2007-02885/BQU, and CAM-CSIC 200580M133).

Supporting information for this article is available on the WWW under <http://www.angewandte.org> or from the author.

Communications

Table 17. Bond lengths [Å] and angles [°] of hydrogen bonds in YNDS and YbAQDS (in italics).¹⁶

D—H...A	<i>d</i> (D—H)	<i>d</i> (H...A)	<i>d</i> (D...A)	\angle (D—H...A)
O _{wp} —H...O (×2)	0.82	2.04	2.81	156
	0.85	1.94	2.77	167
O _{w2} —H...O (×2)	0.85	2.12	2.85	144
O _{w1} —H...O (×2)	0.98	2.00	2.939	163
	1.12	2.32	3.023	179
O _{tr} —H...O	0.98	2.14	3.032	151
	0.92	2.60	3.097	115

[a] The hydrogen bonds are between oxygen atoms from the ligand s...fonate ions and water molecules (O_w) or hydroxy groups (O_h) around the rare-earth ions in the inorganic layers. D=donor, A=acceptor.

b/2. From a crystallographic point of view, a direct relation exists between the brucite-derived hexagonal lattice of the LDHs and that of the new LRHs. Given that in the latter there are two independent well-ordered R atoms because of their asymmetric coordination environments, the ideal hexagonal superlattice would have an *a'* parameter twice that of the mineral (that is, *a'* = 2*a*). As the interatomic distances among R atoms are not uniform, this hexagonal superlattice has a distortion that gives rise to a larger orthorhombic cell. The lattice vectors of the LRH unit cell can be deduced from those of the LDH cell by applying the transformation matrix (2−2*0*, 00−1, 220), as shown in Figure 3.

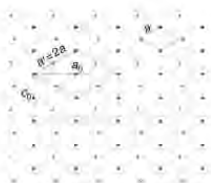


Figure 3. Crystallographic transformation from the ideal brucite-type structure to the new orthorhombic LRH structure. See text for details.

Thermogravimetric analysis and simultaneous differential thermal analysis (TGA-DTA) in an N₂ atmosphere (50 mL min⁻¹) and thermodiffraction X-ray experiments (vacuum) show that the NDS²⁻ compounds are stable up to 600 °C and the AQDS²⁻ compounds up to 500 °C. The IR spectra of these compounds show a broad band near 3500 cm⁻¹, with several maxima corresponding to the ν(M—OH) frequencies of the coordinated hydroxy groups and water molecules. The broadening of this band is due to the hydrogen bonding between these coordinated oxygen atoms and the sulfonate groups. The uncoordinated SO₃ group gives rise to unsplit bands in the region 1000–1100 cm⁻¹, which are consistent with the retention of C_{3v} symmetry.

Rare-earth metals are increasingly being used as catalysts in various organic transformations. These new materials offer the possibility of combining the catalytic properties of rare-earth atoms with the advantages of a solid catalyst. The

capability of the new LRH materials as heterogeneous catalysts has been tested on key processes in green chemistry.

1) In the hydrodesulfurization (HDS) of thiophene, YbAQDS shows a conversion of 50% in 26 h to yield hydrogen sulfide and butane (both components are easily separable) under 7 bar of H₂ at only 70 °C. It is worth pointing out that these results are obtained under much milder conditions than those usually used (high H₂ pressure (30–60 bar) at 350–400 °C^{15,23}). 2) As an alternative to hydrodesulfurization reactions, the removal of refractory sulfur-containing compounds can be accomplished by oxidation. This catalyst effects the oxidation of various alkyl phenyl sulfides. Sulfides were selectively mono-oxygenated to the corresponding sulfoxides (100%) in 30 min by using H₂O₂ as oxidant. The YbAQDS catalyst has a remarkably high turnover frequency (TOF) of 2000 h⁻¹¹⁶ which is due to the small quantity of catalyst (0.1%) needed and the fast conversion of the substrate. The results here are better, both in activity and in selectivity, than those previously obtained with a rare-earth succinate polymeric framework¹⁵. 3) The catalytic activity for the competitive epoxidation of 3,7-dimethylocta-1,6-dien-3-ol (linalool) using an excess of hydrogen peroxide was also tested. Linalool was oxidized to pyranoid and furanoid ethers (ratio 1:1) with >80% conversion over 24 h by using YNDS as a bifunctional redox-acid catalyst. The catalyst activity is comparable with that of both LnPF₆^{16,22} and microporous bifunctional titanium aluminosilicate.¹⁷ The sulfoxidation reaction proceeds through the corresponding peroxo species, as happens in the hydrolysis of phosphodiester¹⁸ and RNA¹⁹ when these are catalyzed by peroxide rare-earth complexes formed in rare-earth/H₂O₂ mixtures.

To verify that the observed process is a heterogeneous catalysis, the reactions were carried out under standard conditions. After about 30% conversion, the solid was removed by filtration whereupon the reactions stopped completely. The solid was then used again without any loss of performance. A powder X-ray diffraction pattern of the recovered catalysts showed no change in the structure of the catalyst.

In conclusion, LRHs have an ordered and tunable porous structure and combine advantages of LDH catalysts with the chemical and physical properties of rare-earth compounds. Although the full range of properties of these compounds have yet to be elucidated,^{10,23} their discovery should be of general interest.

Experimental Section

Synthesis and characterization: All reagents were purchased at high purity (AR) grade from Aldrich and used without further purification. R(NO₃)₃·6H₂O (R = Yb, Dy, Ho, Y) was used as the source of rare-earth cations; the sulfonic acids were used in their disodium salt forms. In a typical synthesis procedure, the initial mixture with molar composition R³⁺/A²⁻/H₂O = 4:1:4400 was adjusted to pH 6.5 with Et₃N (Et₃N/R³⁺ = 2.5). The mixture was stirred for about 20 min and sealed in a 46 mL teflon-lined stainless-steel bomb. The bomb was kept at 180 °C under autogenous pressure for 18 h. After the reaction mixture was cooled to room temperature, the product was removed by filtration and washed with deionized water and acetone. A grayish

white (Dy and Yb) or pink (Ho) powder was obtained for the AQDS²⁻ compounds, and a pale yellow powder for YNDS.

The IR spectra from KBr pellets were recorded in the range 4000–400 cm⁻¹ on a Perkin-Elmer spectrometer. TGA-DTA were performed with a SEIKO TG/DTA 320 apparatus between 25 and 700 °C in N₂ (flow rate of 50 mL min⁻¹) at a heating rate of 5 K min⁻¹.

X-ray structural analyses: Data for single crystals of the YbAQDS and YNDS compounds were collected on a Bruker SMART CCD diffractometer equipped with a normal focus, 2.4 kW sealed-tube X-ray source (MoK α radiation – 0.71073 Å). Data were collected over a hemisphere of the reciprocal space by a combination of three sets of exposures. Each exposure of 20 s covered 0.3° in ω . Unit-cell dimensions were determined by a least-squares fit of 60 reflections with $I > 2\sigma(I)$. The compounds crystallize in the orthorhombic system, space group *Ibam*, with $a = 12.5401(6)$, $b = 35.652(2)$, and $c = 7.0347(4)$ Å for YbAQDS, and $a = 12.639(1)$, $b = 30.525(2)$, and $c = 7.1348(6)$ Å for YNDS. The structures were solved by direct methods. The final cycles of refinement were carried out by full-matrix least-squares analyses with anisotropic thermal parameters for all non-hydrogen atoms. The hydrogen atoms of the hydroxy groups and water molecules were located in difference Fourier maps. Calculations were carried out by using the SMART program for data collection and data reduction, and SHELXTL. CCDC-604276 (YNDS) and CCDC-604277 (YbAQDS) contain the supplementary crystallographic data for this paper. These data can be obtained free of charge from The Cambridge Crystallographic Data Centre via www.ccdc.cam.ac.uk/data_request/cif.

The compounds reported herein are covered under the patent: F. Gándara, J. Perles, N. Snejko, M. Iglesias, B. Gómez-Lor, E. Gutiérrez-Puebla, M. A. Monge (ICMM, CSIC), ES20060422, 2006

Received: June 21, 2006

Revised: September 11, 2006

Published online: November 10, 2006

Keywords: heterogeneous catalysis · hydrogen bonds · intercalations · layered compounds · rare earths

- [1] a) G. R. Williams, T. G. Dunbar, A. J. Beer, A. M. Fogg, D. O'Hare, *J. Mater. Chem.* **2006**, *16*, 1222; b) G. R. Williams, T. G. Dunbar, A. J. Beer, A. M. Fogg, D. O'Hare, *J. Mater. Chem.* **2006**, *16*, 123.
- [2] H. Cai, A. C. Hillier, K. R. Franklin, C. C. Nunn, M. D. Ward, *Science* **1994**, *266*, 1555.
- [3] B. Sels, D. De Vos, M. Buntinx, F. Pierard, A. Kirsch-De Mesmaeker, P. Jacobs, *Nature* **1999**, *400*, 855.
- [4] B. F. Sels, D. E. De Vos, P. A. Jacobs, *Catal. Rev.* **2001**, *43*, 443.
- [5] *Handbook of Layered Materials*, Dekker, New York, **2004**.
- [6] V. Rives, *Layered Double Hydroxides: Present and Future*, Nova Science Publishers, New York, **2001**.
- [7] M. J. Climent, A. Corma, S. Iborra, J. Primo, *J. Catal.* **1995**, *151*, 60.
- [8] M. B. J. Roeffaers, B. F. Sels, H. Uji-i, P. C. De Schryver, P. A. Jacobs, D. E. De Vos, J. Hofkens, *Nature* **2006**, *439*, 572.
- [9] S. Gago, M. Pillingier, R. A. S. Ferreira, L. D. Carlos, T. M. Santos, I. S. Gonçalves, *Chem. Mater.* **2005**, *17*, 5803.
- [10] a) F. Kanazaki, S. Sugiyama, Y. Ishikawa, *J. Mater. Chem.* **1995**, *5*, 1969; b) W. K. Kuk, Y. D. Huh, *J. Mater. Chem.* **1997**, *7*, 1933.
- [11] L. Raki, J. J. Beaudoin, I. Mitchell, *Com. Concr. Res.* **2004**, *34*, 1717.
- [12] N. Snejko, C. Cascales, B. Gómez-Lor, E. Gutiérrez-Puebla, M. Iglesias, C. Ruiz-Valero, M. A. Monge, *Chem. Commun.* **2002**, 1366.
- [13] G. S. Thomas, P. V. Kamath, *J. Chem. Sci.* **2006**, *118*, 127.

- [14] K. R. Shatma, E. S. Olson in *Processing and Utilization of High-Sulfur Coals IV* (E. R. Dugan, D. R. Quigley, Y. A. Attia), Elsevier Science, Amsterdam, **1991**, p. 377.
- [15] T. Chapus, F. Moré, (Institut Français du Pétrole), US 2002195375, **2002**.
- [16] J. Perles, M. Iglesias, C. Ruiz-Valero, N. Snejko, *J. Mater. Chem.* **2004**, *14*, 2683.
- [17] A. Corma, M. Iglesias, E. Sánchez, *J. Chem. Soc. Chem. Commun.* **1995**, 1635.
- [18] Y. Mejía-Racillo, A. K. Yatsimirsky, *Inorg. Chim. Acta* **2002**, *328*, 241, and references therein.
- [19] J. Kamitani, J. Sumaoka, H. Asanuma, M. Koriyama, *J. Chem. Soc. Perkin Trans 2* **1998**, 523.
- [20] R. M. Jones, T. S. Bergstedt, D. W. McBranch, D. G. Whellan, *J. Am. Chem. Soc.* **2001**, *123*, 6726.
- [21] N. D. Hulson, S. A. Speakman, E. A. Payzant, *Chem. Mater.* **2004**, *16*, 135.
- [22] A. I. Khan, D. O'Hare, *J. Mater. Chem.* **2002**, *12*, 3191.
- [23] A. I. Khan, L. X. Lei, A. J. Norquist, D. O'Hare, *Chem. Commun.* **2001**, 2342.

Inorg. Chem. 2007, 46, 3475–3484

Inorganic Chemistry
Article

Rare Earth Arenedisulfonate Metal–Organic Frameworks: An Approach toward Polyhedral Diversity and Variety of Functional Compounds

Felipe Gándara, Alberto García-Cortés, Concepción Cascales, Berta Gómez-Lor, Enrique Gutiérrez-Puebla, Marta Iglesias, Angeles Monge,* and Natalia Snejko

Instituto de Ciencia de Materiales de Madrid, CSIC, Cantoblanco, E-28049 Madrid, Spain

Received September 18, 2006

Eight 2D and 3D metal–organic framework (MOF) rare earth naphthalenedisulfonates have been obtained. The different geometry of the naphthalenedisulfonic acids used as connectors [(1,5-NDS)] gives rise to the three new structure types. In $\text{Ln}(\text{OH})(1,5\text{-NDS})\cdot\text{H}_2\text{O}$, LnPF-1 (lanthanide polymeric framework; Ln = La, Nd, Pr, Sm and Eu), the lanthanide ion is octacoordinated. Its 3D structure is formed by $(\text{Ln}_2\text{O}_4)\text{-S-(Ln}_2\text{O}_4)$ infinite chains, connected through complete NDS connectors. LnPF-2 (Ln = Nd), with the same empirical formula as the former, and the lanthanide in octa- and nonacoordination, owns an arrangement of sulfonate bridges and neodymium polyhedra that gives rise to a 2D structure. $[\text{Ln}_2(2,6\text{-NDS})_2(\text{OH})_2(\text{H}_2\text{O})_2(\text{H}_2\text{O})_2]$, LnPF-3 (Ln = Nd, Eu), demonstrates that it is possible to obtain a 3D structure with (2,6-NDS), when a greater Ln/connector ratio is employed. It is worth pointing out the existence, in this latter family of compounds, of a $\mu^2\text{-OH}$ group, whose hydrogen atom is very close to one-sixth Ln atom (distance $\text{Ln}\cdots\text{H} = 2.09 \text{ \AA}$). The materials, with high thermal stability, act as active and selective bifunctional heterogeneous catalysts in oxidation of linalool yielding cyclic hydroxy ethers. The absence of any 3D Nd–Nd magnetic interaction is explained due to the inner nature of 4f orbitals of Nd^{3+} , which do not favor the magnetic exchange. The influence of the polymeric frame matrix results in a better photoluminescence efficiency for NdPF-1.

Introduction

Current efforts on hybrid metal–organic complexes are directed mostly toward synthesis of diverse frameworks using polycarboxylates^{1–4} and phosphonates.⁵ Many fewer studies are, however, dedicated to polymeric organo-inorganic sulfonates, in spite of the fact that the sulfonic group, being regarded typically as weakly coordinating,⁶ shows, in a

properly planned synthesis, a pronounced effect on the appropriately chosen metal center. The supramolecular chemistry of the sulfonate group in extended solids has been reviewed by Côté and Shimizu,⁷ and that of the metal arene sulfonates, by J. Cai.⁸ Structures of compounds of group I and 2 metal ions with 1,5-NDS are also found.⁹ Mix Ln-sulfonate–phosphonates¹⁰ and an interesting structural study on lanthanide–sulfoisophthalic coordination polymers¹¹

* Corresponding author. E-mail: amonge@icmm.csic.es.

- (1) (a) Perles, J.; Iglesias, M.; Martín Laguna, M. A.; Monge, M. A.; Ruiz-Valero, C.; Snejko, N. *Chem. Mater.* **2005**, *17*, 5837. (b) Gómez-Lor, B.; Gutiérrez-Puebla, E.; Iglesias, M.; Monge, A.; Ruiz-Valero, C.; Snejko, N. *Chem. Mater.* **2005**, *17*, 2568. (c) Monge, A.; Snejko, N.; Gutiérrez-Puebla, E.; Medina, M.; Ruiz-Valero, C.; Iglesias, M.; Gómez-Lor, B. *Chem. Commun.* **2005**, *10*, 1291.
- (2) (a) Tamaki, H.; Zhong, Z. J.; Matsumoto, N.; Kida, S.; Koitava, K.; Ashira, N.; Okawa, H. *J. Am. Chem. Soc.* **1992**, *114*, 6974. (b) Malhotra, C.; Nuttall, C. J.; Corling, S. G.; Day, P. *Inorg. Chem.* **1996**, *35*, 1201. (c) Deurtins, S.; Schmitz, H. W.; Schmeitwy, P.; Ensling, J.; Göttlich, P. *J. Am. Chem. Soc.* **1994**, *116*, 9521. (d) Andrés, R.; Brissard, M.; Gruselle, M.; Train, C.; Vaissermann, J.; Maleszeux, B. N.; Jamet, J. P.; Verduguer, M. *Inorg. Chem.* **2001**, *40*, 4633.
- (3) (a) Deakin, L.; Ariff, A. H.; Müller, J. S. *Inorg. Chem.* **1999**, *38*, 5072. (b) Lo, M. F. S.; Chui, S. Y. S.; Shek, L. Y.; Liu, Z.; Zhang, X. X.; Wang, G. H.; Williams, I. D. *J. Am. Chem. Soc.* **2000**, *122*, 6293.
- (4) Chui, S. Y. S.; Lo, S. M. F.; Charmant, J. P. H.; Orpen, A. G.; Williams, I. D. *Science* **1999**, *285*, 1148.

- (5) (a) Clearfield, A. *Prog. Inorg. Chem.* **1998**, *47*, 371. (b) Mallouk, T. E.; Garvin, J. A. *Acc. Chem. Res.* **1998**, *31*, 209. (c) Byrd, H.; Clearfield, A.; Pojary, D.; Reis, K. P.; Thompson, M. E. *Chem. Mater.* **1996**, *8*, 2239. (d) Vermeulen, L. A.; Snover, J. L.; Sapochak, L. S.; Thompson, M. E. *J. Am. Chem. Soc.* **1993**, *115*, 11767. (e) Kumar, C. V.; Chaudari, A. *Chem. Mater.* **2001**, *13*, 238. (f) Alberti, G.; Constantino, C.; Marmottani, F.; Vivan, R.; Zapelli, P. *Angew. Chem., Int. Ed. Engl.* **1993**, *32*, 1357. (g) Sun, Z. M.; Mao, J. G.; Sun, Y. Q. et al. *New J. Chem.* **2003**, *27*, 1326. (h) Rao, K. P.; Balraj, V.; Mimmeli, M. P. et al. *Inorg. Chem.* **2004**, *43*, 2094. (i) Maeda, K. *Microporous Mesoporous Mater.* **2004**, *73*(1–2), 47. (j) Song, S. Y.; Ma, J. F.; Yang, J. et al. *Inorg. Chem.* **2005**, *44*, 2140.
- (6) Lawrence, G. A. *Chem. Rev.* **1986**, *86*, 17.
- (7) Côté, A. P.; Shimizu, *Coord. Chem. Rev.* **2003**, *86*, 17.
- (8) Cai, J. *Coord. Chem. Rev.* **2004**, *248*, 1061 and references therein.
- (9) Cai, J. W.; Chen, C. H.; Liao, C. Z.; Feng, X. L.; Chen, X. M. *Acta Crystallogr., Sect. B* **2001**, *57*, 520.
- (10) Song, J.-J.; Lei, C.; Mao, J. G. *Inorg. Chem.* **2004**, *43*, 5630.

10.1021/c0617689 CCC: \$37.00 © 2007 American Chemical Society
Published on Web 04/04/2007

Inorganic Chemistry, Vol. 46, No. 9, 2007 3475

Table 1. Main Crystallographic Data for LnPF-1 Structure Type ($L = 1, 5$ -NDS) and for LnPF-2 and LnPF-3 Structure Type ($L = 2, 6$ -NDS)

Compounds	Nd ₂ (OH) ₂ (H ₂ O) ₂ (LnPF-1)	La ₂ (OH) ₂ (H ₂ O) ₂ (LnPF-1)	Eu ₂ (OH) ₂ (H ₂ O) ₂ (LnPF-1)	[Nd ₂ (OH) ₂ (H ₂ O) ₂] ₂ (LnPF-2)	[Nd ₂ (OH) ₂ (H ₂ O) ₂] ₂ (H ₂ O) ₂ (LnPF-3)	[Eu ₂ (OH) ₂ (H ₂ O) ₂] ₂ (H ₂ O) ₂ (LnPF-3)
empirical formula	C ₁₆ H ₁₆ NdO ₈ S ₂	C ₁₆ H ₁₆ LaO ₈ S ₂	C ₁₆ H ₁₆ EuO ₈ S ₂	C ₁₆ H ₁₆ Nd ₂ O ₁₂ S ₄	C ₁₆ H ₁₆ Nd ₂ O ₁₂ S ₄	C ₁₆ H ₁₆ Eu ₂ O ₁₂ S ₄
fw	465.53	460.20	473.25	1862.13	920.59	939.89
cryst syst	triclinic	triclinic	triclinic	monoclinic	monoclinic	monoclinic
space group	<i>P1</i>	<i>P1</i>	<i>P1</i>	<i>Cc</i>	<i>C2/c</i>	<i>C2/c</i>
<i>a</i> (Å)	5.6745(8)	5.7263(2)	5.6309(3)	19.510(1)	34.228(1)	33.933(1)
<i>b</i> (Å)	10.551(2)	10.6104(4)	10.5165(5)	10.559(8)	5.9374(7)	5.857(2)
<i>c</i> (Å)	11.450(2)	11.5533(5)	11.3974(5)	25.340(2)	24.332(3)	24.148(1)
α (deg)	76.156(2)	76.618(4)	76.320(1)	90	90	90
β (deg)	77.484(2)	77.619(1)	77.351(1)	98.448(1)	110.395(2)	110.237(1)
γ (deg)	88.034(2)	87.957(1)	88.063(1)	90	90	90
<i>Z</i>	2	2	2	4	8	8
<i>V</i> (Å ³)	650.5(2)	666.94(4)	639.74(5)	5163.9(7)	4634.9(9)	4563.1(3)
density	2.377	2.292	2.457	2.395	2.639	2.773
(calcd mg/m ³)						
abs coeff (mm ⁻¹)	4.349	3.552	5.266	4.383	5.880	7.251
<i>F</i> (000)	450	444	456	3600	3516	3576
cryst size (mm ³)	0.2 × 0.2 × 0.06	0.16 × 0.16 × 0.16	0.20 × 0.16 × 0.06	0.30 × 0.20 × 0.10	0.10 × 0.07 × 0.05	0.20 × 0.20 × 0.10
θ for data	3.75–30.98°	1.85–29.51°	1.88–26.37°	1.62–28.93°	1.27–29.07°	1.27–26.37°
collection						
index range	(8, 14, 16) (–8, –9, –14)	(7, 14, 15) (–7, –14, –15)	(7, 13, 14) (–6, –12, –14)	(25, 14, 34) (–26, –14, –33)	(45, 7, 32) (–44, –7, –33)	(42, 7, 30) (–40, –7, –30)
reflins collected	4574	7738	5030	22606	20084	16182
unique reflins	3420 [<i>R</i> _{int} = 0.057]	3375 [<i>R</i> _{int} = 0.039]	2407 [<i>R</i> _{int} = 0.027]	11619 [<i>R</i> _{int} = 0.047]	5744 (<i>R</i> _{int} = 0.0417)	4558 (<i>R</i> _{int} = 0.0604)
GOF on <i>F</i> ²	0.799	0.813	1.203	0.993	1.192	1.149
<i>R</i> indices	<i>R</i> ₁ = 0.05	<i>R</i> ₁ = 0.034	<i>R</i> ₁ = 0.049	<i>R</i> ₁ = 0.0406	<i>R</i> ₁ = 0.0546	<i>R</i> ₁ = 0.062
[<i>I</i> > 2 σ (<i>I</i>)]	w <i>R</i> ₂ = 0.12	w <i>R</i> ₂ = 0.071	w <i>R</i> ₂ = 0.13	w <i>R</i> ₂ = 0.0825	w <i>R</i> ₂ = 0.1203	w <i>R</i> ₂ = 0.100
<i>R</i> indices	<i>R</i> ₁ = 0.09	<i>R</i> ₁ = 0.044	<i>R</i> ₁ = 0.057	<i>R</i> ₁ = 0.0557	<i>R</i> ₁ = 0.0747	<i>R</i> ₁ = 0.091
(all data)	w <i>R</i> ₂ = 0.13	w <i>R</i> ₂ = 0.075	w <i>R</i> ₂ = 0.13	w <i>R</i> ₂ = 0.0866	w <i>R</i> ₂ = 0.1354	w <i>R</i> ₂ = 0.109
max diff peak and hole (e Å ⁻³)	2.27 and –1.87	1.25 and –1.16	2.472 and –2.73	2.743 and –1.229	1.669 and –2.941	1.239 and –1.457

have been recently reported. Of special interest are metal-organic frameworks constructed from carefully selected arenesulfonates and rare earth elements, surprisingly, there are only a couple of structural reports on disulfonate coordination compounds, with both sulfonate groups coordinated to the rare earth ions, one of them with mixed ligands,¹² and the other reported in a communication by our group.¹³ In our ongoing studies of arene-sulfonate groups^{14,15} as linkers in the search of multifunctional materials, we report here eight novel two- and three-dimensional Ln³⁺-organic frameworks belonging to three different structural types, in which the metal centers are coordinated to 1,5- and 2,6-naphthalenedisulfonate (NDS²⁻) ligands. Regarding the properties, the aim of this paper is to perform a comparative study of catalytic, magnetic, and optical characteristics for some representatives, and their relationship with the three structural types. This study can be understood as a starting point to tune the required properties with the structural features of new purely disulfonate MOFs, taking into account that these latter species are tailored through the used synthetic conditions.

Experimental Section

General Information. All reagents were purchased at high purity (AR grade) from Aldrich and used without further purification. The

- (11) Liu, Q.-Y.; Xu, L. *Eur. J. Inorg. Chem.* **2005**, 3458.
- (12) Deacon, G. B.; Giffels, A.; Zelesny, G.; Stellfeldt, D.; Meyer, G. Z. *Inorg. Alloys Chem.* **1999**, 623, 764.
- (13) Snejko, N.; Cascales, C.; Gómez-Lor, B.; Gutiérrez-Puebla, E.; Iglesias, M.; Ruiz-Valero, C.; Monge, M. A. *Chem. Commun.* **2002**, 1366.
- (14) Gándara, F.; Fortes-Revilla, C.; Snejko, N.; Gutiérrez-Puebla, E.; Iglesias, M.; Monge, M. A. *Inorg. Chem.*, in press.
- (15) Gándara, F.; Perles, P.; Snejko, N.; Iglesias, M.; Gómez-Lor, B.; Gutiérrez-Puebla, E.; Monge, M. A. *Angew. Chem., Int. Ed.*, in press.

IR spectra were recorded from KBr pellets in the range 4000–400 cm⁻¹ on a Perkin-Elmer spectrometer. Thermogravimetric and differential thermal analysis (TGA-DTA) were performed using a SEIKO TGA/DTA 320 apparatus in the temperature range between 25 and 700 °C in N₂ (flow of 50 mL/min) atmosphere and at a heating rate of 5 °C/min.

Synthesis. Ln(OH)(1,5-NDS)H₂O ($L = \text{La, Nd, Pr, Sm, Eu}$), **LnPF-1**, [1,5-NDS (1,5-naphthalenedisulfonate) and [Ln(2,6-NDS)₂(OH)₂(H₂O)₂](H₂O)₂] ($L = \text{Nd, Eu}$), **LnPF-3** (2,6-NDS = 2,6-naphthalenedisulfonate), were obtained by treating an aqueous solution containing a mixture of equimolar amounts of the corresponding Ln(NO₃)₃·6H₂O and Na₂(1,5-NDS) or Na₂(2,6-NDS) in 7 mL of water under hydrothermal reaction conditions (24 h, 170 °C). **LnPF-3** synthesis was repeated further (after knowing its composition) in a 5:3 Ln³⁺:Na₂(2,6-NDS) ratio, obtaining, as expected, the compound with a higher yield. The synthesis of Nd(OH)(2,6-NDS)H₂O (**LnPF-2**) was carried out by reaction of Nd(NO₃)₃·6H₂O, Na₂(2,6-NDS), and 4,4'-Ibpy or *trans*-1-(2-Py)-2-(4-Py) ethylene (0.82:1:1) in 8 mL of water under hydrothermal reaction conditions (36 h, 180 °C). The organic amines, not being found in the **LnPF-2** structure, play a role not only in creating the appropriate pH, but also in introducing a templating effect in the crystallization of this compound. The crystalline products were separated by suction filtration, washed with water, and dried in air, and their purity checked by X-ray powder diffraction by comparison with the simulated patterns on the basis of the single-crystal data.

X-ray Structure Determinations. A summary of the main crystal and refinement data for the three compounds is given in Table 1. Data for single crystals of **LnPF-1** ($L = \text{La, Nd, Eu}$), **LnPF-2** ($L = \text{Nd}$), and **LnPF-3** ($L = \text{Nd, Eu}$) were collected in a Bruker SMART CCD diffractometer equipped with a normal focus, 2.4 kW, sealed tube X-ray source (Mo K α radiation = 0.71073 Å). Data were collected over a hemisphere of the reciprocal space by a combination of three sets of exposures. Each exposure of 20 s covered 0.3° in ω . Unit cell dimensions were determined

Rare Earth Arenedisulfonate MOFs

by a least-squares fit of 60 reflections with $I > 2\sigma(I)$. The structures were solved by direct methods. Coordinated water molecules in LnPF-3 split into two very close positions; this small disorder is absorbed by the thermal parameter of their oxygen atoms. The final cycles of refinement were carried out by full-matrix least-squares analyses with anisotropic thermal parameters for all non-hydrogen atoms. Hydrogen atoms of the hydroxyl groups and water molecules were located in difference Fourier maps. Calculations were carried out with SMART software for data collection and data reduction and SHELXTL,¹⁶ CCDC reference numbers 182916, 182917, 298197, 298198, 298199, and 298200 contain the supplementary crystallographic data for this paper. These data can be obtained free of charge from the Cambridge Crystallographic Data Center, 12 Union Road Cambridge CB21EZ, U.K. Fax: (+44)-1223-336-033. E-mail: deposit@ccdc.cam.ac.uk.

Catalytic Experiments. Atmospheric pressure, 313 K, using acetonitrile as solvent (5 mL). A 0.01 mmol portion of the catalyst (previously homogenized by milling in an agate mortar) was stirred in a suspension containing the solvent and 1.0 mmol of the allylic alcohol. The oxidant (H₂O₂, 30%, 3 mmol) was added dropwise, while the overall suspension was heated up to 343 K. Samples were taken at regular times and analyzed by gas chromatography.

Physical Measurements. A Quantum Design XL-MPMS superconducting quantum interference device SQUID magnetometer operating in the temperature range 2–300 K at 1000 Oe was used to perform the magnetic susceptibility measurements for the three magnetic samples. Diamagnetic corrections were calculated with conventional values.¹⁷ The room-temperature (RT) photoluminescence (PL) spectra of Nd³⁺ in the three hosts LnPF-1, LnPF-2, and LnPF-3 were recorded by exciting the corresponding ⁴F_{3/2} + ²H_{9/2} multiplets (pump level in the four-level Nd-laser scheme) with a continuous wave Ti:sapphire laser, $\lambda_{exc} = 796.4$, 801.6, and 803 (±0.5 nm), respectively, and collecting the luminescence from ⁴F_{3/2} to ⁴I_{13/2} ($\lambda_{em} \approx 1.35 \mu\text{m}$), ⁴I_{11/2} ($\lambda_{em} \approx 1.06 \mu\text{m}$), and ⁴I_{9/2}. The emission was dispersed with a Spex spectrometer ($f = 34 \text{ cm}$), and the signal was recorded with a cooled Ge photodiode detector, using the lock-in amplifier technique. The PL was corrected, in each case, by the spectral response of the used equipment. Room-temperature optical absorption measurements were made in a Varian spectrophotometer model CARY 5E. Used samples were thin pellets of the stoichiometric Nd-compounds dispersed either on polyethylene or KBr. Further measurement details can be found elsewhere.¹³

Results and Discussion

LnPF-1. X-ray single crystal data and powder diffraction patterns showed that the five La, Nd, Pr, Sm, and Eu compounds own the same structure type. In Ln(OH)(1,5-NDS)H₂O (LnPF-1), the lanthanide ion is octacoordinated (Table 2, Figure 1) to two μ_2 -(OH) groups, one water molecule, and five oxygen atoms of different 1,5-NDS ligands in a LnO₈ triangulated dodecahedron (Figure 2). Every two of these (LnO₈) polyhedra share the (OH)–(OH) edge, giving rise to dimeric units, which are isolated in the *b* direction and joined through S atoms in the *a* direction. Connections along the *c* direction are made via whole 1,5-NDS ligands. Hence, the structure can be thought of as

Table 2. Coordination and Closest Metal–Metal Distances in LnPF-1, LnPF-2, and LnPF-3 Compounds

LnPF-1	La	Nd	Eu
Ln(1)–O(1)	2.602(5)	2.551(7)	2.498(9)
Ln(1)–O(2)	2.341(3)	2.324(7)	2.314(8)
Ln(1)–O(2)	2.379(4)	2.290(7)	2.258(9)
Ln(1)–O(4)	2.570(3)	2.519(6)	2.477(9)
Ln(1)–O(5)	2.508(3)	2.171(7)	2.414(7)
Ln(1)–O(6)	2.688(3)	2.498(6)	2.446(8)
Ln(1)–O(7)	2.630(3)	2.589(6)	2.546(7)
Ln(1)–O(8)	2.527(3)	2.460(6)	2.429(8)
Ln(1)–Ln(1)	3.883(5)	3.801(1)	3.744(1)

LnPF-2	Nd	LnPF-3	Nd	Eu
Ln(1)–O(2)	2.495(7)	Ln(1)–O(4)	2.429(8)	2.402(9)
Ln(1)–O(6)	2.477(7)	Ln(1)–O(5)	2.475(7)	2.364(1)
Ln(1)–O(14)	2.435(8)	Ln(1)–O(9)	2.415(6)	2.373(9)
Ln(1)–O(6)	2.473(7)	Ln(1)–O(10)	2.403(7)	2.373(8)
Ln(1)–O(19)	2.484(9)	Ln(1)–O(11)	2.68(2)	2.63(2)
Ln(1)–O(25)	2.506(7)	Ln(1)–O(12)	2.675(2)	2.473(7)
Ln(1)–O(26)	2.213(8)	Ln(1)–O(13)	2.399(5)	2.352(7)
Ln(1)–O(31)	2.629(8)	Ln(1)–O(14)	2.427(6)	2.382(7)
Ln(1)–Ln(2)	3.903(1)	Ln(1)–O(15)	2.645(1)	2.584(1)
Ln(2)–O(7)	2.497(7)	Ln(1)–Ln(2)	3.752(1)	3.6824(8)
Ln(2)–O(12)	2.538(7)	Ln(1)–Ln(3)	4.007(1)	3.8598(9)
Ln(2)–O(17)	2.563(8)	Ln(2)–O(1)	2.439(8)	2.386(9)
Ln(2)–O(20)	2.516(7)	Ln(2)–O(2)	2.415(8)	2.365(9)
Ln(2)–O(24)	2.464(7)	Ln(2)–O(7)	2.598(6)	2.570(7)
Ln(2)–O(25)	2.404(8)	Ln(2)–O(9)	2.417(6)	2.389(8)
Ln(2)–O(26)	2.388(6)	Ln(2)–O(10)	2.420(6)	2.384(7)
Ln(2)–O(28)	2.742(7)	Ln(2)–O(13)	2.440(6)	2.395(7)
Ln(2)–O(32)	2.630(8)	Ln(2)–O(14)	2.473(6)	2.383(8)
Ln(3)–O(5)	2.513(8)	Ln(2)–O(15)	2.688(1)	2.637(1)
Ln(3)–O(9)	2.496(7)	Ln(2)–O(17)	2.517(1)	2.494(1)
Ln(3)–O(11)	2.459(7)	Ln(2)–Ln(3)	4.038(1)	3.8912(9)
Ln(3)–O(21)	2.180(7)	Ln(3)–O(9)×2	2.470(6)	2.178(7)
Ln(3)–O(22)	2.453(7)	Ln(3)–O(10)×2	2.518(6)	2.411(7)
Ln(3)–O(27)	2.285(7)	Ln(3)–O(13)×2	2.589(6)	2.585(8)
Ln(3)–O(28)	2.453(7)	Ln(3)–O(14)×2	2.496(6)	2.460(7)
Ln(3)–O(30)	2.480(8)	Ln(3)–O(15)×1	2.77(2)	2.76(2)
Ln(3)–Ln(4)	3.876(1)	Ln(3)–H15 ^a	2.09	2.04
Ln(4)–O(3)	2.509(8)	Ln(3)–O(15) ^b	3.161(2)	3.09(2)
Ln(4)–O(4)	2.554(8)	O(15) ^b H15 ^a	1.07	1.05
Ln(4)–O(8)	2.550(9)			
Ln(4)–O(13)	2.436(7)			
Ln(4)–O(18)	2.453(8)			
Ln(4)–O(25)	2.870(7)			
Ln(4)–O(27)	2.337(7)			
Ln(4)–O(28)	2.438(7)			
Ln(4)–O(29)	2.638(9)			

^a Corresponds to the μ_2 -OH group.

formed by (Ln₂O₁₄) dimers that give rise to (Ln₂O₁₄)–S–(Ln₂O₁₄) infinite chains, kept together along the *c* direction through the complete NDS linker. There are two differently coordinated NDS anions, which are perpendicularly oriented along the [210] and the [210] directions. One of them coordinates to six distinct Ln atoms in a symmetric $\eta^3\mu^3-\eta^3\mu^3$ mode, whereas the other is bonded only to four lanthanide atoms in $\eta^2\mu^2-\eta^2\mu^2$ way.

LnPF-2. In Nd(OH)(2,6-NDS)H₂O, there are four crystallographically independent neodymium atoms per asymmetric unit. Two of them are octacoordinated to five oxygen atoms of different sulfonate groups, one μ_2 -OH, one μ_3 -OH, and one water molecule; the other two are nine-coordinated since they share other an extra μ_3 -OH (Table 2, Figure 1). In this way, the inorganic part of this framework is formed by two kinds of polyhedra, one of which is a NdO₈ triangulated dodecahedron similar to that of LnPF-1, and the

(16) Software for the SMART System V3.04 and SHELXTL V5.1; Bruker-Siemens Analytical X-ray Instrument Inc., Madison, WI, 1998.

(17) Boudreaux, E. A.; Mulry, L. N. *Theory and Applications of Molecular Paramagnetism*; Wiley: New York, 1976; p 494.

(18) Cascales, C.; Zaldo, C.; Suez Puche, R. *Chem Mater*. 2005, 17, 2052.

Rare Earth Arenedisulfonate MOFs

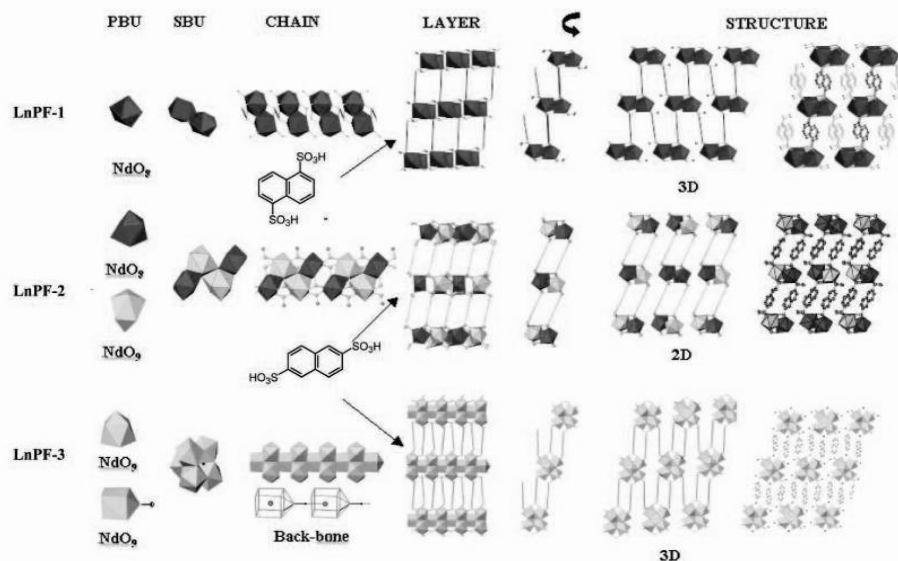


Figure 4. Comparative structural display for $\text{LnL}(\text{OH})(\text{H}_2\text{O})$ (LnPF-1), $\text{NdL}(\text{OH})(\text{H}_2\text{O})$ (LnPF-2), and $[\text{Ln}_2\text{L}_{1.5}(\text{OH})_{4.5}(\text{H}_2\text{O})_2](\text{H}_2\text{O})$ (LnPF-3)

Although all hydrogen atoms were located in Fourier synthesis, concerning that of the $\mu_5\text{-OH}$ group, whose electron density in the Fourier map could be masked by that of the five plus one surrounding Ln atoms, some extra verification was accomplished as follows. Since the only two possibilities to maintain the compound's electrical neutrality are either the oxygen belonging to one OH group, or its position being partially occupied (only one-half), refinements of the O15 with a population factor of 0.5 were performed. The results led to thermal parameters that were very low or even negative for this atom. This fact together with the synthesis media and the ability of lanthanide to coordinate μ_6 hydroxyl groups clearly confirms the formation of the $[\text{O}(15)\text{-H}]$ hydroxyl groups.

IR spectra of LnPF-1, LnPF-2, and LnPF-3 are very similar and indicate both ν_{as} and ν_{s} of the SO_3 groups found at 1240–1180 (ν_{as}) and 1100–1040 (ν_{s}) cm^{-1} , the aromatic C–H stretching mode being situated in the area of 3100–2860 cm^{-1} . The IR spectra of these compounds show additional bands at ca. 3600, 3500–3100, and 1530 cm^{-1} , which correspond to the hydroxy groups and water molecules, respectively.

TG-DTA analysis results for the thermal decomposition of LnPF-1, LnPF-2, and LnPF-3 reveal that their frameworks are stable up to 510 °C (LnPF-1 and LnPF-3) and 550 °C (LnPF-2); above these temperatures the frameworks decompose completely.

For LnPF-1, a weight loss occurs between 240 and 310 °C, accompanied by an endothermic effect corresponding to the loss of the coordinated water molecule per formula

unit (calculated, 1.9%; found, 2% for NdPF-1). For LnPF-2, the loss of the four water molecules (calculated, 5.69%; found, 5.92%) occurs between 240 and 500 °C. LnPF-3 loses the water molecules in two steps, the first from 90 to 230 °C followed by a second step (240–500°). The exceptional thermal stability is to be emphasized (in all cases more than 500 °C) for all MOF compounds.

Catalytic Properties. Linalool oxides are extensively found in nature and are mainly used in perfumery and as fragrances. In addition, they seem to have a strong biological significance in certain pollination systems acting as insect attractants.²² They are obtained usually by extraction from natural products, generally fruits or plants, or by transformation of linalool, but also numerous multistep organic syntheses of pyranoid and furanoid linalool oxides have been reported,²³ some of them highly stereoselective.²⁴ Oxidation of linalool to the corresponding cyclic hydroxy ethers has been achieved previously by some of us using microporous bifunctional titanium–aluminosilicates catalysts.²⁵ As the compounds here presented their own both redox and acid sites, the bifunctional character of these materials as catalysts for the transformation of linalool has been tested. The small size of the pore in these structures avoids the accessibility

(22) Berg-Karlson, A.-K.; Unelius, C. R.; Valterova, I.; Nilsson, L. A. *Phytochemistry* **1996**, *41*, 1477.

(23) Fournier-Nguéfac, Ch.; Lhoste, P.; Snou, D. *Tetrahedron* **1997**, *53*, 4353 and references therein.

(24) (a) Vidari, G.; Di Rosa, A.; Zanoni, G.; Bicchì, C. *Tetrahedron: Asymmetry* **1999**, *10*, 3547. (b) Vidari, G.; Di Rosa, A.; Castronovo, F.; Zanoni, G. *Tetrahedron: Asymmetry* **2000**, *11*, 981.

(25) Corra, A.; Iglesias, M.; Sánchez, F. *Chem. Commun.* **1995**, 1635.

Gándara et al.

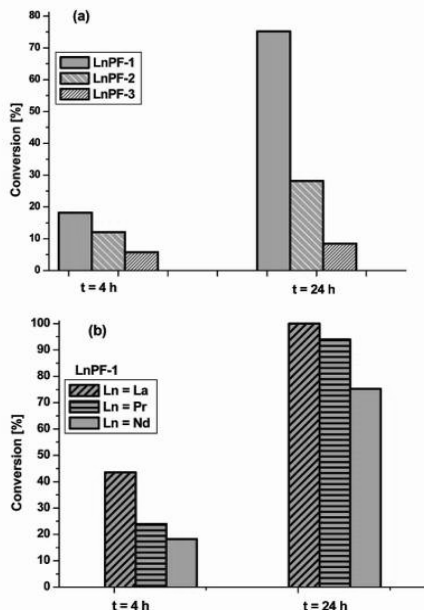
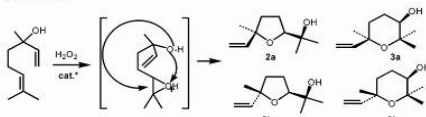


Figure 5. Catalytic oxidation of linalool: (a) activity of compounds LnPF-*n* (*n* = 1–3); (b) comparison of the catalytic activities in LnPF-1 materials (Ln = La, Pr, Nd).

Scheme 1



of the substrate to the metallic centers, the catalytic reactions thus taking place on the surface.

In a first stage, with the purpose of analyzing the coordination sphere influence in the catalyst behavior, only neodymium compounds were tested for the three families of compounds. Subsequently, to study the lanthanide influence in a same framework catalyst, LnPF-1 (Ln = Nd, La, and Pr) compounds were also comparatively tested, Figure 5.

Samples of LnPF-1 (Ln = La, Pr, Nd), LnPF-2, and LnPF-3 (Ln = Nd) were used as catalysts (0.021 mmol) for the transformation of linalool (330 mg, 2.1 mmol) by H₂O₂ (6.3 mmol) and MeCN (5 mL) in a glass reactor at 343 K. A series of blank experiments revealed that each component is essential for an effective catalytic reaction and the system is relatively unaffected by changing the order of mixing. The results show that catalysts LnPF-1 and LnPF-2 are active for the oxidation of linalool to hydroxy ethers (furanoid and pyranoid form) (2–3, Scheme 1), while LnPF-3 presents low

Table 3. Oxidation of Linalool with H₂O₂ Catalyzed by Different Nd–Sulfonates and Oxidation of Linalool with H₂O₂ Catalyzed by LnPF-1

Catalyzed by Different Nd–Sulfonates				
catalyst	conv (%) (h)	furans 2	pyrans 3	2/3
LnPF-1	76 (24)	52	23	2.3
LnPF-2	51 (48)	34.6	16.8	2.0
LnPF-3	17 (48)	11.5	5.2	2.2
Catalyzed by LnPF-1				
catalyst	conv (%) (h)	furans 2	pyrans 3	2/3
LnPF-1Nd	76 (24)	52	23	2.3
LnPF-1Pr	94 (22)	64.0	30.0	2.1
LnPF-1La	100 (22)	64.3	35.7	1.8

activity. All the catalysts are very selective, and no other reaction products were detected.

Looking at the results showed in Table 3, the following should be considered: (i) The 2:3 ratios found in all cases show that all materials behave similarly, indicating that they are produced by parallel reactions, through a common intermediate, and not by an isomerization process. It seems, thus, quite plausible that the process involves first the epoxidation at the metal site of the 2,3 double bond followed by the intramolecular opening of the epoxide ring by the hydroxy group at positions 6 or 7, the latter reaction being catalyzed by the acid sites. (ii) The LnPF-1 catalytic activity is the highest, followed by LnPF-2, with that of LnPF-3 being much lower. From the structural point of view, this behavior is directly related with the neodymium coordination number in each compound. This being 8 in LnPF-1, 8 and 9 in LnPF-2, and 9 in LnPF-3 gives rise to three different arrays involving the lanthanides, in their respective structures. The NdO₉ coordination in LnPF-3 makes it difficult to reach a higher coordination number during the catalytic reaction and explains its low activity. LnPF-1 and LnPF-2 exhibit 3D and 2D related structures, respectively. Although at first sight the 2D structure of LnPF-2 seems to be a better candidate, the fact of having one-half of the neodymium atoms nonacoordinated decreases its coordinative capability and, thus, the catalytic response. LnPF-1 having all Nd atoms octacoordinated offers the possibility of higher coordination during the catalytic process in all the active centers and drives the best results. (iii) Table 3 shows the results for Nd, Pr, and La compounds having the LnPF-1 structure type. In spite of the lack of porosity of this structure type, with, thus, the catalytic reaction being on surface, the activity of this family of catalysts is similar to that obtained when Ti-MCM-41 (yield: 80%) or Ti-Beta (yield: 73.4%) was used as catalyst.²⁶ The 2/3 ratios obtained using these catalysts (2.3–1.8) are much lower than the values obtained by the chemical routes described²⁷ (up to 9.0). The ratio values obtained with our catalyst are closer to that obtained when using epoxidase as catalyst²⁸ (~1).

As expected, the lanthanide size influence is quite clear, with the best catalyst being the lanthanum compound,

- (26) Schofield, L. J.; Kerton, O. J.; McMorn, P.; Bethell, D.; Ellwood, S.; Hutchings, G. J. *J. Chem. Soc., Perkin Trans.* **2002**, 2, 1475–1481.
 (27) Jpn. Kokai Tokkio Koho 59225176, 1984.
 (28) di Stefano, R. *Bull. de L.O.I.V.* **1991**, 721.

Rare Earth Arenedisulfonate MOFs

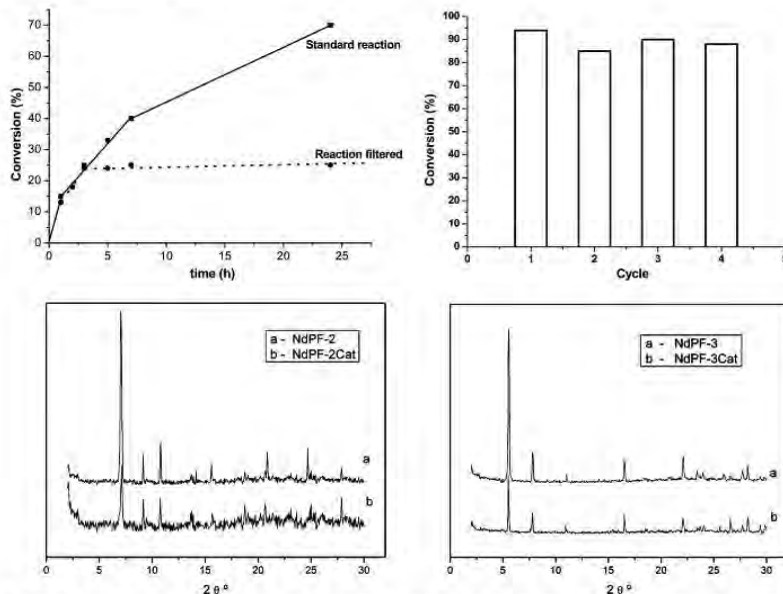


Figure 6. Top: Effect of removing the solid catalyst from the reaction (left) and recycling experiments for catalyst LnPF-IPr (right). Bottom: Catalysts XRPD patterns before and after use.

followed by those of praseodymium and neodymium, corresponding to the decreasing value of their radii.

Separation, Recycling, and Catalyst Reuse. The major advantage of the use of heterogeneous catalysts is the ease with which they can be recovered from the reaction mixtures by simple filtration and reused.

The heterogeneous oxidation of linalool has been carried out until completeness. The five LnPF catalysts were filtered and washed, and then fresh substrate and solvent were added without further addition of catalyst, for four consecutive experiments, and both yield and activity were retained. In order to check the stability of the catalysts, we have characterized the solid before and after reaction (Figure 6). Although extensive studies have been carried out to elucidate the true catalytic species in the heterogeneous metal-catalyzed reaction, it is still unclear in many cases whether the reaction takes place on the surfaces of the solid catalyst or whether the active catalysts are M species solved out from the solid, which simply acts as a reservoir of metal. Taking this into account, it is mandatory to find out if some complex has passed into the solution. To do this, we have investigated the residual activity of the supernatant solution after separation of the catalyst. The potential leaching was studied as follows: the organic phase of a first run was separated from the solid (catalyst). New reagents were added to the clear filtrate, and the composition of the reaction mixture was determined by GC. This homogeneous reaction mixture was

treated as a standard catalytic experiment. After 5 h, the composition was determined, and no reaction was observed, which excludes the presence of active species in solution.

Moreover, to rule out the contribution of homogeneous catalysis in the results shown in Table 3, one reaction was carried out in the presence of the solid until the conversion was $\sim 20\%$, and at that point, the solid was filtered off at the reaction temperature. The liquid phase was transferred to another flask and again allowed to react, but no further significant conversion was observed (Figure 6, 23% after 24 h).²⁹

An important point concerning the use of heterogeneous catalysts is its lifetime, particularly for industrial and pharmaceutical applications. After separation and washing, the heterogeneous catalysts were used several times for the same reaction under the same conditions as for the initial run of the catalyst. We usually see an increase of activity after the first run, followed by a slight decrease of the rate due to the small amount of catalyst lost by manipulation (Figure 6).

Magnetic Susceptibility Measurements. Figure 7 shows the plots of temperature dependence of the reciprocal molar magnetic susceptibility χ_m per Nd^{3+} mol in each LnPF formula for the three Nd materials. It can be observed that these magnetic susceptibilities present Curie–Weiss behavior

(29) Lempers, H. E. B.; Sheldon, R. A. *J. Catal.* **1998**, *175*, 62.

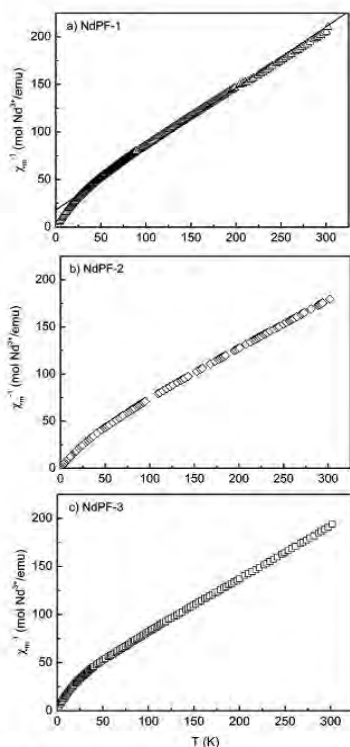


Figure 7. Plots of the reciprocal molar susceptibility (per Nd^{3+} mol) in corresponding NdPF as a function of temperature.

in a wide range of temperature, approximately above 40, 50, and 4–325 K, with expressions $\chi_m^{-1} = 18.1(6) + 0.642(4) \cdot T \text{ mol emu}^{-1}$ ($r = 0.997$), $12.2(7) + 0.571(4) \cdot T \text{ mol emu}^{-1}$ ($r = 0.997$), and $18.9(6) + 0.593(4) \cdot T \text{ mol emu}^{-1}$ ($r = 0.997$), for NdPF-1, NdPF-2, and NdPF-3, respectively. Effective paramagnetic moments were determined to be 3.6, 3.8, and 3.7 μ_B , values which are very close to the expected value, 3.62 μ_B , for the Nd^{3+} free ion and comparable to the values commonly found in Nd compounds for which no magnetic interactions among cations exist. Therefore, observed downward deviations from the Curie–Weiss law below the indicated temperatures reflect only the splitting of the $^4I_{9/2}$ Nd^{3+} ground state under the influence of the crystal field (CF) in each case, and the Weiss constants $\theta = -28$, -21 , and -32 K for NdPF-1, NdPF-2, and NdPF-3, respectively, are thus entirely due to CF effects.³⁰ Despite the existence of Nd-SBU giving rise to structural associations

(30) Colón, C.; Medina, A.; Alonso, F.; Saez Puche, R.; Volkov, V.; Cascales, C.; Zaldo, C. *Chem. Mater.* **2005**, *17*, 6635.

Gándara et al.

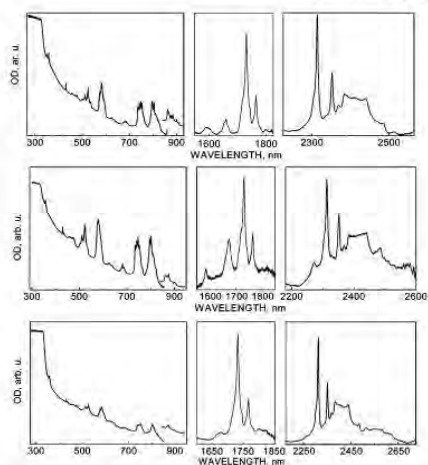


Figure 8. Room-temperature optical absorption spectra for NdPF-1 (top), NdPF-2 (middle), and NdPF-3 (bottom).

where Nd cations are at relatively short distances, the lack of observed three-dimensional Nd–Nd magnetic interaction is explained to be due to the behavior derived from the inner nature of 4f orbitals of Nd^{3+} , which do not favor the magnetic exchange, contrary to the observed situation in other lanthanide-containing structures including 3d cations, too.^{21,31}

Optical Properties. Scarce research on the luminescent properties of rare earth purely sulfonate MOFs has been carried out to date,¹³ although some study on mixed R-sulfonate–phosphonates has been conducted recently.¹⁰ Focusing on optical applications and taking into account that polymer materials doped with rare earths are subjected to growing interest as low-cost alternatives to purely inorganic-based ones, mainly in optoelectronic devices as optical waveguides and optical waveguide amplifiers,³² we are now attempting to give a general overview of room-temperature optical absorption and photoluminescence behavior of new rare earth coordination complexes.

Collected room-temperature optical absorption spectra of the three NdPF species consist of $^{2S+1}L_J \text{ Nd}^{3+}$ multiplets ranging typically from ~ 2600 to 347 nm ($^4I_{13/2}$ up to $^4D_{1/2} + ^3I_{1/2}$). The ultraviolet UV absorption edges, obtained from a linear extrapolation of the stepping absorption, are $\lambda_{\text{th}} = 338$, 344, and 343 nm for NdPF-1, NdPF-2, and NdPF-3,

(31) (a) Cascales, C.; Bucio, L.; Gutiérrez-Puebla, E.; Rasines, I.; Fernández Díaz, M. I. *Phys. Rev. B* **1998**, *57*, 5240. (b) Cascales, C.; Gutiérrez-Puebla, E.; Klimin, S.; Lebeck, B.; Monge, M. A.; Popova, M. N. *Chem. Mater.* **1999**, *11*, 2520. (c) Cascales, C.; Fernández Díaz, M. T.; Monge, M. A. *Chem. Mater.* **2000**, *12*, 3369. (d) Cascales, C.; Monge, M. A.; Fernández Díaz, M. T.; Bucio, L. *Chem. Mater.* **2002**, *14*, 1995. (e) Saez Puche, R.; Climent, E.; Romero de Paz, J.; Martínez, J. L.; Monge, M. A.; Cascales, C. *Phys. Rev. B* **2005**, *71*, 024403. (32) Slooff, L. H.; van Blaaderen, A.; Polman, A.; Hebbink, G. A.; Klink, S. I.; Van Veggel, F. C. J. M.; Reinhoudt, D. N.; Hofstra, J. W. J. *Appl. Phys.* **2002**, *91* (7), 3955.

Rare Earth Arenedisulfonate MOFs

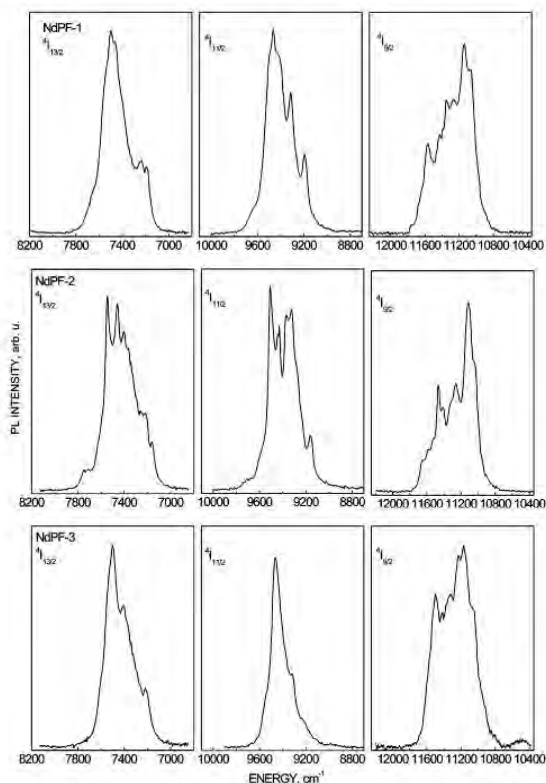


Figure 9. Room-temperature emission spectra from ${}^4F_{3/2}$ for NdPF-1, NdPF-2, and NdPF-3.

respectively, see Figure 8. Expected transitions, with origin in the Nd^{3+} ground state multiplet ${}^4I_{0,2}$, are clearly seen in these spectra. The transition from the lowest Stark component of ${}^4I_{0,2}$ to ${}^2P_{1/2}$, which can be used as an Nd^{3+} point site probe since it appears as a single peak for every independent Nd^{3+} crystal site in the current symmetries, presents the expected number of individual lines, 1, 4, and 3, for the above NdPF-1, NdPF-2, and NdPF-3 hosts. Positions of the most intense peak are significantly different, 23274, 23302, and 23254 cm^{-1} , respectively, which provide evidence for a clear nephelauxetic effect, and for the two Nd^{3+} -multicenter structures the difference between extreme high and low ${}^2P_{1/2}$ energies is from 312 cm^{-1} in PF-2 to 250 cm^{-1} in PF-3. The above higher ${}^2P_{1/2}$ separation value for PF-2 perfectly correlates with its observed wider distribution of Nd–O distances in the four coordination polyhedra, containing the shorter 2.243(8) and the larger 2.870(7) ones, thus yielding the more differentiated crystal field (CF) effects for this host. On the contrary, NdO_9 polyhedra in PF-3 are far more

regular, and also similar among them, and consequently, their CF will be lesser different and somewhat smaller.³³

Figure 9 gives the room-temperature PL spectra corresponding to ${}^4F_{3/2} \rightarrow {}^4I_{13/2}$, ${}^4I_{11/2}$, and ${}^4I_{9/2}$ transitions for the three Nd stoichiometric materials. Differences in these spectra arise from the particular distribution of emitting and final Stark energy levels of Nd^{3+} in every PF host. Because at room temperature photoluminescence from the two ${}^4F_{3/2}$ energy levels of each Nd^{3+} emitting center is expected, observed transitions to ${}^4I_{13/2}$, ${}^4I_{11/2}$, and ${}^4I_{9/2}$ consist of the corresponding overlapped bands, and no conclusions on the position and number of their energy levels can be extracted. Anyway, the above multiplets are split in all cases to the maximum number of crystal field levels, $2(J + 1/2)$, by the low symmetry of Nd^{3+} centers in these PF hosts. Although the inherent uncertainty of optical measurements using

(33) Cascales, C.; Zaldo, C.; Sáez Puche, R. *Chem. Mater.* **2005**, *17*, 2052.

polycrystalline powders was considered, in order to compare their relative emission intensities the same weights of each sample were used in the prepared pellet, with the same pump laser power maintained during all experiments. The results indicate a better luminescence performance for Nd in PF-1 and PF-2 with regards to Nd in PF-3. Taking into account that from the corresponding crystallographic data the Nd^{3+} content per volume of PF unit cell can be calculated as 3.07×10^{-23} , 3.10×10^{-23} , and $4.32 \times 10^{-23} \text{ \AA}^{-3}$ for Nd stoichiometric PF-1, PF-2, and PF-3, respectively, it can be derived that nonradiative energy transfer losses can be greater in PF-3 for its highest Nd^{3+} concentration. Furthermore, along with the large amount of Nd^{3+} centers, the Nd backbone structural feature of PF-3, with the shortest 3.752(7) distance between Nd–Nd pairs, is also contributing to higher losses by cooperative excitation effects in the Nd simulated emission process and some fluorescence lifetime reduction of the ${}^4\text{F}_{3/2}$ multiplet.

Conclusions

In summary, three families of multifunctional materials have been synthesized on the basis of different kinds of rare earth coordination polyhedra. The different geometry of the naphthalenedisulfonic acids used as linker [(1,5-NDS) and (2,6-NDS)] gives rise to the three new structure types. LnPF-1 and LnPF-2 (constitutional isomers, but with 3D and 2D structures, respectively) are the consequence of the sulfonate groups in different position in the NDS linker. LnPF-3 provide evidence that getting a 3D structure with 2,6-NDS is only possible with a greater Ln/linker ratio. It is

Gandara et al.

worth pointing out the existence, in this latter family of compounds, of a $\mu^3\text{-OH}^-$ group, whose hydrogen atom is very close to one of the five coordinated Ln atoms (distance $\text{Ln}\cdots\text{H} = 2.09 \text{ \AA}$).

These materials, with high thermal stability, act as active and selective bifunctional heterogeneous catalysts in oxidation of limonol yielding cyclic hydroxy ethers. Their activity depends more on the number of active centers with possibility of increasing the coordination number during the catalytic reaction, than on other structural effects, and, obviously, for the same structure type, on the rare earth size.

The absence of any three-dimensional Nd–Nd magnetic interaction is explained due to the inner nature of 4f orbitals of Nd^{3+} , which do not favor the magnetic exchange.

The influence of the PF matrix results in a better photoluminescence (PL) efficiency for NdPF-1 , which moreover could be improved by exploring ways to reduce the PL quenching. This can be likely achieved by decreasing the Nd^{3+} concentration in the material, for instance, through the preparation, currently in progress, of mixed La/Nd compositions, since thus Nd–Nd interactions should lessen.

Acknowledgment. This work has been supported by the Spanish MCIT project MAT 2004-2001 and CTQ2004-02865/BQU, Consolider-ingenio 2010 CST2006-0015.

Supporting Information Available: Crystallographic information (CIF). This material is available free of charge via the internet at <http://pubs.acs.org>.

IC0617689

A Rare-Earth MOF Series: Fascinating Structure, Efficient Light Emitters, and Promising Catalysts

F. Gándara,[†] A. de Andrés,[‡] B. Gómez-Lor,[‡] E. Gutiérrez-Puebla,[‡] M. Iglesias,[‡]
M. A. Monge,^{*,§} D. M. Proserpio,[‡] and N. Snejko[‡]

Instituto de Ciencia de Materiales de Madrid, Consejo Superior de Investigaciones Científicas, Madrid, Spain, and Departamento di Chimica Strutturale e Stereochimica Inorganica, Università di Milano, Milano, Italy.

Received August 22, 2007; Revised Manuscript Received November 16, 2007

ABSTRACT: A new family of rare-earth polymeric framework RPF-4 has been obtained and its structure solved from an intrinsically triple twinned crystal. The framework formed by a H—O bond free rare-earth matrix, with the Ln atoms separated in two directions, makes them very promising materials for light-emitting diodes. The properties of the materials as heterogeneous catalysts are reported, too. IR spectroscopy suggests the presence of a peroxo complex that acts as active species in the oxidation reaction.

The research area of metal-organic frameworks (MOFs) has experienced a drastic development during the past decade.¹ Up to the moment, transition-metal-based MOFs are the most studied, and the chemistry of rare-earth (Ln) based MOFs is significantly less explored, probably because lanthanide elements are usually regarded as unsuitable metal centers, whose coordination numbers are too high and coordination geometries are hard to control. However, the situation has been changing over the past few years because of the fact that Ln-based MOFs present a number of interesting opportunities with respect to their intriguing topologies and many scientific and industrial uses. Moreover, high and variable coordination numbers of Ln ions result in their important applications as catalysts for organic transformations.

The interesting optical properties of some Ln cations (Eu, Tb) are very well-known.² However, the extinction effects, which are due to high concentration of active cations in most Ln-based solid compounds,³ have forced preparation of their nonactive cations analogues, like Yttrium, doped with active Ln cations. Another factor with negative influence on the rare-earth compound emission is the presence of O—H bonds in the matrix. To study the luminescence properties of these materials for future applications in optical devices, it is important to obtain water- and OH-free frameworks, in which long linkers provide enough separations between rare-earth cations.

In MOF materials, functionality is introduced from cooperative influence of both inorganic species and organic linker molecules. This paper deals with the self-assembly of the lanthanide series with the 4,4'-(hexafluoroisopropylidene)bis(benzoic acid) ligand (H₂hfpbb). We chose hfpbb as a long hydrophobic linker. This flexible molecule has proven to be able to establish a bridge between different metal centers,⁴ in fact, in our group, two novel frameworks have been obtained that are constructed from Zn or Ln and hfpbb.⁵ In these frameworks, the composition and shape of the intermediate part of the flexible hfpbb linker play an essential role in forming 3D and 2D polymeric structures of corresponding Zn- and Ln-MOFs. As a sequel, we present herein a series of novel lanthanide MOFs, whose synthesis, structure and optical and catalytic properties are reported in this communication.

The hydrothermal reaction of Ln(III) (Ln = Y, La, Ce, Pr, Nd, Sm, Eu, Gd, Tb, Dy, Ho, Er, Yb) salt with H₂ hfpbb in a mixture of solvents leads to the formation of different colored crystalline powders depending on the metal used. The TGA/DTA experiments of the materials reveal that they are thermally stable: the framework

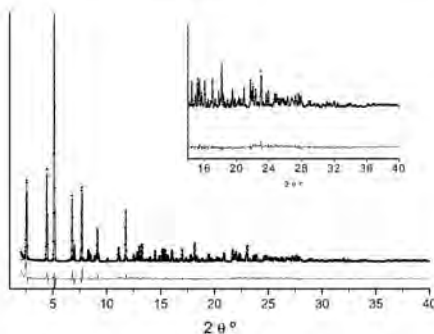


Figure 1. Rietveld refinement of the La-RPF-4 structure showing experimental (dot), simulated (line), and difference patterns.

is stable up to ~470 °C. A sharp endothermic loss between 490 and 550 °C corresponds to the total decomposition of the structure.

Only small twinned crystals were obtained for lanthanum compound. The unit cells found for them were hexagonal, either the one observed for the previously reported^{5(a)} Zn compound ($a = b = 21.32$ Å, $c = 7.71$ Å; $V = 3009.4$ Å³) or another with double a and b and quadruple volume. Only after carefully analysis of the data could we deduce the matrix to obtain the final orthorhombic cell that gave us the solution. The structure could then be solved in the space group $Pnma$ ($a = 7.79$ Å, $b = 21.37$ Å, $c = 37.00$ Å; $V = 6160.2$ Å³). Subsequently, the presence of three orthorhombic components in the twinned crystal was confirmed and refined to a composition of 47:29:24 (%). The structure solution was also confirmed with the Rietveld refinement of the X-ray synchrotron data (Figure 1).

Upon determining the crystal structure, the composition was found to be $[La_2(C_{12}H_4F_6O_4)_3]$ (1). Powder diffraction patterns show that the compounds for all rare-earth elements are isostructural (see the Supporting Information). The asymmetric unit comprises one-half of the formula. The Ln ion is nine-coordinated to three different ligand anions. The hfpbb linker coordinates to four Ln ions in a $\eta^4\mu^2$ way. For 1, the La—O distances lie in the range 2.44 Å–2.77 Å. Chains of Ln atoms are formed along the a axis via the μ_2 oxygen atoms (Figure 2, bottom left).

The anion links these chains giving rise to a 3D channelled structure with three parallel tunnels along the a axis: two square-

* To whom correspondence should be addressed. E-mail: amonge@icmm.csic.es.

[†] Consejo Superior de Investigaciones Científicas.

[‡] Università di Milano.

Communications

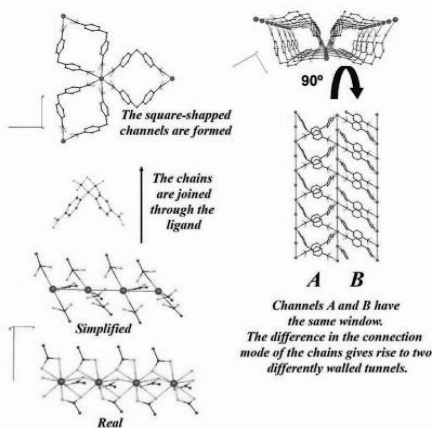


Figure 2. Ln chains and views of the two kinds of square-shaped tunnels.

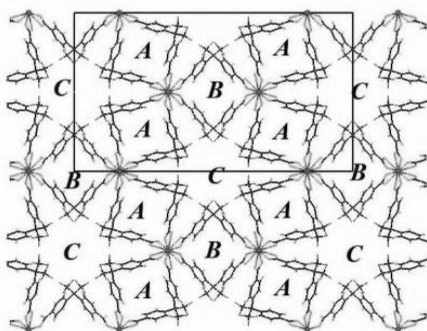


Figure 3. View of the structure along the *a* direction, with the different channels presented.

shaped (A, B) and one hexagonal (C) (Figure 3). All three channels are empty and have a free void cylindrical space with a window of diameters 5.2–5.5 Å, as computed by Platon⁶ (cavity routine). The different distribution of the A and B channels breaks the hexagonal symmetry and probably explains the preference for triple twins. Because of the bent geometry of the ligand, its central atom being a sp^3 carbon, the fluorine atoms are all pointing into the C hexagonal channels. Consequently, the walls of the hexagonal tunnel are formed by CF groups, giving rise to hydrophobic fluoro-lined Teflon-like channels.

Although the structure looks quite similar to that of the zinc compound,^{5a} they have a different topology. The network of the Zn compound is uninodal 4-connected (short symbol $\{6^2.8\}$), whereas in the La compound, the net is uninodal 5-connected. Each node/La ion is directly connected to two other La ions of the same chain via bridging carboxylate oxygen atoms of the ligand, and to three other La ions from different chains via the whole ligand as linkers.

Crystal Growth & Design, Vol. 8, No. 2, 2008 379

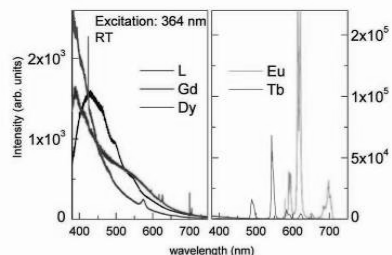


Figure 4. Emission spectra in the visible region (*L* = hfipbb).

Table 1. Methyl-Phenyl Sulfide Oxidation with H_2O_2 Using RPF-4 As Catalysts

rare earth	<i>t</i> (min)	conv. (%)	% sel. sulfoxide	TOF (h^{-1})
Yb	180	92	30	60
Er	300	85	52	32
Gd	300	82	60	48
Sm	300	78	72	22
Nd	300	80	70	20
La	300	80	75	18

The result is a net with Schläfli symbol $\{4^2.6^8\}$ (this net has been recently found in a search for net relations^{7a} and named **hxgd-5-Imma**;^{7b} topological analysis was performed using TOPOS.⁸

In contrast to what happened for the Zn compound, where all the metallic chains are connected through the ligand anions in a crossing way, in the Ln compounds, these connections are established in two different manners: two of them crossing (for the channels of A-type), and one parallel (for the channels of B-type) (Figure 2, right).

We give now a general overview of the room-temperature luminescence behavior of the new Ln materials. Under UV excitation at 364 nm, the pure hfipbb ligand presents a bluish-white emission with the band peaking around 450 nm. The emission corresponding to the different materials either present an emission similar to the ligand (Figure 4, left panel), slightly modified depending on the rare earth, or an intense emission (note the change of y-scale in right panel) of narrow lines due to crystal field transitions of the rare earth. In the second case, the broad white emission almost disappears, indicating that either the incoming light is mainly absorbed by the Ln or that the absorbed energy by the ligand is transferred to the Ln ions, which relax radiatively. It is noticeable the very intense observed emission. In fact, the integrated intensity in the whole visible range of the Eu compound emission is on the same order as compared to that corresponding to a standard red luminescent material ($Y_2O_3:Eu$). Therefore, Eu compound is a very promising material for red light emitting diodes. Tb compound is also a very efficient green luminescent material, whereas Gd can be used as white emitter. The peculiarities of the structure of the materials may avoid the concentration quenching of the luminescence: Ln ions form well-separated chains along the *a* axis with interchain distances around 12.5 Å. The Ho compound (not shown) shows another mechanism: the white emission presents inverted peaks indicating that emitted photons are absorbed by Ho 4f electrons. Deeper optical studies are to be carried out to understand the different mechanisms for the observed behaviors in order to increase the luminescence efficiency and to obtain a blue luminescent compound.

Another dimension in exploring the obtained materials properties lies in the area of heterogeneous catalysis. Generally, Ln compounds are increasingly being used as catalysts in various organic transformations. The new materials obtained offer a possibility of combining the catalytic properties of rare-earth ions with the

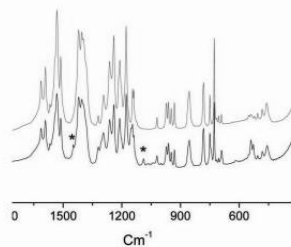


Figure 5. IR spectra of the catalyst before (blue) and after (black) being activated.

advantages of a heterogeneous catalyst. Their capability as redox catalysts has been tested in the reaction of oxidation of sulfides. The methyl phenyl sulfide was oxidized by H_2O_2 , in presence of the catalyst, to sulfoxide or sulfone. Differences both in reactivity and selectivity are observed. Table 1 shows that the activity increases in the series from lanthanum to ytterbium, whereas the selectivity goes in the opposite direction.

To start the reaction, an activation period is needed (see experimental details), which indicates that the active intermediate species are formed during this period. From a reaction mechanism viewpoint, the sulfoxidation reaction has to go through the corresponding peroxo species, as it happens in the hydrolysis of phosphodiester⁹ and RNA,¹⁰ catalyzed by peroxide Ln complexes formed in Ln– H_2O_2 mixtures. A comparison of the IR spectra of the catalysts before and after the activation period (Figure 5) reveals the appearance of new bands at 1090 and 1448 cm^{-1} , which could be assigned to the new Ln–O bond in these active peroxide species. Further experiments are needed for a more accurate identification of this intermediate specie.

In summary, by using hfpbb acid as ligand, a new family of rare-earth polymeric framework (RPF) has been obtained with the following features: (i) Their crystals are intrinsically triple twinned; the topological study explains the breaking of the hexagonal symmetry and likely the cause of the twin. (ii) The framework formed by a H–O bond-free Ln matrix, with the Ln atoms separated in two directions, gives rise to efficient different color emission, which makes them very promising materials for light-emitting diodes. (iii) The capability of the obtained materials as heterogeneous catalysts has been proved in oxidation of sulfides reactions. During the catalytic tests, the intermediate active specie could be identified.

Acknowledgment. F.G. acknowledges a FPI fellowship from Ministerio de Educación y Ciencia (MEC) and Fondo Social

Europeo from the EU. This work has been supported by the Spanish MCYT Project Mat 2004-2001 and Consolider-Ingenio CSD2006-0015. The authors also acknowledge to MEC, CSIC, and the staff of the Spline (BM25, ESRF) for support and assistance during the beamtime.

Supporting Information Available: X-ray crystallographic files in CIF format. Experimental details: crystallographic data for 1; comparative experimental and simulated powder pattern for all the RPF-4 compounds synthesized (PDF). This material is available free of charge via the Internet at <http://pubs.acs.org>.

References

- (1) (a) Sudik, A. C.; Cote, A. P.; Wong-Foy, A. G.; O'Keeffe, M.; Yaghi, O. M. *Angew. Chem., Int. Ed.* **2006**, *45*, 2528. (b) Kondo, A.; Noguchi, H.; Kajiro, H.; Carlucci, L.; Mercandelli, P.; Proserpio, D. M.; Tanaka, H.; Kaneko, K.; Kanoh, H. *J. Phys. Chem. B* **2006**, *110*, 25565. (c) Rowsell, J. L. C.; Yaghi, O. M. *J. Am. Chem. Soc.* **2006**, *128*, 1304. (d) Jhung, S. H.; Lee, Jin-Ho; Cheetham, A. K.; Ferey, G.; Chang, J. S. *J. Catal.* **2006**, *239*, 97. (e) Hong, M. *Cryst. Growth Des.* **2007**, *7*, 10. (f) Vertova, A.; Cucchi, I.; Fermo, P.; Porta, F.; Proserpio, D. M.; Rondinini, S. *Electrochim. Acta* **2007**, *52*, 2603. (g) Janiak, C. *Dalton Trans.* **2003**, *14*, 2781. (h) Braga, D.; Polito, M.; D'Addario, D.; Grepioni, F. *Cryst. Growth Des.* **2004**, *4*, 1109. (i) Hyde, S. T.; Delgado-Friedrichs, O.; Ramsden, S. J.; Robins, V. *Solid State Sci.* **2006**, *740*.
- (2) Hill, R. J.; Long, D. L.; Hubberstey, P.; Schroder, M.; Champness, N. R. *J. Solid State Chem.* **2005**, *178*, 2414.
- (3) (a) Snejko, N.; Cascales, C.; Gómez-Lor, B.; Gutiérrez-Puebla, E.; Iglesias, M.; Ruiz-Valero, C.; Monge, M. A. *Chem. Commun.* **2002**, 1366. (b) Gándara, F.; Perles, J.; Snejko, N.; Iglesias, M.; Gómez-Lor, B.; Gutiérrez-Puebla, E.; Monge, M. A. *Angew. Chem., Int. Ed.* **2006**, *45*, 7998–8001. (c) Gándara, F.; García-Cortés, A.; Cascales, C.; Gómez-Lor, B.; Gutiérrez-Puebla, E.; Iglesias, M.; Monge, A.; Snejko, N. *Inorg. Chem.* **2007**, *46*, 3475.
- (4) (a) Pan, L.; Sander, M. B.; Huang, X.; Li, J.; Smith, M.; Bitner, E.; Brockrath, B.; Johnson, K. J. *J. Am. Chem. Soc.* **2004**, *126*, 1308. (b) Pan, L.; Olson, D. H.; Ciemnomolski, L. R.; Heddy, R.; Li, J. *Angew. Chem., Int. Ed.* **2006**, *45*, 616.
- (5) (a) Monge, A.; Snejko, N.; Gutiérrez-Puebla, E.; Medina, M.; Cascales, C.; Ruiz-Valero, C.; Iglesias, M.; Gómez-Lor, B. *Chem. Commun.* **2005**, 1291. (b) Gándara, F.; Gomez-Lor, B.; Gutiérrez-Puebla, E.; Iglesias, M.; Monge, M. A.; Proserpio, D. M.; Snejko, N. *Chem. Mater.* **2008**, in press.
- (6) Spek, A. L. () *PLATON, A Multipurpose Crystallographic Tool*; Utrecht University: Utrecht, The Netherlands, 2007.
- (7) (a) Blatov, V. A. *Acta Crystallogr., Sect. A* **2007**, *63*, 329. (b) VSI[4.4.6.6.6;6;6;6,6,6,6] and Coordination sequence (5,18,45,82,128,190,262,340,437,544).
- (8) (a) Blatov, V. A. *IUCr Compcomm Newsl.* **2006**, *7*, 4. (b) Blatov, V. A.; Carlucci, L.; Ciani, G.; Proserpio, D. M. *CrystEngComm.* **2004**, *6*, 377.
- (9) Mejia-Radillo, Y.; Yatsimirsky, A. *Inorg. Chim. Acta* **2002**, *328*, 241 and references therein.
- (10) Kamitani, J.; Sumaoka, J.; Asanuma, H.; Komiyama, M. *J. Chem. Soc., Perkin Trans.* **1998**, *2*, 523.

CG700796M

Controlling the Structure of Arene-disulfonates toward Catalytically Active Materials

Felipe Gándara,[†] Enrique Gutiérrez Puebla,[†] Marta Iglesias,[†] Davide M. Proserpio,[‡]
Natalia Snejko,[†] and M. Angeles Monge^{*†}

*Instituto de Ciencia de Materiales de Madrid, CSIC, Madrid, Spain, and Dipartimento di Chimica
Strutturale e Stereochimica Inorganica, Università di Milano, Milano, Italy*

Received September 3, 2008

By adjusting the solvothermal synthesis conditions, two ytterbium catalytically active MOF (metal organic framework) materials aimed at two different heterogeneous processes have been obtained as pure phases. Yb-LRH belongs to the first family of layered rare-earth hydroxides (LRH). With a 2D structure, highly related to that of the layered double hydroxides, Yb-LRHs have cationic inorganic layers with formula $[Yb_2(OH)_2(H_2O)_4]^{2+}$ and is a very active and selective catalyst in the sulfide oxidation reaction. The second, Yb-RPF-5, is a 3D rare-earth polymeric framework material, with formula $[Yb(OH)(2,6-AQDS)(H_2O)]$ (AQDS = anthraquinone-2,6-disulfonate). With lower coordination for the Yb atom and additional acidity from the coordinated ligands, it acts as a good catalyst in hydrodesulfurization (HDS) reactions. Both materials are bifunctional catalysts in redox and acid processes. Structural features of the materials, as well as their catalytic activity and topology, have been studied.

Introduction

The design and synthesis of new materials with desirable properties is one of the main purposes of solid-state chemistry. In this area, metal organic frameworks MOFs have received immense interest in the last years, because of their great possibilities in different applications,¹ such as heterogeneous catalysis.^{2,3} On the other hand, layered double hydroxides (LDHs), also known as hydrotalcite-like materials or synthetic anionic clays, with a brucite-like structure and the formula $[M^{II}_xM^{III}_y(OH)_z]^{+} (A^{n-})_{m \cdot y} \cdot nH_2O$ have attracted increasing attention in recent years because of their potential applications as adsorbents, ionic conductors, and catalysts.⁴

In our ongoing research of rare-earth coordination networks,^{5–7} we have reported in a recent communication⁸

the first layered rare-earth hydroxide (LRH), a new type of layered⁹ crystalline material very related with the LDH materials, in which the positive charge of the inorganic layer is created by varying the number of hydroxyl groups coordinated to the R^{3+} cation instead of introducing two different cations (as it occurs in LDH compounds). This arises from the high and variable coordinative capability of the rare-earth centers and to the tendency of the hydroxide ion to form μ_n connections in structures that contain these rare-earth centers. Rigid organic anions are intercalated to neutralize the positive charge.

One of the conclusions that could be deduced from the previous studies of LRH compounds is that to a certain extent, apart from the more convenient configuration of the organic linker, the LRH structure seemed to be kinetically favored for small rare-earth cations. However, previous screenings on the synthesis conditions did not rule out the possibility to obtain 3D materials also for the same linker and rare-earth cation. A correct choice of the synthesis conditions seems to be decisive to obtain either, 2D layered hydroxide or 3D polymeric framework material as pure phases. In this paper, we report the complete study of the different synthesis conditions that lead to the different structures, and thus to materials designed for heterogeneous catalysis of different specific reactions. A new rare earth polymeric framework (named Yb-RPF-5) compound has been obtained, and its structure, topology, and catalytic properties are here compared with those of the Yb-LRH

* To whom correspondence should be addressed. E-mail: amonge@icmm.csic.es

[†] Instituto de Ciencia de Materiales de Madrid.

[‡] Università di Milano.

- (1) (a) Janiak, C. *Dalton Trans* 2003, 14, 2781. (b) James, S. L. *Chem. Soc. Rev.* 2003, 32, 276.
- (2) (a) Alacris, L.; Seguin, E.; Poelman, H.; Thibaut-Starzyk, F.; Jacobs, P. A.; De Vos, D. F. *Chem. - Eur. J.* 2006, 12, 7353. (b) Mueller, U.; Schubert, M.; Teich, F.; Puetter, H.; Schiele, A.; Andt, K.; Pastre, J. J. *Mater. Chem.* 2006, 16, 626. (c) De Rosa, S.; Giordano, G.; Grimaldo, T.; Katsvici, A.; Siciliano, A.; Tripicchio, F. *J. Agric. Food Chem.* 2005, 53, 8306. (d) Seo, J. S.; Wang, D.; Lee, H.; Jun, S. I.; Oh, J.; Jeon, Y. J.; Kim, K. *Nature* 2000, 404, 982. (e) Schlichte, K.; Knatzke, T.; Kaskel, S. *Microporous Mesoporous Mater.* 2004, 73, 81.
- (3) Gándara, F.; Fortes-Revilla, C.; Snejko, N.; Gutiérrez-Puebla, E.; Iglesias, M.; Monge, M. A. *Inorg. Chem.* 2006, 45, 9680.
- (4) Rives, V. *Layered Double Hydroxides: Present and Future*; Nova Science Publishers: New York, 2001.
- (5) Snejko, N.; Cascales, C.; Gómez-Lor, B.; Gutiérrez-Puebla, E.; Iglesias, M.; Ruz-Valero, C.; Monge, M. A. *Chem. Comm.* 2002, 1366.
- (6) Gándara, F.; García-Cortés, A.; Cascales, C.; Gómez-Lor, B.; Gutiérrez-Puebla, E.; Iglesias, M.; Monge, M. A.; Snejko, N. *Inorg. Chem.* 2007, 46, 3475.
- (7) Gándara, F.; de Andrés, A.; Gómez-Lor, B.; Gutiérrez-Puebla, E.; Iglesias, M.; Monge, M. A.; Proserpio, D. M.; Snejko, N. *Cryst. Growth Des.* 2008, 8, 378.

(8) Gándara, F.; Perles, J.; Snejko, N.; Iglesias, M.; Gómez-Lor, B.; Gutiérrez-Puebla, E.; Monge, M. A. *Angew. Chem., Int. Ed.* 2006, 45, 7998.

(9) (a) Holman, K. T.; Pivovar, A. M.; Swift, J. A.; Ward, M. D. *Acc. Chem. Res.* 2001, 34, 107. (b) Pivovar, A. M.; Holman, K. T.; Ward, M. D. *Chem. Mater.* 2001, 13, 3018. (c) Russell, V. A.; Etter, M. C.; Ward, M. D. *J. Am. Chem. Soc.* 1994, 116, 1941.

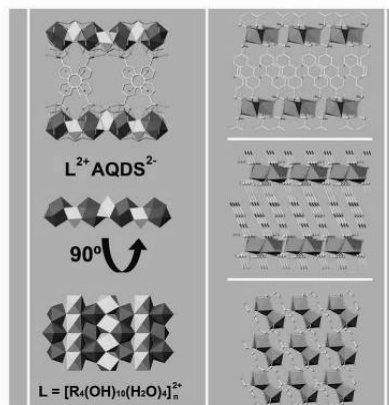


Figure 1. Left: Structure of Yb-LRH, $[\text{Yb}(\text{OH})_{10}(\text{H}_2\text{O})_4]^{2+}$ [2,6-AQDS]. Right: Structure of Yb-RPF-5, $[\text{Yb}(\text{OH})_{10}(2,6\text{-AQDS})(\text{H}_2\text{O})]$.

material. In addition, a new refinement of the crystal structure for the Yb-LRH⁸ is also included.

Experimental Section

General Information. All reagents and solvents employed were commercially available and used as supplied without further purification: anthraquinone-2,6-disulfonic acid disodium salt, 2,6-AQDSNa₂ (97% Sigma-Aldrich); ytterbium nitrate pentahydrate, Yb(NO₃)₃·5(H₂O), (99% Strem Chemicals). The IR spectra were recorded from KBr pellets in the range 4000–400 cm⁻¹ on a Perkin-Elmer spectrometer. Thermogravimetric and differential thermal analyses (TGA-DTA) were performed using a SEIKO TG/DTA 320 apparatus in the temperature range between 25 and 800 °C in N₂ (flow of 50 mL/min) atmosphere and at a heating rate of 5 °C/min. A thermostat QMS200 M3 quadrupole mass spectrometer detector was employed. Power X-ray diffraction (PXRD) patterns were measured with a Bruker D8 diffractometer, with step size = 0.02° and exposure time = 0.5 s/step.

Synthesis. The compounds were synthesized under hydrothermal conditions, by heating an aqueous solution of molar compositions given in table 1, with an initial pH of 6.5, at 175 °C for 18 h in a Teflon-lined stainless steel autoclave. For Yb-LRH (ytterbium-layered rare-earth hydroxide), typically 0.112 g (0.25 mmol) of 2,6-AQDSNa₂ and 0.510 g (1 mmol) of Yb(NO₃)₃·5(H₂O) were dissolved in 19.8 mL of water (1100 mmol), and then 0.032 mL (2.375 mmol) of triethylamine was added. For Yb-RPF-5 (ytterbium-rare earth polymeric framework-5), 0.320 g (0.78 mmol) of 2,6-AQDSNa₂ and 0.350 g (0.78 mmol) of Yb(NO₃)₃·5(H₂O) were dissolved in 21.1 mL of water (1170 mmol), and then 0.77 mL of a 1 M solution of NaOH (0.77 mmol NaOH) was added. After being cooled to room temperature, the products were filtered and washed with deionized water and acetone. In all cases, the products were isolated as a unique phase: large yellow crystals of Yb-RPF compound (65% yield) and a grayish white powder of Yb-LRH compound (94% yield). Only a few single crystals of Yb-LRH were obtained. The purity of the products was tested by comparing the experimental and simulated PXRD patterns and through the elemental CHNS analysis. Calcd for Yb-LRH: C, 12.9; H, 1.8; S,

Table 1. Synthesis Conditions

Yb/AQDS ^a	H ₂ O/AQDS ^a	base	product
4	4400	Et ₃ N	pure LRH phase
4	4400	Py	pure LRH phase
1	1500	NaOH	pure RPF phase
4	4400	NaOH	RPF majority phase + LRH presence
4	1500	NaOH	RPF + LRH
1	4400	Et ₃ N	pure LRH phase
1	1500	Et ₃ N	pure LRH phase

^a Molar ratio.

4.9. Found: C, 13.0; H, 2.2; S, 4.6. Calcd for Yb-RPF: C, 29.2; H, 1.6; S, 11.1. Found: C, 28.1; H, 1.7; S, 10.6.

X-ray Structure Determination. Single crystals suitable for X-ray crystallography were carefully selected and mounted in a Bruker SMART CCD diffractometer equipped with a normal focus, 2.4 kW sealed tube X-ray source (Mo K α radiation = 0.71073 Å). Data were collected over a hemisphere of the reciprocal space by a combination of three sets of exposures. Each exposure of 20 s covered 0.3° in ϕ . Unit-cell dimensions were determined by a least-squares fit of 60 reflections with $I > 20\sigma(I)$. The structures were solved by direct methods. The final cycles of refinement were carried out by full-matrix least-squares analyses with anisotropic thermal parameters for all non-hydrogen atoms. Hydrogen atoms of the hydroxyl groups and water molecules were located in difference Fourier maps. Calculations were carried out with SMART software for data collection and data reduction and SHELXTL.¹⁰

Catalytic Experiments. Hydrodesulfurization of thiophene was carried out in a Parr reactor, under 7 bar of H₂. For thiophene decomposition, 10 mL (125 mmol) of substrate and 0.040 g of Yb-LRH or 0.072 g of Yb-RPF5 (0.125 mmol of Yb catalyst) were mixed and heated at different temperatures, with stirring. After selected time intervals, the reactor was cooled and then opened; the remaining amount of thiophene was then measured. For sulfide oxidation, 2 mmol of the substrate (methylphenylsulfide) was added to a flask containing a suspension of the Yb catalyst (0.002 mmol) in acetonitrile. Under stirring, and after being heated to 60 °C, an excess of the oxidant (5 mmol of H₂O₂) was added dropwise. For epoxidation of linalool, a suspension containing 1 mmol of the substrate and the catalyst (100:1 linalool:Yb) in 5 mL of acetonitrile was heated to 80 °C, under stirring. An excess of oxidant (H₂O₂) was then added. Chemical yield was measured by gas chromatography (GC), in a Hewlett-Packard 5890 II coupled with a mass detector. A methylsilicone column was employed.

Results and Discussion

Synthesis. As indicated in experimental section, time, pH, and temperature are similar for the synthesis of both compounds. From the synthesis conditions summarized in Table 1, some conclusions can be made: Despite the fact that for all the syntheses the pH is 6.5, the source of OH⁻ anions seems to be a decisive factor. When using an amine, the LRH phase is obtained, whereas with an inorganic base such as Na(OH), a mixture of 2D LRH and 3D RPF phase can appear independently of the reagent ratio (see the Supporting Information). The only way to get the 3D structure as single product is by adjusting its molecular formula with an equimolar amount of OH⁻ anions. It seems that the presence of any other different compound added to

(10) Software for the SMART System V5.04 and SHELXTL V 5.1; Bruker-Siemens Analytical X-ray Instrument Inc., Madison, WI, 1998.

Table 2. Crystallographic Data for Yb-LRH and Yb-RPF-5

	Yb-LRH	RPF-5
empirical formula	C ₁₄ H ₂ O ₁₂ S ₂ Yb ₆	C ₁₄ H ₂ O ₁₀ S ₂ Yb
<i>f</i> _w	1300.61	574.37
cryst syst	orthorhombic	triclinic
space group	<i>Ibam</i>	<i>P1</i>
<i>a</i> (Å)	12.5401(6)	7.3843(8)
<i>b</i> (Å)	35.6519(19)	7.8665(8)
<i>c</i> (Å)	7.0347(4)	13.7366(15)
α (deg)	90	86.119(2)
β (deg)	90	86.097(2)
γ (deg)	90	86.398(2)
Volume	3145.1(3)Å ³	792.90(15)Å ³
Z	4	2
Density(calculated)	2.747 Mg/m ³	2.406 Mg/m ³
Absorption coefficient	12.000 mm ⁻¹	6.219 mm ⁻¹
theta range for data collection (deg)	1.72–33.14	1.49–28.27
cryst size	0.20 × 0.10 × 0.05 mm ³	0.20 × 0.15 × 0.10 mm ³
independent reflns	2606 [R _{int} = 0.0628]	3717 [R _{int} = 0.0450]
data/restraint/params	2606/12/105	3717/1/244
GOF on F ²	1.024	1.036
final R indices	R1 = 0.0719, wR2 = 0.1883	R1 = 0.0560, wR2 = 0.1292
R indices (all data)	R1 = 0.0947, wR2 = 0.2007	R1 = 0.0678, wR2 = 0.1349

control the pH, such as triethylamine or pyridine in the mixture, releases more hydroxide anions as the reaction runs, in a such way that the formation of the cationic layer with a higher OH⁻/Ln³⁺ ratio (molecular formula [Yb₄(OH)₁₀]²⁺) is favored, and the Yb-LRH product is obtained. This factor seems to be more important than the possible amine template effect, or even the influence of the Brønsted/Lewis acid character of the used base.

Crystal Structure Description. Details of unit cell, data collection, and refinement for the two compounds are given in Table 2.

The molecular formulas of the two compounds are [Yb₄(OH)₁₀(H₂O)₄] [2,6-AQDS] (Yb-LRH) and [Yb(OH)(2,6-AQDS)(H₂O)] (Yb-RPF-5) (2,6-AQDS = anthraquinone-2,6-disulfonate).

Yb-LRH. As we previously reported,⁸ the structure of the LRH family of compounds is highly related to that of the LDH materials, with positively charged layers, and the anions situated in the interlayer space. The layers have a formula [Yb₄(OH)₁₀(H₂O)₄]_n²⁺. Two crystallographically independent Yb atoms are found, with coordination numbers 8 and 9. Each Yb ion is coordinated to a water molecule and to the μ_3 -hydroxyl groups, thanks to which the cations are linked giving rise to the inorganic layer. Two different coordination polyhedra are formed: one dodecahedron and a monocapped square antiprism. Polyhedra of the same type are placed in alternated rows parallel to the 001 direction forming the layers parallel to the *ac* plane. The AQDS²⁻ anions are located in the interlayer space, linked to the layers through hydrogen bonds. They are highly ordered, with a tilting angle formed between the organic anion S–S axes and the normal of the respective hydroxide layers of 30.86°. The value of the basal spacing is one-half of the *b* parameter. The AQDS²⁻ anions are situated parallel to the *ab* plane in an alternated configuration, and separated 3.5 Å (*c*/2) and 12.5 Å (*a*) along the [001] and [100] directions, respectively (Figure 1, left).

This arrangement gives rise to π – π and O– π stacking interactions of the parallel type¹¹ among the AQDS²⁻ central

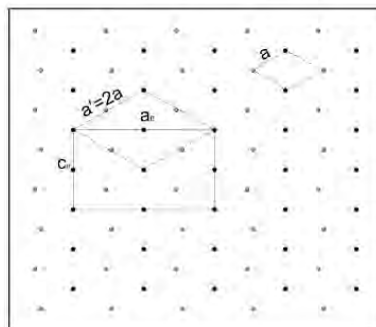


Figure 2. Crystallographic transformation from the LDH material structure to the new orthorhombic LRH structure.

rings and among one of the quinonic oxygen atoms and lateral aromatic rings, respectively, at a distance of 3.52 Å. Thanks to this well-ordered disposition of the anions in the interlayer space, this compound has a porous structure, with channels running along the *c* direction. The potential solvent area is 16.4%, as computed by Platon.¹²

From a crystallographic point of view, a direct relation exists between the brucite derived LDH hexagonal lattice and that of the LRHs. Given that in the latter there are two independent well-ordered Yb atoms by asymmetric unit, the ideal hexagonal superlattice would have an *a'* parameter twice that of the mineral. As the distances among Yb atoms are not uniform, this hexagonal superlattice is not real but it has a distortion that gives rise to orthorhombic larger cell for Yb-LRH compound. Vectors of the LRH unit cell can be deduced from those of the LDH by roughly applying the transformation matrix (220, 001, 220) (Figure 2).

In terms of topology, the cationic [Yb₂(OH)₁₀]²⁺_n layer can be described as a pentanodal 3,7,8 connected net, with stoichiometry (3-c)₅(7-c)(8-c), where the 7c and 8c nodes are given by the ytterbium atoms, and the 3c by the hydroxylic oxygen atoms (Figure 4, top left). To study the 3D net formed through the hydrogen bonds, the model has been simplified as follows: First of all, the oxygen atoms of the layer are omitted, giving rise to a (3,6) sheet of Yb atoms (Figure 3, top right). Second, the intercalated AQDS molecules are directly connected to the [Yb₂(OH)₁₀]²⁺ layers via hydrogen bonds (Figure 3, bottom left). The result is a trinodal, octa- and pentaconnected net with stoichiometry (5-c)(8-c)₂, and point (Schläfli) symbol (3¹⁰,4¹²,5⁶) (3³,4⁴,6²,7²) (3³,4¹¹,5⁷,6²) (Figure 3, bottom right).

Yb-RPF-5. The new RPF-5 has a 3D structure, with the AQDS²⁻ anions coordinated to the Yb atoms. Different from the Yb-LRH phase, in [Yb(OH)(2,6-AQDS)(H₂O)], the lanthanide ion is heptacoordinated (table 3), to two μ_2 -(OH) groups, one water molecule, and four oxygen atoms, belong-

(11) Janiak, C. *J. Chem. Soc., Dalton Trans.* **2000**, 3885.

(12) Spek, A. L. 2008 PLATON, A Multipurpose Crystallographic Tool; Utrecht University: Utrecht, The Netherlands.

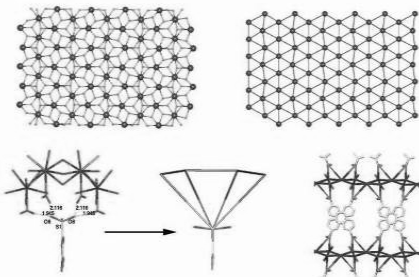


Figure 3. Topological analysis of Yb-LRH. Top, ball-and-stick (left) and simplified without oxygen atoms (right) view of the Yb–O layer; bottom, depiction of Yb-LRH structure considering hydrogen bonds.

ing to four different sulfonate groups in a YbO_7 monocapped trigonal prism. Every two of these (YbO_7) polyhedra form Yb_2O_{12} sharing edges dimeric units via two $\mu_2\text{-OH}^-$, which are isolated in the b direction and joined through S atoms in the a direction. The SO_3 groups, with $\mu^2\text{-}\eta^2$ coordination mode, join the $\text{Yb}_2(\text{OH})_2$ units, with the S atom acting as a bridge between every two dimeric units in a such way that an entirely inorganic layer is formed parallel to the ab plane (Figure 1, bottom right). These layers are not as condensed as those of LRH, because they are $10R$ ($6\text{Yb} + 4\text{S}$) containing layers with the coordinated water molecules pointing inside the rings (in the LRH compounds, the coordinated water molecules point toward the interlamellar space and play a important structural role by forming the H-bonds with the intercalated AQDS molecules).

In the Yb-RPF-5 3D structure, the layers are connected along the c direction by $\eta^2\mu^2\text{-}\eta^2\mu^2$ bonded AQDS^{2-} with a tilt angle of 66.27° between the ab plane, and that involving the three aromatic rings (Figure 1, right middle). These molecules are disposed along the 100 direction occupying two different position in the b axis, in an alternating configuration, and separated by 3.692 \AA ($a/2$). Because the molecules in both position have the same slope trend, $\pi\text{-}\pi$ stacking interactions between rings are not given. In Figure 1, right top, the projection of the bc plane is shown.

From a topological point of view, we can describe an inorganic layer formed by the Yb atoms, where each atom is connected to the other three, one of them directly by hydroxyl groups and the other two through sulfonate bridges, resulting in a (6,3) honeycomb layer (Figure 4, left). The three-dimensional real net, with these layers linked through the whole ligand, can be described as a binodal net, where the S atoms are 3-connected nodes, and the ytterbium atoms are 5-connected nodes (Figure 4, middle). This network, with poing (Schläfli) symbol $(4.6^2)_2(4^2.6^2.8^6)$ has maximum symmetry in the space group $Fm\bar{3}m$ and it is found with the code sqc707 in the EPINET database,¹³ where no previous examples of networks with this topology are described

(Figure 4, right). Topological study of both Yb-LRH and Yb-RPF-5 structure was made with TOPOS.¹⁴

The comparison of the experimental and simulated X-ray powder diffraction patterns shows that both compounds appear as the only product of their respective optimized reactions. The X-ray patterns also demonstrate a high crystallinity of the obtained materials. Figure 5 shows both experimental and simulated patterns.

Thermal Behavior. Yb-LRH. TGA-DTA analysis (Figure 6) shows a first mass loss (3.5%) before 60°C , which is due to the loss of adsorbed water molecules. In the temperature range of $100\text{--}400^\circ\text{C}$, there are three steps in the TG curve, corresponding to a total mass loss of $\sim 10\%$. Only the signal corresponding to a mass of 18 was found in the mass detector in this temperature range. Consequently, a loss of 7 water molecules is assumed from the TG value (calculated value = 9.7%). Four of them are the 4 coordinated water molecules, present in the initial structure. The remaining three molecules come from the inorganic layer, in such a way that the formula of this layer after the heating, should be $[\text{Yb}_4\text{O}_2(\text{OH})_4]^{2+}$. An elemental analysis made to the sample after being heated at 500°C (under the same conditions than in the TG experiments) shows that all the organic components remain in the structure. The result of this analysis (14% C, 0.6% H, and 5.1% S) demonstrates that the AQDS^{2-} anion remains intact in the structure (experimental $\text{C/S} = 7.3$, calculated = 7.0). The PXRD patterns of the heated samples show no changes in the peaks positions until 300°C (Figure 7). At this temperature, a shift in the first peak to higher angle happens, and consequently, a diminution of the basal space to a value of 17.0 \AA . Only the three first peaks are observed, indicating that the layered structure remains, but the layer is not so ordered. Finally, at 500°C , a new diminution of the interlayer space takes place, with a final basal space of 16.5 \AA , before the decomposition of the structure begins.

RPF-5. The first mass loss starts at $\sim 285^\circ\text{C}$, corresponding to the loss of the only water molecule present in the structure (experimental 3%, calculated 3.1%). There is an irreversible phase transition associated to this change, showing the PXRD pattern a different crystalline phase when the sample is heated above this temperature (see the Supporting Information). This crystalline phase remains until the decomposition of the product, which begins at $\sim 485^\circ\text{C}$. After an initial weight lost of $\sim 21\%$ in a 80 degrees interval, the product decomposes gradually until a final weight loss of $\sim 62\%$, which indicates the almost total loss of the organic molecule (calculated = 69.6%). PXRD shows ytterbium oxide as main final residue, and the difference in percent mass loss is probably due to the presence of coke residue.

FTIR. The band ($3300\text{--}3650 \text{ cm}^{-1}$) corresponding to the $\nu(\text{Yb-OH})$ frequencies of the coordinated hydroxyl groups and water molecules is more narrow in the IR spectra of Yb-RPF-5 compound than in the Yb-LRH, which has a broadband at $3000\text{--}3700 \text{ cm}^{-1}$. This broadening is due to the hydrogen bonds between the coordinated oxygen atoms

(13) Hyde, S.; Friedrichs, O. D.; Ramsden, S. J.; Robins, V. *Solid State Sci.* **2006**, *8* (7), 740.

(14) (a) Blatov, V. *IUCr Compcomm Newsletter* **2006**, *7*, 4; <http://www.topos.ssu.samara.ru>. (b) Blatov, V. A.; Carlucci, L.; Ciani, G.; Proserpio, D. M. *CrystEngComm* **2004**, *6*, 377.

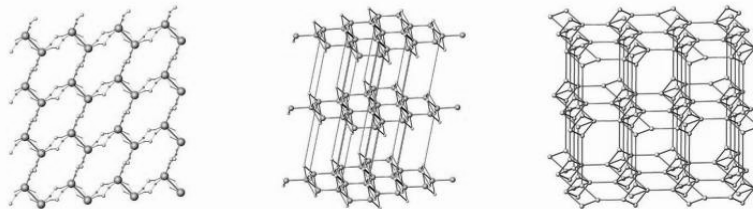


Figure 4. Topological analysis for Yb-RPF-5 showing: left, honeycomb inorganic layer; middle, simplified 3D real net; right, idealized $(4,6^2)(4,3,6,3^8)$ network.

Table 3. Bond Lengths (Å) in Yb-LRH and Yb-RPF-5

LRH ^a			
O(1)–Yb(1)	2.538(11)	O(3)–Yb(2)	2.430(8)
O(2)–Yb(1)	2.275(12)	Yb(2)–O(3)#8	
O(3)–Yb(1)#3	2.242(8)	O(4)–Yb(2)#5	2.415(7)
Yb(1)–O(3)#2		O(4)–Yb(2)	
Yb(1)–O(3)#3		Yb(2)–O(4)#8	
O(5)–Yb(1)	2.386(15)	O(6)–Yb(2)	2.79(2)
O(4)–Yb(1)#3	2.274(11)	Yb(1)–Yb(2)#2	3.5221(6)
Yb(1)–O(4)#3		Yb(1)–Yb(2)#3	
Yb(1)–O(3)#4	2.324(8)	Yb(2)–Yb(1)#3	
O(3)–Yb(1)		Yb(1)–Yb(1)#6	3.7362(5)
O(1)–Yb(2)#2	2.300(7)	Yb(1)–Yb(1)#3	3.5173(2)
O(1)–Yb(2)#3		Yb(2)–Yb(2)#4	
Yb(2)–O(1)#7		Yb(2)–Yb(2)#5	
Yb(2)–O(1)#3			
O(2)–Yb(2)	2.392(7)		
O(2)–Yb(2)#4			
Yb(2)–O(2)#8			
RPF ^b			
Yb(1)–O(9)	2.183(6)	Yb(1)–O(3)	2.299(6)
Yb(1)–O(9)#1	2.199(6)	Yb(1)–O(5)	2.310(6)
Yb(1)–O(6)	2.282(6)	Yb(1)–O(10)	2.325(7)
Yb(1)–O(2)	2.283(6)	Yb(1)–Yb(1)#1	3.5954(7)

^a Symmetry transformations used to generate equivalent atoms: #1 $-x, -y + 1, -z + 1$; #2 $-x + 1/2, -y + 1/2, z + 1/2$; #3 $-x + 1/2, -y + 1/2, -z + 1/2$; #4 $x, y, -z + 1$; #5 $x, y, -z$; #6 $-x + 1/2, -y + 1/2, -z + 3/2$; #7 $x - 1/2, -y + 1/2, z$; #8 $-x + 0, y + 0, -z + 1/2$.

^b Symmetry transformations used to generate equivalent atoms: #1 $-x, -y + 2, -z + 1$.

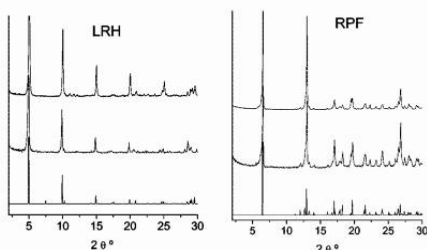


Figure 5. Comparison of the calculated (lower) and experimental powder X-ray diffraction pattern before (medium) and after (upper) catalytic reactions.

and the sulfonate group. In **Yb-RPF-5**, the coordination of the SO_3 group to the metal causes a shift of the band at 1040 cm^{-1} to higher wavenumber ($\sim 1060 \text{ cm}^{-1}$), while in **Yb-LRH**, the uncoordinated $-\text{SO}_3$ group gives rise to nonsplit bands in the region $1000\text{--}1100 \text{ cm}^{-1}$, corresponding to the C_{3v} symmetry that the group retains.

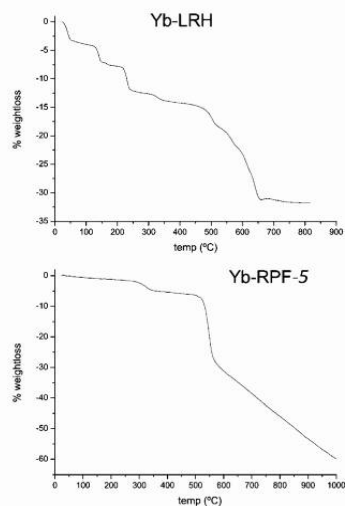


Figure 6. TG curves for Yb-LRH and Yb-RPF-5.

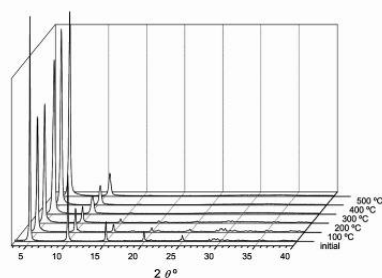


Figure 7. PXRD patterns of Yb-LRH heated samples.

Catalytic Activity. Rare earth metals are increasingly used as catalysts in a wide variety of organic transformations. MOF materials of these elements offer the possibility of combining the Lanthanide catalytic properties with the advantages of being heterogeneous catalysts. Both Yb-LRH

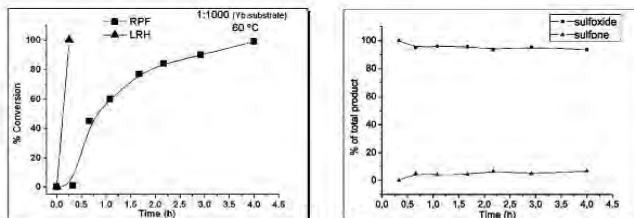


Figure 8. (Left) Kinetic profile and (right) selectivity curves of the oxidation of sulfides for Yb-RPF-5.

and Yb-RPF-5 materials bear a great number of active centers with capability of varying the coordination number in catalytic processes, which confers them great possibilities in the green chemistry field. These compounds help to control the activity and selectivity of a catalytic process by tuning geometrical features of their frameworks. The differences in the coordination environment of the active rare earth metal will lead to materials with specific activities in different catalytic processes. The properties of the new materials as heterogeneous catalysts have been tested in key processes, such as:

Hydrodesulfurization of Thiophene (HDS). The Yb-LRH under 7 bar of H_2 at only 70 °C shows a conversion of 50% in 26 h, with a ratio substrate/Yb = 1000, giving hydrogen sulfide and butane (both components easily separable). It is worth pointing out that these results are obtained under much milder conditions than those usually utilized (high pressure of H_2 , i.e., 30–60 bar, at 350–400 °C^{15,16}). For the Yb-RPF-5, a higher grade of conversion is obtained with the same rate of substrate vs active center and the total decomposition of the thiophene is achieved after 24 h. By increasing the temperature, the reaction becomes faster in such a way that only 16 h are needed at 100 °C, and a conversion of 90% is found after only 4.3 h at 120 °C. Although the Yb-RPF-5 structure is less open than that of Yb-LRH and thus, the catalytic reaction should take place only on surface, the activity of the former is higher because of the low Yb coordination number in this compound, which allows an easier access of the substrate to the active center, and to the acidity coming from the coordinated ligand, that favors the heterolytic rupture of the hydrogen molecule.

Oxidation of Sulfides. As an alternative to hydrodesulfurization reactions the removal of refractory sulfur containing compounds can be accomplished by oxidation. The present systems also catalyze the oxidation of various alkyl phenyl sulfides (figure 8).

Yb-LRH. Sulfides were selectively mono-oxygenated to the corresponding sulfoxides (100%) in 30 min, using H_2O_2 as oxidant. It is remarkable the excellent $TOF = 2000\ h^{-1}$ value reached by the material, due to the small quantity of catalyst (0.1%) needed and the fast conversion of the substrate¹⁷ ($TOF = \text{turnover frequency}$, here defined as $[\text{mol substrate}]/[\text{mol}$

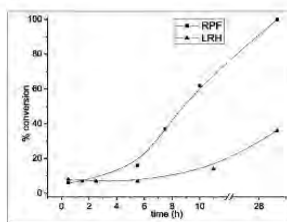


Figure 9. Catalytic activity of both materials for the conversion of linalool.

Yb-**LRH**). Its activity is comparable to that of microporous bifunctional titanium aluminosilicates, and better, both in activity and selectivity, than that of previously studied rare earth succinate polymeric framework.¹⁸

Yb-RPF-5 also presents catalytic activity, with a TOF value of $706\ h^{-1}$ at 60 °C, which is smaller than that of Yb-LRH compound. The catalyst is highly selective, with the sulfoxide (>90%) being the main product of the oxidation. Kinetic profile and selectivity curve of the oxidation of sulfides are shown in Figure 8 left and right, respectively.

From a reaction mechanism viewpoint, the sulfoxidation reaction has to go through the corresponding peroxy species, as happens in the hydrolysis of phosphodiester¹⁹ and RNA,²⁰ catalyzed by peroxide rare earth complexes formed in rare earth- H_2O_2 mixtures. Accordingly, the different catalytic behavior of the two compounds in sulfides oxidation is a consequence of the different charge density over the rare earth cation, caused by the ligand nature: In the cationic layer of Yb-LRH, the coordination sphere of the Yb atom is composed only by oxygen atoms of μ_3 -OH anions and one water molecule. In the 3D Yb-RPF-5, the charge density over the Yb cation is higher, because most oxygen atoms of the coordination sphere come from SO_3^- groups, and thus, the formation of the active peroxy complex is slower when using this later system as catalyst.

Oxidation of Linalool. The two materials were also tested as bifunctional redox-acid catalyst in the transformation of 3,7-dimethylocta-1,6-dien-3-ol (linalool) to hydroxy ethers

(15) Sharma, K. R.; Olson, E. S. *Catalytic Hydrodesulfurization with Hydrotalcites. Processing and Utilization of High-Sulfur Coals IV*. Elsevier Science Publisher B.V.: Amsterdam, 1991; p 377.

(16) Chapus, T.; Morel, F. U.S. Patent 2002195375.

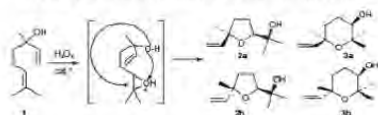
(17) Corma, A.; Iglesias, M.; Sánchez, F. *Catal. Lett.* **1996**, *39*, 153.

(18) Perles, J.; Iglesias, M.; Ruiz-Valero, C.; Snejko, N. *J. Mater. Chem.* **2004**, *14*, 2683.

(19) Mejía-Radillo, Y.; Yatsimirsky, A. *Inorg. Chim. Acta* **2002**, *328*, 241.

(20) Kamitani, J.; Sumaoka, J.; Asanuma, H.; Komiyama, M. *J. Chem. Soc., Perkin Trans.* **1998**, *2*, 523.

Scheme 1. Transformation of Linalool Reaction



(furanoid and pyranoid forms, 2 and 3 in Scheme 1), in acetonitrile, at 353 K, with an excess of H_2O_2 . In the reaction scheme, the first step involves the epoxidation of the 2,3 double bond, promoted by the metal as active center. In the second step, the presence of acid sites is needed for the intramolecular opening of the epoxide ring by the hydroxyl group at position 6 or 7. As it has been shown above, the Yb-LRH material is very active as redox catalyst but acts poorly as acid catalyst, so that only 36% of conversion occurs after 28 h, with a ratio 1:100 Yb:substrate. In the case of Yb-RPF-5, a total conversion is achieved after 28 h, with the same Yb:substrate ratio, and with a high selectivity to the furanoid versus pyranoid products (9:1 in the first run; 7:3 in the second run). Figure 9 shows the activity of both products for the oxidation of linalool.

Recycling Experiments. To verify the observed catalysis is truly heterogeneous, the catalytic reactions were carried out under standard conditions. After $\sim 30\%$ conversion, the solid was removed by filtration. The reactions were completely stopped when removing it. The solid was then used again without any loss of catalytic performance. X-ray diffraction powder pattern of the recovered catalysts showed no change in their structures. The analysis of ytterbium content (measured by ICP emission spectroscopy) in the solution after removal of the active Yb catalyst shows that only a 1% of the solid has been

dissolved during the catalytic experiment. The PXRD patterns of the solids after the experiments show that no changes have occurred in the structure (Figure 3).

Conclusions

In summary, by controlling the source of hydroxyl anions in a mild hydrothermal method of synthesis and starting from the same components, that is, ytterbium and anthraquinone-2,6-disulfonate, two active catalytic materials aimed at two different heterogeneous processes have been obtained as pure phases. $[\text{Yb}_4(\text{OH})_{10}(\text{H}_2\text{O})_4]$ [2,6-AQDS] (Yb-LRH) has a 2D structure with cationic inorganic layers that make this material a very active and selective catalyst in sulfides oxidation.

$[\text{Yb}(\text{OH})(2,6\text{-AQDS})(\text{H}_2\text{O})]$ (Yb-RPF-5) with a 3D structure, in which the Yb cation bears more charge density, yields in poorer activity in sulfides oxidation reaction. However, the Yb low coordination number and the additional acidity coming from the coordinated sulfonate ligands make this material a good catalyst in hydrodesulfurization of thiophene (HDS) reactions.

Both materials behave as bifunctional catalyst for catalyzed redox and acid processes.

Acknowledgment. F.G. acknowledges a FPI fellowship from Ministerio de Educación y Ciencia (MEC) and Fondo Social Europeo from the EU. This work has been supported by the Spanish MCYT Project Mat 2007-60822, CTQ MAT 2006-14274-C02-02, and Consolider-Ingenio CSD2006-2001.

Supporting Information Available: X-ray crystallographic files in CIF format; PXRD patterns (PDF). This material is available free of charge via the Internet at <http://pubs.acs.org>.

CM8029517

Three Lanthanum MOF Polymorphs: Insights into Kinetically and Thermodynamically Controlled Phases

Felipe Gándara,[†] Víctor A. de la Peña-O'Shea,[‡] Natalia Snejko,[†] David M. Proserpio,[§] Enrique Gutiérrez-Puebla,[†] M. Angeles Monge,^{†,¶} and Francesc Illas[†]

[†]Instituto de Ciencia de Materiales de Madrid, CSIC, Madrid, Spain, [‡]Instituto Madrileño de Estudios Avanzados en Energía (IMDEA Energía), and [§]Dipartimento di Chimica Strutturale e Stereochimica, Inorganica and Università di Milano, Milano, Italy and [¶]Departament de Química Física & IQTCUB, Universitat de Barcelona, Barcelona, Spain

Received September 17, 2008

RPF-4 is a family of polymeric frameworks prepared with rare-earth elements and the versatile ligand 4,4'-(hexafluoroisopropylidene)bis(benzoic acid). We have found that during the synthesis procedure up to three different polymorphs can be obtained. Their crystal structures are here presented. The three networks have unusual topologies, the three being uninodal penta-coordinated, two of them unknown up to now, and the other named **hxg-d-5-Imma**. They are here described and compared. DFT calculations of the relative energies for the three polymorphs show that the most often obtained structure is a metastable phase, which appears to be, next to others, thermodynamically more stable.

Introduction

The design and synthesis of microporous coordination networks with a novel structural topology obtained using polydentate ligands and a metal center have been of a great interest across disciplines because these metal-organic frameworks (MOFs) have been found to be a platform for immense potential applications^{1–9} in gas storage, catalysis, magnetism, nonlinear optics, ion exchange reactions, separation processes, and so forth. Numerous studies have been presented of transition metal MOFs with the chemistry of rare-earth (Ln) based MOFs that are significantly less studied. However, the situation has been changing over the past few years due to the fact that Ln-based MOFs present a number of interesting opportunities with respect to their intriguing topologies and many interesting

properties that may give rise to industrial applications from catalysis to optical materials.^{10–12} In MOF materials, functionality is introduced from a cooperative influence of both inorganic species and organic linker molecules. This paper deals with the self-assembly of the lanthanide series with the 4,4'-(hexafluoroisopropylidene)bis(benzoic acid) ligand (H₂hfpbb). The long hydrophobic linker H₂hfpbb is a flexible molecule, which, being a dicarboxylate, establishes a bridge between different metal centers;^{13–16} two novel frameworks have been recently obtained in our group, constructed from Zn¹⁴ or In¹⁶ and hfpbb. In these frameworks, the composition and shape of the intermediate part of the hfpbb^{2–} linker play an essential role in forming 3D and 2D polymeric structures of corresponding Zn and In MOFs. As a followup, we previously presented a short communication¹⁷

*To whom correspondence should be addressed. E-mail: amonge@icmm.csic.es.

- (1) Sudic, A. C.; Coia, A. P.; Wong-Foy, A. G.; O'Keefe, M.; Yaghi, O. M. *Inorg. Chem. Int. Ed.* **2006**, *45*, 2528.
- (2) Kanō, A.; Noguchi, H.; Kajiro, H.; Carlucci, L.; Mercandalli, P.; Proserpio, D. M.; Tanaka, H.; Kaneko, K.; Kanoh, H. *J. Phys. Chem. B* **2006**, *110*, 23565.
- (3) Rowell, J. L. C.; Yaghi, O. M. *J. Am. Chem. Soc.* **2006**, *128*, 1304.
- (4) Jiang, S. H.; Lee, J.-H.; Cheetham, A. K.; Ferey, G.; Chang, J. S. *J. Catal.* **2006**, *239*, 97.
- (5) Heng, M. *Cryst. Growth Des.* **2006**, *7*, 10.
- (6) Vertova, A.; Cucchi, I.; Fermo, P.; Porta, F.; Proserpio, D. M.; Rencimmi, S. *Electrochim. Acta* **2006**, *52*, 2603.
- (7) Jannak, C. *Balton Trans* **2003**, *34*, 2781.
- (8) Braga, D.; Polito, M.; D'Alcamo, D.; Giropiana, F. *Cryst. Growth Des.* **2006**, *6*, 1169.
- (9) Hyée, S. T.; Delgado-Friedrichs, O.; Ramsden, S. J.; Rebins, V. *Solid State Sci.* **2006**, *740*.

- (10) Snejko, N.; Cascales, C.; Gómez-Lor, B.; Gutiérrez-Puebla, E.; Iglesias, M.; Ruiz-Valero, C.; Monge, M. A. *Chem. Commun.* **2002**, 1366.
- (11) Gándara, F.; García-Cortés, A.; Cascales, C.; Gómez-Lor, B.; Gutiérrez-Puebla, E.; Iglesias, M.; Monge, A.; Snejko, N. *Inorg. Chem.* **2006**, *45*, 3433.
- (12) Gándara, F.; Parles, J.; Snejko, N.; Iglesias, M.; Gómez-Lor, B.; Gutiérrez-Puebla, E.; Monge, M. A. *Angew. Chem., Int. Ed.* **2006**, *45*, 7998.
- (13) Pan, L.; Sander, M. B.; Hwang, X.; Li, J.; Smith, M.; Biter, E.; Brockrath, B.; Johnson, K. J. *J. Am. Chem. Soc.* **2004**, *126*, 1308.
- (14) Monge, A.; Snejko, N.; Gutiérrez-Puebla, E.; Medina, M.; Cascales, C.; Ruiz-Valero, C.; Iglesias, M.; Gómez-Lor, B. *Chem. Commun.* **2005**, 1291.
- (15) Pan, L.; Olsen, D. H.; Ciomolowski, L. R.; Heddy, R.; Li, J. *Angew. Chem., Int. Ed.* **2006**, *45*, 616.
- (16) Gándara, F.; Gómez-Lor, B.; Gutiérrez-Puebla, E.; Iglesias, M.; Monge, M. A.; Proserpio, D. M.; Snejko, N. *Chem. Mater.* **2008**, *20*, 72.
- (17) Gándara, F.; Andrés, A. J.; Gómez-Lor, B.; Gutiérrez-Puebla, E.; Iglesias, M.; Monge, M. A.; Proserpio, D. M.; Snejko, N. *Cryst. Growth Des.* **2008**, *8*(2), 378.

Table 1. Main Crystallographic and Refinement Data for the Three La-RPF-4 Polymorphs.

	RPF-4- α	RPF-4- β	RPF-4- γ
empirical formula	C ₅₂ H ₁₂₃ F ₁₈ La ₂ O ₁₂	C ₅₁ H ₁₂₄ F ₁₈ La ₂ O ₁₂	C ₅₁ H ₂₄ F ₁₈ La ₂ O ₁₂
<i>V</i>	1448.52	1948.52	1448.52
cryst syst, space group	orthorhombic, <i>P2₁2₁2₁</i>	monoclinic, <i>P2₁/n</i>	orthorhombic, <i>C222₁</i>
unit cell dimensions	<i>a</i> = 7.7910(9) Å <i>b</i> = 21.372(3) Å <i>c</i> = 36.997(3) Å	<i>a</i> = 7.5600(3) Å <i>b</i> = 25.8914(1) Å <i>c</i> = 29.6752(1) Å	<i>a</i> = 7.7910(9) Å <i>b</i> = 21.372(3) Å <i>c</i> = 36.997(3) Å
volume	6160.2(13) Å ³	5583.6(4) Å ³	5235.7(10) Å ³
<i>Z</i> , calculated density	1.362 Mg/m ³	1.723 Mg/m ³	1.838 Mg/m ³
abs coeff	1.475 mm ⁻¹	1.628 mm ⁻¹	1.736 mm ⁻¹
<i>F</i> (000)	2808	2898	2808
cryst size	0.06 × 0.04 × 0.02 mm	0.20 × 0.10 × 0.06 mm	0.12 × 0.10 × 0.07
Θ range for data collection	1.10–28.62°	1.07–25.18°	1.31–26.48°
limiting indices	0 ≤ <i>h</i> ≤ 10 0 ≤ <i>k</i> ≤ 28 0 ≤ <i>l</i> ≤ 48	−9 ≤ <i>h</i> ≤ 9 −30 ≤ <i>k</i> ≤ 30 −35 ≤ <i>l</i> ≤ 36	−9 ≤ <i>h</i> ≤ 9 −38 ≤ <i>k</i> ≤ 38 −27 ≤ <i>l</i> ≤ 28
reflns collected/unique	22622/7622	36747/10356	21371/5360
Absorption correction	semiempirical from equivalents	semiempirical from equivalents	semiempirical from equivalents
max. and min. transmission	0.9211 and 0.9167	0.9087 and 0.7367	0.8882 and 0.8188
refinement method	full-matrix least-squares on <i>F</i> ²	full-matrix least-squares on <i>F</i> ²	full-matrix least-squares on <i>F</i> ²
Data/restraints/parameters	22866/160/293	10356/355/748	5360/0/376
goodness-of-fit on <i>F</i> ²	0.863	1.130	1.264
final <i>R</i> indices [<i>I</i> > 2 σ (<i>I</i>)]	<i>R</i> ₁ = 0.1355, <i>wR</i> ₂ = 0.3388	<i>R</i> ₁ = 0.0892, <i>wR</i> ₂ = 0.1691	<i>R</i> ₁ = 0.0898, <i>wR</i> ₂ = 0.2019
<i>R</i> indices (all data)	<i>R</i> ₁ = 0.4358, <i>wR</i> ₂ = 0.3620	<i>R</i> ₁ = 0.1547, <i>wR</i> ₂ = 0.1979	<i>R</i> ₁ = 0.0973, <i>wR</i> ₂ = 0.2114
largest diff. peak and hole	2.454 and −3.197 e Å ⁻³	0.946 and −2.283 e Å ⁻³	2.050 and −5.090 e Å ⁻³

reporting a series of novel isostructural lanthanide MOFs with the same ligand, called RPF-4, showing excellent optical properties, as well as catalytic activity. In this paper, we report the extended data of the synthesis study of the Ln–hfpbb system. During the synthesis procedure, up to three different polymorphs have been identified, named α , β , and γ , and their crystal structures determined. Polymorphism is an interesting and well-known phenomenon: there exist numerous examples of compounds with more than one crystalline phase, being of special interest those of pharmacologically important molecules.¹⁸ In the case of MOFs, however, there are not too many examples of real polymorphism.¹⁹ In the current work, a topological analysis for the three new polymorphs is now reported, together with DFT calculations with a comparison of the relative energy for the three networks.

Experimental Section

All chemicals were of reagent grade and were used as commercially obtained without further purification. The IR spectrum was recorded from KBr pellets in the range 4000–400 cm⁻¹ on a Perkin-Elmer spectrometer. The powder X-ray diffraction was performed with a Bruker D8 diffractometer at the European Synchrotron Radiation Facility (ESRF), Grenoble, France.

General Synthesis Procedure. During the first attempts to synthesize the new Ln³⁺-based materials with the ligand H₂hfpbb, a mixture of phases with different crystal structures was obtained. Only after determining their crystal structures did the same formula, Ln₂(hfpbb)₃, for the three phases result, three polymorphs for the RPF-4 family, that we call α , β , and γ . By adjusting the synthesis conditions, we could get the materials as pure phases. The materials of the new family of the rare-earth

polymeric framework, RPF-4- α , were synthesized via hydrothermal reactions of R₃(III) (R = Y, La, Ce, Pr, Nd, Sm, Eu, Gd, Tb, Dy, Ho, Er, Yb) salts with H₂hfpbb in a mixture of solvents. Typically, a mixture of Ln(NO₃)₃ (0.1 mmol), H₂hfpbb acid (C₁₄H₁₆F₂O₄; 0.15 mmol), ethylene glycol (2 mL), ethylenediamine (0.2 mL), and H₂O (12 mL) was put in a Teflon-lined acid digestion bomb (internal volume of 43 mL) and heated at 170 °C for 2 days, followed by cooling to room temperature. The crystalline products (the color of the crystalline powder depends on the metal used) were collected after washing with H₂O (3 × 20 mL) and acetone (2 × 10 mL). Yields were 60–70%. The pure RPF-4- β (R = La) was obtained from a mixture of La(NO₃)₃ (0.1 mmol), H₂hfpbb acid (0.15 mmol), triethylamine (0.3 mL), and H₂O (5 mL). Heating this mixture in a Teflon-lined acid digestion bomb at 170 °C for 5 days, followed by cooling to room temperature, resulted in pure white crystalline product La-RPF-4- β . The RPF-4- γ (R = La) polymeric framework was obtained from a mixture of La(NO₃)₃ (0.1 mmol), H₂hfpbb acid (0.15 mmol), 4,4'-bipyridyl (0.1 mmol), and H₂O (6 mL). Heating this mixture in a Teflon-lined acid digestion bomb at 180 °C for 4 days, followed by cooling to room temperature, resulted in a mixture of crystalline powder La-RPF-4- α and colorless large crystals of La-RPF-4- γ . All attempts to obtain La-RPF-4- γ as a pure phase were not successful. It is worth noting that, if we use the synthesis conditions that lead to the obtaining of RPF-4- α , but augmenting the time of the reaction (up to 5 days), a mixture of RPF-4- α and RPF-4- β is obtained.

Crystal Structure Determination. The data collection of La-RPF-4- α was reported in ref 17. Main crystallographic and refinement data are given in Table 1, for comparison with those of La-RPF-4- β and La-RPF-4- γ . For La-RPF-4- β and La-RPF-4- γ , the data were collected at room temperature, on a SMART-CCD Bruker diffractometer, with Mo K α radiation (λ = 0.71073 Å). Data were collected over a hemisphere of the reciprocal space through a combination of sets of exposures. Each exposure of 20 s covered 0.5° in ϕ . Unit cell dimensions were determined by a least-squares fit of 60 reflections with *I* > 2 σ (*I*). The structures were solved by direct methods. The final cycles of refinement were carried out by full-matrix least-squares analyses with anisotropic thermal parameters for all non-hydrogen atoms. Hydrogen atoms of the hydroxyl groups and water molecules were located in difference Fourier

(18) (a) Munshi, P.; Skellon, B. W.; McKinnon, J. J.; Spackman, M. A. *CrystEngComm* **2008**, *10*, 197. (b) Barsky, I.; Bernstein, J. *CrystEngComm* **2008**, *10*, 669. (c) Katamura, M. *Cryst. Growth Des.* **2004**, *4*, 1153. (d) Harstein, F. H. *Cryst. Growth Des.* **2004**, *4*, 1419.

(19) (a) Chen, B.; Fronczek, F. R.; Mavrick, A. W. *Chem. Commun.* **2003**, 2166. (b) Chen, B.; Ockwig, N. W.; Fronczek, F. R.; Contreras, D. S.; Yaghi, O. M. *Inorg. Chem.* **2005**, *44*, 181. (c) Li, Z.-G.; Wang, G.-H.; Jia H.-Q.; Liu, N.-H.; Xu, J.-W. *CrystEngComm* **2007**, *9*, 882.

Article

inaps. Calculations were carried out with SMART software for data collection and data reduction and SHELXTL.²⁹

Computational Details. Density functional plane-wave calculations have been carried out with the help of the VASP code^{21,22} for the three lanthanum MOFs. There are 428 atoms in the unit cell ($C_{27}H_{66}F_{17}La_3O_{48}$). The energy is calculated employing the generalized gradient approximation, in particular, the exchange and correlation functional of Perdew and Wang (PW91).^{23,24} The density was expanded in a plane-wave basis set, whereas the effect of the inner cores was taken into account through the projected augmented plane wave method.^{25,26} The cutoff for kinetic energy of the plane waves has been set to 415 eV throughout, which ensures a total energy convergence of better than 10^{-6} eV. A Gaussian smearing technique with a 0.2 eV width has been applied to enhance convergence, but all energies presented have been obtained by extrapolating to zero smearing (0 K). Geometry optimization on selected starting geometries obtained from single-crystal X-ray diffraction (for corresponding experimental details) was carried out using a gradient-conjugate method until forces on all atoms were less than 0.3 eV/nm. All calculations have been carried out on a parallel CESA supercomputer.

Results and Discussion

The $La_3(\text{hflpbb})_3$ MOF presents three different polymorphs, named α , β , and γ . The polymorphs α and β tend to appear together in most of the synthesis experiments. Only after a fine adjustment of the hydrothermal conditions (see the Experimental Section) were these two polymorphs obtained as pure phases. The polymorph **La-RPF-4- γ** could not be obtained as a pure phase. Crystals of the monoclinic polymorph **La-RPF-4- β** (isostructural with one of Eu^{2+} recently reported) and orthorhombic polymorph **La-RPF-4- γ** are quite good, and the structures can be easily determined. The orthorhombic polymorph **La-RPF-4- α** , however, is only obtained as fine crystalline powders, with few small twinned crystals in some cases. Powder diffraction patterns of this orthorhombic phase show that the compounds for all rare-earth elements are isostructural and quite similar to that of our Zn(hflpbb) compound previously reported¹⁰ and also to that of, later reported,²⁷ with cell parameters $a = b = 21.32 \text{ \AA}$, $c = 7.71 \text{ \AA}$, and $V = 3009.4 \text{ \AA}^3$.

Only small twinned crystals apt for the structure determination were obtained in the case of the lanthanum compound. The careful analyses of the diffraction pattern gave us another hexagonal cell unit with double a and b and quadruple volume. Only after thorough study of the data could we solve the twin by applying the matrix

$$\begin{pmatrix} 0 & 0 & 1 \\ 1 & 0 & 0 \\ 1 & 2 & 0 \end{pmatrix}$$

(20) SMART System, V.3.04; SHELXTL, V.5.1; Bruker-Siemens Analytical X-ray Instrument Inc.; Madison, WI, 1998.

(21) Kresse, G.; Furthmüller, J. *Comput. Mater. Sci.* **1996**, *6*, 15.

(22) Kresse, G.; Hafner, J. *Phys. Rev. B* **1993**, *47*, 558.

(23) Perdew, J. P.; Wang, Y. *Phys. Rev. B* **1992**, *45*, 13244.

(24) Perdew, J. P.; Chevary, J. A.; Vosko, S. H.; Jackson, K. A.; Pedersen, M. R.; Singh, D. J.; Fiolhais, C. *Phys. Rev. B* **1992**, *46*, 6671.

(25) Blöchl, P. E. *Phys. Rev. B* **1994**, *50*, 17953.

(26) Kresse, G.; Joubert, D. *Phys. Rev. B* **1999**, *59*, 1758.

(27) Harbuziani, B. V.; Curma, A.; Rey, F.; Atienzar, P.; Jordá, J. L.; Garcia, H.; Ananias, D.; Carlos, L. D.; Rocha, J. *Angew. Chem., Int. Ed.* **2008**, *47*(6), 1080.

to a hexagonal cell quite similar to that of the Zn compound, which drove us to the final orthorhombic cell. The structure could then be solved in the space group $P6mm$ ($a = 7.79 \text{ \AA}$, $b = 21.37 \text{ \AA}$, $c = 37.00 \text{ \AA}$, $V = 6160.2 \text{ \AA}^3$). Subsequently, the presence of three orthorhombic components in the twinned crystal was confirmed and refined to a composition of 47:29:24%. The structure solution was also employed to refine the obtained bulk samples of the compounds with the Rietveld refinement of the X-ray synchrotron data for La¹⁷ and with laboratory X-ray data for the whole family (Figure 1).

Upon determining the crystal structure, the composition of the three compounds was found to be $[\text{La}_2(\text{C}_7\text{H}_6\text{F}_6\text{O}_4)_3]$. The La ion is always nine-coordinated (Table 2). In **La-RPF-4- α** and **La-RPF-4- γ** , the asymmetric unit comprises one-half of the formula, while in **La-RPF-4- β** , there are two independent La atoms, and therefore one molecular formula per unit cell. In the three structures, chains of La atoms are formed along the a axis via the μ_2 oxygen atoms (Figure 2, bottom). The anions link these chains, giving rise to 3D structures.

In the case of **RPF-4- α** , a channelled structure with three parallel tunnels down the a axis is formed. Two of the channels are square-shaped (A and B), and one is hexagonal (C; Figure 3). All of these channels are empty and have a free void cylindrical space with a window of diameters 5.2–5.5 Å, as computed by Platon²⁸ (cavity routine). Although the structure looks quite similar to that of the previously reported zinc compound,¹⁰ it has a different topology. The network of the Zn compound is unimodal four-connected (short symbol (6³.8)), while in the La compound, the net is unimodal five-connected. Each node/La ion is directly connected to two other La ions of the same chain via bridging carboxylate oxygen atoms of the ligand, and also to three other La ions from different chains via the whole ligand as linkers. The result is a net with a point symbol of (4².6³) (this net has been recently found in a search for net relations^{29,30} and named **hxg-d-5-Imma**²¹); topological analysis was performed using TOPOS.^{31,32} In contrast to what happened for the Zn compound, where all of the metallic chains are connected through the ligand anions in a crossing way, in the Ln compounds, these connections are established in two different manners: two of them crossing (for the channels of A-type) and one parallel (for the channels of B-type) (Figure 3, right). The different distribution of the A and B channels breaks the hexagonal symmetry and explains the preference for triple twins. Due to the bent geometry of the ligand, its central atom being a sp^3 carbon, the fluorine atoms are all pointing into the C hexagonal channels. Consequently, the walls of the hexagonal tunnel are formed by CF_3 groups, giving rise to hydrophobic fluoro-lined Teflon-like channels.

The two other polymorphs (Figure 4) exhibit a more dense structure, with smaller cell volumes than the first structure; **RPF-4- α** has a cell volume of $6160.2(13) \text{ \AA}^3$, with

(28) Spek, A. L. *PLATON*; Utrecht University, Utrecht, The Netherlands, 2007.

(29) Blatov, V. A. *Acta Crystallogr., Sect. A* **2007**, *63*, 329.

(30) VS [4.4.6.6.6; 6.6.6.6.6.6] and coordination sequence (5,18,45;82,128;190;262;340;437;540).

(31) Blatov, V. A. *IUCr Commission Newsletter* **2006**, *7*, 4. <http://www.tpos.ssa.suunra.ru> (accessed Apr 2009).

(32) Blatov, V. A.; Carlucci, L.; Ciani, G.; Proserpio, D. M. *CrystEngComm* **2004**, *6*, 377.

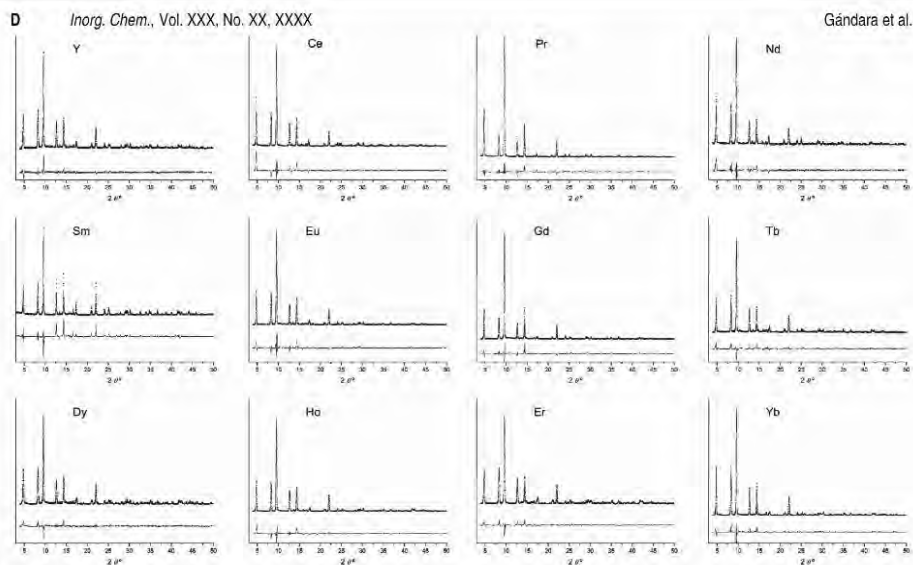


Figure 1. Rietveld refinement of the **La-RPF-4- α** structure showing experimental (dot), simulated (line), and difference patterns.

Table 2. Interatomic Distances in the Coordination Sphere of the Three **La-RPF-4** Polymorphs

RPF-4-α^a		RPF-4-β^b		RPF-4-γ^c	
La(1)–O(1)	2.443(12)	La(1)–O(12)#a	2.473(7)	La(2)–O(10)	2.470(7)
La(1)–O(6)#a	2.443(12)	La(1)–O(6)	2.491(7)	La(2)–O(8)#b	2.487(8)
La(1)–O(2)#a	2.456(14)	La(1)–O(9)	2.499(8)	La(2)–O(11)	2.500(8)
La(1)–O(4)	2.467(11)	La(1)–O(1)	2.501(8)	La(2)–O(2)	2.536(7)
La(1)–O(3)#b	2.471(12)	La(1)–O(4)#a	2.501(7)	La(2)–O(3)	2.539(7)
La(1)–O(5)	2.560(12)	La(1)–O(7)	2.526(8)	La(2)–O(5)	2.568(8)
La(1)–O(6)	2.668(11)	La(1)–O(10)	2.622(7)	La(2)–O(4)	2.612(7)
La(1)–O(2)	2.712(13)	La(1)–O(2)	2.658(7)	La(2)–O(12)	2.616(7)
La(1)–O(3)	2.769(11)	La(1)–O(8)	2.803(7)	La(2)–O(6)	2.677(7)
				La(1)–O(6)#b	2.505(10)
				La(1)–O(4)#a	2.505(11)
				La(1)–O(1)	2.521(10)
				La(1)–O(3)	2.533(11)
				La(1)–O(2)#b	2.545(12)
				La(1)–O(5)	2.578(10)
				La(1)–O(6)	2.637(10)
				La(1)–O(1)#b	2.675(11)
				La(1)–O(4)	2.878(11)

^aSymmetry transformations used to generate equivalent atoms. #a: $x - 1/2, -y + 1, z$; #b: $x + 1/2, -y + 1, z$. ^bSymmetry transformations used to generate equivalent atoms. #a: $x + 1, y, z$; #b: $x - 1, y, z$. ^cSymmetry transformations used to generate equivalent atoms. #a: $x - 1/2, -y - 1/2, -z$; #b: $x + 1/2, -y + 1/2, -z$.

a 23.8% of free volume, while those for **RPF-4- β** and **RPF-4- γ** are 5583.6(4) Å³ and 5235.7(10) Å³, with a free volume of 15.9% and 3.7%. The networks of **RPF-4- β** and **RPF-4- γ** can also be simplified as rods of La atoms, running along the *a* axis. The ligand is then considered as a linker between two La nodes from different chains. Opposite of **RPF-4- α** , where all of the interchain connections are made through two linkers, above and below the chains, in **RPF-4- β** and **RPF-4- γ** , there is a connection between chains which is made only by one ligand: in **RPF-4- β** , along the *b* axis and, in **RPF-4- γ** , along the *c* axis. The joining along the remaining direction is made by two linkers, above and below the chains. However, this connection is different in each case: in **RPF-4- β** , they are all made in a parallel mode, with no edge-crossing presence, while in **RPF-4- γ** , they are all arranged in an edge-crossing manner (Figure 2, top). As a result, these two networks, also uninodal pentacoordi-

nated, have different unprecedented topologies³³ with a point (Schläfli) symbol of (4⁶.6⁴.8²) for **RPF-4- β** and (6¹⁰) for **RPF-4- γ** . Notwithstanding that the infinite chains give simple rod packings for all three compounds (α , hexagonal type I, β and γ square type II),³⁴ the bent ligands give a final topology more complex than the simplest possible five-connected bnn and six-connected pcu nets derived from two such kinds of rod packings.

(33) RPF-4- β : vertex symbol, [4.4.4.4.6.6.6.8₁₃.8₁₃*]; coordination sequence, (5:16:45:96:169:264:377:508:657:824). RPF-4- γ : vertex symbol, [6₁.6₁.6₁.6₁.6₁.6₁.6₁.6₁.6₁.6₁]; coordination sequence, (5:20:52:112:188:284:391:516:653:808). The maximum symmetry embedding of the nets (the "ideal nets") observed in the polymorphs α and γ present edge-crossings similar to the 3D net in the Zn derivative (ref 10) and the two-periodic 3D in the In layers (ref 16). Such crossings are avoided in the real structures due to the flexible ligands that bend over.

(34) Rosi, N. L.; Kim, J.; Eddaoudi, M.; Chen, B.; O'Keefe, M.; Yaghi, O. M. *J. Am. Chem. Soc.* **2005**, *127*, 1504.

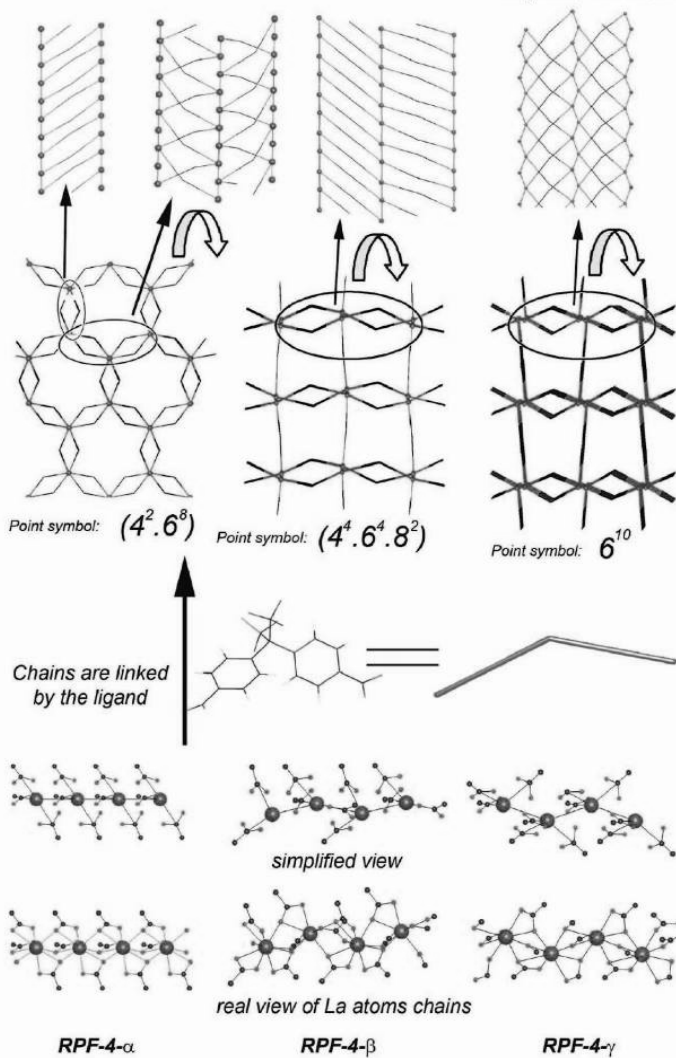


Figure 2. Topological analysis of the three RPF-4 polymorphs.

The three nets can also be compared in other ways, describing layers of square (more or less deformed) channels, parallel to the ab plane for the α and the β , and to the ac plane in the case of γ polymorph (figure 5). Thus, in both α and γ polymorphs, the layers are ligand-crossed. In the γ polymorph, the layers stack on 010 joined by the remaining ligand; in the α polymorph, the layers are

undulated, stacking on 001 and joined by the no crossing ligands. Actually, in this α polymorph, we can also find the undulated layers containing the square channels by rotating the cell $\pm 60^\circ$ over the a axis, but then the distribution of the crossing and no crossing ligands is different, which may be the cause of the triple twinning in this structure.

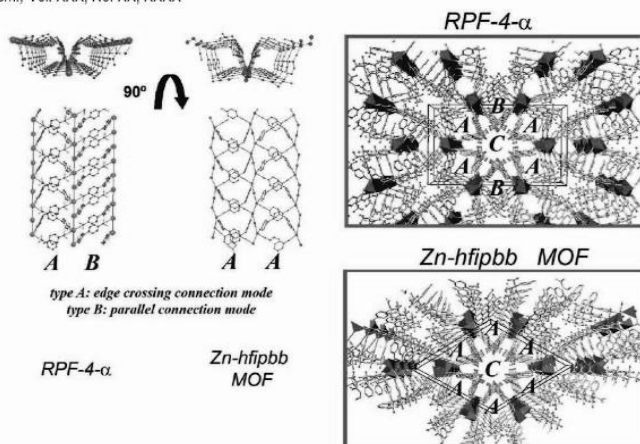


Figure 3. Comparison between RPF-4- α and Zn-hfipbb MOFs.

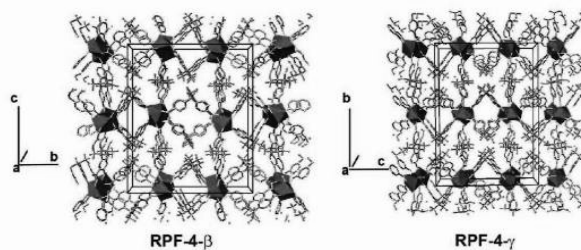


Figure 4. A view of the two new La-hfipbb polymorphs.

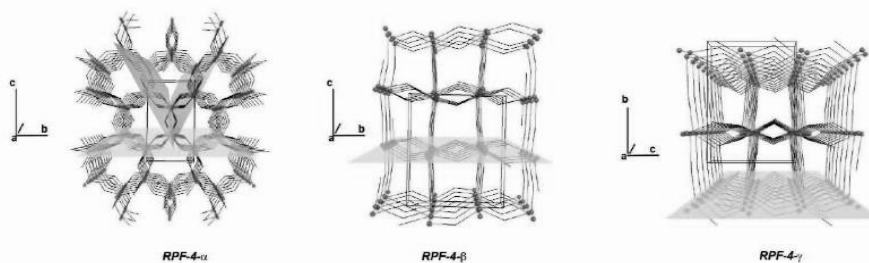


Figure 5. Comparison of the three simplified networks. Layers containing the La atoms and the square channels are represented. In the case of the α polymorph, the two other possible orientations for these planes, the cause of the twinning, are shown with different colors.

Conformational and energetic DFT-based calculations are commonly used in several chemistry fields as organic and inorganic systems. In the case of MOFs, the majority of works that raise these studies are performed using molecular mechanics calculations, due to the size of these systems. Only

a limited number of studies use an ab initio DFT methodology. DFT plane wave periodic calculations have been extensively performed in solid-state chemistry (perovskites and catalysts, among others) because they offer a better interpretation of periodic solid frameworks. However, these

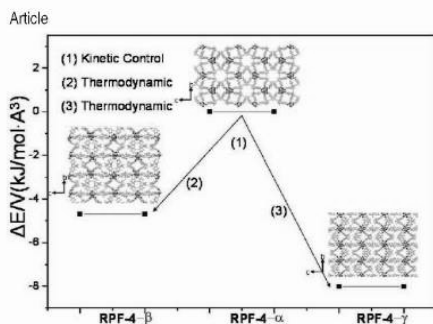


Figure 6. Energy gap diagram of different polymorphs, obtained by DFT calculations.

studies are much less applied to MOF materials, although some groups have begun to use these kinds of methods.³⁵

A study of the relative energies of the three polymorphs in the La–hfipbb RPF-4 system has also been carried out. The geometry optimization always converged to a stable structure with the same topology that the experimental structures exhibited as obtained by X-ray diffraction, even though no symmetry constraints were imposed. As observed in Figure 6 and taking into account the experimental results, the α polymorph is a metastable structure kinetically controlled. The changes of the synthesis conditions give rise to the other two different polymorphic phases (that often are observed together with α). The DFT calculation shows that these crystal polymorphs (β and γ) are more stable than α , and therefore they are thermodynamically controlled.

(35) (a) Keskin, S.; Liu, J.; Rankin, R. V.; Karl Jhonson, J.; Sholl, D. S. *Ind. Eng. Chem. Res.* **2009**, *48*, 2355 and references therein. (b) Coombes D. S.; Cora, F.; Mellot-Draznieks, C.; Bell, R. G. *J. Phys. Chem. C* **2009**, *113*, 544. (c) Sillar, K.; Hofmann, A.; Sauer, J. *J. Am. Chem. Soc.* **2009**, DOI: 10.1021/ja8099079.

The solution-phase synthesis, especially hydro- or solvothermal synthesis, is often controlled kinetically, giving rise to the growth of metastable phases. Thus, the optimization of the synthesis conditions is critical and can play a crucial role in the design of thermodynamically unstable unknown structures with interesting properties that are technologically useful.

Conclusions

In summary, up to three polymorphs can be obtained in the La–hfipbb system. The crystal structures for the three of them have been solved and refined, including one with a triple twinned structure. The structural and topological analysis here reported demonstrate that the use of a versatile ligand such as hfipbb can lead to the formation of different networks with different features, some of them with very interesting properties, as it has been already reported.¹⁷ In addition, the energetic calculations carried out for the three compounds demonstrate that the most frequently found structure is a metastable phase, which appears to be, next to others, thermodynamically more stable. The formation of this metastable phase is controlled by kinetic factors, and it can be obtained purely with a fine control of the synthesis conditions.

Acknowledgment. F.G. acknowledges an FPI fellowship from Ministerio de Educación y Ciencia (MEC) and Fondo Social Europeo from the EU. This work has been supported by the Spanish MCYT Project Mat 2007-60822, CTQ 2007-28909-E/BQU, and Consolider-Ingenio CSD2006-2001. Generous allocation of computational time on the CESCA supercomputer of the Centre de Supercomputació de Catalunya is gratefully acknowledged.

Supporting Information Available: X-ray crystallographic files in CIF format. This material is available free of charge via the Internet at <http://pubs.acs.org>.



DOI: 10.1021/cg900704c

Isolated Hexanuclear Hydroxo Lanthanide Secondary Building Units in a Rare-Earth Polymeric Framework Based on *p*-Sulfonatocalix[4]arene

Felipe Grándara, Enrique Gutiérrez-Puebla, Marta Iglesias, Natalia Snějko, and M. Angeles Monge*

Instituto de Ciencia de Materiales de Madrid (ICM), CSIC, C/Sor Juana Inés de la Cruz 3, 28049 Madrid, Spain

Received June 23, 2009; Revised Manuscript Received September 15, 2009

ABSTRACT: RPF9 is a new family of catalytically active metal–organic frameworks (MOFs) prepared with rare-earth elements and *p*-sulfonatocalix[4]arene, hexanuclear hydroxo lanthanide clusters forming the secondary building units in an open-framework with two-dimensional channels. The synthesis, characterization, and evaluation of sorption properties and catalytic activity of this new rare-earth polymeric framework type are here described.

Introduction

Calixarenes and their analogues are fascinating basket-shaped compounds that possess the ability to hold metal ions, as well as molecules, in their interior.^{1–3} In the solid state, the cone shapes of the calixarenes give bowl cavities that can encapsulate some small molecules, both charged and neutral, by weak interactions including H-bonding, H–aromatic, etc., so these compounds have been widely regarded as important macrocyclic host molecules in host–guest chemistry.^{4–8} As a result of their very easy synthesis from phenols and aldehydes,^{9–11} they are receiving increasingly wide attention. Water-soluble calixarenes have been exploited in all areas of supramolecular chemistry over the past two decades.^{12–18} Some reports deal with complexes or coordination polymers of *p*-sulfonatocalix[4]arenes with transition metals^{19–26} in the case of rare earth elements (REEs), not many reports can be found, most being dedicated to isolated complexes or those linked through weak interactions (H bond or $\pi-\pi$). On the other hand, the synthesis of inorganic clusters continues attracting considerable attention, due to the interesting properties of the metallic aggregates.^{27,28} Rare earth element clusters still remain less studied than those of transition metals. The control of the hydrolysis of the lanthanide salts in the presence of appropriate ligands appears as a common strategy for the synthesis of hydroxo lanthanide clusters. However, the cluster-forming ability of *p*-sulfonatocalix[4]arenes as multidentate and multimetalating ligands has not been described up to now. Such ability has been discovered for thiacalix[4]arenes,²⁹ in which the introduction of the S heteroatom enforces significantly a coordinative capacity of the ligand molecule. Only tri- and tetranuclear clusters were found to be supported by thiacalix[4]arenes and only up to pentanuclear clusters by a larger and more flexible thiacalix[6]arene. Octalanthanide and dodecalanthanide wheels were reported to be supported by *p*-tert-butylsulfonocalix[4]arene.^{30,31}

Among the lanthanide clusters, the hexanuclear hydroxo lanthanide cluster of the M₆X₈ type appears as a common

unit, both as an independent cluster and as a core of a larger aggregate. In this M₆X₈ hydroxo lanthanide cluster, the Ln atoms are disposed octahedrally, linked by μ_3 -OH⁻ groups, and in most cases with a central μ_6 oxygen atom. This latter has been suggested to have an influence on the stability of the Ln₆ units, but some examples of octahedral Ln₆ aggregates can be found without it.^{32–35} Despite that the hydroxo lanthanide clusters in most of the examples are discrete units, a great effort is being done to incorporate these types of lanthanide aggregates into polymeric frameworks,^{36–38} and in many cases, they are in combination with transition metals in the framework.^{37,40–45} The utilization of metal aggregates as secondary building units (SBU's) is a common strategy in the preparation of metallorganic frameworks.⁴⁶ However, when sulfonate derivative ligands are used, the most common pattern is the formation of inorganic chains or layers,^{44,45} and there are few examples of structures with a discrete inorganic SBU.⁴⁶ In this paper, we present the synthesis, crystal structure, and catalytic activity study of the first example of a rare earth polymeric framework (RPF) composed of hexanuclear hydroxo-lanthanide clusters and *p*-sulfonatocalix[4]arene.

Experimental Section

Synthesis. The products were obtained under hydrothermal conditions. The molar composition of the initial mixture was 11n/14.5/300(1.0/9) Sr₂N (pH = 8). The Ln³⁺ ions were added in their hydrate nitrate form. H₂L is the calix[4]arene *p*-sulfonic acid. In a typical synthesis, 0.197 g of Ln(NO₃)₃·6H₂O and 0.117 g of H₂L are solved in 13.5 mL of water. Et₃N (0.18 mL) is then added, and the solution is magnetically stirred at room temperature for 5 min. After this, the solution is placed into a Teflon lined stainless steel autoclave and heated at 160 °C for 10 h. After cooling to room temperature, the product is filtered, then washed with water and acetone and dried in air. Equivalent synthesis procedures are carried out employing Pr(NO₃)₃·6H₂O and Nd(NO₃)₃·6H₂O to obtain the corresponding products. The pH control seems to be critical: experiments with pH values lower or higher than 8 were unsuccessful, and no product was obtained. The product appears with good yield after only 5 h of heating. With heating times longer than 10 h, the yield decreases significantly (36% yield after 20 h), suggesting that the product decomposes in the reaction media. Under these synthesis conditions, obtaining products with smaller lanthanides was unsuccessful. Only in the case of ytterbium, a few crystals were

*To whom correspondence should be addressed. E-mail: amonge@icmm.csic.es.

obtained with slightly modified conditions: a mixture of molar composition $10Yb/HfL_{10}9000H_2O$ heated at 160 °C for 24 h. For the La, Pr, and Nd preparations, only a few single crystals were obtained in the case of Pr and Nd, and in all cases, they were very small crystals.

Single-Crystal X-ray Diffraction. A small, square-shaped crystal of each product was selected and glued on a glass fiber for X-ray diffraction experiments. X-ray intensity data were collected in a Bruker D8 diffractometer equipped with an Axien detector and a X-ray microsource (Cu K α radiation = 1.54178 Å) and in a Bruker SMART CCD diffractometer equipped with a normal focus, 2.4 kW sealed tube X-ray source (Mo K α radiation = 0.71073 Å). Data were collected at room temperature by a combination of several sets of exposures. Each exposure of 20 s covered 0.5° or 0.3° in θ . Unit cell dimensions were determined by a least-squares fit of 60 reflections with $I > 3\sigma(I)$. The structures were solved by direct methods. The final cycles of refinement were carried out by full-matrix least-squares analyses with anisotropic thermal parameters for all non-hydrogen atoms except for the disordered water molecules. Hydrogen atoms were geometrically calculated. Up to three different single crystals of RPF9 were measured, three of them of Pr and one of Nd. In the Pr compound, the coordinated oxygen O8 of the water molecule is disordered in two positions with relative occupancy factor of 0.7/0.3, and the occupancy factor of the coordinated water molecule O6 was refined to 0.4; in the Nd and Yb crystals, no disorder was found for the coordinated water molecules. In the three cases, a solvent water molecule was also located. Calculations were carried out with APEX II and SMART software for data collection and data reduction and SHELXTL for the structure solution and refinement. The small size and bad quality of the crystals, especially in that of Yb, did not allow better refinements.

X-ray Powder Diffraction. X-ray powder patterns were measured in a D8 Bruker diffractometer with a step size of 0.2° and an exposure time of 2 s/step. For the thermogravimetric experiments, the samples were heated at a rate of 5 °C/min, and after 10 min heating, the powder patterns were collected. At 125 °C, the sample was heated for 65 min, measuring the diffraction patterns at several times until no changes in the patterns were observed.

Catalytic Activity Experiments. One millimole of methyl phenyl sulfide was added to a suspension containing the corresponding amount of catalyst (ratio Ln/substrate = 1:1000) in 5 mL of acetonitrile. The suspension was heated to 80 °C under stirring, and then hydrogen peroxide (H $_2$ O $_2$ 50%, 3 mmol) was added dropwise. At selected intervals of time, the grade of conversion was measured in a gas chromatograph. A powder X-ray pattern of the catalyst was measured after the reaction to check that the structure did not suffer any change.

After the reaction cycles, the catalyst was separated by decantation of the solution and re-used with fresh solvent and substrate, starting a new cycle of reaction when the oxidizing agent is added. While the oxidation of sulfide continued in presence of the catalysts, there was no further significant conversion when the catalyst was removed from the reaction system. The blank experiments, carried out in absence of catalyst, showed no conversion after 4 h.

Surface Area Analysis and Gas Sorption Properties. Specific surface area and pore size distribution were determined by nitrogen adsorption-desorption isotherms at 77 K obtained on a Microsorbitics TriStar 3000 sorptometer. Before adsorption measurements, the sample was outgassed at 383 K. N $_2$ adsorption isotherms were performed in the relative pressure range of 10^{-5} to 1 atm. The gas adsorption studies with H $_2$, CH $_4$, and CO $_2$ were performed using a Hiden Isochem (Warrington, U.K.) intelligent gravimetric analyzer (IGA) equipped with a microgram balance, and two baratron pressure transducers in the ranges 0–2 mbar and 0–10 bar were used to monitor the pressure. The microbalance had a long-term stability of $\pm 1 \mu\text{g}$ with a weighing resolution of 0.2 μg . These measurements were carried out using high purity gases. The gas entrance was made by means of a BRONKHORST mass flow controller. All isotherms were measured to 1 bar at 304 K. The sample was outgassed under high vacuum at 403 K prior to the admission of any gas into the system. The buoyancy effects were corrected as a function of temperature taking into account the void

Table 1. Main crystallographic and refinement data for Pr- and Nd-RPF9 compounds

identification code	Pr-RPF9	Nd-RPF9
empirical formula	C $_2$ H $_2$ O $_2$ Ln $_2$ (Pr, Nd)	C $_2$ H $_2$ O $_2$ Nd $_2$ (Pr, Nd)
formula weight	1391.61	1593.56
temp, K	296(2)	296(2)
wavelength, Å	1.54178	1.54178
crystal system	tetragonal	tetragonal
space group	<i>I</i> 4/m	<i>I</i> 4/m
unit cell dimensions		
<i>a</i> , Å	11.9761(3)	11.9612(6)
<i>b</i> , Å	11.9761(3)	11.9612(6)
<i>c</i> , Å	11.399(1)	11.377(1)
α , deg	90	90
β , deg	90	90
γ , deg	90	90
vol, Å 3	1503.5(2)	1488.5(6)
Z	4	4
calcd density, Mg/m 3	2.035	2.062
abs coeff, mm $^{-1}$	27.075	28.650
<i>F</i> (000)	2276	2720
crystal size, mm 3	0.045 × 0.03 × 0.03	0.02 × 0.02 × 0.01
θ range for data collection, deg	3.95–60.29	2.82–59.66
limiting indices	$-11 \leq h \leq 9$ $-9 \leq k \leq 13$ $-35 \leq l \leq 35$	$-13 \leq h \leq -13$ $-13 \leq k \leq 17$ $-27 \leq l \leq 34$
reflns collected/unique	6560/1623	6701/1660
completeness	$\theta = 59.50$ 96.0%	$\theta = 59.66$ 97.6%
abs corr.	semiempirical from equivalents	
max and min transmission	0.6140 and 0.4111	0.7626 and 0.5981
refinement method	full-matrix least squares on <i>F</i> 2	
data/restraints/params	1523/0/132	1660/0/141
GOE on <i>F</i> 2	1.047	0.892
final <i>R</i> indices	$R_1 = 0.0389$, $wR_2 = 0.11166$	$R_1 = 0.1002$, $wR_2 = 0.1989$
<i>R</i> indices (all data)	$R_1 = 0.0461$, $wR_2 = 0.1205$	$R_1 = 0.1209$, $wR_2 = 0.2163$
largest diff. peak and hole, e $^-$ Å $^{-3}$	1.129 and -0.872	1.932 and -1.880

volume of the cell determined with He gas at 77 K and assuming that the amount of He adsorbed is negligible.

Results and Discussion

The RPF9 crystal structure was solved in the tetragonal system, space group *I*4/m (Table 1). There are two crystallographically independent Ln atoms; one of them (Ln1) is on a 4-fold axis and coordinated to four μ_2 -OH $^-$ groups, four O atoms from SO $_4$ groups, and, in the case of the Pr crystals, a water molecule with occupancy factor lower than one. The other lanthanide atom (Ln2) coordinates to four μ_2 -OH $^-$ groups, two oxygen atoms from two SO $_4$ groups, and two water molecules, one of them disordered in two positions in Pr crystals. This arrangement gives rise to the formation of hexameric clusters, in which the octahedrally disposed lanthanide atoms are joined through eight μ_2 -OH $^-$ groups to give rise to a rhombic dodecahedron (Figure 1). This type of cluster, which has already been reported in other lanthanide compounds, is depicted in most cases with a central oxygen atom coordinated to the six Ln atoms.^{47–50} There are also some examples in which this central atom does not appear in the cluster.^{51,52} In the present metal-organic frameworks (MOFs), a high electronic density was located at the center of the cluster, which was effectively assigned to an oxygen atom. The structure of three different Pr crystals and one Nd crystal were refined, finding this atom in all of them, and its

Article

Crystal Growth & Design, Vol. XXX, No. XX, XXXX C

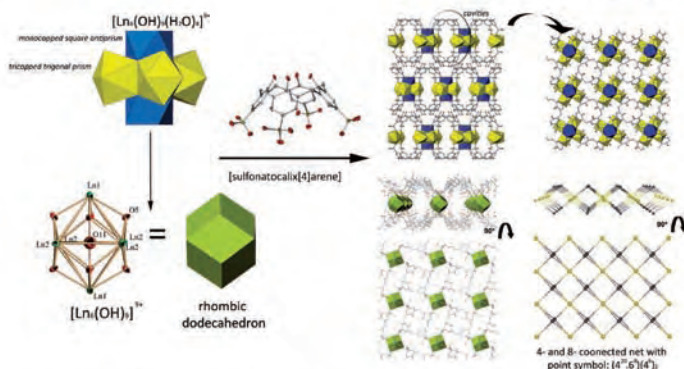


Figure 1. Representation (top left) of the real coordination polyhedra on the Ln atoms, view (top right) of the structure along the *a* axis and projection of one double layer in the *ab* plane, ORTEP representation (bottom left; 50% probability) of the Ln and O atoms in the cluster and their representation as rhombic dodecahedron, and perspective view (bottom right) of a double layer (water molecules are omitted for clarity) and its topological representation.

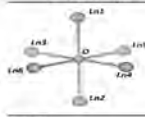
thermal parameters showed in all cases relatively high values, which is unexpected for a hexacoordinated O atom (see Figure 1, left). The population factors refinement indicated total occupancy for this atom in all cases. In order to allow differences in the Ln–O distances and at the same time to study the possibility that the high thermal parameter values for the central oxygen are due to pseudosymmetry effects (they are positioned on a 4-fold center), the crystal structure for the compounds was also refined in *P1*, in the primitive cell with parameters $a = 17.839 \text{ \AA}$, $b = 17.839 \text{ \AA}$, $c = 11.988 \text{ \AA}$, $\alpha = 109.63^\circ$, $\beta = 109.63^\circ$, $\gamma = 123.26^\circ$, and cell volume = 2255.7 \AA^3 resulting from applying the matrix $(-0.5a - 0.5b - 0.5c; -0.5a - 0.5b + 0.5c; b)$ to the tetragonal cell. The results of these refinements confirmed the occupancy obtained for this atom in the *I4/m* space group and showed that effectively this oxygen atom position is slightly shifted from the rhombic dodecahedron center, bearing a considerable anisotropy in the direction in which (as we will see later) the hydrogen atom could be situated.

Oxygen or Hydroxyl Group? Another matter related to the presence of central oxygen in the hydroxo cluster is the chemical nature of this atom. All papers reporting this type of hexanuclear Ln cluster with a central oxygen atom indicate that this is an O^{2-} anion. An exception is LnPF-3,⁵¹ a MOF previously prepared in our group with 2,6-naphthalenedisulfonate as ligand and with framework composition $[\text{Nd}_4\text{Ln}(\text{OH})(\text{H}_2\text{O})_4]$. In LnPF-3, the oxygen atom is clearly identified as OH^- not only on the basis of the structural data but also on the electrical neutrality. Regarding to the charge balancing in RPF9, in the H_3L ligand, there are five acidic hydrogen atoms, four of them coming from the sulfonate groups and the fifth from one phenolic group.⁵² If the central oxygen atom were an O^{2-} , all the ligands should be HL^+ , if it were a hydroxyl group, there should coexist HL^+ and L^{3-} species, and in the absence of this atom, all the ligands should be in the L^{3-} form. Under our synthesis conditions ($\text{pH} \approx 8$), the major protonation state of the ligand is L^{3-} , being

difficult to find all the ligands as HL^+ species. This makes possible the presence of a hydroxyl group instead of an O^{2-} ion. We therefore consider that the obtained composition could be $[\text{Ln}_4(\text{OH})(\text{HL})(\text{L})(\text{H}_2\text{O})_4]$ ($\text{Ln} = \text{La, Pr, and Nd}$; $8 < y < 9$), with one-half of the calixarene molecules monoprotonated. The presence of a hydrogen atom in the OH^- central group is also sterically feasible. In LnPF-3,⁵¹ the hydrogen atom is positioned along one of the Ln–O longest distance (Table 2). In the RPF9 case, the interatomic Ln– μ_6 -O distances are symmetrically related in the tetragonal cell. However, the results of the *P1* refinements for all the crystals demonstrate that a hydrogen atom could be accommodated inside the cluster and placed along one of these O–Ln longest distances, which also could justify the high anisotropy of this oxygen atom.

Additionally, bond valence calculations also support the assignment of the central O atom as a hydroxyl group. With the bond valence method,⁵³ the formal oxidation state of an atom in a crystal is calculated according to valence-sum rule: $V_i = \sum_j v_{ij}$. The parameter v_{ij} is the bond valence value, and it is related to the bond length between nearest-neighboring atoms *i* and *j* (d_{ij}). It has the expression $v_{ij} = e^{(R_0 - d_{ij})/b}$; b is a constant⁵⁴ with value 0.37 Å. R_0 is known as the bond-valence parameter, and it is calculated for each element in a given oxidation state. We have performed the calculations with the R_0 values calculated for lanthanide compounds by Breese and O’Keeffe⁵⁵ and by Trzesowska et al.⁵⁶ We have carried out the bond valence sum calculations of the central oxygen atom with the RPF9 crystal data, as well as with other reported compounds in which an μ_6 -O atom is present,^{57–61} either as O^{2-} or as OH^- . The bond valence sum values of the RPF9 compound are in the same range as those of the LnPF-3 compound and other reported μ_6 -OH groups and lower than those corresponding to other reported μ_6 - O^{2-} atoms (see Table 3).

On the other hand, attempts to obtain RPF9 with smaller lanthanides under the current synthesis conditions only gave

Table 2. Comparison of the Interatomic O–La Distances for the *I4/m* and *P1* Refinements and Those of the LnPF-3 Compound (Ref 51)^a


	Pr-RPF9, crystal a		Pr-RPF9, crystal b		Pr-RPF9, crystal c		Nd-RPF9		Nd-LnPF-3_ref 51
	<i>I4/m</i>	<i>P1</i>	<i>I4/m</i>	<i>P1</i>	<i>I4/m</i>	<i>P1</i>	<i>I4/m</i>	<i>P1</i>	
O–Ln1	2.691	2.656	2.655	2.624	2.609	2.449	2.567	2.562	2.645
O–Ln2	2.691	2.725	2.655	2.692	2.609	2.901	2.567	2.600	2.645
O–Ln3	2.769	2.701	2.751	2.886	2.756	2.779	2.678	2.440	2.764
O–Ln4	2.769	2.860	2.751	2.620	2.756	2.771	2.678	2.917	3.174
O–Ln5	2.769	3.051	2.751	2.790	± 6	2.627	2.688	2.688	2.688
O–Ln6	2.769	2.489	2.751	2.719	2.756	2.902	2.678	2.800	2.688

^a The pairs of distances with a higher variation in the *P1* refinement and the one along which the H atom is found in the LnPF-3 compound are marked in bold.

Table 3. Comparison of the Bond Valence Sum of the $\mu_6\text{-O}$ Atoms. Calculated with the R_b Bond-Valence Parameters Reported by Trzesowska et al.⁵⁸ and by Breese and O’Keefe⁵⁹

compound	$\mu_6\text{-O}$ atom bond valence sum		
	R_b by Trzesowska et al.	R_b by Breese and O’Keefe	
Nd-LnPF-3 [ref 51]	1.006(1)	1.094(1)	
Eu-LnPF-3 [ref 51]	0.994(9)	1.102(10)	
Nd-RPF9	<i>I4/m</i>	1.253(5)	1.471(4)
	<i>P1</i>	1.305(12)	1.420(13)
Pr-RPF9, crystal a	<i>I4/m</i>	1.056(2)	1.167(2)
	<i>P1</i>	1.006(10)	1.171(11)
Pr-RPF9, crystal b	<i>I4/m</i>	1.129(1)	1.248(1)
	<i>P1</i>	1.087(33)	1.201(37)
Pr-RPF9, crystal c	<i>I4/m</i>	1.105(3)	1.221(4)
	<i>P1</i>	1.177(24)	1.301(27)
[Nd(NO ₃) ₃] ₂ (Nd(L) ₂ ($\mu_6\text{-OH}$)) ⁶⁰	1.006(1)	1.094(1)	
Eu ₂ (OH) ₂ (H ₂ O) ₂ O ₂ C–C–H ₄ CO ₂ H ⁶¹	1.163(14)	1.289(16)	
[Yb ₂ (CH ₃ CO ₂ S ₂) ₂ (OH) ₂ (H ₂ O) ₂] ⁶²	1.634(0)	1.685(2)	
[DMF] ₂ Yb ₂ ($\mu_6\text{-O}$)($\mu_2\text{-OH}$) ₂ ⁶³	1.462(3)	1.807(4)	
(μ -NC) ₂ (μ -CN) ₂ (μ -CN) ₂ [Pd(CN) ₄] ⁶⁴			
[C(Me) ₃ (Sm) ₂ O ₂ H ₂] ⁶⁵	1.752(8)	1.874(9)	

^a L = 1-azobisindaneethanol Nd compound including a $\mu_6\text{-OH}$ group [ref 57]. ^b Eu compound including a $\mu_6\text{-OH}$ group [ref 58]. ^c Yb compound including a $\mu_6\text{-O}$ atom [ref 59]. ^d Yb compound including a $\mu_6\text{-O}$ atom [ref 60]. ^e Sm compound including a $\mu_6\text{-O}$ atom [ref 61].

a few crystals of the Yb compound. The crystal structure showed that the Yb compound belongs also to the RPF9 family but in this case without any electron density at the center of the cluster, the formula being thus [Yb₂(OH)₂–L₂(H₂O)₂] with all the ligand molecules completely deprotonated (L²⁻). All in all, we do not rule out the possible existence of an O²⁻ anion, but we opt for the presence of a hydroxyl group inside the RPF9 clusters, as it is in LnPF-3, or even the coexistence of both, depending on a narrow pH value synthesis range.

In the new RPF9 MOFs, the usual calixarene up–down “bilayer” arrangement is maintained, and the calixarene molecules are bonded to each other through the hexanuclear Ln clusters. Each [Ln₆(OH)₆] cluster joins eight sulfonato-calixarene ligands through the SO₃⁻ groups. Thus, one sulfonate oxygen atom is bonded to the axial Ln1 atom, another to an equatorial Ln2, and the third remains uncoordinated. The hydroxo-lanthanide clusters located in the *ab* plane are joined to each other through the calixarene anions, up and down this plane. This arrangement gives rise to the formation of double layers with intersecting channels (Figure 1), forming cavities with a maximum height of 11.87 Å (distance between calixarene molecules) and

maximum width of 8.32 Å (distance between clusters). The double layers stack along the *c* direction in an AB sequence, not allowing any channel along this direction. The topology of the double layers is of the Al₂O₃ type, binodal 8 and 4 connected, the clusters being the 8-connected centers and the calixarene anions the 4-connected nodes. The point symbol of this network is (4²⁰.6³)(4⁴)₂ (Figure 1, bottom right). RPF9 is one of the few examples of sulfonate-based MOFs with isolated inorganic SBUs.

The La, Pr, and Nd RPF9 compounds were obtained as pure phases. In Figure 2, the Rietveld refinements for these compounds are shown. The differences in the intensity of the experimental patterns might be attributed to the presence of adsorbed water molecules inside the channels of the structure. These water molecules are responsible for the first mass loss observed in the thermogravimetry (TG) curves. The loss of these water molecules has an influence on the structure. A variable-temperature X-ray powder diffraction study was carried out with the Nd-RPF9 sample. As it can be seen in Figure 3, as the sample is heated, the relative intensity of the peaks varies, due to the progressive loss of the adsorbed molecules. Finally, a phase transition is observed when the sample is heated above 125 °C. The high-temperature powder pattern could be indexed in the tetragonal system with the following parameters: *a* = *b* = 11.600 Å, *c* = 28.276 Å; cell volume = 3793.8 Å³. These parameters are quite similar to those of the original structure, suggesting that after the water molecule evaporate, the rest of the framework should remain without significant changes. The powder pattern of the new crystalline phase, however, is not of sufficient quality to refine the atomic positions in the new cell. The second step in the TG curve at ~240 °C corresponds to the loss of the coordinated water molecules. The total decomposition of the framework, with the loss of the organic part, begins above 350 °C.

Given that the framework remains intact after evacuation of the solvent molecules, the sorption properties of the Nd-RPF9 material have been tested. First, a nitrogen adsorption–desorption isotherm was performed at 77 K in the relative pressure range 10⁻⁵ to 1 atm. The apparent surface area was calculated with these data, obtaining the low BET area value of 13.45 m² g⁻¹. Despite this disappointing value, sorption isotherms were carried out with H₂, CO₂, and CH₄, and for a better comparison, these measurements were performed at 304 K and high pressures. These three isotherms are compared in Figure 4. Despite the low nitrogen sorption exhibited by the material, RPF9 shows a high adsorption of hydrogen, with an uptake of 2.12 mmol·g⁻¹ at

Article

Crystal Growth & Design, Vol. XXX, No. XX, XXXX E

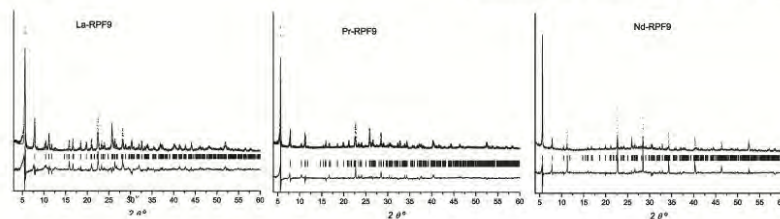


Figure 2. Rietveld refinements for the RPF9 compounds, showing experimental (•••), calculated (—), and difference patterns. Bragg positions are marked as columns.

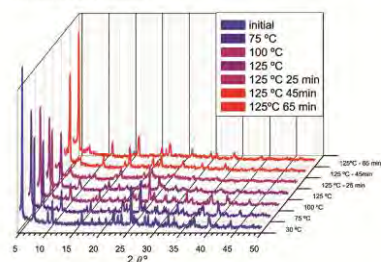


Figure 3. Variable-temperature X-ray diffraction for the Nd-RPF9 compound.

$P = 20$ atm, while the adsorption amounts of CO_2 and CH_4 are $0.92 \text{ mmol} \cdot \text{g}^{-1}$ and $0.24 \text{ mmol} \cdot \text{g}^{-1}$, respectively. These results show that RPF-9 could act as a H_2 absorber due to its high selectivity for this gas, compared with CO_2 or CH_4 adsorption.

The new RPF9 materials have been evaluated as heterogeneous catalysts. In previous work, we have studied the activity of several rare-earth polymeric frameworks as redox heterogeneous catalysts.^{64,65} For this purpose, the selected substrate was methyl phenyl sulfide, which is an appropriate molecule to be used as a model in test reactions. From the comparison of the activity of different RPF families previously reported, we could conclude that for the reaction to take place, an induction period is needed to form the active intermediate species. Furthermore, this species could also be identified as a Ln-peroxo species on the basis of spectroscopic studies.^{64,65} Following with this systematic comparison of the catalytic activity of our families of compounds, we have also evaluated the possibilities of the here-reported compounds, under similar reaction conditions. In the case here presented, the RPF9 new materials exhibit an open-framework, which together with the high nuclearity of the inorganic SBUs makes these compounds good candidates to be used as heterogeneous catalysts. Thus, the three La, Pr, and Nd RPF9 compounds have been tested as catalysts for the oxidation of methyl phenyl sulfide (Table 4). The catalysts were reused at least in three consecutive cycles. As it can be seen in Figure 5, where the kinetic curves are represented, in all three cases an increase in the activity is observed after the first reaction cycle. As explained above,

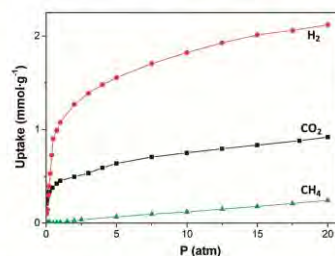


Figure 4. Gravimetric gas sorption isotherms for the uptake of H_2 , CH_4 , and CO_2 at 304 K for the Nd-RPF9 compound.

Table 4. Results of heterogeneous RPF9-catalyzed oxidation of methylphenylsulfide^a

run	La-RPF9			Pr-RPF9			Nd-RPF9		
	1	2	3	1	2	3	1	2	3
TOF (h^{-1})	108	193	509	150	195	212	83	286	870
% sulfoxide	87	95	92	85	86	86	90	92	89

^a Reaction conditions: acetonitrile, 80°C (H_2O_2 , 3 mmol), cat./subs. 1:1000.

this is attributed to the need for an induction period for the formation of the active intermediate, postulated to be an Ln-peroxo species. Thus, in the subsequent cycles, the activity was enhanced, achieving high values of conversion in short periods of time. It is worth pointing out the low amount of the catalyst needed, with a high ratio of substrate to metal (1000:1), and therefore, high values of TOF are obtained. In Table 5, the obtained results are compared with those of the other reported rare earth materials, as well as with the corresponding oxides, showing the good activity evidenced by the RPF9 new materials. After the reaction cycle, the integrity of the catalysts was checked by PXRD. The material was confirmed to be intact.

Conclusions

In conclusion, a new family of rare-earth polymeric frameworks has been obtained in which discrete hydroxo lanthanide clusters act as SBUs, and they are joined by *p*-sulfonatocalix-[4]arene ligands. In the new RPF9 MOFs, the usual calixarene

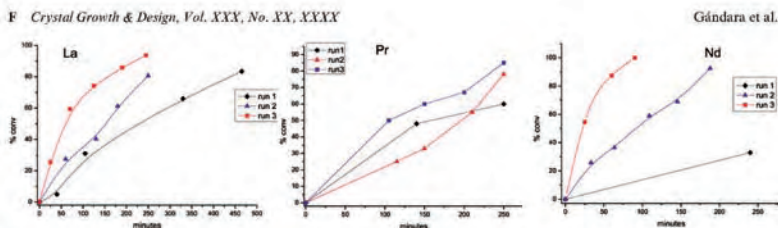


Figure 5. Kinetic curves for the oxidation of methyl phenyl sulfide catalyzed by RPF9 compounds.

Table 5. Average TOF Values (h^{-1}) Shown by Different Catalysts in the Oxidation of Methyl Phenyl Sulfide

family	Ln^{3+}		
	La	Nd	Yb
RPF4(ref 65)	18	20	60
RPF5 (ref 44)		413	241
RPF9 (this work)	270		
LRH (ref 62)			1233
succinate (ref 63)	163.7		457
oxide (ref 63)	100		

up-down "bilayer" arrangement is maintained, to give rise to a $(4^{20}, 6^8)(4^6)$, 4- and 8-connected net. This paper opens the possibility of having a hydroxyl group inside the RPF9 hexanuclear clusters (similar to that existing in LnPF_3). The new materials are active as heterogeneous redox catalysts, and they show selective sorption properties.

Acknowledgment. F.G. acknowledges a FPI fellowship from Ministerio de Educación y Ciencia (MEC, Spain) and Fondo Social Europeo from the EU. This work has been supported by the Spanish MCYT Project Mat 2007-60822, MAT2006-14274-C02-01, and Consolider-Ingenio CSD2006-2001. The authors especially thank Dr. Victor A. de la Peña-O'Shea (IMDEA Energia) for surface area and gas sorption experiments.

Supporting Information Available: X-ray crystallographic files in CIF format. This material is available free of charge via the Internet at <http://pubs.acs.org>.

References

- (1) Orr, G. W.; Barbour, L. J.; Atwood, J. L. *Science* **1999**, *285*, 1049–1052.
- (2) Atwood, J. L.; Barbour, L. J.; Jerga, A.; Schottel, B. L. *Science* **2002**, *298*, 1000–1002.
- (3) Atwood, J. L.; Barbour, L. J.; Jerga, A. *Science* **2002**, *296*, 2367–2369.
- (4) Qin, D. B.; Xu, F. B.; Li, Q. S.; Song, H. B.; Zhang, Z. Z. *Synlett* **2005**, 2987–2989.
- (5) Gutsche, C. D. *Calixarenes: Monographs in Supramolecular Chemistry*; The Royal Society of Chemistry: Cambridge, U.K., 1989.
- (6) Masci, B.; Mortera, S. L.; Persiani, D.; Thuéry, P. *J. Org. Chem.* **2006**, *71*, 504–511.
- (7) Saha, A.; Nayak, S. K.; Chottopadhyay, S.; Mukherjee, A. K. *J. Phys. Chem. B* **2004**, *108*, 7688–7693.
- (8) Turner, B.; Shterenberg, A.; Kapon, M.; Suwinska, K.; Eichen, Y. *Chem. Commun.* **2001**, 13–14.
- (9) Gutsche, C. D.; Levine, J. A. *J. Am. Chem. Soc.* **1982**, *104*, 2652–2653.
- (10) Gutsche, C. D.; Dhawan, B.; No, K. H.; Muthakrishnan, R. *J. Am. Chem. Soc.* **1981**, *103*, 3782–3792.
- (11) Atwood, J. L.; Coleman, A. W.; Zhang, H.; Bott, S. G. *J. Inclusion Phenom.* **1989**, *7*, 203–211.
- (12) Thallapally, P. K.; McGrail, P. B.; Dalgarno, S. J.; Atwood, J. L. *Cryst. Growth Des.* **2008**, *8*, 2090–2092.

- (13) Makha, M.; Alias, Y.; Raston, C. L.; Sobolev, A. N. *New J. Chem.* **2008**, *32*, 83–88.
- (14) Makha, M.; Alias, Y.; Raston, C. L.; Sobolev, A. N. *New J. Chem.* **2007**, *31*, 662–668.
- (15) Ripmeester, J. A.; Enright, G. D.; Ratcliffe, C. I.; Udachin, K. A.; Moudrakovski, I. L. *Chem. Commun.* **2006**, 4986–4996.
- (16) Nichols, P. J.; Raston, C. L. *Dalton Trans.* **2003**, 2923–2927.
- (17) Asfari, Z.; Bohmer, V. *Calixarenes*; Kluwer Academic Publishers: Dordrecht, The Netherlands, 2001.
- (18) Mandolini, L.; Ungaro, R., Eds. *Calixarenes in Action* Imperial College Press: London, 2000.
- (19) Liao, W.; Bi, Y.; Gao, S.; Li, D.; Zhang, H.; Dronsowski, R. *Eur. J. Inorg. Chem.* **2008**, 2959–2962.
- (20) Guo, D. S.; Liu, Y. *Cryst. Growth Des.* **2007**, *7*, 1038–1041.
- (21) Dalgarno, S. J.; Atwood, J. L.; Raston, C. L. *Cryst. Growth Des.* **2007**, *7*, 1762–1770.
- (22) Smith, C. B.; Barbour, L. J.; Makha, M.; Raston, C. L.; Sobolev, A. N. *Chem. Commun.* **2006**, 950–952.
- (23) Dalgarno, S. J.; Atwood, J. L.; Raston, C. L. *Cryst. Growth Des.* **2006**, *6*, 174–180.
- (24) Atwood, J. L.; Ness, T.; Nichols, P. J.; Raston, C. L. *Cryst. Growth Des.* **2002**, *2*, 171–176.
- (25) Selkti, M.; Coleman, A. W.; Nicolis, I.; Douteau-Guével, N.; Villain, F.; Tomas, A.; De Rango, C. *Chem. Commun.* **2000**, 161–162.
- (26) Drjaca, A.; Hardie, M. J.; Raston, C. L.; Spiccia, L. *Chem.—Eur. J.* **1999**, *5*, 2295–2299.
- (27) Schmidt, G. *Cluster and Colloids: From Theory to Applications*; VCH: Weinheim, Germany, 1994.
- (28) de Jongh, L. J. *Physics and Chemistry of Metal Cluster Compounds*; Kluwer: Dordrecht, The Netherlands, 1994.
- (29) Kajiwara, T.; Iki, N.; Yamashita, M. *Coord. Chem. Rev.* **2007**, *251*, 1734–1746.
- (30) Kajiwara, T.; Katagiri, K.; Takahashi, S.; Yamashita, M.; Iki, N. *Chem.—Asian J.* **2006**, *1*, 349–351.
- (31) Kajiwara, T.; Wu, H.; Ito, T.; Iki, N.; Miyano, S. *Angew. Chem., Int. Ed.* **2004**, *43*, 1832–1835.
- (32) Burgstein, M. R.; Ganser, M. T.; Roesky, P. W. *J. Am. Chem. Soc.* **2004**, *126*, 5213–5218.
- (33) Wang, R.; Song, D.; Wang, S. *Chem. Commun.* **2002**, 368–369.
- (34) Wang, R.; Selby, H. D.; Liu, H.; Carducci, M. D.; Jin, T.; Zheng, Z.; Anthis, J. W.; Staples, R. J. *Inorg. Chem.* **2002**, *41*, 278–286.
- (35) Markus, R.; Burgstein, P. W. R. *Angew. Chem., Int. Ed.* **2000**, *39*, 549–551.
- (36) Weng, D.; Zheng, X.; Jin, L. *Eur. J. Inorg. Chem.* **2006**, 4184–4190.
- (37) Zheng, X.-J.; Jin, L.-P.; Gao, S. *Inorg. Chem.* **2004**, *43*, 1600–1602.
- (38) Zheng, Z. *Chem. Commun.* **2001**, 2521–2529.
- (39) Bao-Qing Ma; Zhang, D.-S.; Gao, S.; Jin, T.-Z.; Chun-Hua; Xu, Y. G.-X. *Angew. Chem., Int. Ed.* **2000**, *39*, 3644–3646.
- (40) Xiang, S.; Hu, S.; Sheng, T.; Fu, R.; Wu, X.; Zhang, X. *J. Am. Chem. Soc.* **2007**, *129*, 15144–15146.
- (41) Gu, X.; Xue, D. *Inorg. Chem.* **2007**, *46*, 5349–5353.
- (42) Zhang, M. B.; Zhang, J.; Zheng, S. T.; Yang, G. Y. *Angew. Chem., Int. Ed.* **2005**, *44*, 1385–1388.
- (43) Tranchemontagne, D. J.; Mendoza-Cortez, J. L.; O'Keeffe, M.; Yaghi, O. M. *Chem. Soc. Rev.* **2009**, *38*, 1257–1283.
- (44) Gándara, F.; Gutiérrez-Puebla, E.; Iglesias, M.; Proserpio, D. M.; Snejko, N.; Monge, M. A. *Chem. Mater.* **2009**, *21*, 655–661.
- (45) Cao, A. P.; Shimizu, G. K. H. *Coord. Chem. Rev.* **2003**, *245*, 49–64.
- (46) Shimizu, G. K. H.; Vaidyanathan, R.; Taylor, J. M. *Chem. Soc. Rev.* **2009**, *38*, 1430–1449.

Article

- (47) Chruszalkowa, I. A.; Dem Aower, C. *Crystallog. Rep.* **2007**, *52*, 226–229.
- (48) Muijing, A. V.; Babai, A. Z. *Angew. Allg. Chem.* **2005**, *631*, 261–263.
- (49) Mahé, N.; Guillou, O.; Daiguzbonne, C.; Gérauld, Y.; Cameschi, A.; Singarayer, C.; Chme-Cheing, J. Y.; Car, P. E.; Rolinet, T. *Inorg. Chem.* **2005**, *44*, 7754–7759.
- (50) Zhang, D.-S.; Ma, B.-Q.; Ju, T.-Z.; Guo, S.; Yan, C.-H.; Mak, T. C. W. *New J. Chem.* **2000**, *24*, 61–62.
- (51) Gándara, F.; Gatola-Cortés, A.; Cascales, C.; Gómez-Lor, B.; Gutiérrez-Puebla, E.; Iglesias, M.; Monge, A.; Snejko, N. *Inorg. Chem.* **2007**, *46*, 3475–3484.
- (52) Scharif, J.-P.; Malacubi, M. *New J. Chem.* **1991**, *15*, 883–887.
- (53) Brown, I. D. *The Chemical Bond in Inorganic Chemistry: The Bond Valence Model*; Oxford Science Publications: Oxford, UK, 2002.
- (54) Brown, I. D.; Allenmaul, D. *Acta Crystallogr., Sect. B: Struct. Sci.* **1985**, *11*, 263–267.
- (55) Bresso, N. E.; O'Keefe, M. *Acta Crystallogr., Sect. B: Struct. Sci.* **1991**, *17*, 192–197.
- (56) Trzesnowska, A.; Kruszynski, R.; Bernczak, I. J. *Acta Crystallogr., Sect. B: Struct. Sci.* **2004**, *60*, 174–178.
- (57) Thompson, M. K.; Lough, A. J.; White, A. J. P.; Williams, D. J.; Kahwa, L. A. *Inorg. Chem.* **2003**, *42*, 8528–8531.
- (58) Serre, C.; Pella, F.; Gardani, N.; Férey, C. *Chem. Mater.* **2004**, *16*, 1177–1182.
- (59) Zhang, Z.-C. *Acta Crystallogr., Sect. C: Cryst. Struct. Commun.* **2008**, *64*, m381–m383.
- (60) Liu, J.; Meyers, E. A.; Shore, S. G. *Inorg. Chem.* **1998**, *37*, 5110–5111.
- (61) Evans, W. J.; Allen, N. T.; Greci, M. A.; Ziller, J. W. *Organometallics* **2001**, *20*, 2936–2937.
- (62) Gándara, F.; Perles, J.; Snejko, N.; Iglesias, M.; Gómez-Lor, B.; Gutiérrez-Puebla, E.; Monge, M. A. *Angew. Chem., Int. Ed.* **2006**, *45*, 7998–8001.
- (63) Perles, J.; Iglesias, M.; Ruiz-Valero, C.; Snejko, N. *J. Mater. Chem.* **2004**, *14*, 2683–2689.
- (64) Barini, M. C.; Gándara, F.; Iglesias, M.; Snejko, N.; Gutiérrez-Puebla, E.; Brusca, E. V.; Narda, G. I.; Monge, M. A. *Chem.—Eur. J.* **2009**, *15*, 4896–4905.
- (65) Gándara, F.; Andrés, A. J.; Gómez-Lor, B.; Gutiérrez-Puebla, E.; Iglesias, M.; Monge, M. A.; Proserpio, D. M.; Snejko, N. *Cryst. Growth Des.* **2008**, *8*, 378–380.

